



TECHNISCHE
UNIVERSITÄT
DARMSTADT

Investigating SMAD Signaling Dynamics and Function in Single Cells

vom Fachbereich Biologie
der Technischen Universität Darmstadt

zur Erlangung des Grades

Doctor rerum naturalium

(Dr. rer. nat.)

Dissertation von Zixin Huang

Erstgutachter: Prof. Dr. Alexander Löwer

Zweitgutachter: Prof. Dr. Stefan Legewie

Darmstadt 2024

Zixin Huang: Investigating SMAD Signaling Dynamics and Function in Single Cells

Darmstadt, Technische Universität Darmstadt,

Jahr der Veröffentlichung der Dissertation auf TUpriints: 2024

URN: urn: nbn:de:tuda-tuprints-287257

Tag der mündlichen Prüfung: 25.10.2024

Veröffentlicht unter CC BY-SA 4.0 International

<https://creativecommons.org/licenses/>

Contents

Contents.....	i
Abstract.....	v
1 Introduction	1
1.1 The SMAD Signaling Pathway.....	1
1.1.1 Ligand Diversity in TGF-beta Superfamily.....	1
1.1.2 Receptors in the TGF-beta Superfamily.....	2
1.1.3 Functional Differences Among SMADs.....	3
1.1.4 The Inhibitory Proteins of the SMAD Pathway.....	4
1.1.5 Pathological Implications of SMAD Signaling Dysregulation.....	5
1.2 Live-Cell Imaging and Single-Cell Analysis of SMAD Signaling.....	5
1.3 Decoding the Complexity of SMAD Signaling in Cell Fate Decisions.....	7
1.4 SMAD Signaling in Vascular Development and Disease.....	9
1.5 Aims of the Study.....	13
2 Result.....	14
2.1 Result of Part 1	14
2.1.1 EGF-Dependent SMAD2 Translocation Intensity Dictates Cellular Fate.....	14
2.1.2 Loss of SMAD2 Linker Phosphorylation Sites Independently Regulates Ligand-Induced Dynamics and Cell State.....	18
2.1.3 Loss of SMAD3 Enhances GDF11-Regulated SMAD2 response in Proliferating Cells.....	26
2.1.4 Reconstituted SMAD3 Reduced the SMAD2 Dynamic.....	33
2.1.5 Mechanisms of SMAD2/3 Pathway Modulation.....	38
2.2 Result of Part 2:	47
2.2.1 Quantifying SMAD Dynamics in Response to BMP Treatment Using Fluorescent Reporters.....	47
2.2.2 FKBP12 Modulates the Activity of ALK2 in EA.hy926 Cells.....	51
2.2.3 FKBP12 Regulates the Balance of SMAD1/5/9 and SMAD2/3 Activation by Ligands of the BMP Family.....	56
2.2.4 Different Receptor Complexes Determine SMAD Response Branches for Various Ligands.....	61
2.2.5 SMAD1/5/9 and SMAD2/3 Induce Distinct Cell Fates Independent of Activating Ligands.....	64

3	Discussion	67
3.1	Discussion of Part 1:	67
3.1.1	Conservation of SMAD Signaling Mechanisms in TGF-beta Family.	67
3.1.2	EGF-Induced Rewiring of SMAD Signaling.	68
3.1.3	Role of SMAD2 Linker Region Phosphorylation in Signal Integration and Cellular Response.	69
3.1.4	Impact of Receptor Expression and SMAD Proteins on TGF-beta Signaling.	71
3.1.5	SMAD3 Knockout Reveals Ligand-Specific Regulation of SMAD2 Dynamics.	72
3.1.6	Dissecting the Roles of SMAD2 and SMAD3 in Cellular Apoptosis and Motility.	73
3.1.7	Exploring SMAD3's Role in SMAD2 Modulation.	74
3.1.8	Upstream Regulation of SMAD3 and Its Impact on SMAD2 Dynamics.	75
3.1.9	Exploring SMAD2-Regulation through Gene Expression Profiling.	76
3.1.10	Future research.	77
3.2	Discussion of Part 2:	79
3.2.1	Live-Cell Imaging of SMAD Dynamics in Response to BMP9 Stimulation.	79
3.2.2	Investigating the Role of FKBP12 and Non-Signaling Complexes (NSCs) in BMP Signaling.	82
3.2.3	Novel Insights into the Balance of SMAD1 and SMAD2 Signaling.	84
3.2.4	Investigating Mechanisms Underlying the shift from SMAD2 to SMAD1 Signaling and Pathway Integration.	85
3.2.5	Unveiling the Complexity of TGF-beta Family Signaling: Receptor Dynamics and FKBP12 Modulation.	85
3.2.6	Investigating Single and Dual Pathway Inputs: Insights into Endothelial Cell Responses regulated by FKBP12.	86
3.2.7	Implications for Disease and Therapeutic Strategies.	88
4	Material and Methods.....	90
4.1	Material and Methods of Part 1:	90
4.1.1	Cell Lines.	90
4.1.2	Generating SMAD2 Knockout Cell Line.	91
4.1.3	Generating SMAD3 Knockout Cell Line.	94
4.1.4	Generating SMAD2-Replacement Cell Lines.	95
4.1.5	Generating SMAD3 Knockin Cell Line.	95

4.1.6	Generating LTBP2, MMP9, PMEPA1 Overexpression Cell Line.	98
4.1.7	Transfection and Generation of Monoclonal Cell Lines.....	100
4.1.8	PCR Amplification of DNA Fragments.	101
4.1.9	Analysis and Purification of DNA by Agarose Gel Electrophoresis.	101
4.1.10	Electroporation and Cultivation of Escherichia coli.	101
4.1.11	Genomic and Plasmid DNA Isolation.	102
4.1.12	Restriction Digest.	102
4.1.13	Sequencing.	103
4.1.14	Live-Cell Time-Lapse Imaging.	103
4.1.15	Ligand and Inhibitor Treatment.....	103
4.1.16	Wound Healing Assay.	104
4.1.17	RNA Sequencing.	104
4.1.18	Bioinformatic Analysis of RNA Sequencing Data.	105
4.1.19	Filter the Data.	105
4.1.20	Data Analysis of Live-Cell Microscopy Experiments.	106
4.1.21	Quantification of Cell Death.....	106
4.1.22	Quantification of Cell Motility.	107
4.1.23	Statistical Assessment of Differences in Cell Motility.	107
4.1.24	Protein Quantification and Western Blot Assay.	107
4.1.25	RNA Isolation and Quantification.	109
4.1.26	Software and Website.....	110
4.2	Material and Methods of Part 2:	111
4.2.1	Cell Maintenance of EA.hy926 Cell Lines.	111
4.2.2	Generated the Reporter Cell Line.	112
4.2.3	Live-Cell Time-Lapse Microscopy.....	112
4.2.4	Ligand and Inhibitor Treatments.	112
4.2.5	Western Blot Assay.	113
4.2.6	Real-Time Quantitative PCR (RT-qPCR).	114
4.2.7	Image Analysis and Cell Tracking.	114
4.2.8	EC50 and IC50 analysis.	115

4.2.9	Timing of Nuclear Translocation.....	115
4.2.10	Investigating Single-Cell SMAD1 and SMAD2 First Response Dynamics.....	115
4.2.11	Single Cell Dual Single Correlation Assay.....	116
4.2.12	Peak Value for Dual Single Assay.....	116
4.2.13	Radar Chart.....	116
4.2.14	Tube Formation Assay.	117
4.2.15	Softwares Used for the Assay.....	117
5	Reference.....	119
6	Appendix.....	140
6.1	List of Abbreviation.....	140
6.2	List of Figures.....	144
6.3	Supplementary Figures	146
6.4	Number of Tracked Cells in Time-Lapse Microscopy Experiments	153
6.4.1	Number of Tracked Cells in Time-Lapse Microscopy Experiments (Part 1):	153
6.4.2	Number of Tracked Cells in Time-Lapse Microscopy Experiments (Part 2):	160
	Acknowledgments	165
	Ehrenwörtliche Erklärung.....	167

Abstract

SMAD signaling is crucial for regulating key cellular processes such as differentiation, proliferation, apoptosis, migration, and extracellular matrix production. The pathway gets activated when ligands of the TGF-beta superfamily bind to specific serine/threonine kinase receptors on the cell surface and induce the formation of receptor complexes that phosphorylate SMAD proteins at their C-terminal domains. Phosphorylated SMADs then form oligomes that translocate to the nucleus to regulate gene expression. Despite extensive knowledge of TGF-beta pathway components, understanding how pathway activation translates into distinct cellular responses, especially at the single-cell level and across various ligands, remains limited. To address this, I explored SMAD signaling dynamics using quantitative, time-resolved measurements of fluorescent reporters and computer-aided data analysis. Through live-cell imaging and fluorescent reporter systems, I investigated the signaling dynamics of SMAD2/3 and SMAD1/5/9 in response to different ligands and cellular conditions, focusing on their roles in cells of the mammary gland epithelium and endothelium. This research aims to deepen our understanding of the mechanisms underlying SMAD dynamics in regulating cell fate decisions.

Our previous studies of TGF-beta superfamily ligands revealed varied SMAD2 responses depending on cellular states. TGF-beta triggered a strong SMAD2 response in proliferating cells, which was diminished in quiescence. In contrast, Activin A induced consistent SMAD2 responses across different cellular states and GDF11 led to opposing effects—enhanced SMAD2 activity in quiescent cells and attenuated responses in proliferating cells. Interestingly, there was evidence that the resulting cell fate decisions at the single-cell level are more influenced by SMAD signaling intensity than by ligand specificity. To build on these findings, the first part of my research addressed two key questions: Is the intensity of the SMAD response indeed correlated with cell fate decisions across different TGF-beta superfamily ligands? And what mechanisms modulate the SMAD response across cell states in the presence of different ligands? Using Activin A treatment, I could show that SMAD2 nuclear accumulation in MCF10A cells correlates strongly with cellular phenotype, with cell state being a more significant factor than ligand type. EGF was identified as a crucial modulator of the SMAD2 response network, capable of rescuing apoptosis in quiescent cells regardless of the ligand. Furthermore, I dissected the role of phosphorylation in the SMAD2 linker region for stimulus- and state-specific signaling by generating reporter cell lines with mutations of the corresponding phosphorylation sites. When examining the role of SMAD3, I observed that its knockout led to uniform SMAD2 nuclear translocation in both proliferating and quiescent cells upon GDF11 stimulation, but did not change the response pattern to TGF-beta. Reintroducing SMAD3 attenuated SMAD2 accumulation in response to GDF11, with attenuation levels correlating with SMAD3 expression. To gain deeper insights into the factors influencing state- and ligand-specific SMAD signaling, I utilized RNA sequencing to identify proteins that modulate the SMAD3-mediated SMAD2 response induced by GDF11. This analysis

highlighted several genes regulated by the SMAD3 pathway. From these observations, I propose that an extracellular feedback mechanism driven by SMAD3 may play a critical role in modulating the SMAD2 response, offering new perspectives on how SMAD signaling is dynamically regulated in different cellular contexts.

Building on insights from SMAD2/3 signaling in epithelial cells, I investigated the SMAD1/5/9 pathway in vascular endothelial cells. My primary goal was to compare how SMAD1, SMAD5, and SMAD9 respond to various TGF-beta superfamily ligands, revealing both unique and overlapping activation effects of these signaling components. Furthermore, I aimed to explore how the balance between the SMAD1/5/9 and SMAD2/3 pathways shifts with different ligands and impacts cellular responses. To achieve this, I developed fluorescent reporter cell lines for SMAD1, SMAD5, and SMAD9 in EA.hy926 vascular endothelial cells and characterized the dynamics and sensitivities of the signaling mediators. To understand how SMAD1/5/9 respond to various TGF-beta superfamily ligands, I focused on their distinct and overlapping effects. My findings revealed that only BMP9 and BMP10 robustly induced SMAD nuclear accumulation. I identified FKBP12 as a key inhibitor of ALK2-mediated SMAD1/5/9 activation which restricts their activation by ligands such as BMP7 and Activin A. Notably, these ligands activate both the SMAD2/3 and SMAD1/5/9 pathways in the absence of FKBP12. Using a dual SMAD1-SMAD2 reporter system, I investigated the balance between SMAD1 and SMAD2 and I identified distinct receptor complexes involved in SMAD2/3 activation: BMP7-induced activation relies on ALK4/ALK2 heterodimers, while Activin A-induced activation involves both ALK4/ALK2 heterodimers and ALK4 homodimers. Both ligands use ALK2 homodimers for SMAD1/5/9 activation. Finally, I investigated the cellular responses initiated through SMAD1/5/9 and/or SMAD2/3 activation and confirmed a cooperative interaction between the SMAD1/5/9 and SMAD2/3 pathways, highlighting FKBP12's role as a key regulator of SMAD1/5/9 activity.

Collectively, these findings offer new insights into how SMAD dynamics influence single-cell outputs in both epithelial and endothelial cells. Specifically, SMAD3 mediates the GDF11-induced SMAD2 response in MCF10A cells in a dose-dependent manner, while FKBP12 plays a crucial role in regulating SMAD1/5/9 responses to BMP7 and Activin A in EA.hy926 cells. This research elucidates key factors involved in the regulation of SMAD signaling in response to various ligand stimuli, deepening our understanding of their roles in diverse cellular processes.

Zusammenfassung

Die SMAD-Signalübertragung ist entscheidend für die Regulierung wichtiger zellulärer Prozesse wie Differenzierung, Proliferation, Apoptose, Migration und Produktion extrazellulärer Matrix. Der Signalweg wird aktiviert, wenn Liganden der TGF-beta-Superfamilie an spezifische Serin/Threonin-Kinaserezeptoren auf der Zelloberfläche binden und die Bildung von Rezeptorkomplexen induzieren, die SMAD-Proteine an ihren C-terminalen Domänen phosphorylieren. Die phosphorylierten SMADs bilden dann Oligome, die in den Zellkern wandern und die Genexpression regulieren. Trotz des umfangreichen Wissens über die Komponenten des TGF-beta-Signalwegs ist das Verständnis darüber, wie die Aktivierung des Signalwegs zu unterschiedlichen zellulären Reaktionen führt, insbesondere auf Einzelzellebene und bei verschiedenen Liganden, noch begrenzt. Um dieses Problem zu lösen, habe ich die Dynamik der SMAD-Signalübertragung mithilfe quantitativer, zeitaufgelöster Messungen von Fluoreszenzreportern und computergestützter Datenanalyse untersucht. Mit Hilfe von Live-Cell-Imaging und Fluoreszenzreportersystemen untersuchte ich die Signaldynamik von SMAD2/3 und SMAD1/5/9 als Reaktion auf verschiedene Liganden und zelluläre Bedingungen, wobei ich mich auf ihre Rolle in Zellen des Brustdrüsenepithels und des Endothels konzentrierte. Diese Forschung zielt darauf ab, unser Verständnis der Mechanismen zu vertiefen, die der SMAD-Dynamik bei der Regulierung von Zellschicksalsentscheidungen zugrunde liegen.

Unsere früheren Studien mit Liganden der TGF-beta-Superfamilie haben gezeigt, dass SMAD2 je nach Zellzustand unterschiedlich reagiert. TGF-beta löste in proliferierenden Zellen eine starke SMAD2-Reaktion aus, die in der Ruhephase abgeschwächt war. Im Gegensatz dazu löste Activin A konsistente SMAD2-Reaktionen in verschiedenen Zellstadien aus, und GDF11 führte zu gegensätzlichen Effekten - erhöhte SMAD2-Aktivität in ruhenden Zellen und abgeschwächte Reaktionen in proliferierenden Zellen. Interessanterweise gab es Hinweise darauf, dass die daraus resultierenden Entscheidungen über das Zellschicksal auf Einzelzellebene eher von der Intensität der SMAD-Signalisierung als von der Ligandenspezifität beeinflusst werden. Aufbauend auf diesen Erkenntnissen beschäftigte sich der erste Teil meiner Forschung mit zwei Schlüsselfragen: Ist die Intensität der SMAD-Reaktion tatsächlich mit den Entscheidungen über das Zellschicksal bei verschiedenen Liganden der TGF-beta-Superfamilie korreliert? Und welche Mechanismen modulieren die SMAD-Antwort in verschiedenen Zellstadien in Gegenwart unterschiedlicher Liganden? Durch die Behandlung mit Activin A konnte ich zeigen, dass die Akkumulation von SMAD2 im Zellkern von MCF10A-Zellen stark mit dem zellulären Phänotyp korreliert, wobei der Zellzustand ein wichtigerer Faktor ist als der Ligandentyp. EGF wurde als entscheidender Modulator des SMAD2-Reaktionsnetzwerks identifiziert, der in der Lage ist, die Apoptose in ruhenden Zellen unabhängig vom Liganden zu retten. Darüber hinaus untersuchte ich die Rolle der Phosphorylierung in der SMAD2-Linker-Region für die stimulus- und zustandsspezifische Signalübertragung, indem ich Reporterzelllinien mit Mutationen der entsprechenden

Phosphorylierungsstellen erzeugte. Bei der Untersuchung der Rolle von SMAD3 stellte ich fest, dass sein Knockout zu einer einheitlichen SMAD2-Kerntranslokation sowohl in proliferierenden als auch in ruhenden Zellen nach GDF11-Stimulation führte, aber das Reaktionsmuster auf TGF-beta nicht veränderte. Die Wiedereinführung von SMAD3 schwächte die SMAD2-Akkumulation als Reaktion auf GDF11 ab, wobei die Schwächungswerte mit der SMAD3-Expression korrelierten. Um tiefere Einblicke in die Faktoren zu gewinnen, die die zustands- und ligandspezifische SMAD-Signalgebung beeinflussen, habe ich die RNA-Sequenzierung genutzt, um Proteine zu identifizieren, die die durch GDF11 induzierte SMAD3-vermittelte SMAD2-Reaktion modulieren. Diese Analyse ergab, dass mehrere Gene durch den SMAD3-Signalweg reguliert werden. Aus diesen Beobachtungen schließe ich, dass ein extrazellulärer Rückkopplungsmechanismus, der von SMAD3 angetrieben wird, eine entscheidende Rolle bei der Modulation der SMAD2-Antwort spielen könnte, was neue Perspektiven für die dynamische Regulierung der SMAD-Signalübertragung in verschiedenen zellulären Kontexten eröffnet.

Aufbauend auf den Erkenntnissen über die SMAD2/3-Signalübertragung in Epithelzellen habe ich den SMAD1/5/9-Signalweg in vaskulären Endothelzellen untersucht. Mein primäres Ziel war es, zu vergleichen, wie SMAD1, SMAD5 und SMAD9 auf verschiedene Liganden der TGF-beta-Superfamilie reagieren, und dabei sowohl einzigartige als auch überlappende Aktivierungseffekte dieser Signalkomponenten aufzudecken. Darüber hinaus wollte ich untersuchen, wie sich das Gleichgewicht zwischen den SMAD1/5/9- und SMAD2/3-Signalwegen bei verschiedenen Liganden verschiebt und die zellulären Reaktionen beeinflusst. Zu diesem Zweck entwickelte ich fluoreszierende Reporterzelllinien für SMAD1, SMAD5 und SMAD9 in EA.hy926-Gefäßendothelzellen und charakterisierte die Dynamik und Empfindlichkeit der Signalüberträger. Um zu verstehen, wie SMAD1/5/9 auf verschiedene Liganden der TGF-beta-Superfamilie reagieren, konzentrierte ich mich auf deren unterschiedliche und sich überschneidende Wirkungen. Meine Ergebnisse zeigten, dass nur BMP9 und BMP10 eine robuste Akkumulation von SMAD im Zellkern bewirken. Ich identifizierte FKBP12 als einen wichtigen Inhibitor der ALK2-vermittelten SMAD1/5/9-Aktivierung, der deren Aktivierung durch Liganden wie BMP7 und Activin A einschränkt. Bemerkenswert ist, dass diese Liganden in Abwesenheit von FKBP12 sowohl den SMAD2/3- als auch den SMAD1/5/9-Weg aktivieren. Mit einem dualen SMAD1-SMAD2-Reportersystem habe ich das Gleichgewicht zwischen SMAD1 und SMAD2 untersucht und verschiedene Rezeptorkomplexe identifiziert, die an der SMAD2/3-Aktivierung beteiligt sind: Die BMP7-induzierte Aktivierung beruht auf ALK4/ALK2-Heterodimeren, während die Activin A-induzierte Aktivierung sowohl ALK4/ALK2-Heterodimere als auch ALK4-Homodimere umfasst. Beide Liganden nutzen ALK2-Homodimere für die Aktivierung von SMAD1/5/9. Schließlich untersuchte ich die zellulären Reaktionen, die durch die Aktivierung von SMAD1/5/9 und/oder SMAD2/3 ausgelöst werden, und bestätigte eine kooperative Interaktion

zwischen den SMAD1/5/9- und SMAD2/3-Wegen, wobei ich die Rolle von FKBP12 als Schlüsselregulator der SMAD1/5/9-Aktivität hervorhob.

Insgesamt bieten diese Ergebnisse neue Einblicke in die Art und Weise, wie die SMAD-Dynamik die Leistung einzelner Zellen sowohl in Epithel- als auch in Endothelzellen beeinflusst. Insbesondere vermittelt SMAD3 die GDF11-induzierte SMAD2-Reaktion in MCF10A-Zellen in einer dosisabhängigen Weise, während FKBP12 eine entscheidende Rolle bei der Regulierung der SMAD1/5/9-Reaktionen auf BMP7 und Activin A in EA.hy926-Zellen spielt. Diese Forschung klärt Schlüsselfaktoren auf, die an der Regulierung der SMAD-Signalübertragung als Reaktion auf verschiedene Ligandenstimuli beteiligt sind, und vertieft unser Verständnis ihrer Rolle in verschiedenen zellulären Prozessen.

1 Introduction

1.1 The SMAD Signaling Pathway.

Few cell signals match the impact of the highly conserved SMAD pathway in metazoan biology, as it plays a crucial role in regulating processes from embryonic development to adult cellular functions (David & Massagué, 2018; Feng & Derynck, 2005; M. Y. Wu & Hill, 2009; Zhu et al., 1999). The input for the SMAD pathway is generated at the cell surface, where TGF-beta superfamily ligands bind to specific serine/threonine kinase receptors. Upon ligand binding, these receptors form heteromeric complexes that phosphorylate SMAD proteins at their C-terminal domains. This phosphorylation promotes the formation of SMAD complexes that translocate to the nucleus to modulate gene expression (Figure 1A) (Attisano & Wrana, 2002; Heldin et al., 1997; Massagué, 2012). SMAD signaling governs critical cellular functions, including differentiation, proliferation, apoptosis, migration, and extracellular matrix production (Derynck & Zhang, 2003; Dijke et al., 2002; Massagué & Gomis, 2006). These processes are essential for embryogenesis, immune system regulation, wound healing and cancer progression (Finsson et al., 2013; Ikushima & Miyazono, 2010).

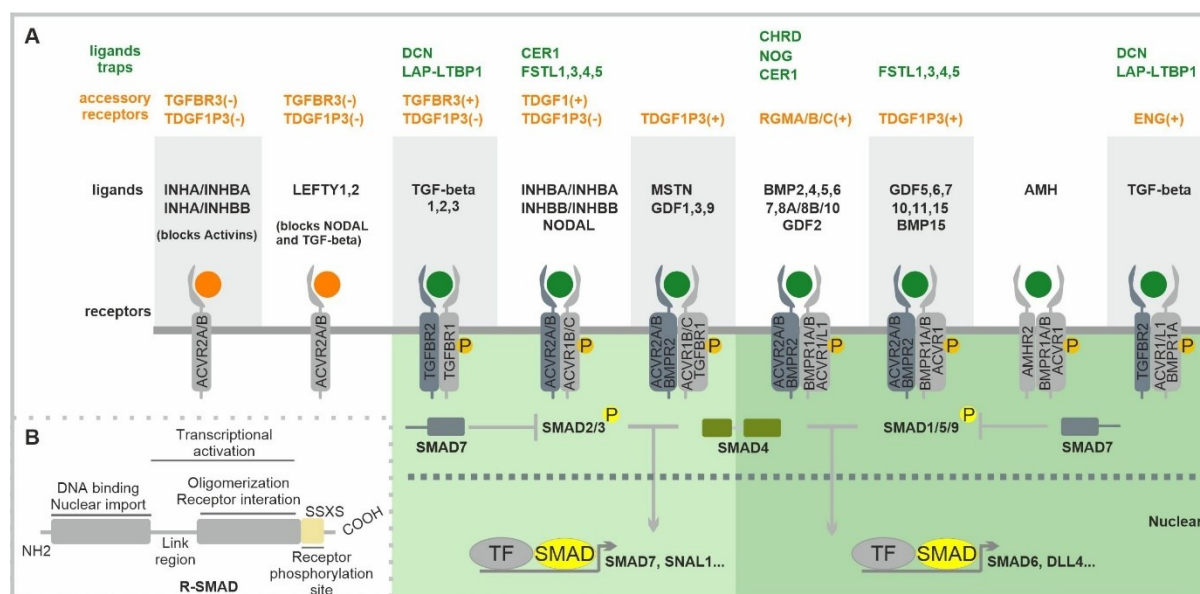


Figure 1 Schematic Representation of the SMAD Pathway Elements.

(A) This schematic representation highlights key components of the SMAD signaling pathway, illustrating the SMAD signaling cascade, including members of the TGF-beta family (ligands), their traps, and accessory receptors. This schematic is adapted from Kramer et al. (2016). **(B)** The schematic illustrates the structure of R-SMADs, highlighting their key domains. This schematic is adapted from Zhang et al. (2020).

1.1.1 Ligand Diversity in TGF-beta Superfamily.

The TGF-beta superfamily comprises a diverse array of over 30 cytokines, each with unique roles across various biological contexts (Attisano & Wrana, 2002; Schmierer & Hill, 2007). This rich ensemble includes TGF-betas, Bone Morphogenetic Proteins (BMPs), Growth and Differentiation Factors (GDFs), Activins, Inhibins, Anti-Müllerian Hormone (AMH), and Nodal (Figure 1A) (PIEK et al., 1999; Weiss & Attisano, 2013). The ligands in this superfamily are categorized into two main pathways: the TGF-beta and BMP pathways. The TGF-beta pathway, encompassing TGF-beta ligands, GDFs, Activins, and Inhibins, regulates the cell cycle, immune responses, and extracellular matrix production (Tzavlaki & Moustakas, 2020). It is involved in growth inhibition, fibrosis, cancer progression, muscle growth, stem cell differentiation, reproduction, and wound healing. The BMP pathway, originally identified for bone formation, is essential for embryonic development, vascular homeostasis, osteogenesis, chondrogenesis, neurogenesis, and angiogenesis (D. Chen et al., 2004; Miyazono et al., 2010).

1.1.2 Receptors in the TGF-beta Superfamily.

Central to the TGF-beta superfamily signaling pathway is a network of transmembrane serine/threonine kinase receptors, which act as the primary intermediaries between extracellular ligands and intracellular signaling mechanisms (Massagué, 2000). These receptors are broadly categorized into three main types: type I receptors, type II receptors and co-receptors. Upon ligand binding, type II receptors recruit and phosphorylate type I receptors, forming a heteromeric receptor complex that is crucial for downstream signaling. This receptor complex's composition is ligand-specific (Figure 1A) (Heldin et al., 1997; Heldin & Moustakas, 2016; Massagué et al., 2005).

Type I receptors, also known as Activin receptor-Like Kinases (ALKs), comprise seven distinct members in mammals, designated ALK1 through ALK7. Each of these receptors is characterized by unique structural features and ligand-binding specificities, enabling them to mediate diverse signaling pathways. ALK1, ALK2, ALK3, and ALK6 are primarily involved in BMP signaling. ALK4, ALK5, and ALK7 predominantly mediate TGF-beta and Activin signaling. Type II receptors, including TGF-beta Receptor II (TGFBR2), BMP Receptor II (BMPRII), and Activin Receptors (ACVRIIA, ACVRIIB), are constitutively active kinases that phosphorylate type I receptors upon ligand binding and formation of a tetrameric complex (López-Casillas et al., 1991; Vander Ark et al., 2018).

The receptor system's complexity is further enhanced by the presence of co-receptors. Co-receptors such as betaglycan (TGFBR3) and endoglin (ENG) can modulate the interactions between ligands and their primary receptors, influencing the signaling outcomes (Lastres et al., 1996; Lebrin et al., 2004; Lewis et al., 2000). Additionally, the expression of different receptor types and co-receptors can vary between cell types, adding another layer of specificity to the signaling process.

1.1.3 Functional Differences Among SMADs.

SMAD proteins are integral to TGF-beta/BMP signal transduction (Massagué et al., 2005). They are classified into three categories: receptor-regulated SMADs (R-SMADs: SMAD1, 2, 3, 5, and 9 (often referred to as SMAD8)), the common mediator SMAD (co-SMAD: SMAD4), and inhibitory SMADs (I-SMADs: SMAD6 and 7) (Figure 1A) (Miyazawa & Miyazono, 2017). R-SMADs are activated through phosphorylation at a conserved Ser-Ser-X-Ser (SSXS) motif, which enables them to form heteromeric complexes with SMAD4 and translocate to the nucleus to regulate gene expression (Figure 1B) (Miyazono, 1999). Each R-SMAD has distinct roles that contribute to the specificity of signaling, with SMAD2/3 being part of the TGF-beta pathway and SMAD1/5/9 being activated by the BMP pathway (Miyazawa et al., 2002). SMAD4, as the co-SMAD, acts as a central mediator that forms complexes with activated R-SMADs, facilitating their binding to DNA and the regulation of target genes (Schwarte-Waldhoff & Schmiegel, 2002). Meanwhile, I-SMADs, such as SMAD6 and SMAD7, provide critical negative feedback by inhibiting R-SMAD activation, thus ensuring precise control over the signaling pathway and preventing excessive or aberrant activation function (Miyazawa & Miyazono, 2017; Nakao et al., 1997).

At the core of TGF-beta and BMP signaling pathways are the receptor-regulated SMADs (R-SMADs), which are pivotal in transducing extracellular signals to the nucleus where their nucleocytoplasmic translocation regulates access to target genes and influences transcriptional outcomes based on their nuclear concentration and retention time (Xu, 2006). Structurally, R-SMADs consist of two domains—the N-terminal Mad Homology 1 (MH1) domain and the C-terminal Mad Homology 2 (MH2) domain—connected by a flexible linker region (Figure 1B). The MH1 domain is mainly responsible for nuclear import, DNA binding, and interactions with transcription factors (Shi et al., 1998), whereas the MH2 domain mediates interactions with type I receptors and the formation of SMAD complexes (Macias et al., 2015; Shi et al., 1998). A distinctive feature of R-SMADs is the conserved SSXS motif at the C-terminus, which is phosphorylated by activated type I receptors. This phosphorylation is crucial for SMAD activation, leading to the formation of SMAD complexes with SMAD4 and subsequent nuclear translocation. Meanwhile, the linker regions are subject to phosphorylation by various other kinases, including MAP kinases, CDKs, and GSK3, which can modulate SMAD activity and stability, known as the non-classical SMAD pathway (Moustakas & Heldin, 2005; Wrighton & Feng, 2008; Y. E. Zhang, 2009).

Despite their common role in transducing signals from TGF-beta superfamily receptors, R-SMADs exhibit distinct structural and functional characteristics that influence their specific roles in signaling. SMAD2, for instance, contains a unique E3 insert within its MH1 domain that affects its DNA-binding capacity, making it more reliant on interactions with other transcription factors compared to SMAD1, SMAD3, SMAD5, and SMAD9, which can directly bind DNA (Aragón et al., 2019; Hill, 2016; Macias

et al., 2015). Functionally, these SMADs exhibit varying degrees of redundancy and specialization. SMAD1 and SMAD5 demonstrate considerable functional overlap in BMP signaling, often compensating for each other's absence in many biological contexts (Retting et al., 2009; Salazar et al., 2016). This redundancy ensures robustness in BMP signal transduction, which is critical for numerous developmental processes. However, there are still functional differences between them. Smad5 knockout results in embryonic lethality due to defects in angiogenesis (Yang et al., 1999), while Smad1 knockout also leads to embryonic lethality but at a different developmental stage with distinct phenotypes (McReynolds et al., 2007; Tremblay et al., 2001). SMAD9, while is also involved in BMP signaling, shows more specialized functions, particularly in pulmonary vascular remodeling as demonstrated by the SMAD9 mutation patient (Machado et al., 2015). In contrast, SMAD2 and SMAD3, which primarily mediate TGF-beta signaling, display both overlapping and distinct functions (Nakao, Imamura, et al., 1997). They can often substitute for each other in many responses, yet they also have unique roles in specific developmental processes like gastrulation and epithelial-to-mesenchymal transition (EMT). The knockout of the Smad2 gene in mice leads to early embryonic lethality. This lethality occurs due to defects in primitive streak formation and the failure to establish the anterior-posterior axis, as well as the formation of the three germ layers (Brown et al., 2007; Heyer et al., 1999; Waldrip et al., 1998; Weinstein et al., 1998). In contrast, Smad3 knockout mice survive embryogenesis but exhibit other significant issues, including impaired immune function, accelerated wound healing, and reduced fertility (Falanga et al., 2004; Tomic et al., 2002; Yang, 1999).

1.1.4 The Inhibitory Proteins of the SMAD Pathway.

The regulation of SMAD signaling is crucial for maintaining cellular homeostasis and ensuring appropriate cellular responses to TGF-beta and BMP signals. There are many regulatory proteins and mechanisms that also contribute to the inhibition of the SMAD pathway, which can be categorized based on their protein location.

Intracellular inhibitory proteins include SMAD6, which primarily inhibits BMP signaling by competing with R-SMADs for receptor binding, preventing their activation and reducing BMP-mediated transcriptional responses, and SMAD7, which inhibits TGF-beta signaling by directly interacting with type I receptors to prevent R-SMAD (SMAD2/3) phosphorylation (Figure 1A) (Imamura et al., 1997; Nakao, Afrakhte, et al., 1997). SMAD7 also recruits ubiquitin ligases like Smurf1 and Smurf2 to degrade the receptors, further attenuating the signaling cascade (Ebisawa et al., 2001; Kavsak et al., 2000). Other intracellular regulators include nuclear oncoproteins such as Ski and SnoN, which inhibit TGF-beta signaling by binding to activated SMAD complexes and blocking their interaction with DNA (Deheuninck & Luo, 2009).

Negative regulators located at the cell membrane also play a role in blocking receptor-activated SMADs. For example, FKBP12 (FK506-binding protein 12, also called FKBP1A) binds to type I receptors in their inactive state, thereby preventing their inappropriate activation in the absence of ligands (Huse et al., 1999).

Extracellular negative regulators such as Noggin, Chordin, and Follistatin play crucial roles in modulating the availability of TGF-beta superfamily ligands, particularly BMPs (Figure 1A) (Canalis et al., 2003; Correns et al., 2021). These extracellular antagonists bind to specific ligands with high affinity, sequestering them and preventing their interaction with cell surface receptors. For example, Noggin is a potent inhibitor of BMP2 and BMP4 (C. Chen et al., 2012; La Rosa et al., 2011; Pregizer & Mortlock, 2015), while Follistatin primarily targets activins and some BMPs (Gajos-Michniewicz et al., 2010; Lin et al., 2003). The expression and distribution of these ligand traps can create local gradients of ligand availability, which is particularly important during embryonic development and tissue patterning (Perrimon et al., 2012). This multilayered regulation allows for context-dependent cellular responses crucial for normal physiological functions while safeguarding against aberrant pathway activation (Richardson et al., 2023).

1.1.5 Pathological Implications of SMAD Signaling Dysregulation.

The broad influence of the SMAD signaling pathway on cellular processes makes it a key player in numerous diseases. In cancer, SMAD signaling can function as both a tumor suppressor and promoter, depending on the context and tumor stage (Derynck et al., 2001; Kubiczkova et al., 2012; Labelle et al., 2011). Mutations in SMAD proteins can lead to various developmental disorders, including skeletal abnormalities (M. Wu et al., 2016). Additionally, TGF-beta plays a significant role in the pathogenesis of fibrosis across a wide range of disease models. For instance, the overexpression of TGF-beta 1 has been shown to induce renal fibrosis (Meng et al., 2016). Furthermore, cardiovascular diseases like atherosclerosis, pulmonary arterial hypertension (PAH) and hereditary hemorrhagic telangiectasia (HHT) have been linked to SMAD signaling dysregulation, highlighting its importance in vascular homeostasis (Miyazono et al., 2010). Understanding and targeting SMAD signaling thus holds promise for improving outcomes across a broad range of health conditions.

1.2 Live-Cell Imaging and Single-Cell Analysis of SMAD Signaling.

The study of cellular signaling pathways has long been constrained by the limitations of traditional research methods. Population-level analyses, while informative, often obscure the intricate heterogeneity of individual cellular responses. However, the emergence of live-cell imaging has introduced a new era of cellular biology research, offering unprecedented insights into the dynamic world of intracellular signaling (Batchelor et al., 2011; Loewer & Lahav, 2011). By leveraging

advanced microscopy technologies and fluorescent markers, researchers can visualize and track the dynamic behaviors of proteins and organelles in real-time, providing unprecedented detail and temporal resolution (Figure 2A) (Ankers et al., 2008). This approach allows for the long-term observation of individual cells, enabling the correlation of signaling dynamics with subsequent cellular behaviors such as proliferation, apoptosis, and differentiation (Blanpain & Simons, 2013; Y. Xu et al., 2013). This integration provides insights into cellular heterogeneity, the influence of cellular context on signaling interpretation, and the effects of perturbations on both signaling dynamics and cellular responses.

This approach has been employed to study other critical signaling pathways. For instance, live-cell imaging of Notch signaling has revealed oscillatory patterns of pathway activation in neural progenitor cells, crucial for maintaining the balance between proliferation and differentiation, ultimately influencing cell fate decisions in neurogenesis (Ninkovic et al., 2010). Single-cell analysis of NF- κ B signaling has uncovered oscillatory nuclear translocation patterns in response to TNF- α stimulation, encoding information about the stimulus and affecting gene expression patterns that influence immune responses and inflammation (Tay et al., 2010). Additionally, live-cell imaging of p53 dynamics has revealed pulsatile activation patterns in response to DNA damage, which regulate the cellular decision to undergo cell cycle arrest, senescence, or apoptosis (Finzel et al., 2016; Lahav et al., 2004; Loewer et al., 2010; Purvis et al., 2012).

SMAD proteins function as classical transcription factors, with their activation relying on cytoplasm-to-nucleus translocation, a process crucial for understanding SMAD signaling dynamics, and live-cell imaging serves as a pivotal technique for observing this translocation and protein response to ligand stimulation in real-time. A study by Strasen exemplifies this approach, where SMAD2-reporter cell lines were employed alongside time-lapse imaging and automated image analysis to meticulously dissect TGF- β signaling dynamics at the single-cell level (Strasen et al., 2018). Through this method, significant heterogeneity in SMAD2 activation patterns among TGF- β -treated cell populations were uncovered. Leveraging dynamic time-warping algorithms, thousands of SMAD2 activation profiles were clustered, revealing six distinct cellular sub-populations characterized by diverse signaling behaviors. This comprehensive analysis underscores the complex and variable nature of SMAD signaling responses within cell populations, shedding light on how individual cells interpret and respond to extracellular signals.

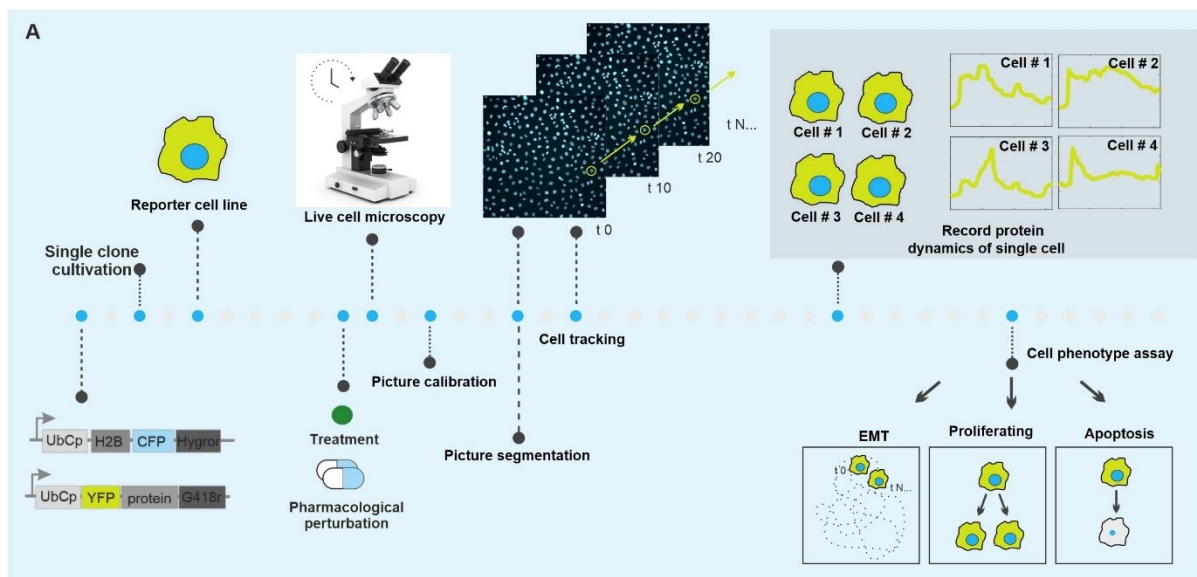


Figure 2 Schematic Representation of Live-Cell Time-Lapse Microscopy and Single-Cell Analysis.

(A) To perform time-lapse microscopy, a reporter cell line expressing fluorescently labeled proteins is essential. In this study, we utilized a reporter cell line expressing a target protein fused to yellow fluorescent protein (YFP) and histone 2B fused to cyan fluorescent protein (H2B-CFP). Both transgenes are driven by a constitutive human Ubiquitin C promoter (UbCp). This setup allows for high-resolution, temporal imaging of protein dynamics over several hours in response to different stimuli. Time-lapse microscopy generates extensive datasets of time-series images, which are analyzed using automated image processing. This approach enables tracking of hundreds of individual cells over time, facilitating measurement of protein dynamics within each cell. To assess protein translocation, the nuclear-to-cytoplasmic ratio of the fluorescently labeled proteins is quantified. Furthermore, single-cell data obtained from tracking are analyzed to study additional cellular behaviors such as motility, apoptosis, and proliferation.

1.3 Decoding the Complexity of SMAD Signaling in Cell Fate Decisions.

The TGF-beta signaling pathway, mediated by SMAD proteins, plays a crucial role in maintaining tissue homeostasis and orchestrating cellular responses to environmental cues (David & Massagué, 2018; Richardson et al., 2023). Our recent study has shed new light on how cells interpret and respond to TGF-beta superfamily signals in different cellular states (Bohn et al., 2023).

In healthy tissues, most cells remain quiescent with low metabolic activity and halted cell cycles, yet can re-enter proliferation upon specific signals (Figure 3A). The mammary gland illustrates this dynamic, cycling through proliferation, differentiation, and involution in response to hormonal cues during puberty, pregnancy, and lactation (J. L. Inman et al., 2015). These processes, involving proliferation, migration, and apoptosis, are regulated by signaling pathways like TGF-beta/SMAD. Interestingly, while TGF-beta/SMAD signaling supports tissue homeostasis and controlled cell growth in normal conditions, its role becomes more complex in cancer (Katsuno et al., 2013).

In normal epithelial cells and early-stage cancers, TGF-beta primarily acts as a potent growth inhibitor by upregulating cyclin-dependent kinase inhibitors and repressing c-Myc expression (Yagi et al., 2002). It also induces apoptosis, promoting programmed cell death through genes like p21, reinforcing its tumor-suppressive role in early cancer stages (Figure 3B) (Smith et al., 2012; Villalba et al., 2017; Y. Zhang et al., 2017). However, in advanced cancers, TGF-beta paradoxically shifts to promoting cell survival and proliferation (Connolly et al., 2012; Heldin et al., 2009). Beyond growth regulation and apoptosis, TGF-beta is a key regulator of epithelial-to-mesenchymal transition (EMT) (Hao et al., 2019; Labelle et al., 2011). During EMT, epithelial cells lose their characteristics and gain migratory and invasive properties, driven by genes like Snail and E-Cadherin, facilitating tumor progression (Figure 3B) (Dongre & Weinberg, 2019; Wang et al., 2014).

Through long-term microscopy, we observed that SMAD2 nuclear translocation correlates with distinct cellular outcomes depending on the cell's state: in quiescence, elevated nuclear SMAD2 intensity is associated with apoptosis, while in proliferation, it correlates with increased cell motility and proliferation (Figure 3B) (Bohn et al., 2023). Importantly, our previous investigation of various TGF-beta superfamily ligands revealed diverse SMAD2 responses. TGF-beta induces a high SMAD2 response in proliferating cells, which diminishes when the cells become quiescent. While some ligands like GDF3 and Activin A evoked similar SMAD2 responses across cellular states, others such as GDF8 and GDF11 induced opposing effects—heightened SMAD2 activity in quiescence and reduced activity in proliferation (Figure 3C). Perhaps most intriguingly, our research demonstrated that cell fate decisions at the single-cell level were influenced more by the intensity of SMAD signaling than by ligand specificity.

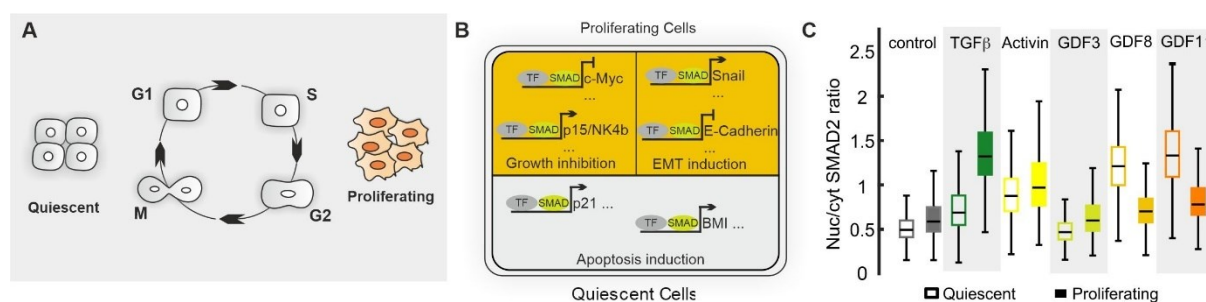


Figure 3 Context-Dependent Effects of TGF-beta Signaling on Cellular Outcomes.

(A) Schematic representation of the cell cycle transition from quiescent to proliferating states. Quiescent cells, characterized by low metabolic activity and cell cycle arrest, can re-enter the cell cycle and proliferate in response to specific signals. **(B)** Illustration of TGF-beta-induced effects in proliferating and quiescent cells. In proliferating cells, TGF-beta signaling inhibits cell proliferation and enhances epithelial-to-mesenchymal transition (EMT), promoting migratory and invasive properties. In quiescent cells, TGF-beta induces apoptosis, leading to programmed cell death. **(C)** Graph depicting the differential SMAD2 response levels induced by various TGF-beta superfamily ligands. Different ligands elicit distinct SMAD2 activation patterns, highlighting the complexity and specificity of TGF-beta signaling in determining cellular outcomes (Bohn et al., 2023).

Despite significant advances in understanding SMAD2/3-mediated processes, critical gaps persist in our comprehension of TGF-beta signaling's intricate regulation and context-dependent functions. The interaction between TGF-beta and other major signaling cascades, such as MEK/ERK and PI3K/AKT, complicates our understanding of how these pathways collectively modulate cellular outcomes (Luo, 2017). Moreover, the mechanisms by which cells interpret and discriminate between different TGF-beta superfamily ligands via SMAD2/3 remain poorly understood, particularly in light of our recent findings that cells appear to interpret SMAD signals quantitatively rather than based on ligand identity. Our previous research has revealed that cellular state (quiescent vs. proliferating) significantly influences SMAD2/3 signaling dynamics and outcomes. However, the molecular basis of this state-dependent response and its implications for cell fate decisions require further investigation. These gaps in knowledge highlight the need for a more comprehensive understanding of the complex interplay between cellular state, signaling dynamics, and cell fate determination in the context of TGF-beta/SMAD signaling. This thesis aims to address these critical gaps by elucidating the mechanisms by which cellular state modulates SMAD2/3 signaling dynamics and subsequent cellular responses. We will investigate the molecular basis of quantitative SMAD signal interpretation and its role in determining cell fate decisions, explore the interplay between SMAD2/3 signaling and other major signaling pathways. The significance of this research lies in its potential to deepen our understanding of how quantitative variations in signaling lead to qualitative differences in cellular behavior, shedding light on the intricate role of TGF-beta signaling in maintaining tissue homeostasis and driving disease progression, such as cancer and fibrotic disorders (David & Massagué, 2018).

1.4 SMAD Signaling in Vascular Development and Disease.

As outlined in the preceding section, SMAD signaling pathways are pivotal in regulating vascular development, maintaining vascular homeostasis, and influencing disease processes (Cai et al., 2012; Ten Dijke & Arthur, 2007). These pathways are particularly integral to angiogenesis, the process by which new blood vessels are formed from pre-existing ones (Figure 4A) (Carmeliet & Jain, 2011; Conway et al., 2001; Hiepen et al., 2020). This complex process requires the coordinated interaction of various cell types, underscoring the essential role of SMAD signaling in orchestrating these events.

During angiogenesis, different branches of the SMAD signaling pathways play distinct yet complementary roles across various stages and regions of vascular development. At the leading edge, tip cells—which guide the migration and formation of new vessel branches—rely on the SMAD1/5/9 signaling pathway. This pathway, activated by BMP2/6/7, is crucial for navigating and establishing new branches in the growing vessel network (Figure 4B) (Benn et al., 2017, 2020; Heinke et al., 2008; Hiepen et al., 2020). In the middle region, stalk cells—which follow the tip cells and contribute to forming the vessel lumen—are regulated by the SMAD2/3 pathways. Activated by TGF-beta, this pathway ensures proper vessel maturation and stability, facilitating cell proliferation and maintaining

the structural integrity of the developing vessels (Figure 4C) (Benn et al., 2017; Gaengel et al., 2009; Ito et al., 2009; Mallet et al., 2006). Finally, in mature vessels, the SMAD1/5/9 pathway continues to play a critical role. It ensures that endothelial cells receive the appropriate signals to maintain vascular quiescence and homeostasis. BMP9 and BMP10, promoted by shear stress, are key to this process, helping to preserve the stability and functionality of the mature vascular system (Figure 4D) (Desroches-Castan et al., 2022; Goumans et al., 2018; Hiepen et al., 2020).

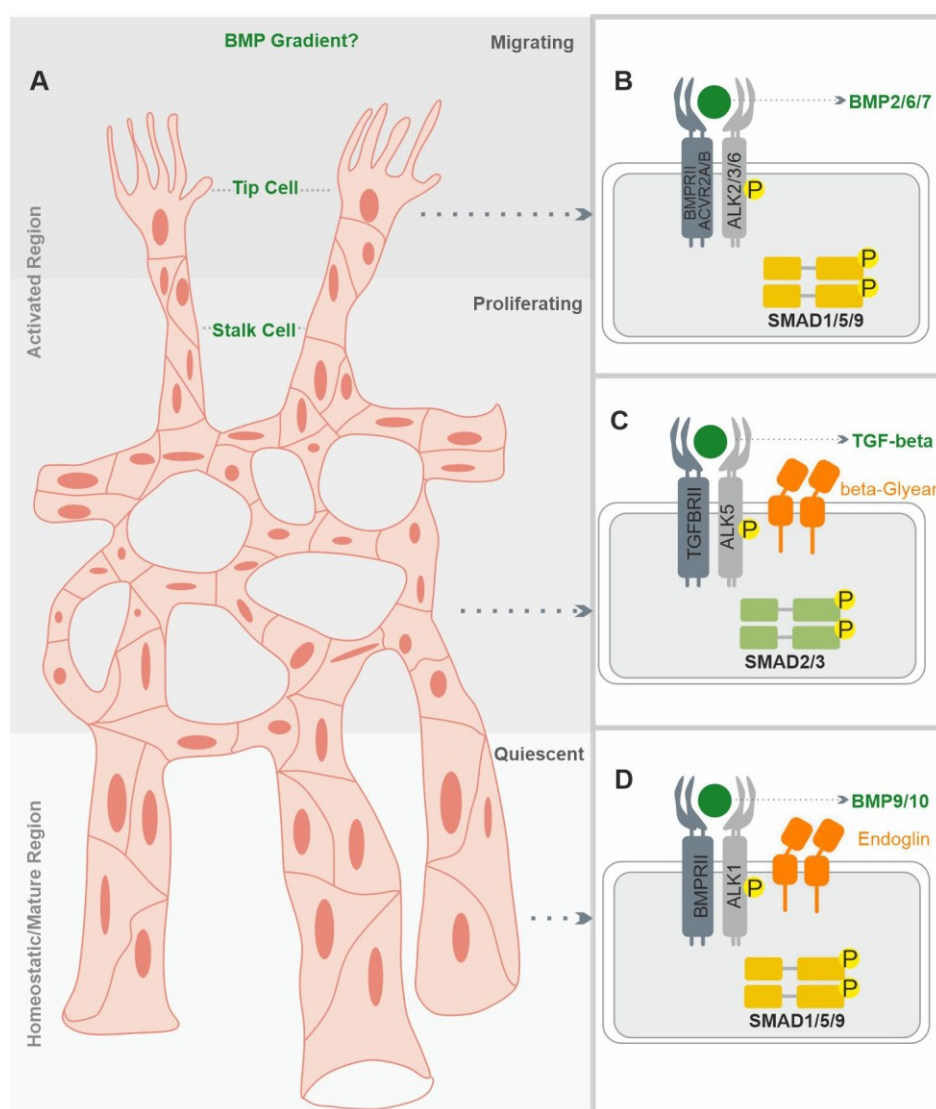


Figure 4 SMAD Signaling in Angiogenesis and Vascular Homeostasis.

Schematic representation modified from Hiepen et al. (2020). **(A)** Overview of the angiogenesis process, illustrating the structure of a sprouting blood vessel. The image shows the organization of tip cells leading the vascular sprout, followed by proliferating stalk cells, and the established homeostatic and mature region of the vasculature. This panel provides a comprehensive view of the different cellular states and regions involved in angiogenesis. **(B)** The image depicts how activation of the SMAD1/5/9 pathway promotes the migratory and invasive phenotype characteristic of tip cells, driving the directional growth of new blood vessels. **(C)** Detailed view of the stalk cell region, emphasizing the role of SMAD2/3 signaling. This panel illustrates how SMAD2/3 activation contributes to stalk cell proliferation and lumen formation, supporting the

elongation and stabilization of the growing vessel behind the tip cell. **(D)** Representation of the homeostatic and mature region of the vasculature. This image demonstrates how SMAD1/5/9 activation in established vessels promotes a quiescent endothelial phenotype, contributing to the long-term stability and function of mature blood vessels.

The balance between these SMAD pathways is vital for vascular development and homeostasis. Disruptions in this balance are implicated in various vascular diseases (Goumans et al., 2009; Lowery & de Caestecker, 2010; Miyazono et al., 2010). For instance, Hereditary Hemorrhagic Telangiectasia (HHT) and Pulmonary Arterial Hypertension (PAH) both highlight the critical role of SMAD signaling. HHT, also known as Osler-Weber-Rendu syndrome, is a rare autosomal dominant genetic disorder characterized by abnormal blood vessel formation (Robert et al., 2020). The genetic basis of HHT primarily involves mutations in three genes crucial for SMAD signaling: ENG (encoding endoglin, 50-60% of cases), ACVRL1 (encoding ALK1, 30-40% of cases), and SMAD4 (1-2% of cases) (Figure 5A) (Gallione et al., 2004; Lesca et al., 2006; Robert et al., 2020). It is important to note that the reported percentages of cases attributed to each gene can vary across different studies and populations. These variations may be due to differences in patient cohorts, diagnostic criteria, and detection methods employed in various research settings. Despite these variations, the overall distribution of genetic causes in HHT remains consistent, with ENG and ACVRL1 mutations accounting for the vast majority of cases. These mutations lead to impaired SMAD1/5/9 signaling, disrupting vascular stability and promoting the formation of telangiectases and arteriovenous malformations in various organs (Figure 5B) (Pardali et al., 2010). Pulmonary arterial hypertension (PAH) is a progressive and potentially fatal disease marked by elevated blood pressure in the pulmonary arteries, driven by sustained vasoconstriction and vascular remodeling (Thenappan et al., 2018). The genetic basis of PAH is closely linked to SMAD signaling pathways, with BMPR2 gene mutations being the primary cause, present in 75-80% of familial PAH (HPAH) cases and 20-25% of sporadic cases (IPAH). Mutations in other BMP pathway genes like ACVRL1, ENG, and SMAD9 also contribute, though less frequently, accounting for about 1-4% of PAH cases (Figure 5C) (Garcia-Rivas et al., 2017; Morrell et al., 2019). In PAH, pathological vascular changes include excessive proliferation and migration of vascular smooth muscle cells, endothelial dysfunction, and increased extracellular matrix deposition (Figure 5D) (Humbert et al., 2004; Rajagopal & Yu, 2022).

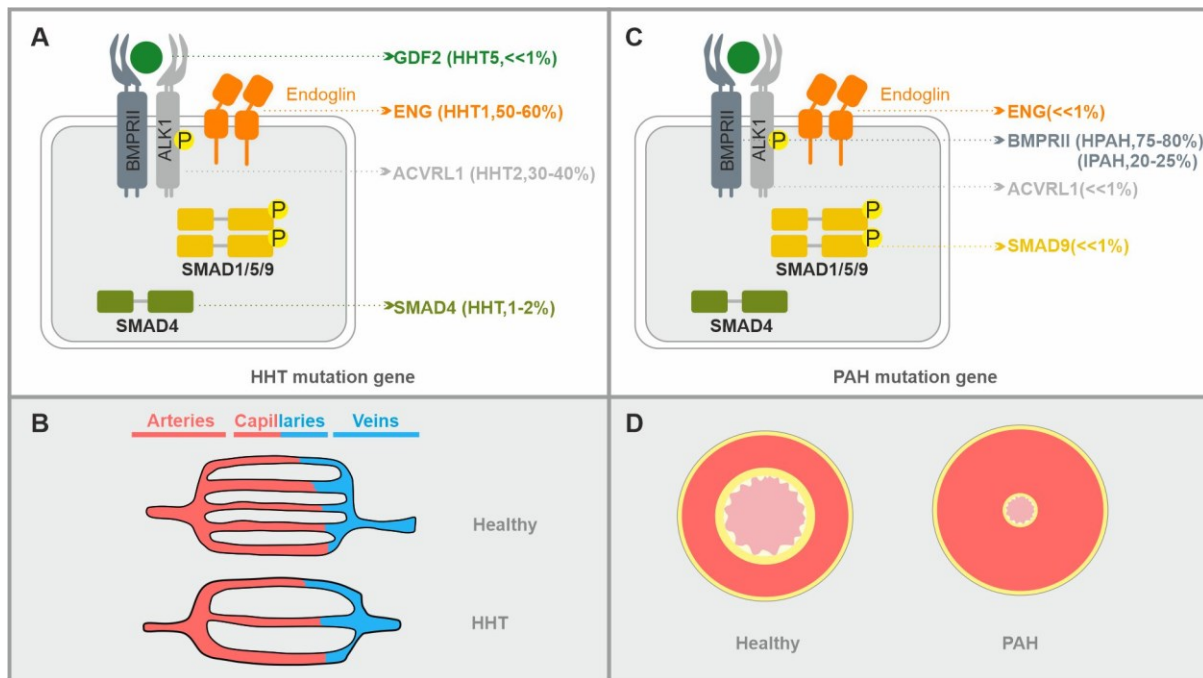


Figure 5 Genetic Basis and Vascular Manifestations of Hereditary Hemorrhagic Telangiectasia (HHT) and Pulmonary Arterial Hypertension (PAH).

(A) Schematic illustration of the distribution of causative gene mutations in Hereditary Hemorrhagic Telangiectasia (HHT). ENG mutations (HHT1) account for 50-60% of cases, ACVRL1 mutations (HHT2) for 30-40% of cases, SMAD4 mutations for 1-2% of cases, and GDF2 mutation less than 1%. A small percentage represents unknown mutations (Robert et al., 2020). **(B)** Schematic representation of vascular abnormalities characteristic of HHT, with normal vessels included for comparison. **(C)** Schematic showing the distribution of known genetic mutations associated with Pulmonary Arterial Hypertension (PAH). BMPR2 mutations are the most common, accounting for 75-80% of familial cases (HPAH) and 20-25% of sporadic cases (IPAH). Other less common mutations in genes such as ACVRL1, ENG, and SMAD9 collectively represent about 1-4% of cases. The remaining portion represents cases with unknown genetic causes. **(D)** Illustration of the vascular changes in PAH. The image contrasts normal pulmonary arteries with those affected by PAH, showing the characteristic narrowing of the vessel lumen due to vascular remodeling.

Despite significant advances in understanding SMAD signaling, critical gaps persist in our knowledge of this complex pathway. The redundancy and compensatory mechanisms within the TGF-beta superfamily signaling add layers of complexity that are not fully understood. Mutations in individual receptors often only partially impair pathway activity due to these compensatory processes, involving redundant or differentially functional ligand-receptor pairs. Additionally, the coexistence of multiple TGF-beta family ligands in the extracellular environment creates intricate signaling inputs, with some ligands acting synergistically while others exhibit antagonistic effects (M. Y. Wu & Hill, 2009). Key areas requiring further investigation include the mechanisms underlying partial loss of function due to receptor mutations, the distinct effects of different SMAD proteins (SMAD2/3 vs. SMAD1/5/9) in response to varying ligand levels, and the live cell dynamics of the SMAD pathway, which remain poorly understood. Understanding these pathways is crucial for developing treatments for vascular

disorders like Hereditary Hemorrhagic Telangiectasia (HHT) and Pulmonary Arterial Hypertension (PAH). This study aims to fill gaps in SMAD signaling knowledge, enhancing our grasp of cellular communication and potentially advancing disease modeling, drug discovery, and targeted therapies.

1.5 Aims of the Study.

This study aims to elucidate the mechanisms by which different SMAD proteins and ligands regulate cell fate decisions across two distinct biological contexts: mammary gland epithelia and vascular. The research is structured into two main parts, each focusing on specific aspects of SMAD signaling pathways.

In the first part, the focus is on the SMAD2/3 signaling pathways in mammary gland development. The objective is to unravel the regulatory networks governing SMAD responses to various ligands under different cell states. This will be achieved through CRISPR/Cas9-mediated gene editing to investigate the role of the SMAD2 linker region, alongside exploring how SMAD3 contributes to SMAD2 responses and cell fate decisions. Integration of time-resolved single-cell measurements of signaling dynamics with pharmacological and genetic perturbations, complemented by RNA sequencing, aims to provide a detailed understanding of how these pathways influence cell fate decisions in mammary gland development.

In the second part, the study addresses the complexities of SMAD signaling in vascular biology. The challenge lies in predicting how specific ligands function in combination and deciphering the underlying molecular determinants of their interactions. To tackle these challenges, the research will establish SMAD fluorescent reporter cell lines to dissect pathway responses in living cells. Employing fluorescent reporters, live-cell microscopy, and automated image analysis, the study will track SMAD translocation from the cytoplasm to the nucleus in human vascular endothelial cells (EA.hy926) with high resolution. This approach aims to uncover how SMAD signaling dynamics vary within cells over time and how BMP network architecture influences these responses. Additionally, I will investigate receptor roles in the BMP pathway and ligand effects on long-term cellular dynamics and decision-making.

2 Result

2.1 Result of Part 1

Figures 6, 7, and 13 in Part 1 of this work are based on a study recently published by Bohn, S., Hexemer, L., **Huang, Z.**, Strohmaier, L., Lenhardt, S., Legewie, S., & Loewer, A. (2023) titled "State- and stimulus-specific dynamics of SMAD signaling determine fate decisions in individual cells," in *Proceedings of the National Academy of Sciences of the United States of America*, 120(10). <https://doi.org/10.1073/pnas.2210891120>. All experiments were conducted by me, with RNA-seq materials prepared by Stefan Bohn and data analysis carried out in collaboration with Lorenz Ripka (IMB Mainz). The figures and text have been adapted specifically for this thesis.

2.1.1 EGF-Dependent SMAD2 Translocation Intensity Dictates Cellular Fate.

To further validate our hypothesis that SMAD2 nuclear accumulation determines cell fate and depends on cell states rather than specific ligands, I expanded our investigation to include Activin A alongside TGF-beta and GDF11, investigating how cell phenotype changes under proliferating and quiescent cell states. The rationale for selecting Activin A was that it induced SMAD2 intensity intermediate to the other two ligands and elicited a similar SMAD2 response in both cell states, as proven by previous live cell experiments. Consistent with our previous observations, GDF11 induced a weak SMAD2 response in proliferating cells, while TGF-beta elicited a robust response under similar conditions over a three-day period (Figure 6A). Activin A triggered a SMAD response similar to that induced by TGF-beta (Figure 6A).

Next, I analyzed cell motility and found that cells with higher SMAD2 translocation, stimulated by TGF-beta and Activin A, exhibited more pronounced mobility, while GDF11 only weakly increased cell motility compared to the control (Figure 6B). These findings support our hypothesis linking SMAD2 activation to cell fate decisions in proliferating cells. Given the strong correlation between the SMAD2 response and cell motility at the population level, I calculated the area under the curve (AUC) of the nuclear-to-cytoplasmic SMAD2 ratio as an integrated measure of pathway activity and correlated this with individual cell motility (see Method 2.3.23) (Figure 6C). Single-cell motility closely correlated with SMAD2 AUC; cells with higher AUC values exhibited higher motility scores, indicating that stronger pathway activation corresponded with more significant phenotypic responses in individual cells.

To further confirm my cell motility assay, I evaluated epithelial-to-mesenchymal transition (EMT) using wound healing assay. Comparing TGF-beta and GDF11 treated conditions, TGF-beta stimulation significantly enhanced cell migration compared to GDF11, where weaker SMAD activation was

associated with less cell mobility (Figure 6D). Comparing the untreated condition and GDF11-treated group, cells treated with TGF-beta exhibited significant EMT. This process was characterized by the nuclear translocation of SMAD2, which drives the transition from epithelial to mesenchymal states, resulting in the loss of epithelial characteristics and the acquisition of mesenchymal-like properties (Figure 6E) (Marconi et al., 2021; Sánchez-Tilló et al., 2012).

Next, I investigated how SMAD translocation dynamics correlate with apoptosis in quiescent cells treated with those ligands. As anticipated, GDF11 induced the highest SMAD response, followed by Activin A, with TGF-beta showing the lowest response, consistent with previous findings (Figure 6F). Notably, GDF11 treatment resulted in significant cell death, corresponding to its robust SMAD2 nuclear accumulation (Figure 6G). In contrast, TGF-beta induced minimal apoptosis, aligning with its lower SMAD2 response, while Activin A caused a moderate level of cell death. To further explore this relationship, I analyzed the correlation between SMAD AUC and apoptosis at the single-cell level. Higher SMAD AUC values were clearly associated with increased cell apoptosis in quiescent cells (Figure 6H). These findings underscore the role of SMAD nuclear accumulation in determining cell fate, with stronger pathway activation linked to higher cellular responses.

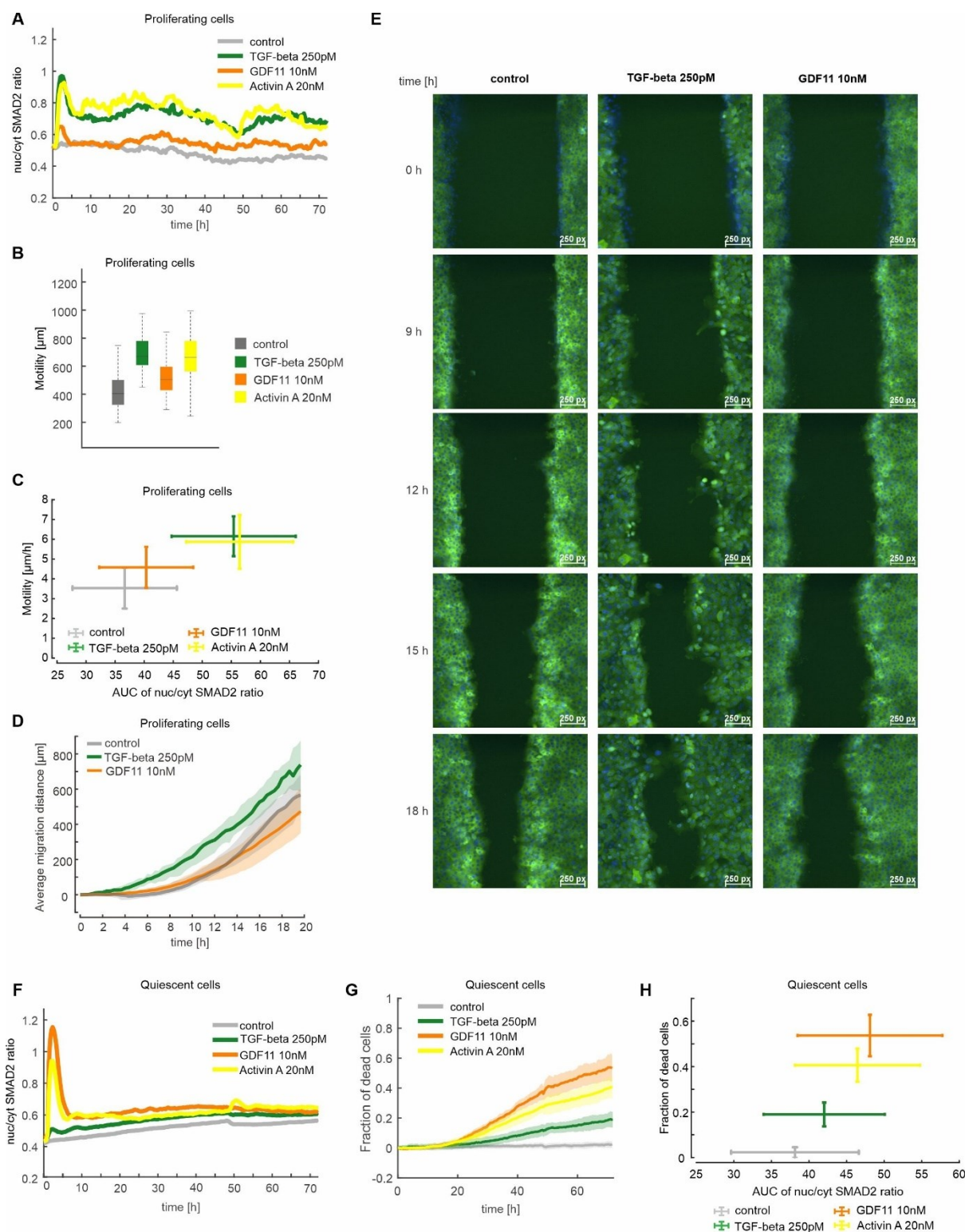


Figure 6 Phenotypic Responses Correlate with SMAD Translocation in a State-Specific Manner Independent of Ligand Type.

(A) Median nuclear-to-cytoplasmic SMAD2 ratio in proliferating SMAD2-reporter cells treated with TGF-beta (250 pM), GDF11 (10 nM), or Activin A (20 nM) over 72 hours. Cells were imaged 0.5 hours before ligand stimulation. Medium was refreshed with ligands every 48 hours. **(B)** Cell movement in proliferating SMAD2-reporter cells treated as in (A), represented by boxplots showing distance moved per cell. Cell motility was measured in pixels and converted to micrometers using a

conversion factor of 1 pixel = 0.361 μm (derived from dividing 1 by 2.77). The generated boxes include data between the 25th and 75th percentiles. The black line indicates the mean and whiskers extend to maximum values within 1.5 \times the interquartile range. **(C)** Correlation between median cell mobility fraction and mean integrated nuclear-to-cytoplasmic SMAD2 ratio (area under the curve, AUC; hours). Error bars: standard deviation (SD) across cell population (x axis) and fields of view (y axis). **(D)** Wound healing assay. After 72 hours stimulation with TGF-beta (250 pM) or GDF11 (10 nM), cell layer was scraped and cultured with corresponding ligands. Images were taken every 20 minutes for 20 hours. Average migration distance measured for each condition. **(E)** Representative images from (D) show cell activation and movement at the indicated time points, merging the channels with CFP and YFP. **(F)** Nuclear-to-cytoplasmic SMAD2 ratio in quiescent SMAD reporter cells treated as in (A). **(G)** Fraction of dead cells over time. Bold lines represent median fraction per field of view; shaded areas represent standard deviation (SD). **(H)** Correlation between median dead cell fraction and mean integrated nuclear-to-cytoplasmic SMAD2 ratio (AUC) in quiescent cells treated with indicated ligands for 72 hours.

After proving our hypothesis, I aimed to further investigate the factors that could modify SMAD dynamics based on the cell state. Our previous results showed that EGF, a growth factor known to switch cell states in MCF10A cells (Chou et al., 1999), increased the SMAD2 response upon TGF-beta treatment after 8 hours of incubation with EGF in quiescent cells. However, the duration required for EGF to rescue the SMAD2 response remained unclear. Additionally, I aimed to determine whether EGF could modulate the GDF11-induced SMAD2 response in quiescent cells, and if so, whether this modulation would ultimately influence cell fate decisions.

To address these questions, I incubated quiescent cells with EGF for varying durations before TGF-beta stimulation. Shorter EGF incubation times partially rescued the SMAD2 response, with SMAD2 levels peaking and plateauing after 4-8 hours of EGF treatment (Figure 7A). This suggests that EGF's effect on SMAD2 response is indirect and likely involves downstream gene expression changes. Interestingly, EGF pre-incubation downregulated the GDF11-induced SMAD2 response, with a noticeable decrease in SMAD2 levels beginning around 3 hours (Figure 7B). The similar timeframe required for EGF to affect SMAD2 responses to both TGF-beta and GDF11 (approximately 3-4 hours).

Next, I monitored cell apoptosis following EGF incubation to determine whether this modulation would ultimately influence cell fate decisions. EGF pre-incubation rescued cells from apoptosis, whether incubated for a long duration (8 hours) or even with just 1 hour of pre-incubation (Figure 7C). Additionally, adding EGF 16 hours after ligand stimulation, when cells typically begin to undergo apoptosis, still effectively rescued cells from apoptosis in both ligand stimulation conditions.

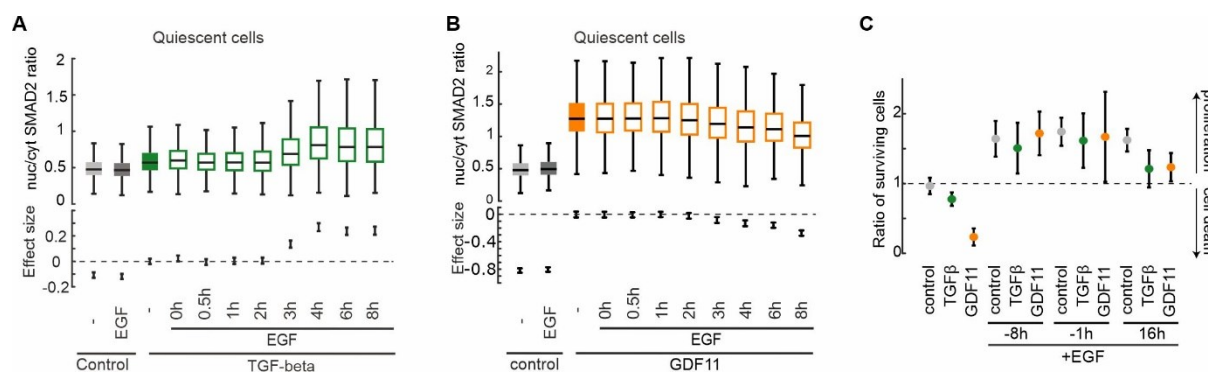


Figure 7 EGF treatment Rewrites SMAD Response to Ligands in Quiescent Cells and Rescues Cells from Apoptosis.

(A and B) Single-cell quantification of maximum nuclear-to-cytoplasmic SMAD2 ratio in quiescent SMAD2-reporter cells within 5 hours after stimulation with (A) 100 pM TGF-beta or (B) 10 nM GDF11. EGF was added at indicated times before ligand stimulation. Boxplots show the distribution of the cell population, with boxes including data between the 25th and 75th percentiles, black lines indicating the median and whiskers extend to maximum values within 1.5× the interquartile range. Estimated changes compared to untreated cells of each condition are shown for each replicate in lower plot; error bars represent 95% confidence intervals determined by permutation testing. Dashed lines serve as guides to the eye. **(C)** Phenotypic conversion toward proliferation by EGF treatment. Quiescent cells were treated with 250 pM TGF-beta or 10 nM GDF11 for 72 hours or left untreated. EGF was added either before (-8 h or -1 h) or 16 hours after TGF-beta family ligand treatment. Mean ratio of surviving cells at endpoint (120 hours) relative to initial cell number (0 hours) is shown. Ratio > 1 indicates overall proliferation; ratio < 1 indicates prevalence of cell death. Error bars represent SD across fields of view. Dashed lines serve as guides to the eye.

2.1.2 Loss of SMAD2 Linker Phosphorylation Sites Independently Regulates Ligand-Induced Dynamics and Cell State.

Following the observations from my experiments, I aimed to uncover the mechanism behind SMAD dynamic regulation. Prior research indicates that SMAD2 regulation by EGF involves phosphorylation in the SMAD2 linker region, through its interaction with the EGF-MAPK pathway (Figure 8A) (Ooshima et al., 2019; Wrighton et al., 2009). This interaction serves as a cross-talk point between the TGF-beta/SMAD pathway and other signaling cascades, thereby regulating SMAD dynamics. However, there is no information on how the SMAD2 linker region functions in MCF10A cells or if it regulates cell fate based on different cell states.

To systematically explore these questions and determine if linker phosphorylation underlies EGF's ability to reverse SMAD2 responses, I employed gene editing and mutagenesis techniques. Initially, I needed a cell line where endogenous SMAD2 was removed to insert a SMAD2 protein mutated at specific phosphorylation sites. Using the CRISPR-Cas9 system, I disrupted endogenous SMAD2 in MCF10A H2B-CFP cells by targeting exon 2 with designed single guide RNAs (sgRNAs) (Figure 8B) (see Method 4.1.2.). This approach facilitated the removal of native SMAD2 while integrating a blasticidin resistance cassette. Extensive screening confirmed the successful knockout of endogenous

SMAD2 in the MCF10A-H2B-CFP cell line (clone #6), validated by clonal selection and further analyses, including Western blotting (Figure 8C), PCR (Figure 8D), and sequencing (Figure 8E). Specifically, the PCR results revealed that one allele harbored a blasticidin insertion, while the other allele had a deletion. PCR1 amplified the Cas9 endonuclease site region, showing bands of 3,716 bp and 2,486 bp, indicative of a heterozygous genotype. PCR2 amplified the blasticidin sequence, indicating successful donor DNA integration with a 2,199 bp fragment. Collectively, these results demonstrate the effective knockout of SMAD2 in the cell line. Given that the SMAD2 linker region contains four phosphorylation sites (Figure 8A), each potentially influencing SMAD2 function based on their specific location and kinase interactions, I engineered plasmids to introduce mutations targeting these sites: T220, S245, S250, and S255 (Figure 8F). To explore how loss of SMAD2-linker phosphorylation impacts SMAD2 dynamics, I also generated 3x and 4x mutations to investigate the collective inhibition of phosphorylation and its effect on SMAD2 response to ligand stimulation (Figure 8F), considering indications that EGF may affect multiple sites similarly. These mutations were integrated into plasmids under the UbCp with a G418 selection cassette, and CRISPR-Cas9 facilitated their insertion into the AAVS1 locus (Figure 8G), with wild-type (WT) SMAD2 sequences used as a reference for comparative analyses (Figure 8F).

Following plasmid insertion and selection under specialized conditions, I isolated clones and characterized them through sequencing (Figure 8H) to confirm the incorporation of mutations. These engineered cell lines now serve as tools for unraveling the intricate regulatory dynamics of the linker region and understanding its consequential impact on SMAD2 behavior in response to diverse ligand stimulations and within varying cellular contexts.

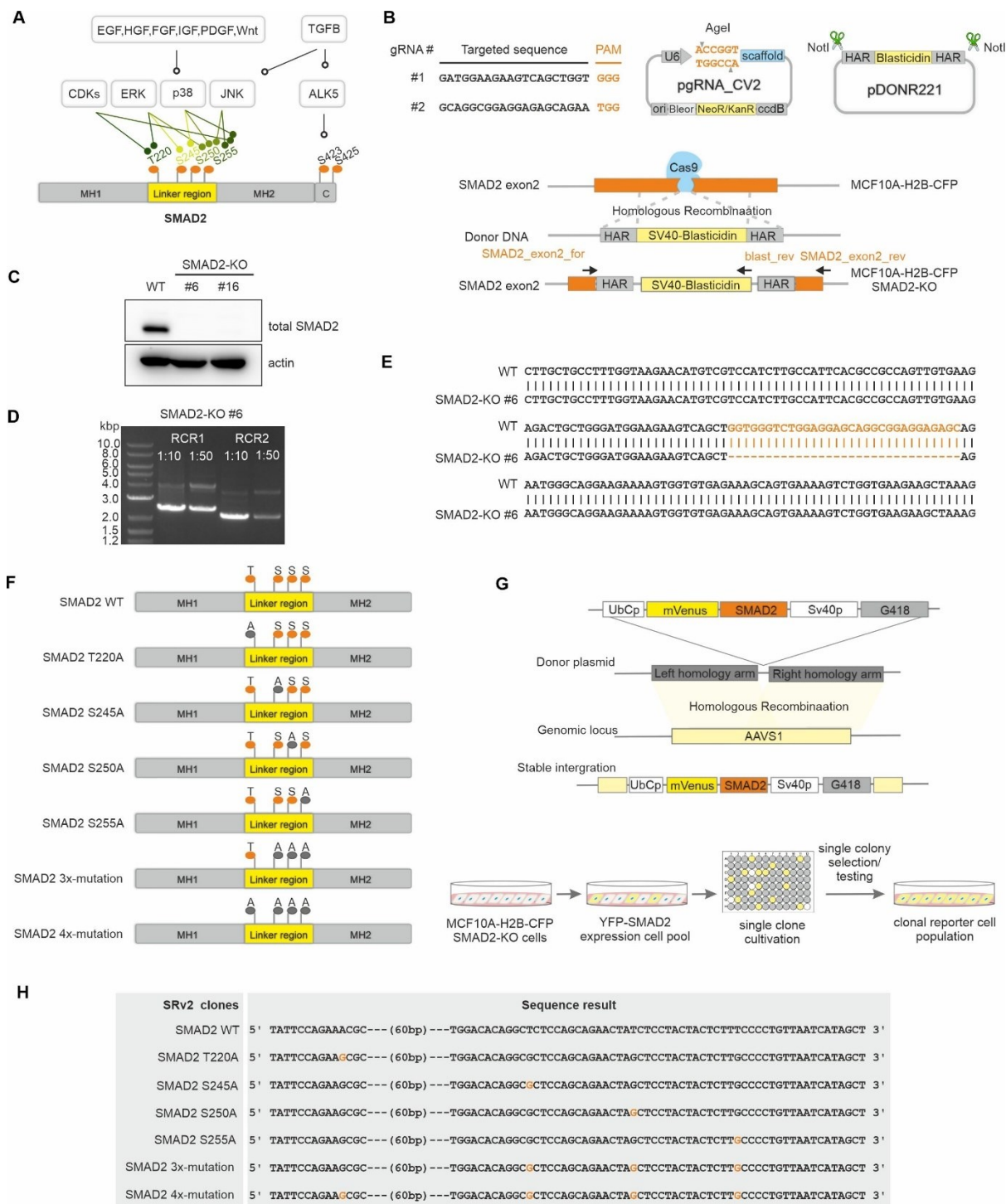


Figure 8 Generation of SMAD2 Linker Region Mutation Clones.

(A) Schematic depicting the regulatory regions of SMAD2, including the linker region and C-terminal domain. (B) CRISPR/Cas9 knockout strategy for SMAD2. Top left: Insertion of sgRNA into Cas9 vector using Agel. Top right: Generation of repair template by amplifying homology arms from MCF10A genomic DNA and SV40-Blasticidin from pVE10 vector, followed by assembly cloning. (For details, see Method 4.1.2.). Below: To achieve complete loss of SMAD2, both alleles of the gene were targeted through homology-directed repair in MCF10A H2B-CFP cells. This was accomplished by co-transfecting the cells with a plasmid expressing Cas9 endonuclease, a plasmid containing a single guide RNA (sgRNA), and linearized donor DNA designed to insert a blasticidin resistance gene under the control of a constitutive SV40 promoter (SV40-Blasticidin). The

SV40-Blasticidin was specifically inserted into exon 2 of the SMAD2 gene. **(C)** Western blot assay confirming SMAD2 knockout in two selected clones compared to MCF10A H2B-CFP control cells, with Actin as a loading control. **(D)** Agarose gel (0.75%) electrophoresis of PCR products from SMAD2 knockout clones. PCR1: The allele with deletion in exon 2 exhibited a band at 2,486 bp, while the allele with the blasticidin insertion showed a band at 3,716 bp. Homozygous samples for the insertion displayed a single band at 3,716 bp, whereas heterozygous samples presented both bands at 3,716 bp and 2,486 bp. The results revealed that the selected clone is heterozygous. PCR2: Amplification of blasticidin sequence indicating successful donor DNA integration with a 2,199 bp fragment. The two lanes with different indicated ratios demonstrate varying dilutions of the DNA template, illustrating the PCR efficiency with different template concentrations. DNA Ladder 1 kb Plus served as marker. **(E)** Sequencing validation of SMAD2 knockout in lower bands from PCR1. **(F)** Schematic illustrating various mutations in the SMAD2 linker region. **(G)** Schematic of AAVS1 locus post-integration of SMAD2 mutations and G418R selection cassette. **(H)** Sequencing results confirming successful knock-in of different SMAD2 mutations into the AAVS1 locus.

Following the establishment of the SMAD2-reporter cell lines, I had to ensure that the newly developed SMAD2 replacement reporter system maintained physiological relevance without disrupting pathway behavior compared to the previous SMAD2-R cell line (Figure 9A). Initially, I evaluated the phosphorylation kinetics of YFP-SMAD2 in SRv2 WT cells upon TGF-beta stimulation. The phosphorylation dynamics of YFP-SMAD2 in SRV2 WT cells mirrored those of endogenous SMAD2 in MCF10A wildtype cells (Figure 9B, up panel) and SMAD2-R cells (Figure 9B, down panel) over a 0 to 9 hours time course post-stimulation in proliferating cells. Live-cell microscopy further confirmed that YFP-SMAD2 in SRV2 WT cells faithfully reproduced canonical nucleocytoplasmic shuttling upon TGF-beta stimulation (Figure 9C), consistent with observations in SMAD2-R cells (Figure 9D). Dose-dependent patterns of SMAD2 nuclear accumulation were observed in both SRv2 WT and SMAD2-R cells following TGF-beta stimulation (Figure 9E) and GDF11 stimulation (Figure 9F). While the overall response patterns remained consistent, individual clones displayed subtle differences in their responses to the same stimulus intensity, resulting in slight variations in the magnitude of both early and late responses. These findings underscore that the new SMAD2 replacement reporter system faithfully represents TGF-beta/SMAD2 pathway dynamics, similar to the established SMAD2-R line, without altering cellular responses to TGF-beta family ligands. Consequently, this system proves to be an effective tool for studying SMAD2 regulation in diverse cellular contexts. After validating the SRv2 WT reporter, I addressed whether the linker region, potentially regulated by EGF, alters SMAD2 response based on cell state. Using mutant cell lines, I probed the roles of specific linker phosphorylation sites upon TGF-beta stimulation in proliferating cells. Compared to SRv2 WT, mutations at S245 and S250 did not affect SMAD2 nucleocytoplasmic shuttling (Figure 10A, B), whereas mutation at S255 enhanced SMAD2 nuclear translocation (Figure 10C), suggesting S255 phosphorylation inhibits SMAD2 nuclear accumulation. Similarly, T220 mutation augmented the SMAD2 response (Figure 10D). Consistent with expectations, SMAD2-3x-mutation cells with functional T220 showed heightened SMAD2 nuclear accumulation (Figure 10E), similar to S255

mutation cells. However, simultaneous silencing of T220 and S255 (4x mutation) did not further enhance the SMAD2 response (Figure 10F).

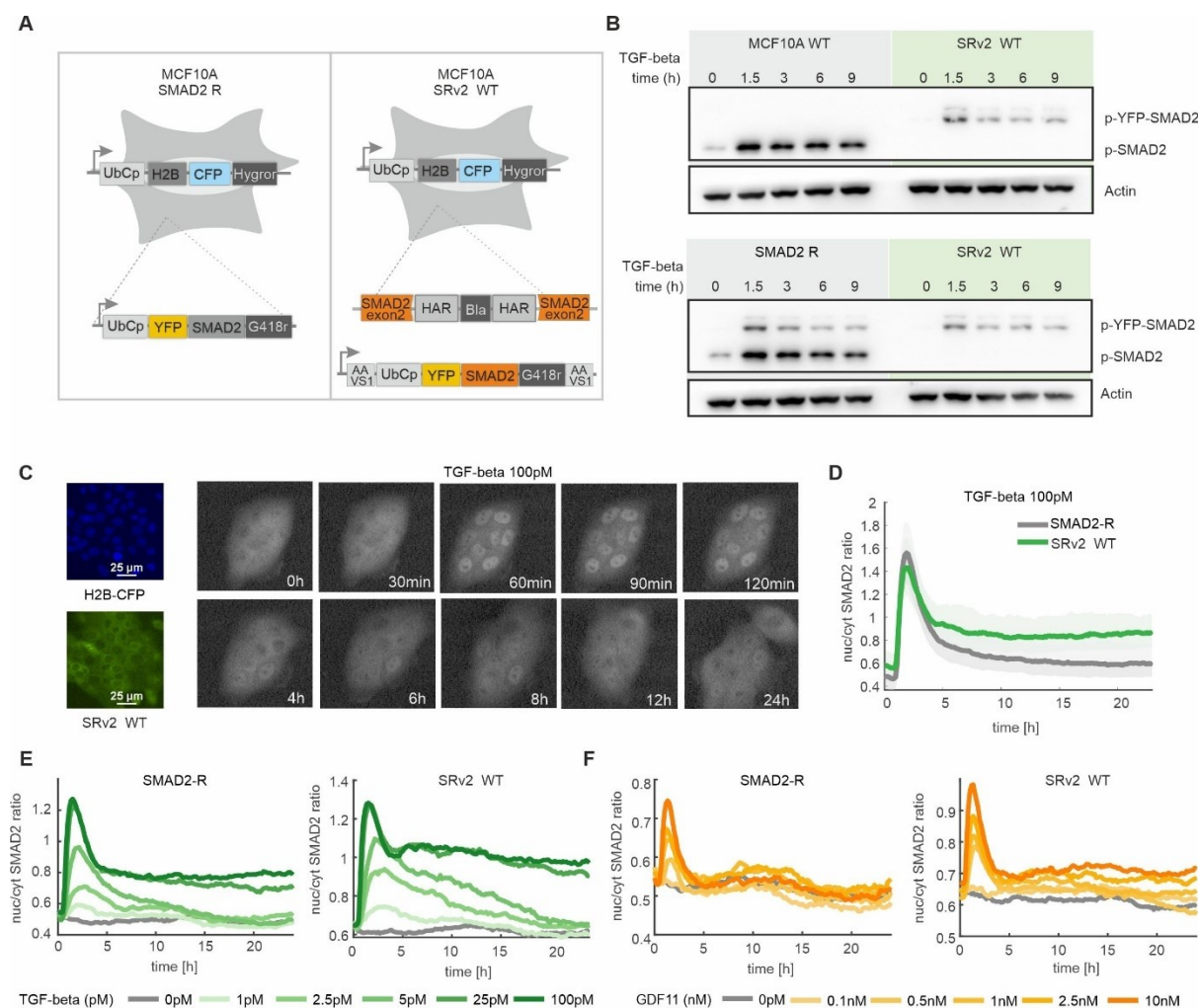


Figure 9 Validation of SRv2 WT Clone.

(A) Schematic comparison of SMAD2-R and SRv2 WT cell lines. **(B)** Western blot assay of SMAD2 activation in SRv2 WT and parental MCF10A wildtype cells (upper panel) and SRv2 WT and SMAD2-R cells (lower panel) stimulated with 100 pM TGF-beta under proliferating conditions. Phosphorylated SMAD2 levels were assessed at indicated time points, with Actin used as a loading control. **(C)** Representative live-cell time-lapse microscopy images showing YFP-SMAD2 WT localization in individual cells at specified time points following 100 pM TGF-beta treatment in proliferating conditions. **(D)** Median nuclear-to-cytoplasmic SMAD2 ratio in SRv2 WT (green) and SMAD2-R (gray) cells upon 100 pM TGF-beta stimulation in proliferating conditions. Solid lines represent median values, while shaded areas indicate the 25th to 75th percentiles. **(E)** Median nuclear-to-cytoplasmic SMAD2 ratio in SMAD2-R and SRv2 WT cells following stimulation with various concentrations of TGF-beta over 24 h. **(F)** Median nuclear-to-cytoplasmic SMAD2 ratio in SMAD2-R and SRv2 WT cells following stimulation with varying concentrations of GDF11 over 24 h in proliferating conditions.

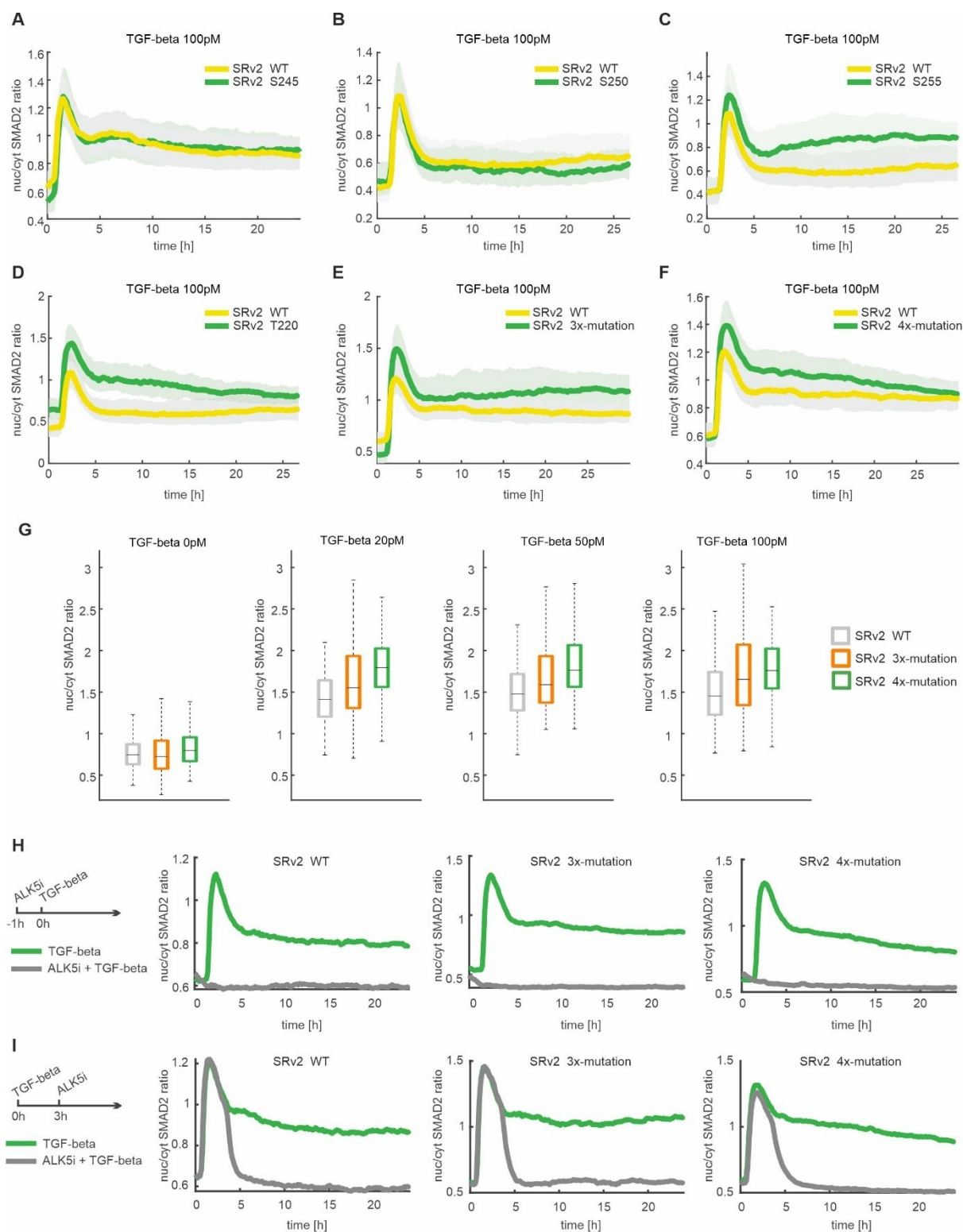


Figure 10 Analysis of SMAD2 Dynamics in Different Clones with TGF-beta Induction.

(A-F) Median trajectories of nuclear-to-cytoplasmic SMAD2 ratios following treatment with 100 pM TGF-beta1 in proliferating conditions for (A) SRv2 S245, (B) SRv2 S250, (C) SRv2 S255, (D) SRv2 T220, (E) SRv2 3x-mutation, and (F) SRv2 4x-mutation (green), compared to SRv2 WT (yellow). Solid lines indicate median values, and shaded areas represent the 25th to 75th percentiles. (G) Single-cell quantification of maximum nuclear-to-cytoplasmic SMAD2 ratios in SRv2 3x-mutation (orange), SRv2 4x-mutation (green), and SRv2 WT (grey) cells within 5 h after stimulation with various doses of TGF-beta in

proliferating conditions. **(H)** Efficacy of ALK5 inhibitor (SB525334) in SRv2 3x-mutation, SRv2 4x-mutation, and SRv2 WT cells prior to TGF-beta induction in proliferating conditions. Cells were treated with 10 μ M ALK5i 1 h before 100 pM TGF-beta stimulation (grey). DMSO served as control (green). **(I)** Efficacy of ALK5 inhibitor (SB525334) in SRv2 3x-mutation, SRv2 4x-mutation, and SRv2 WT cells after TGF-beta induction in proliferating conditions. Cells were treated with 10 μ M ALK5i 3 h after 100 pM TGF-beta stimulation (grey). DMSO served as control (green).

To explore whether the amplified SMAD2 response observed in high-dose TGF-beta stimulation extends across a range of doses compared to SRv2 WT, SMAD2-3x-mutation and SMAD2-4x-mutation clones were stimulated with varying doses of TGF-beta (Figure 10G). As anticipated, both mutations showed enhanced SMAD2 responses at peak time points across all TGF-beta doses. Interestingly, despite the enhanced responses due to linker region mutations, these mutations exhibited dose-dependent patterns similarly to wildtype cells across all tested doses. These findings highlight that SMAD2 nuclear translocation is specifically influenced by phosphorylation at T220 and S255, without showing cumulative effects across varying doses of TGF-beta stimulation in proliferating cells.

To determine if the increased nuclear accumulation of SMAD2 caused by linker region mutations requires activation of the SMAD C-terminus, I treated SMAD2-3x-mutation and SMAD2-4x-mutation clones with the ALK5 receptor inhibitor SB525334 (ALK5i). Pre-treatment with the inhibitor both before TGF-beta stimulation (Figure 10H) and post-stimulation (Figure 10I) abolished SMAD2 translocation, highlighting the continual requirement for receptor-mediated activation across all experimental conditions. This underscores that the linker region alone cannot initiate SMAD2 shuttling, affirming the persistent role of receptor-dependent mechanisms under all tested scenarios.

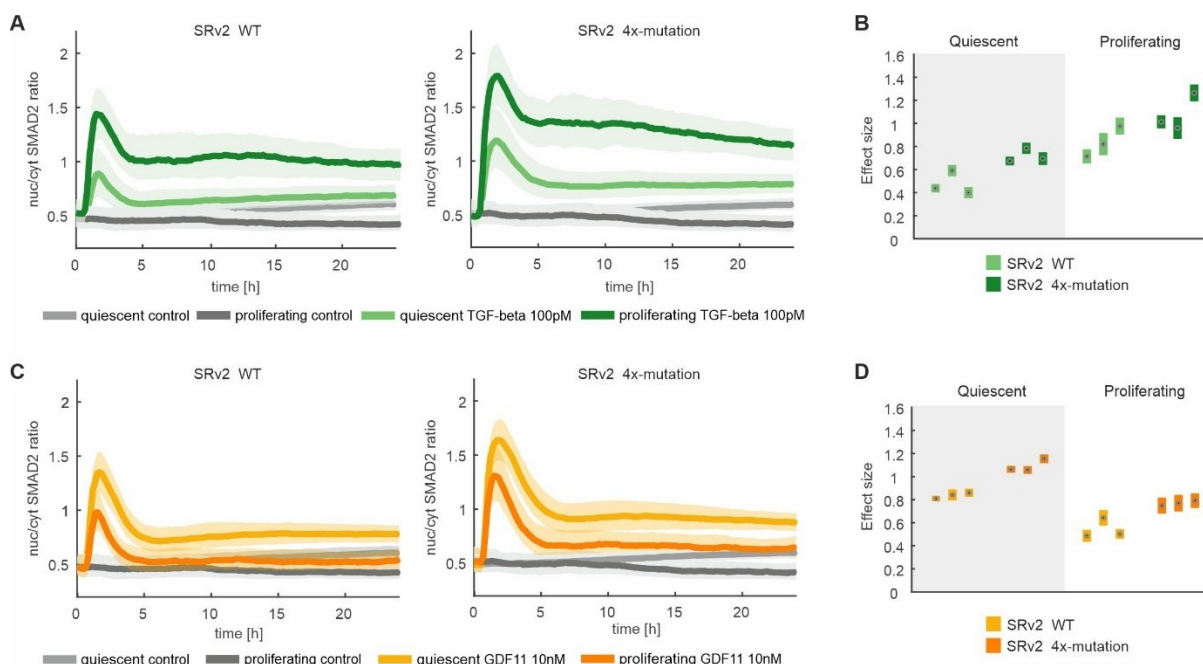


Figure 11 SMAD2 Linker Region Inhibits SMAD2 Nuclear Translocation Upon Stimulation Independent of Cellular State.

(A) Median nuclear-to-cytoplasmic SMAD2 ratio upon stimulation with 100 pM TGF-beta in SRv2 WT (left) and SRv2 4x-mutation (right) cells. Cells were treated with TGF-beta (green) 0.5 h after the experiment started or left unstimulated (grey) in both quiescent and proliferating conditions. Solid lines represent the median values, and shaded areas indicate the 25th to 75th percentiles of the population. **(B)** Effect size intervals are depicted for three replicate experiments described in (A). Confidence intervals were estimated using permutation testing (1,000 permutations), with unstimulated conditions as controls for comparison with TGF-beta stimulation. **(C)** Median nuclear-to-cytoplasmic SMAD2 ratio upon stimulation with 10 nM GDF11 in SRv2 WT (left) and SRv2 4x-mutation (right) cells. Cells were either treated with GDF11 (orange) 0.5 hours after the start of the experiment or left unstimulated (grey), under both quiescent and proliferating conditions. Solid lines represent the median values, and shaded areas indicate the 25th to 75th percentiles of the population. **(D)** Effect size confidence intervals (25th to 75th percentiles) are shown for three replicate experiments described in (C). Confidence intervals were estimated using permutation testing (1,000 permutations), with unstimulated conditions as controls for comparison with GDF11 stimulation.

However, solely examining TGF-beta stimulation in proliferating cells does not fully elucidate whether EGF-mediated SMAD2 linker region phosphorylation plays a pivotal role in altering SMAD2 responses based on cell states. To further investigate this, I evaluated the effects of linker mutations in quiescent cells. Given that cumulative effects of linker phosphorylation site loss were not observed, I specifically focused on the SMAD2-4x-mutation line. If the linker region is indeed influenced by EGF-mediated cross-talk pathways, the SMAD2-4x-mutation line would be expected to exhibit comparable SMAD2 responses in both proliferating and quiescent states upon TGF-beta stimulation. However, contrary to this hypothesis, SMAD2-4x-mutation cells showed a consistently attenuated SMAD2 response to TGF-beta stimulation compared to proliferating cells, resembling the response of SRv2 WT cells in the quiescent state (Figure 11A, B). Notably, despite being in a quiescent state, the SMAD2-4x-mutation cell line consistently exhibited enhanced SMAD2 nuclear translocation upon TGF-beta stimulation compared to SMAD2-WT-R cells (Figure 11A, B). These findings suggest that the SMAD2 linker region imposes an inhibitory effect on SMAD2 nuclear accumulation in response to TGF-beta, irrespective of the cellular state being proliferating or quiescent.

Next, I investigated whether mutations in the linker region would affect the SMAD2 response to GDF11 differently. If the linker region is influenced by GDF11-mediated signaling, mutations might enhance nuclear translocation specifically in the proliferating cell state upon GDF11 stimulation. However, contrary to this hypothesis, my results showed that linker region mutations resulted in a similar nuclear shuttling pattern as SRv2 WT cells in response to GDF11 across both proliferating and quiescent cell states (Figure 11C, D). Comparing WT and mutant clones, loss of the linker region consistently increased the magnitude of the SMAD2 response in both cell states, akin to the response observed with TGF-beta. In summary, these findings highlight the SMAD2 linker region as a key regulatory node that modulates the intensity of SMAD2 nuclear translocation upon stimulation, irrespective of cellular state.

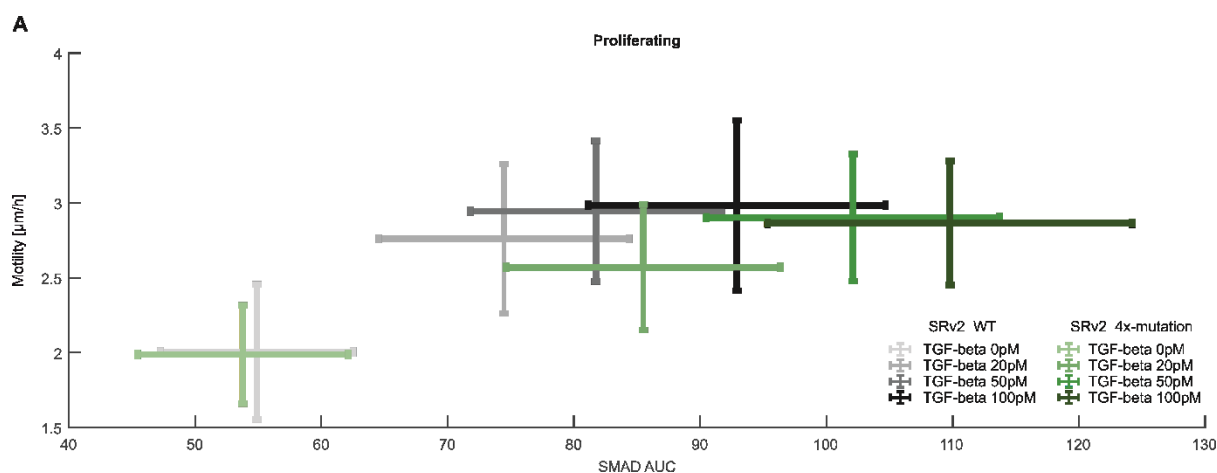


Figure 12 SMAD2 Linker Region Does Not Alter Cell Mobility Upon TGF-beta Stimulation.

(A) Correlation between median cell motility fraction and mean integrated nuclear-to-cytoplasmic SMAD2 ratio (area under the curve, AUC) in SRv2 WT (grey) and SRv2 4x-mutation (green) cells following stimulation with varying concentrations of TGF-beta over 48 hours. Error bars depict the standard deviation across the cell population (x-axis) and fields of view (y-axis). This analysis highlights the relationship between SMAD2 signaling dynamics and cell motility in response to different TGF-beta concentrations.

Despite observing increased SMAD2 nuclear accumulation due to loss of the SMAD2 linker region independent of cellular state, I investigated whether this alteration correlates with cell fate decisions, particularly focusing on cell motility. I treated cells carrying SMAD2 4x-mutation with varying doses of TGF-beta and monitored cell motility over 48 hours while quantifying SMAD2 AUC across all conditions (Figure 12A). Interestingly, although mutant line exhibited higher SMAD2 AUC, they did not show a corresponding increase in motility compared to SMAD2 WT cells. These results suggest that while the SMAD2 linker region plays a role in regulating SMAD2 dynamics, mutations in this region do not fundamentally alter SMAD2-induced cell fate decisions, such as epithelial-mesenchymal transition (EMT).

2.1.3 Loss of SMAD3 Enhances GDF11-Regulated SMAD2 response in Proliferating Cells.

Since the SMAD2 linker region loss cell line did not support the hypothesis of it being a key point of crosstalk leading to pathway rewriting, I redirected my focus to other potential factors within the SMAD pathway. Given that SMAD is primarily activated through receptor activation, I investigated whether changes in cell state influence receptor levels. I assessed the expression of type I and type II receptors for GDF11 and TGF-beta, crucial for pathway activation and potentially limiting SMAD activation. Our previous RNA-seq data indicated that cell state switches did not affect the expression of type I receptors ALK4 and ALK5 (Figure 13A). EGF treatment of quiescent cells did not alter ALK4 expression but slightly reduced ALK5 expression, suggesting that type I receptors may not significantly contribute to pathway rewriting. Turning to type II receptors, ACVR2A, a GDF11 type II receptor,

showed no notable expression changes across different conditions. Interestingly, ACVR2B, the other GDF11 type II receptor, was upregulated in quiescent cells but downregulated upon EGF treatment. However, given its lower RPKM values and similar binding affinities for GDF11, ACVR2A appears to be the primary GDF11 type II receptor in MCF10A cells. Thus, the GDF11 receptor does not significantly change with EGF or cell state switch, suggesting that other factors may modulate pathway response. In contrast, the TGF-beta type II receptor TGFBR2 was downregulated in quiescent cells but upregulated with EGF stimulation. This indicates that increased TGFBR2 expression in proliferating cells may enhance SMAD2 sensitivity to TGF-beta, contributing to the observed high SMAD2 activity.

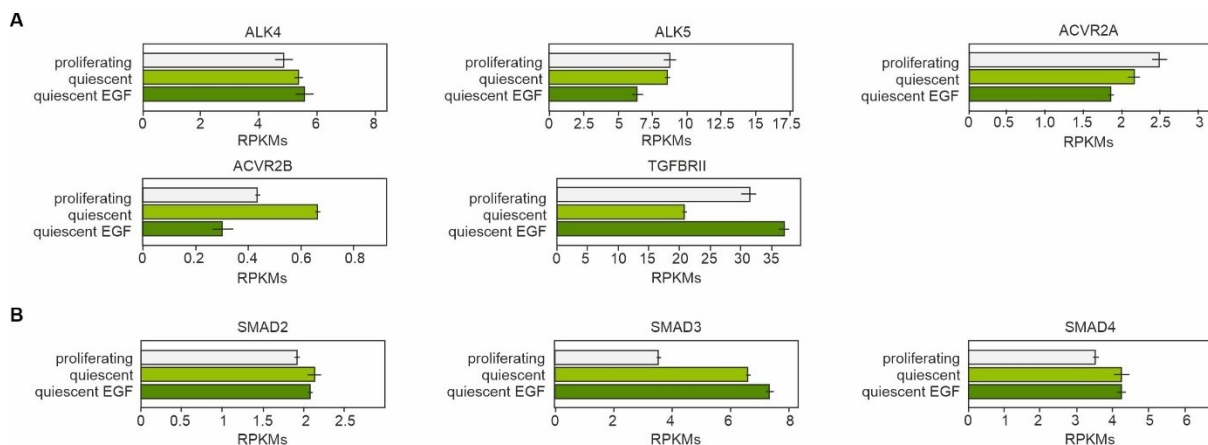


Figure 13 Gene Expression Analysis Identifies Receptors and SMADs in TGF-beta Pathway.

The analysis was conducted collaboratively with Lorenz Ripka from the University of Stuttgart. RNA-seq data was normalized using RPKM (Reads Per Kilobase Million). **(A)** Schematic depicting TGF-beta receptor gene expression levels (RPKM) in MCF10A wildtype cells under proliferating conditions, quiescent conditions, and EGF-stimulated quiescent conditions. **(B)** SMADs gene expression levels (RPKM) under the same cellular conditions as shown in (A).

Beyond receptors, SMAD proteins themselves likely play a role in pathway rewriting. As critical transcription factors, SMADs regulate target genes that profoundly influence pathway responses (Hill, 2016). In my assessment of SMAD protein expression within the TGF-beta pathway, I observed that SMAD2 and the co-SMAD SMAD4 remained unchanged with variations in cell state or EGF treatment (Figure 13B). SMAD3, another pivotal transcription factor in the TGF-beta pathway, exhibited upregulation in quiescent cells. However, despite expectations, RNA-seq results did not reveal EGF-induced downregulation of SMAD3 expression. Previous studies indicate that SMAD3 is notably active, predominantly localized in the nucleus even without TGF-beta signaling activation or SMAD4 binding (L. Liu et al., 2016). The elevated expression and distinct localization of SMAD3 in quiescent cells compared to SMAD2 suggest potential alterations in target gene regulation within the TGF-beta pathway. Moreover, while the SMAD2 linker region loss did not rewrite the cellular response, the possibility that SMAD3's activated linker region may be regulated by growth factors and ultimately

alter SMAD2 dynamics warrants consideration. These observations imply that SMAD3's activity could potentially rewrite pathway responses, emphasizing the need for further detailed investigation into its role in different cellular contexts.

To investigate the role of SMAD3 in regulating SMAD2 dynamics, I generated a SMAD3 knockout (SMAD3 KO) cell line from SRV2 WT cells using the CRISPR/Cas9 system. As with the SMAD2 knockout approach, I designed a single guide RNA (sgRNA) targeting exon 6 of the SMAD3 gene and integrated a puromycin resistance selection cassette (Figure 14A) (see Method 4.1.3.). After confirming successful SMAD3 knockout in SRV2 WT cells through Western blot (Figure 14B) and qPCR analyses (Figure 14C), I investigated how the absence of SMAD3 specifically affects the initial peak of SMAD2 response to ligand stimulation across different cellular states (Figure 14D). In quiescent cells, SMAD3 knockout did not alter the SMAD2 response pattern: SMAD2 exhibited a robust initial peak upon GDF11 stimulation, whereas TGF-beta induced only a weak SMAD2 response. In contrast, in proliferating cells, the absence of SMAD3 resulted in an enhanced initial SMAD2 response to GDF11, reaching levels similar to those observed with TGF-beta. Additionally, I explored how SMAD3 removal influences the SMAD2 response compared to cells with intact SMAD3 activity (Figure 14E). Interestingly, SMAD3 knockout did not alter the TGF-beta-induced SMAD2 dynamics in either cellular state, providing further evidence that SMAD3 does not modulate the TGF-beta-induced SMAD2 response. Upon GDF11 treatment, in quiescent cells, SMAD3 knockout did not affect the peak of SMAD2 levels but increased SMAD2 activity at later response post-stimulation (Figure 14AF). In contrast, in proliferating cells treated with GDF11, SMAD3 knockout enhanced the SMAD2 response during both the initial and subsequent phases. These findings emphasize the specific role of SMAD3 in regulating GDF11-induced SMAD2 dynamics across different cellular states.

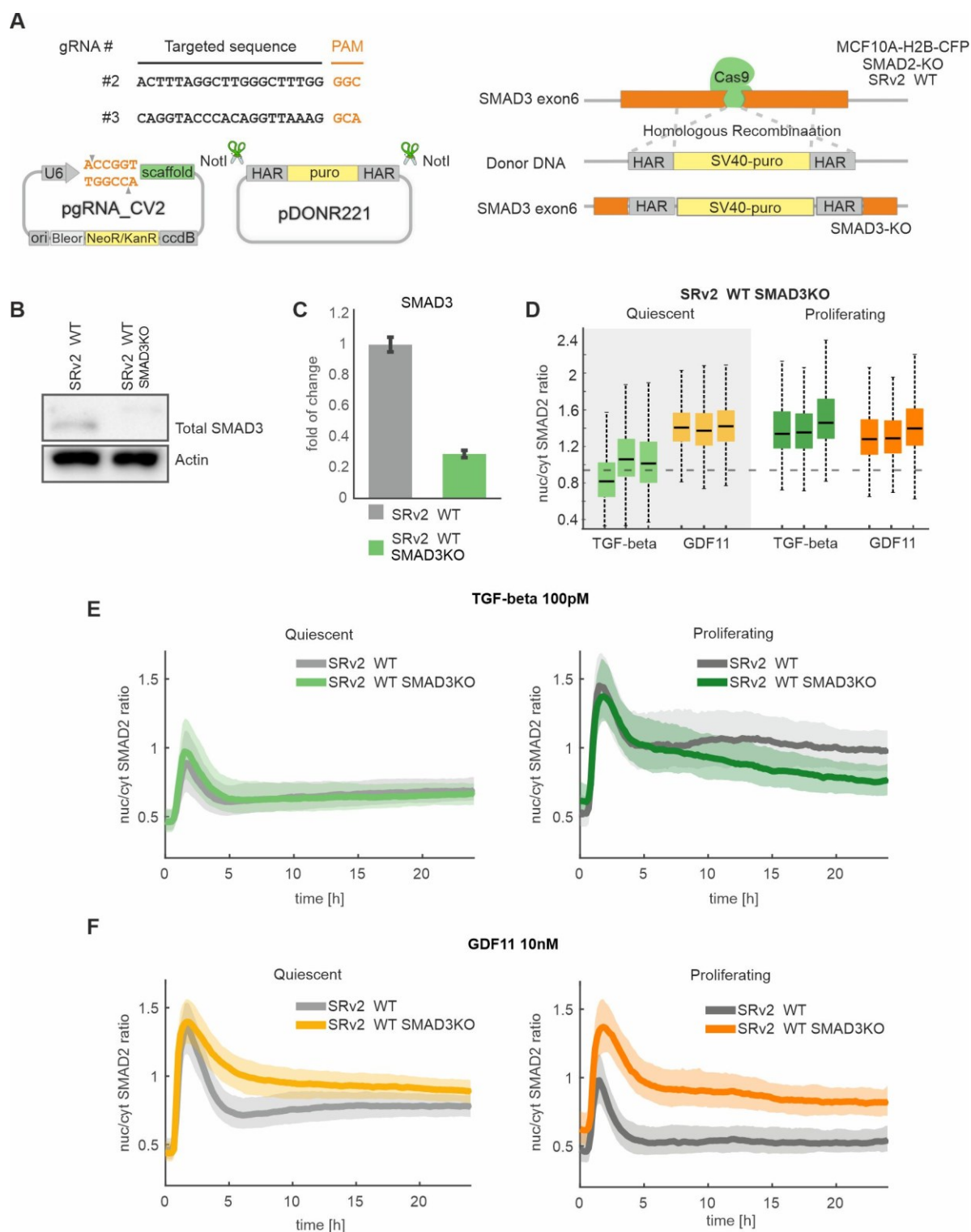


Figure 14 Loss of SMAD3 Enhances GDF11-Regulated SMAD2 response in Proliferating Cells.

(A) CRISPR/Cas9 knockout strategy for SMAD3. Left: sgRNA insertion into Cas9 vector using AgeI. Right: Generation of repair template by amplifying homology arms from MCF10A genomic DNA and SV40-puro, followed by assembly cloning. Linearized donor DNA and Cas9/sgRNA vectors were transfected into SRv2 WT cells for homology-directed repair. **(B)** Western blot analysis of selected SMAD3 knockout clones and SRv2 WT control cells, with actin as loading control. **(C)** RT-qPCR analysis comparing SMAD3 expression kinetics in SRv2 WT and SMAD3KO cells, normalized to beta-actin. Data show mean \pm SD of

technical triplicates. **(D)** Single-cell quantification of maximum nuclear-to-cytoplasmic SMAD2 ratio in SRv2 WT and SMAD3KO cells within 5 h after stimulation with 100 pM TGF-beta (green) or 10 nM GDF11 (orange) in quiescent and proliferating cells. Each bar represents one repeat experiment; boxes indicate data between 25th and 75th percentiles, with median (black line). Dashed lines serve as guides to the eye. **(E)** Nuclear-to-cytoplasmic SMAD2 ratio upon stimulation with 100 pM TGF-beta in quiescent cells (left) and proliferating cells (right) of SRv2 WT (grey) and SMAD3KO (green) cells. Solid lines depict median ratios; shaded areas represent 25th to 75th percentiles. **(F)** Nuclear-to-cytoplasmic SMAD2 ratio upon stimulation with 10 nM GDF11 in quiescent cells (left) and proliferating cells (right) of SRv2 WT (grey) and SMAD3KO (orange) cells. Solid lines indicate median ratios; shaded areas represent 25th to 75th percentiles.

After assessing that SMAD3 influences GDF11-induced SMAD2 responses, I proceeded to investigate whether this effect is specific to GDF11 or extends to other ligands within the TGF-beta superfamily. I treated SRv2 WT SMAD3KO cells with various ligands under both quiescent and proliferating states (Figure 15A). Interestingly, upon SMAD3 knockout, I observed consistent SMAD2 responses to Activin A and GDF3 across both cell states. This aligns with previous experiments using the SMAD2-R, suggesting that the presence or absence of SMAD3 does not alter SMAD2 responses to these ligands. Furthermore, GDF8 induced a similar SMAD2 response pattern as GDF11 following SMAD3 loss, enhancing SMAD2 responses in proliferating cells over both short and long periods. This consistent pattern indicates that SMAD3 specifically mediates SMAD2 nuclear translocation responses to GDF11 and GDF8, but not to other ligands.

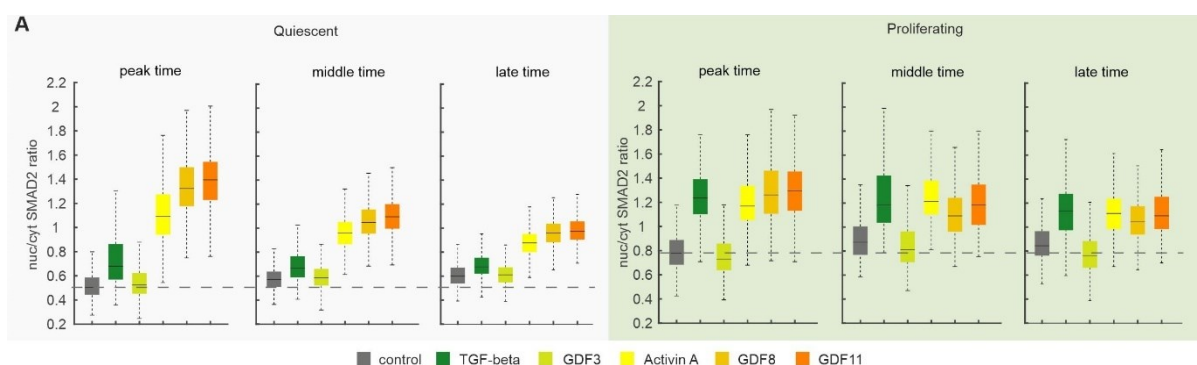


Figure 15 SMAD2 Nuclear Translocation in SMAD3KO Cells in Response to TGF-beta Superfamily Ligands.

(A) Single-cell quantification of maximum nuclear-to-cytoplasmic SMAD2 ratio in SRv2 WT SMAD3KO cells under quiescent (left) and proliferating (right) conditions following stimulation with different TGF-beta superfamily ligands. TGF-beta was administered at 100 pM, GDF11 at 10 nM, and other ligands at saturating concentrations of 20 nM. Each boxplot represents data between the 25th and 75th percentiles of the cell population.

Next, I revisited the question of whether SMAD2 nuclear accumulation still correlates with cell fate decisions after the loss of SMAD3, particularly upon GDF11 stimulation. Thus, I monitored SMAD3 removal cells (SRv2 WT SMAD3KO) under ligand stimulation over a 72-hour period in both quiescent and proliferating states, comparing them to SRv2 WT cells. Initially, consistent with previous experiments, both TGF-beta and GDF11 induced similar early SMAD2 responses regardless of SMAD3

presence in quiescent cells. However, upon SMAD3 knockout, GDF11 induced a significantly stronger secondary SMAD2 response (Figure 16A). Importantly, SMAD3 removal did not induce cell apoptosis on its own. Interestingly, the loss of SMAD3 partially rescued apoptosis induced by both ligands. Under TGF-beta stimulation, SMAD3 knockout nearly completely inhibited apoptosis, whereas GDF11, which promoted strong SMAD2 translocation, still induced cell death in the absence of SMAD3 (Figure 16B). These results suggest that SMAD3 knockout can partially rescue cells from apoptosis. Moreover, SMAD2, acting as a transcription factor, can independently regulate apoptosis-related gene expression, influencing cell fate decisions in the absence of SMAD3, particularly under potent stimuli like GDF11.

Furthermore, in proliferating cells where I assessed cell motility, I found that SMAD3 knockout reduced baseline motility compared to SRV2 WT cells, even without ligand stimulation (Figure 16C). Interestingly, treatments with ligands did not significantly enhance motility in SMAD3 knockout cells, contrasting with the observed enhancement in cells with intact SMAD3 (Figure 16D). Upon closer examination at the single-cell level, I observed that high SMAD AUC did not correlate with increased motility (Figure 16E). These results indicate that SMAD2 alone does not drive EMT-related gene expression or influence cell motility in the absence of SMAD3. This suggests that SMAD3 plays a critical role in regulating cell motility and EMT-related gene expression, and its absence cannot be compensated for by SMAD2.

In conclusion, these findings highlight distinct roles for SMAD2 and SMAD3 in cell fate regulation. SMAD2 can influence apoptosis-related gene expression and cell fate independently, but its impact is diminished without SMAD3. In contrast, SMAD3 is essential for regulating EMT-related gene expression and cell motility, playing a primary role in these processes.

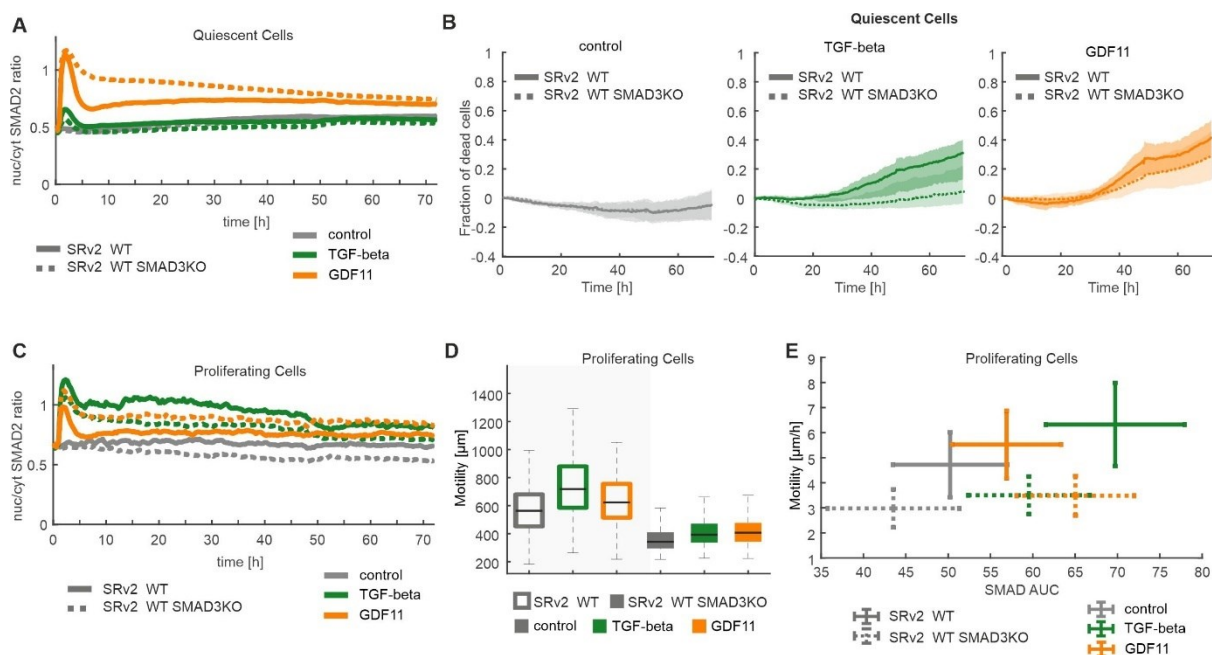


Figure 16 Loss of SMAD3 Alters Cell Phenotype Response Upon Ligand Stimulation.

(A) Median nuclear-to-cytoplasmic SMAD2 ratio in quiescent SRv2 WT SMAD3KO cells treated with TGF-beta (250 pM) or GDF11 (10 nM) over 72 h. Images are taken 0.5 h before ligand stimulation and ligands were refreshed every 48 h. **(B)** Fraction of dead cells over time from the experiment described in (A), showing bold lines for median fraction per field of view and shaded areas indicating standard deviation (SD). **(C)** Median nuclear-to-cytoplasmic SMAD2 ratio in proliferating SRv2 WT SMAD3KO cells treated with TGF-beta (250 pM) or GDF11 (10 nM) over 72 h, with images taken 0.5 h before ligand stimulation and media refreshed every 48 h. **(D)** Cell motility in proliferating SRv2 WT SMAD3KO cells treated as in (C), represented by boxplots showing distance moved per cell. Cell motility was measured in pixels and converted to micrometers using a conversion factor of 1 pixel = 0.361 μm (derived from dividing 1 by 2.77). **(E)** Correlation between median cell mobility fraction and mean integrated nuclear-to-cytoplasmic SMAD2 ratio (area under the curve, AUC; hours) in SRv2 WT and SRv2 WT SMAD3KO cells following stimulation with TGF-beta and GDF11 over 72 h, with error bars indicating SD across the cell population (x-axis) and fields of view (y-axis).

After understanding how SMAD3 regulates the GDF11-induced SMAD2 response and its impact on cell fate decisions as a transcription factor, I investigated whether mutating the SMAD2 linker region alone affects SMAD2 responses to ligands, especially TGF-beta, when SMAD3 is absent. My previous experiments indicated that the TGF-beta-regulated SMAD2 response is modified by EGF, possibly through the linker region. Loss of the SMAD2 linker region did not change the TGF-beta-induced SMAD2 response in either cell state. This suggests that the intact SMAD3 linker region may influence this response, potentially through the MAPK pathway, which regulates SMAD3 and could also impact SMAD2 responses. To test if removing SMAD3 changes the SMAD2 response to TGF-beta, I used CRISPR/Cas9 to generate an SRv2 4x-mutation SMAD3KO cell line, confirmed by Western blot analysis (Figure 17A). Subsequently, I stimulated these cells with TGF-beta and, for comparison, GDF11 under quiescent and proliferating conditions. In quiescent cells lacking SMAD3, the SRv2 4x-

mutation response to GDF11 remained unchanged. Similarly, its response to TGF-beta was unaffected after the loss of SMAD3 (Figure 17B). In proliferating cells without SMAD3, the SMAD2 response to TGF-beta remained unaltered, while the response to GDF11 was significantly amplified, mirroring the results observed in the SRv2 WT SMAD3KO cells (Figure 17C). This pattern suggests a consistent regulatory effect of SMAD2 linker region mutations on SMAD2 nuclear accumulation, even in the absence of SMAD3. These findings underscore that mutations in the SMAD2 linker region modulate SMAD2 responses by inhibiting nuclear accumulation, a regulatory mechanism that persists independently of SMAD3. This highlights the robustness and autonomy of linker region mutations in influencing SMAD2 dynamics across different cellular contexts and ligand stimulations.

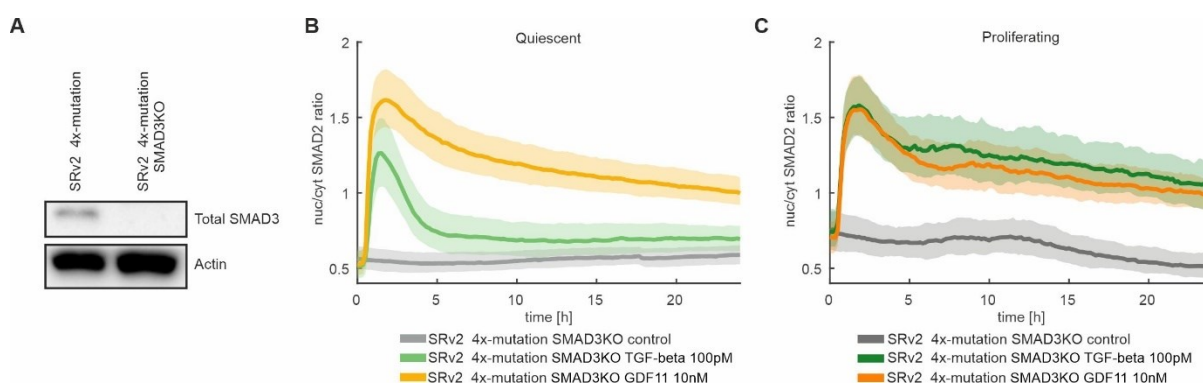


Figure 17 Loss of SMAD3 Does Not Alter SMAD2 response in Cells Lacking the SMAD2 Linker Region Upon Ligand Stimulation.

(A) Western blot analysis of selected SRv2 4x-mutation SMAD3KO clones and SRv2 4x-mutation control cells, with Actin as the loading control. (B) Nuclear-to-cytoplasmic SMAD2 ratio in quiescent SRv2 4x-mutation SMAD3KO cells treated with 100 pM TGF-beta (green) or 10 nM GDF11 (orange) over 72 h. Ligands were added 0.5 h after the beginning of the experiment, with unstimulated conditions shown in grey. Median ratios are represented by solid lines, and shaded areas indicate the 25th to 75th percentiles. (C) Nuclear-to-cytoplasmic SMAD2 ratio in proliferating SRv2 4x-mutation SMAD3KO cells following stimulation with 100 pM TGF-beta (green) or 10 nM GDF11 (orange) over 72 h. Ligands were added 0.5 h after the beginning of the experiment, with unstimulated conditions depicted in grey. Solid lines denote median ratios, and shaded areas show the 25th to 75th percentiles.

2.1.4 Reconstituted SMAD3 Reduced the SMAD2 Dynamic.

Building on previous findings that SMAD3 is crucial for regulating the SMAD2 response to GDF8 and GDF11, I reintroduced SMAD3 into SRv2 WT SMAD3KO cells to test if it would reduce the SMAD2 response to GDF11 in proliferating cells. Using the Gateway cloning method, I constructed an mCherry-SMAD3 plasmid under the UbCp with Zeocin selection (For details, see Method 4.1.5.). Following lentiviral transduction into SRv2 WT SMAD3KO cells and subsequent clonal selection (Figure 18A), Western blot results confirmed that clone #3 (named SRv2 WT SMAD3 R) successfully expressed mCherry-SMAD3, allowing it to be utilized in subsequent experiments (Figure 18B).

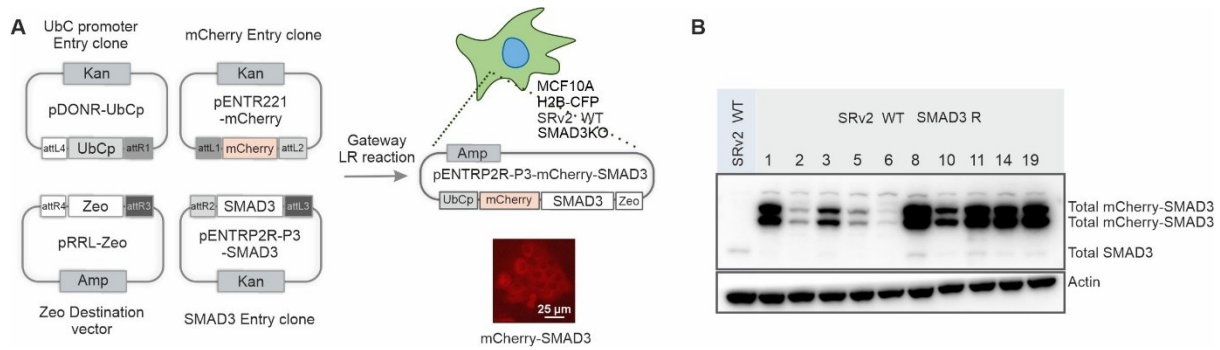


Figure 18 Generation and Validation of mCherry-SMAD3 Double Reporter Clones.

(A) Schematic depiction of the mCherry-SMAD3 plasmid construction using MultiSite Gateway LR Recombination Reaction. The construct incorporates a UbCp and Zeocin selection marker. Following lentiviral transduction into SRv2 WT SMAD3KO cells, double reporter clones were chosen based on Zeocin resistance. **(B)** Assessment through Western blot of various mCherry-SMAD3 clones and SRv2 WT control cells, with Actin used as a loading control.

First, to validate the functionality of the double reporter clone in reflecting SMAD3 activation dynamics, I treated these cells with TGF- β . Upon treating proliferating cells with TGF- β , I observed similar dynamics of SMAD2 and SMAD3 at the population level (Figure 19A), confirming the fidelity of the double reporter cells in reflecting SMAD3 activation. To explore whether the SMAD3 response mirrors the ALK5-mediated pathway observed in SMAD2, I conducted experiments where cells were treated with an ALK5 inhibitor before and after TGF- β stimulation at various time points (Figure 19B). These investigations revealed that both SMAD2 and SMAD3 responses were entirely dependent on receptor activity across all tested time points. Additionally, dose-titration experiments with TGF- β demonstrated that both SMAD2 and SMAD3 exhibited comparable dose-dependent responses in both quiescent and proliferating cell states (Figure 19C). Notably, in proliferating cells, SMAD3 displayed a distinct late-phase response at higher ligand concentrations (>25 pM), which differed from SMAD2 dynamics. This suggests potential cross-talk with other signaling pathways, indicating that while SMAD2 and SMAD3 share similar initial activation mechanisms, SMAD3 may engage additional regulatory pathways during prolonged or intense stimulation.

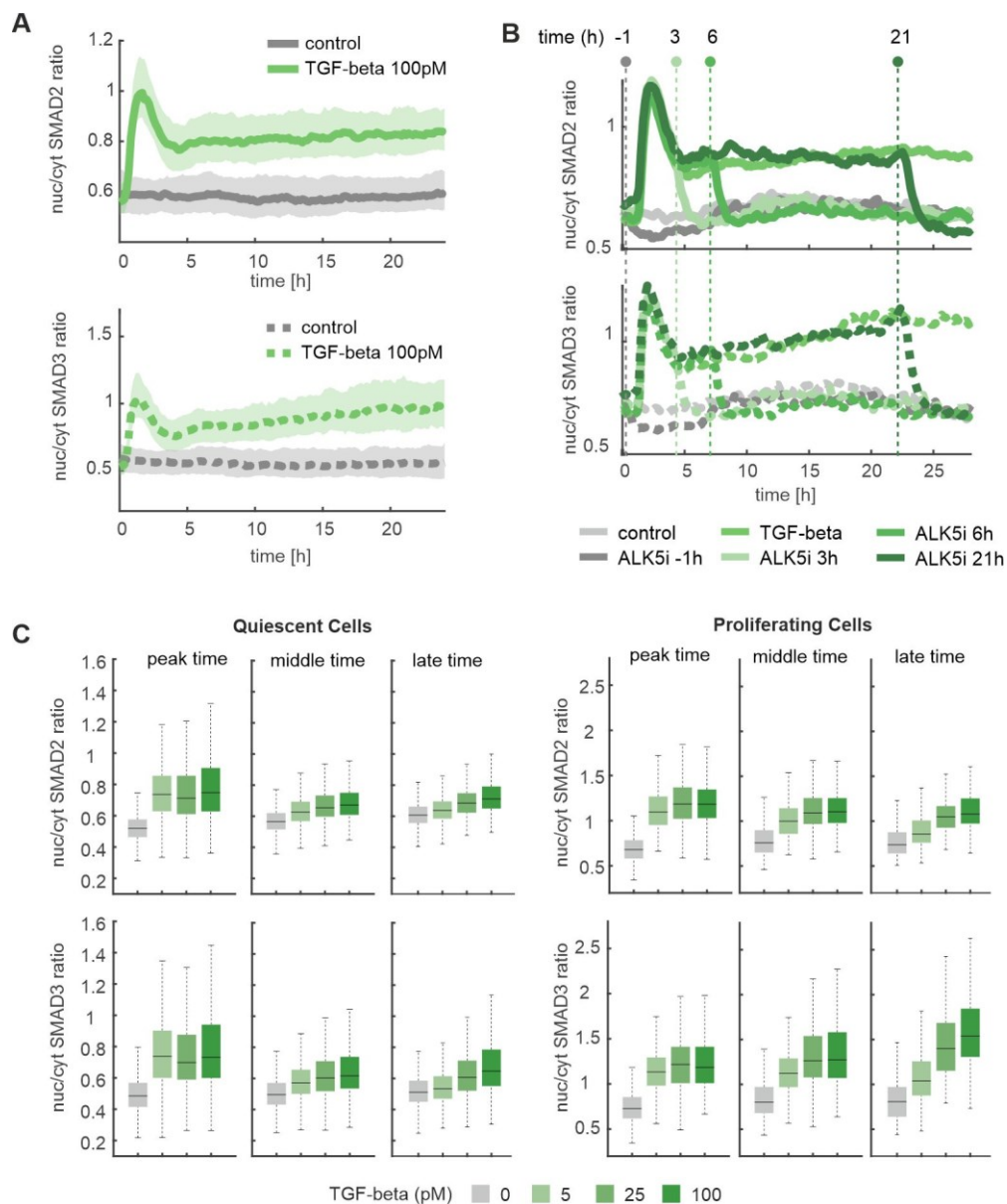


Figure 19 SMAD2 and SMAD3 Dynamics in Double Reporter Clones in Response to TGF-beta.

(A) Median nuclear-to-cytoplasmic ratios of SMAD2 (top) and SMAD3 (bottom) upon stimulation with 100 pM TGF-beta (green) in proliferating SRv2 WT SMAD3 R cells. Cells were treated with TGF-beta 0.5 h after the start of the experiment or left unstimulated (grey). Solid lines represent median ratios, and shaded areas indicate the 25th to 75th percentiles. **(B)** Nuclear-to-cytoplasmic ratios of SMAD2 (top) and SMAD3 (bottom) illustrating ALK5 inhibitor efficacy at different time points relative to TGF-beta induction in proliferating cells. Cells were treated with 10 μ M ALK5 inhibitor at indicated time points (1 h before or 3 h, 6 h, 21 h post 100 pM TGF-beta stimulation), with DMSO serving as control. **(C)** Single-cell quantification of maximum nuclear-to-cytoplasmic ratios of SMAD2 (top) and SMAD3 (bottom) in quiescent (left) and proliferating (right) SRv2 WT SMAD3 R cells treated with varying doses of TGF-beta. Boxes represent data between the 25th and 75th percentiles of the cell population.

After confirming that the double reporter cells effectively reflected SMAD pathway activation upon TGF-beta stimulation, I refocused on my primary question: could reconstituted SMAD3 alter pathway

dynamics? Upon stimulating cells with GDF11, I observed a significant reduction in the SMAD2 response in proliferating cells reintroduced with SMAD3 compared to SMAD3KO cells (Figure 20A). This finding supports the hypothesis that SMAD3 mediates the downregulation of the SMAD2 response to GDF11, highlighting its pivotal role as a regulator in this context. Interestingly, I also noted that reconstituted SMAD3 similarly attenuated the GDF11-mediated SMAD2 response in quiescent cells (Figure 20B). This observation underscores the broader regulatory influence of SMAD3 across different cellular states.

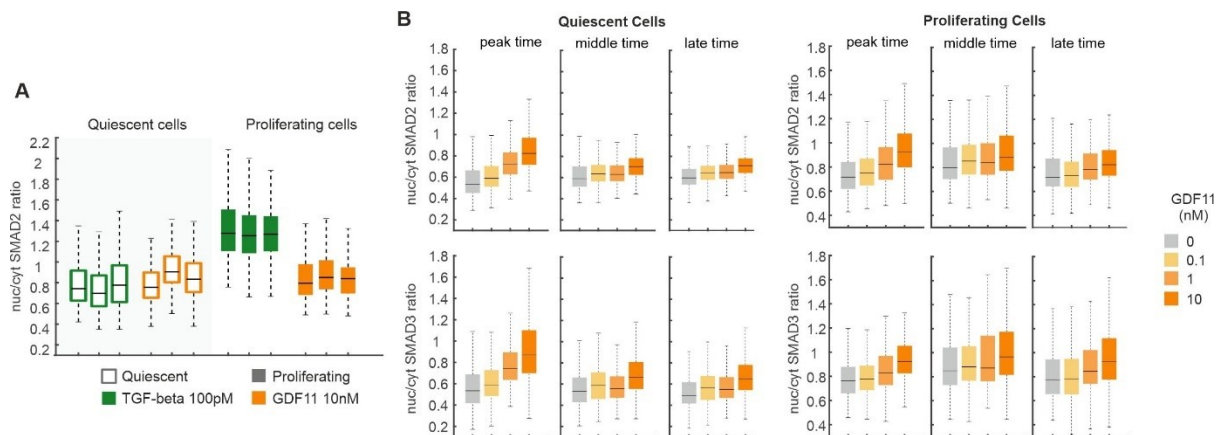


Figure 20 SMAD2 and SMAD3 Dynamics in Double Reporter Clones in Response to GDF11.

(A) Single-cell quantification of maximum nuclear-to-cytoplasmic SMAD2 ratio in SRv2 WT SMAD3 R cells within 5 h after stimulation with 100 pM TGF-beta (green) or 10 nM GDF11 (orange) in quiescent and proliferating conditions. Each bar represents one repeat experiment. Boxes show data between 25th and 75th percentiles. **(B)** Single-cell quantification of maximum nuclear-to-cytoplasmic ratios of SMAD2 (top) and SMAD3 (bottom) in proliferating (left) and quiescent (right) SRv2 WT SMAD3 R cells treated with varying doses of GDF11. Boxes represent data between 25th and 75th percentiles of the cell population.

These results prompted me to investigate whether the reduction in the SMAD2 response was influenced by the concentration of GDF11 or the elevated expression level of SMAD3 in the clone compared to wild-type levels. To address this, first, I stimulated cells with various concentrations of GDF11 and monitored both SMAD2 and SMAD3 responses in a dose-dependent manner. Upon all tested concentrations, I consistently observed lower SMAD2 translocation in the double reporter cell clone (Figure 20B).

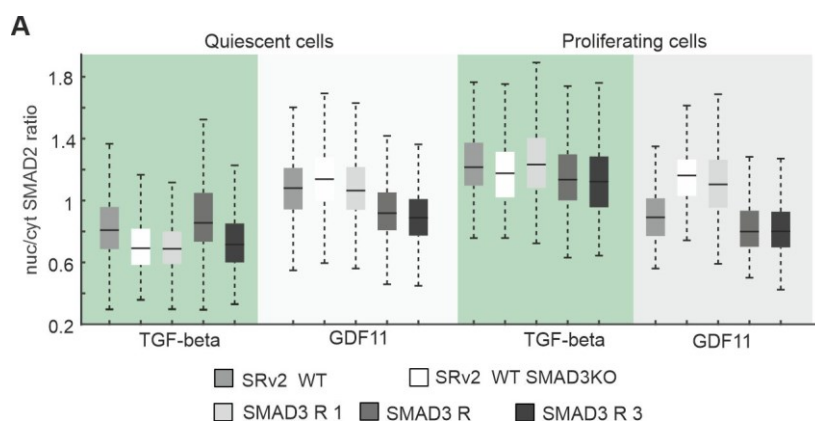


Figure 21 SMAD3 Regulates GDF11-Mediated SMAD2 Dynamics in a Dose-Dependent Manner.

(A) Single-cell quantification of maximum nuclear-to-cytoplasmic SMAD2 ratio in SRv2 WT, SRv2 WT SMAD3KO, SRv2 WT SMAD3 R1, SRv2 WT SMAD3 R, and SRv2 WT SMAD3 R3 cells within 5 h after stimulation with 100 pM TGF-beta (green) or 10 nM GDF11 (grey) in quiescent (left) and proliferating (right) conditions. Each bar represents one repeat experiment. Boxes show data between the 25th and 75th percentiles of the cell population.

To further investigate whether the observed reduction in the SMAD2 response to GDF11 was influenced by elevated SMAD3 expression levels, I tested additional clones expressing varying amounts of SMAD3 (#5 as SMAD3 R1, #3 as SMAD3 R, #10 as SMAD3 R3). Consistently, higher levels of SMAD3 expression correlated with a diminished SMAD2 response to GDF11 stimulation, while the effect was more pronounced in proliferating cells, it remained observable in quiescent cells (Figure 21A). In contrast, SMAD3 expression levels did not impact the TGF-beta-induced SMAD2 response in either cell state. This specificity underscores that SMAD3 specifically regulates the GDF11-induced SMAD2 response in a dose-dependent manner.

After observing that SMAD3 reconstitution reduced the SMAD2 response to GDF11, I proceeded to examine its influence on SMAD2 responses induced by other ligands. As expected, SMAD3 reconstitution specifically diminished the SMAD2 response to GDF8 and GDF11, consistent with our previous findings from SMAD3 knockout experiments (Figure 22A). In contrast, ligands such as Activin A and GDF3 did not alter SMAD2 responses upon SMAD3 reconstitution. Furthermore, the results indicated that all ligands induced similar SMAD2 and SMAD3 responses regardless of the cell state.

These findings offer deeper insights into the intricate regulatory mechanisms within the TGF-beta superfamily signaling pathways, emphasizing how SMAD3 selectively modulates cellular responses to ligands.

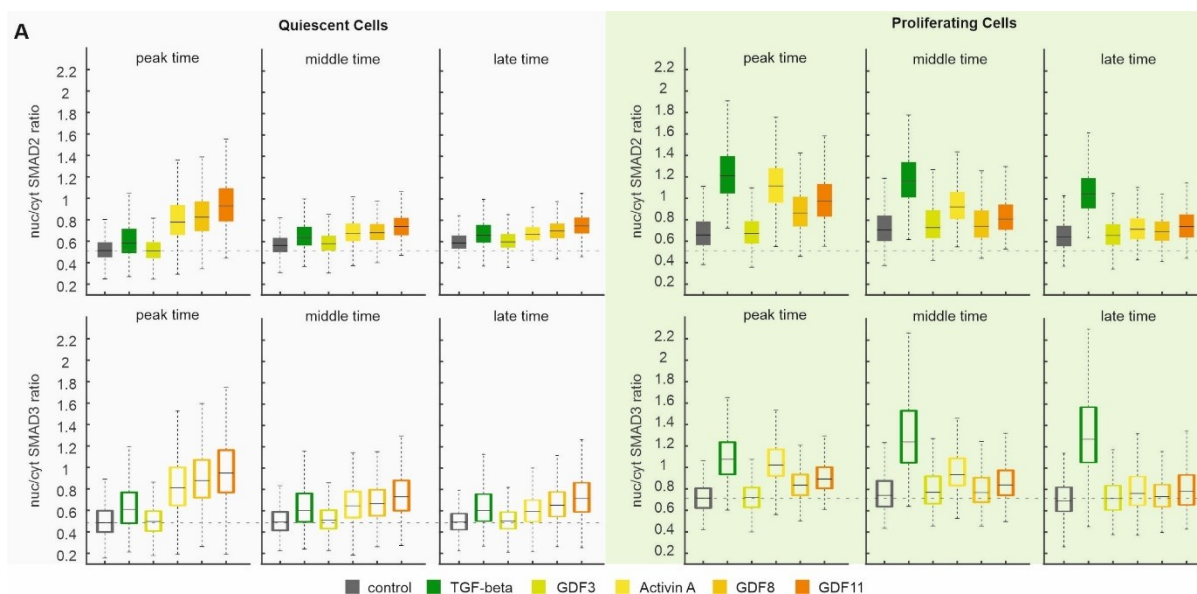


Figure 22 SMAD2 and SMAD3 Responses to TGF-beta Superfamily Ligands.

(A) Single-cell quantification of maximum nuclear-to-cytoplasmic ratios of SMAD2 (top) and SMAD3 (bottom) in quiescent (left) and proliferating (right) SRv2 WT SMAD3 R cells stimulated with different TGF-beta superfamily ligands. TGF-beta was applied at 100 pM, GDF11 at 10 nM, and other ligands at saturating concentrations of 20 nM. Boxes represent data between the 25th and 75th percentiles of the cell population. Dashed lines serve as guides to the eye.

2.1.5 Mechanisms of SMAD2/3 Pathway Modulation.

Based on my previous findings, I aimed to delve deeper into understanding the SMAD3-regulated, GDF11-mediated SMAD2 response by exploring two fundamental questions: the dependency of this regulation on the ALK5 receptor, and the downstream genes regulated by SMAD3 that reshape this pathway.

Given that the SRv2 4x-mutation SMAD3KO data suggested that the SMAD2 linker region is not crucial for regulating the SMAD2 response to various stimuli, I shifted my focus to investigating the C-terminal region of SMADs. The ALK5-TGFBR2 complex phosphorylates SMADs at this region, prompting my investigation into SMAD3's role in mediating the GDF11-induced SMAD2 response and its reliance on ALK5.

Initially, I employed Western blot analysis to assess phosphorylated SMAD3 (p-SMAD3) levels under various conditions, including treatment with an ALK5 inhibitor and presence or absence of EGF, across quiescent and proliferating cell states in MCF10A cell line (Figure 23A). Notably, p-SMAD3 levels were lower in quiescent cells compared to proliferating cells. Moreover, administration of EGF restored p-SMAD3 levels in quiescent cells, whereas inhibition of the EGF receptor reduced p-SMAD3 in proliferating cells (Figure 23A). These findings suggest an interaction between EGF signaling and SMAD3 activation, influencing its phosphorylation status under different cellular growth conditions.

Subsequent inhibition of ALK5 resulted in the absence of p-SMAD3 in proliferating cells, highlighting that SMAD3 activation in MCF10A cells is indeed dependent on ALK5.

To further investigate the dependency of SMAD3 activation on the ALK5 receptor and its impact on downstream signaling, I designed a wash-off experiment to assess how altering SMAD3 phosphorylation affects the SMAD2 response network. Proliferating SRv2 WT cells were pre-treated with ALK5i for 8 hours, followed by washing off the inhibitor (Figure 23B). Subsequently, the cells were stimulated immediately with GDF11 or TGF-beta. Remarkably, ALK5 inhibition significantly reduced SMAD3 activation, which led to an enhanced SMAD2 response specifically to GDF11 in proliferating cells (Figure 23C, D). In contrast, TGF-beta induced consistent SMAD2 responses regardless of SMAD3's activation status, confirming its independence from SMAD3 regulation. To confirm these observations, I used the SMAD2-R cell line to ensure consistency and conducted the same wash-off experiment with SMAD2-R cells. As illustrated in Figure 23E and F, the results were analogous to those observed in SRv2 WT cells. Although there is a slight increase in the SMAD2 response induced by TGF-beta after washing off the ALK5 inhibitor, GDF11 still induces a stronger amplification after the inhibitor wash-off. This may be due to differences in the behavior of individual cells, leading to the observed slight increase upon the TGF-beta stimulation. Using the double reporter system further validated that modulation of the ALK5-SMAD3 pathway influenced both SMAD2 and SMAD3 dynamics (Figure 23G, H). In summary, these findings collectively underscore that SMAD3 activation is predominantly receptor-dependent and plays a crucial role in regulating SMAD2 dynamics specifically in response to GDF11.

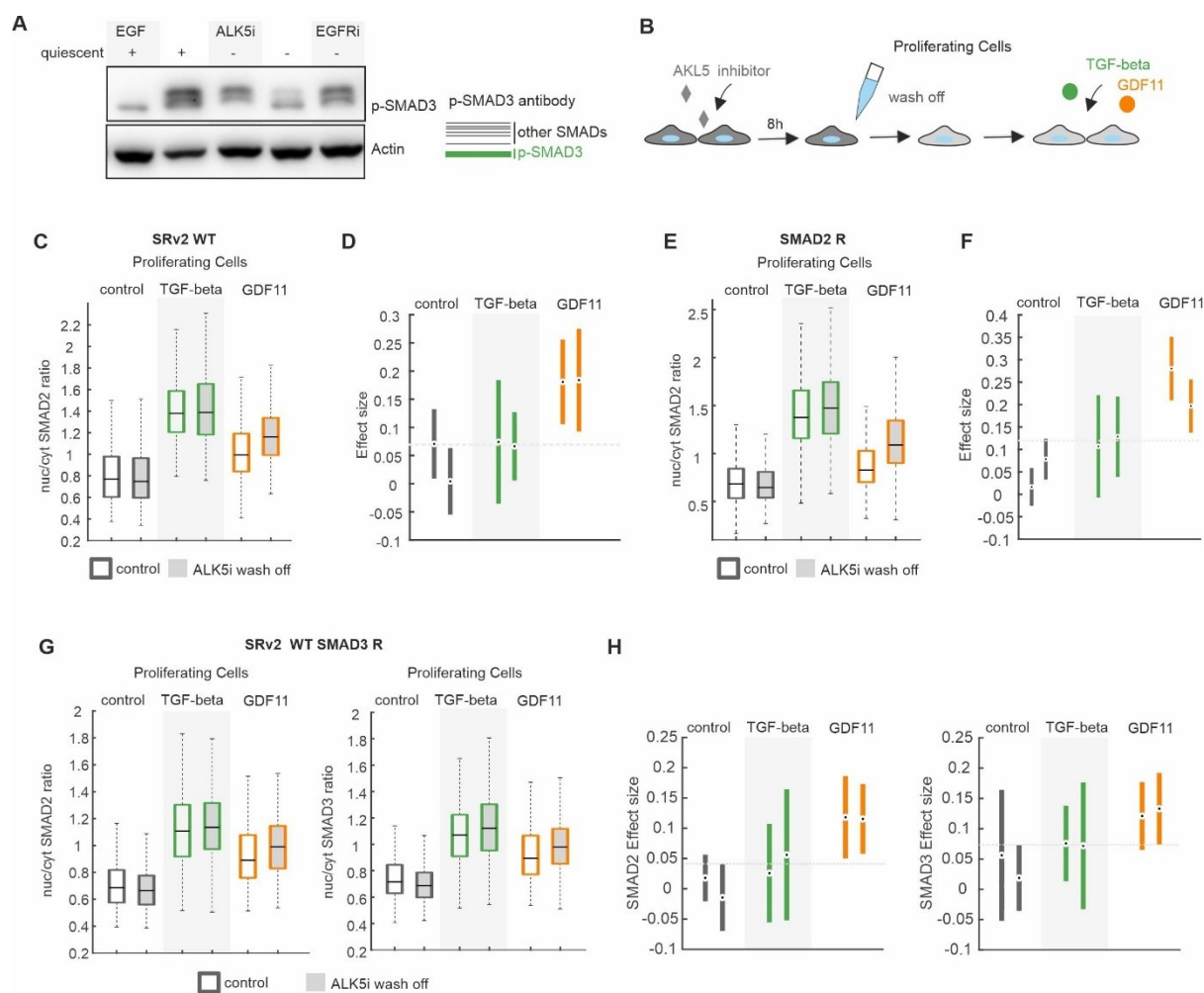


Figure 23 SMAD3 Regulates GDF11-Mediated SMAD2 response via ALK5.

(A) Western blot analysis of SMAD3 phosphorylation in MCF10A wildtype cells. Cells were treated with EGF (50 ng/ml), ALK5 inhibitor (10 μ M), or EGFR inhibitor (10 μ M) as indicated. The figure shows the phosphorylation status of SMAD3, with Actin serving as the loading control. Specifically, the lower band corresponds to phosphorylated SMAD3, and the upper band corresponds to phosphorylated SMAD1/5/9. For confirmation of band identities, see Figure 36A. **(B)** Schematic representation of the ALK5 inhibitor wash-off experiment procedure. **(C)** Single-cell quantification of maximum nuclear-to-cytoplasmic SMAD2 ratio in proliferating SRv2 WT cells within 5 h after stimulation with 100 pM TGF-beta (green) or 10 nM GDF11 (orange). ALK5 inhibitor wash-off condition is indicated in grey, with DMSO wash-off serving as the control. Boxes represent data between the 25th and 75th percentiles of the cell population. Each box represents a single repeat experiment. **(D)** Effect size intervals are depicted for two replicate experiments described in (C). Confidence intervals were estimated using permutation testing (1,000 permutations), comparing the washed-off condition to the unwashed control condition with the same ligand stimulation. Dashed lines serve as guides to the eye. **(E)** Single-cell quantification of maximum nuclear-to-cytoplasmic SMAD2 ratio in proliferating SMAD2-R cells within 5 h after stimulation with 100 pM TGF-beta (green) or 10 nM GDF11 (orange). ALK5 inhibitor wash-off condition is indicated in grey, with DMSO wash-off serving as the control. Boxes represent data between the 25th and 75th percentiles of the cell population. Each box represents a single repeat experiment. **(F)** Effect size intervals are depicted for two replicate experiments described in (E). Confidence intervals were estimated using permutation testing (1,000 permutations), comparing the washed-off condition to the unwashed control condition with the same ligand stimulation. Dashed lines serve as guides to the eye. **(G)** Single-cell quantification of maximum nuclear-

to-cytoplasmic ratios of SMAD2 (left) and SMAD3 (right) in proliferating SRv2 WT SMAD3 R cells within 5 h after stimulation with 100 pM TGF-beta (green) or 10 nM GDF11 (orange). ALK5 inhibitor wash-off condition is indicated in grey, with DMSO wash-off serving as the control. Boxes represent data between the 25th and 75th percentiles of the cell population. Each box represents a single repeat experiment. **(H)** Effect size intervals are depicted for two replicate experiments described in (G). Confidence intervals were estimated using permutation testing (1,000 permutations), comparing the washed-off condition to the unwashed control condition with the same ligand stimulation. Dashed lines serve as guides to the eye.

After confirming that the upstream regulation is indeed ALK5-dependent, I proceeded to investigate my next research question using RNA-seq to identify key proteins involved in regulating this pathway. This approach aimed to pinpoint candidate genes that could modulate the GDF11-induced SMAD2 response mediated by SMAD3. To begin, I compared SRv2 WT SMAD3KO cells with SRv2 WT cells to delineate genes regulated by SMAD3 under basal conditions (Figure 24A). This comparison provided a foundational understanding of SMAD3's regulatory impact on gene expression. Next, I compared SRv2 WT cells treated with an ALK5 inhibitor to untreated SRv2 WT cells (Figure 24A). This comparison was essential to identify genes whose expression changes in response to ALK5 inhibition, implicating them in the ALK5-SMAD3 regulatory pathway. By analyzing overlaps between these two comparisons, I aimed to identify proteins potentially involved in mediating the regulatory effects of SMAD3 downstream of ALK5 activation.

After filtering for a significance threshold of $p < 0.05$ and selecting genes with a log₂ fold change greater than 1, I identified 995 genes that were upregulated and 836 genes that were downregulated in the comparison between SRv2 WT and SRv2 WT SMAD3KO cells (Figure 24A). In the ALK5 inhibitor-treated SRv2 WT cells, 595 genes were upregulated and 691 genes were downregulated. Further analysis revealed that 281 genes were upregulated and 449 genes were downregulated in both comparison groups (Figure 24A, Figure 37). The substantial number of identified genes highlights the integral role of the ALK5-SMAD3 pathway in transcriptional regulation. However, the presence of numerous genes that did not overlap the stringent filtering criteria suggests that not all gene expression changes are solely dependent on SMAD3. This indicates the potential for SMAD3-independent transcriptional regulation in certain genes. Moreover, it suggests that ALK5 may exert its influence on gene expression through pathways involving SMAD2 or other downstream transcription factors, further illustrating the complexity and interconnectedness of TGF-beta signaling cascades.

Next, I employed additional criteria to narrow down potential candidates for further investigation. Building on insights from the ALK5 inhibitor wash-off experiment, which showed an immediate increase in the SMAD2 response upon GDF11 stimulation, I focused on identifying membrane or secreted proteins from the gene list. Using the protein prediction tools available at Protein Atlas (<https://www.proteinatlas.org/>) and Compartments (<https://compartments.jensenlab.org/>), I found 27 membrane proteins and 15 secreted proteins among the upregulated genes, and 133 membrane proteins and 75 secreted proteins among the downregulated genes (Figure 24C, D). Given that Activin A utilizes

ALK2 and ALK4 as type I receptors and shares a type II receptor with GDF11, it suggests that the SMAD3-mediated regulation of GDF11-induced SMAD2 dynamics may involve factors beyond receptor activity, potentially including secreted proteins that modulate downstream signaling. I hypothesized that these secreted proteins could act as inhibitors of GDF11 and GDF8, influencing their signaling effects. Consequently, I selected two genes for further investigation: LTBP2 and MMP9. Additionally, considering membrane regulators that might block SMAD signaling, I identified PMEPA1 as a third candidate.



Figure 24 Global Gene Expression Analysis Identifies Potential Key Regulators of SMAD Signaling.

(A) Schematic representation of gene filtering strategy. Left: Comparison of SRv2 WT cells to SRv2 WT SMAD3KO cells ($p < 0.05$), identifying up- (orange) or downregulated (green) genes with fold change ≥ 1.0 . Right: Comparison of SRv2 WT cells to SRv2 WT cells treated with ALK5 inhibitor ($p < 0.05$), identifying up- or downregulated genes with fold change ≥ 1.0 . **(B)** Scaled Venn diagram showing the number of overlapping genes between the two comparison groups. **(C)** Schematic representation of protein localization (intracellular (yellow), membrane (orange), secreted (green), not available (grey)) in

upregulated (left) and downregulated (right) gene lists. **(D)** List of membrane and secreted proteins from upregulated gene sets. **(E)** List of membrane and secreted proteins from downregulated gene sets.

LTBP2, MMP9, and PMEPA1 play crucial roles in the TGF-beta signaling pathway, albeit having distinct mechanisms. LTBP2 (Latent Transforming Growth Factor Beta Binding Protein 2) is integral to the TGF-beta signaling pathway, influencing growth, differentiation, and extracellular matrix production (Robertson et al., 2015). It regulates GDF11 activation by controlling its cleavage, thereby reducing GDF11 signaling and the subsequent SMAD response (Sun et al., 2011). In contrast, PMEPA1 (also called TMEPAI, transmembrane prostate androgen-induced) inhibits the SMAD-mediated transcriptional responses triggered by GDF11 and other TGF-beta ligands by binding to SMAD proteins (Singha et al., 2014). This interaction sequesters SMADs, preventing their transmission of signals from activated TGF-beta receptors to the nucleus, thereby modulating cellular processes such as cell growth and differentiation. In addition, although matrix metalloproteinase (MMP) pathway cross-talk with the TGF-beta pathway, whether MMP9 cross talk with SMAD signaling remains less explored (Gordon et al., 2009). Its presence suggests potential feedback mechanisms that could affect overall SMAD signaling dynamics, influencing cellular responses in various contexts.

To investigate whether LTBP2, MMP9, and PMEPA1 can regulate the GDF11-induced SMAD2 response, I employed an approach inspired by Konermann (Konermann et al., 2015). Instead of using functional Cas9, I utilized a dead Cas9 (dCas9) fused to the transcription activation domain VP64 (Figure 25A) (see Method 4.1.6.). This complex was guided to the endogenous loci of LTBP2, MMP9, and PMEPA1, specifically targeting regions within 200 base pairs upstream of the transcriptional start site (TSS). The objective was to upregulate the expression of these proteins and assess their impact on the SMAD2 response induced by GDF11 in SRv2 WT SMAD3KO cells. To ensure efficient targeting, two specific sgRNAs were designed for each gene (Figure 25B) (For details, see Method 4.1.5.). After constructing plasmids containing the specified sgRNAs, these plasmids were transduced into cells using lentiviral transduction. Cells expressing the transgenes were selected using zeocin, and the expression levels of LTBP2, MMP9, and PMEPA1 were validated using RT-qPCR. Subsequently, two stable clones were selected for each sgRNA based on their expression levels. In the case of LTBP2, which is strongly regulated by SMAD3, the overexpression system only partially rescued its expression level compared to SRv2 WT (Figure 25C). Conversely, MMP9 and PMEPA1, which showed strong reduction upon SMAD3 removal, were restored to baseline expression levels by the dCas9 system (Figure 25C).

Upon generating stable cell lines expressing upregulated LTBP2, MMP9, and PMEPA1 proteins, I conducted time-lapse microscopy to assess the dynamics of SMAD2 response to GDF11 stimulation in proliferating cells, with TGF-beta serving as a reference (Figure 25D). Contrary to expectations, neither the initial nor subsequent responses of SMAD2 to GDF11 were downregulated compared to

TGF-beta stimulation in all clones. The lack of observed downregulation suggests several potential reasons for these findings. Firstly, the expression levels attained using the dCas9-VP64 system may not have been sufficient to exert a significant impact on the pathway. Moreover, biological pathways often involve the coordinated action of multiple genes and proteins. While LTBP2, MMP9, and PMEPA1 were selected based on their theoretical roles, it is plausible that additional factors or a combination of proteins are necessary for effective rewiring of the SMAD2 response network to GDF11.

In conclusion, while my research successfully elucidated the ALK5-SMAD3 mediated pathway for GDF11-induced SMAD2 response, the initial investigation into LTBP2, MMP9, and PMEPA1 as potential downstream regulators did not yield the anticipated outcomes. Future studies should aim to uncover other potential contributors that may influence the SMAD2 response to GDF11, thereby broadening our understanding of cellular signaling dynamics.

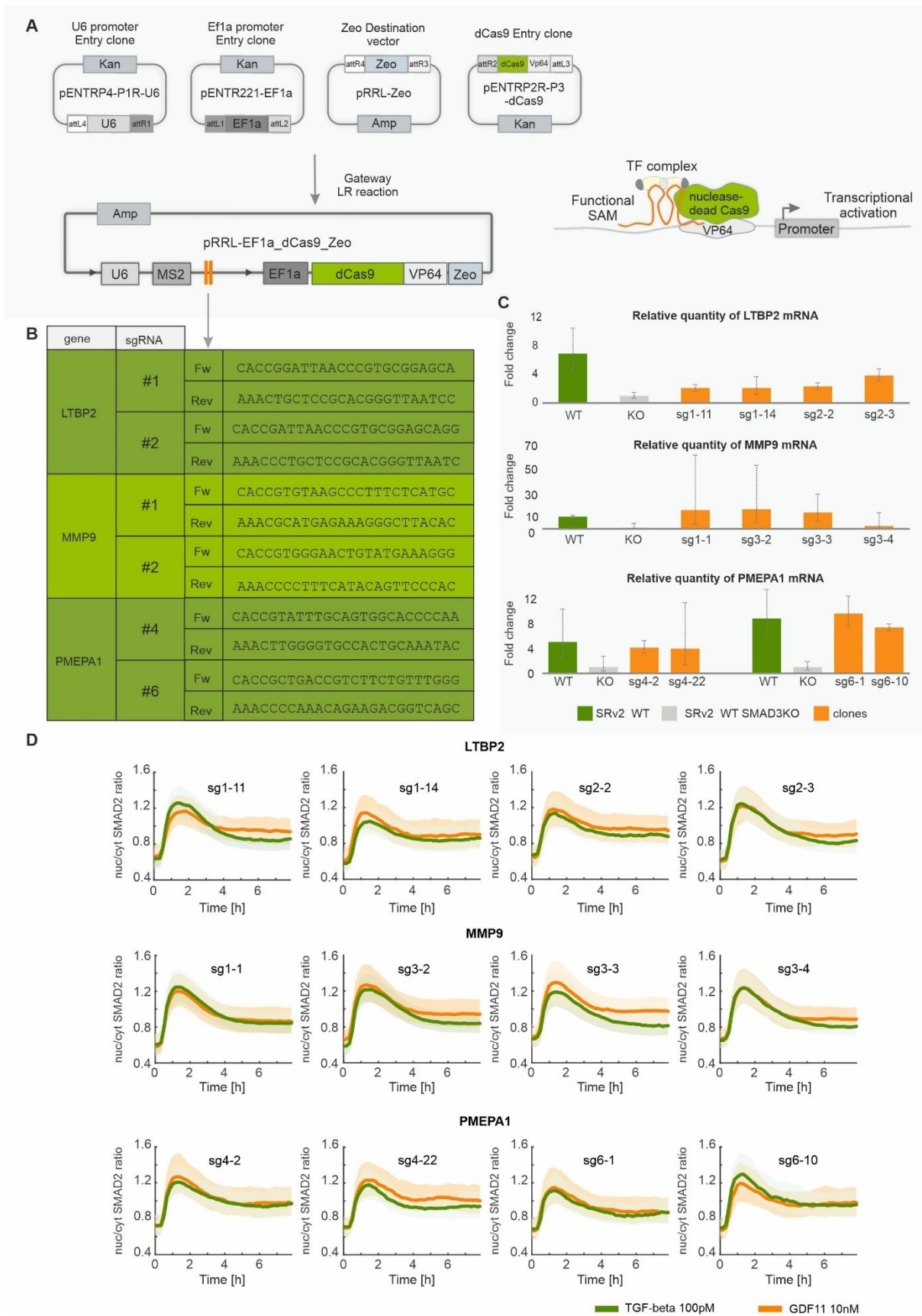


Figure 25 LTBP2, MMP9, and PMEPA1 Do Not Regulate GDF11-Mediated SMAD2 response in Proliferating Cells.

(A) Schematic representation of dCas9 plasmid construction using MultiSite Gateway LR Recombination Reaction. The construct includes a U6 promoter and Zeocin selection marker. Following lentiviral transduction into SRv2 WT SMAD3KO cells, clones were selected using Zeocin. Transcriptional activation through dCas9 modified after Konermann is shown (Konermann et al., 2015). The dCas9 is fused to the activation domain VP64 and guided to the target gene's TSS by sgRNAs. **(B)** List of sgRNAs for LTBP2, MMP9, and PMEPA1. **(C)** RT-qPCR analysis comparing gene expression in SRv2 WT (green), SRv2 WT SMAD3KO (grey), and different overexpression clones for LTBP2 (top), MMP9 (middle), and PMEPA1 (bottom) (orange). beta-Actin served as control. Data represent mean \pm SD of technical triplicates. **(D)** Nuclear-to-cytoplasmic SMAD2 ratio upon stimulation with 100 pM TGF-beta (green) or 10 nM GDF11 (orange) in proliferating cells. Cells were treated with ligands 0.5 h after experiment start. Solid lines represent median ratios; shaded areas represent 25th to 75th percentiles.

2.2 Result of Part 2:

2.2.1 Quantifying SMAD Dynamics in Response to BMP Treatment Using Fluorescent Reporters.

Having elucidated the intricate role of SMAD2/3 signaling in epithelial cell fate determination, I now turn my attention to the SMAD1/5/9 pathway in vascular endothelial cells. This strategic shift in focus allows for the exploration of the broader implications of SMAD-mediated signaling across diverse cellular contexts, providing a more comprehensive understanding of these critical pathways. While SMAD2/3 signaling is pivotal in regulating epithelial cell behaviors, the SMAD1/5/9 axis plays an equally crucial role in endothelial cell function and vascular homeostasis (Cai et al., 2012). Despite its importance, the dynamic changes of SMAD1/5/9 signaling in live cells and its role in driving endothelial cell fate decisions remain largely unexplored. To address this knowledge gap, I have developed fluorescent reporter cell lines that enable real-time visualization of SMAD1/5/9 activity in vascular endothelial cells. This innovative approach allows for elucidating how various ligands modulate SMAD1/5/9 signaling and subsequently influence endothelial cell behaviors within their unique microenvironment. In the following section, I will delve into the mechanistic aspects of SMAD1/5/9 signaling, exploring its temporal and spatial dynamics, and investigating its impact on endothelial cell fate decisions. By comparing and contrasting these findings with those from the SMAD2/3 pathway in epithelial cells, the aim is to uncover both common principles and cell-type specific features of SMAD signaling. This comprehensive analysis will not only enhance our understanding of vascular biology but also provide insights into potential therapeutic strategies for vascular disorders.

To systematically elucidate SMAD dynamics and monitor pathway activation at the single-cell level, I developed stable clonal reporter cell lines for SMAD1 in human vascular endothelial cells (EA.hy926). EA.hy926 cells, frequently used as a model for human vascular endothelial cells, are derived by fusing primary human umbilical vein cells (HUVEC) with the lung carcinoma cell line A549 (Edgell et al., 1983). The reporter cells were constructed by expressing an N-terminal fusion of SMAD1 cDNA with the yellow fluorescent protein mVenus (YFP) under the control of a constitutive ubiquitin promoter (UbCp). Additionally, the cells were engineered to stably express the nuclear marker histone H2B-CFP, facilitating efficient tracking of cell movement and division through automated image analysis, similarly to the SMAD2-reporter in MCF10A cells (Figure 26A) (Strasen et al., 2018). A suitable clone was selected based on expression levels determined by Western blot analysis (Figure 38A). To validate that SMAD1 overexpression did not alter its physiological dynamics, I performed Western blot and RT-PCR assays. For these and all subsequent experiments, serum levels were reduced to 1.5% 20 hours before stimulation to deplete any additional BMP family ligands from the medium. The results showed

that SMAD1 phosphorylation dynamics remained unaltered, with both the reporter and wildtype cell lines displaying similar phosphorylation patterns for endogenous SMAD1/5/9 upon BMP9 stimulation and YFP-SMAD1 (Figure 26B). Phosphorylation levels peaked at approximately 1.5 hours post-stimulation and then gradually decreased over time.

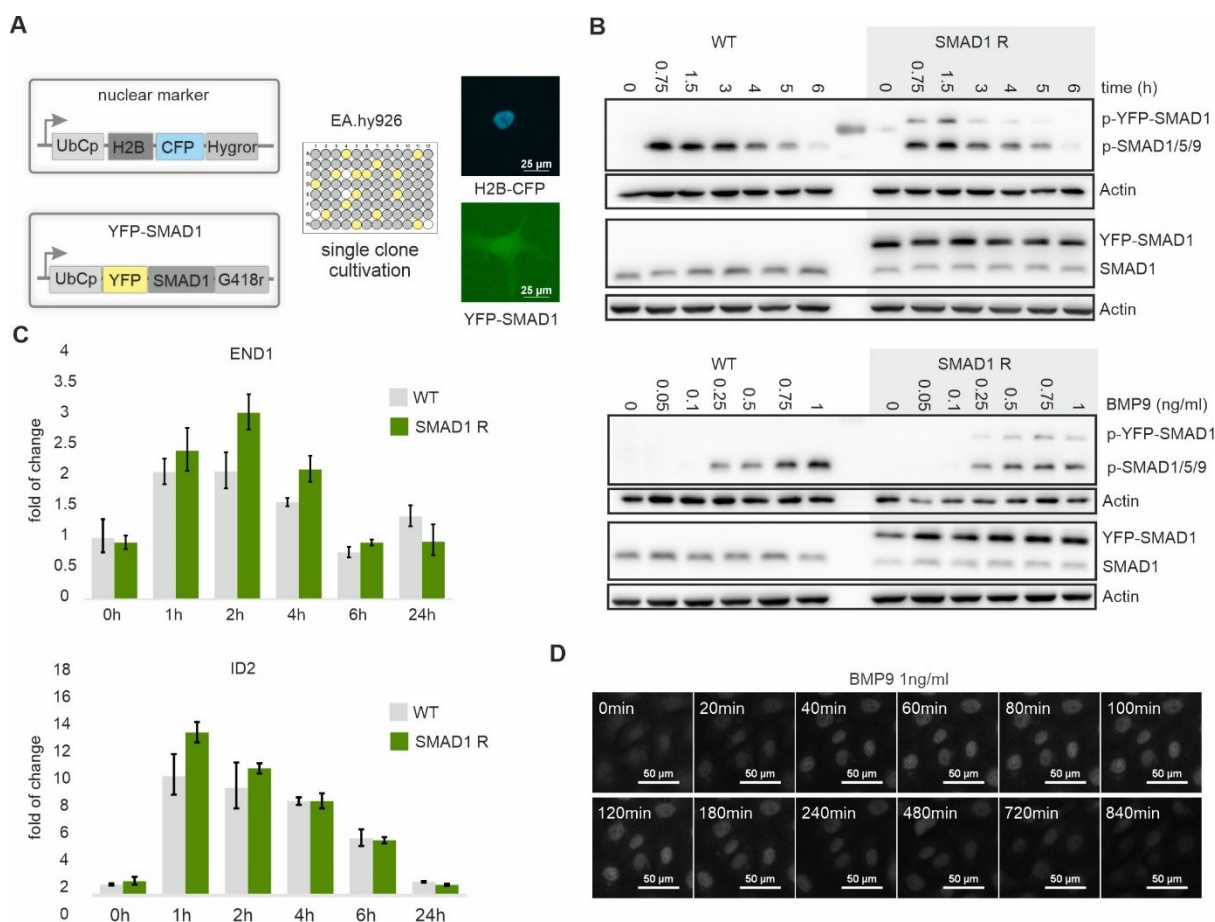


Figure 26 Selection and Validation of SMAD1 Reporter Clone.

(A) Schematic of the fluorescent reporter system. SMAD1 was fused to mVenus (YFP) under the UbCp with G418 selection. Histone 2B (H2B) was fused to mCerulean (CFP) under UbCp with hygromycin selection. **(B)** Western blot analysis of SMAD1 activation in SMAD1 reporter cells and parental EA.hy926 wildtype cells. Cells were pre-cultured in 1.5% FBS medium for 20 hours before ligand stimulation. Upper panel: Cells stimulated with 1 ng/ml BMP9; phosphorylated SMAD1/5/9 and total SMAD1 examined at indicated time points post-stimulation. Lower panel: SMAD1 activation assessed with varying BMP9 dosages; samples harvested 1.5 hours after stimulation. Actin served as loading control. **(C)** RT-qPCR analysis comparing SMAD1 target gene expression kinetics in EA.hy926 WT and EA.hy926 SMAD1 reporter cells following 1 ng/ml BMP9 stimulation; samples harvested at indication time point. Cells were pre-cultured in 1.5% FBS medium for 20 hours before ligand stimulation. β -Actin served as control. Data represent mean \pm SD of technical triplicates. **(D)** Representative live-cell time-lapse microscopy images of cells expressing YFP-SMAD1 post-treatment with 1 ng/ml BMP9. Images show YFP-SMAD1 localization in individual cells at indicated time points.

Dose-response analysis indicated that phosphorylated SMAD1/5/9 levels were dependent on ligand concentration, with both wildtype and reporter cell lines exhibiting comparable responses. RT-qPCR

analysis of well-characterized SMAD1/5/9 target genes, including EDN1 and ID2 (Figure 26C), revealed similar expression levels between the wildtype and reporter cell lines, despite the elevated expression of YFP-SMAD1 compared to endogenous SMAD1. Although there was a slight amplification in the expression of both genes in the reporter cell line, the overall gene response pattern was not altered by SMAD1 overexpression. These validation experiments confirm the reliability of the SMAD1 reporter system in accurately reflecting SMAD pathway dynamics, with SMAD1 overexpression not affecting BMP9-dependent downstream responses. This confirms the utility of our system for monitoring SMAD pathway activity. To broaden my investigation into SMAD1/5/9 dynamics and to facilitate comparative analyses, I extended this approach to develop similar fluorescent reporters for SMAD5 and SMAD9. Sonja and Marc assisted in validating these reporters through Western blot and RT-qPCR analyses, as detailed in Figure 38 (Marc-Andre Fiedler, 2022; Sonja Lenhardt, 2022).

I utilized time-lapse microscopy to explore the intracellular localization dynamics of SMAD1 in live cells. SMAD1 reporter cells were treated with a saturating dose of 1 ng/ml BMP9, and images were captured at 10-minute intervals over a 16-hour period. As illustrated in Figure 26D, a clear temporal pattern of SMAD1 translocation emerged. Shortly after BMP9 stimulation, there was a pronounced nuclear translocation of SMAD1 observed at approximately 1-hour post-stimulation, followed by a gradual relocalization back to the cytoplasm.

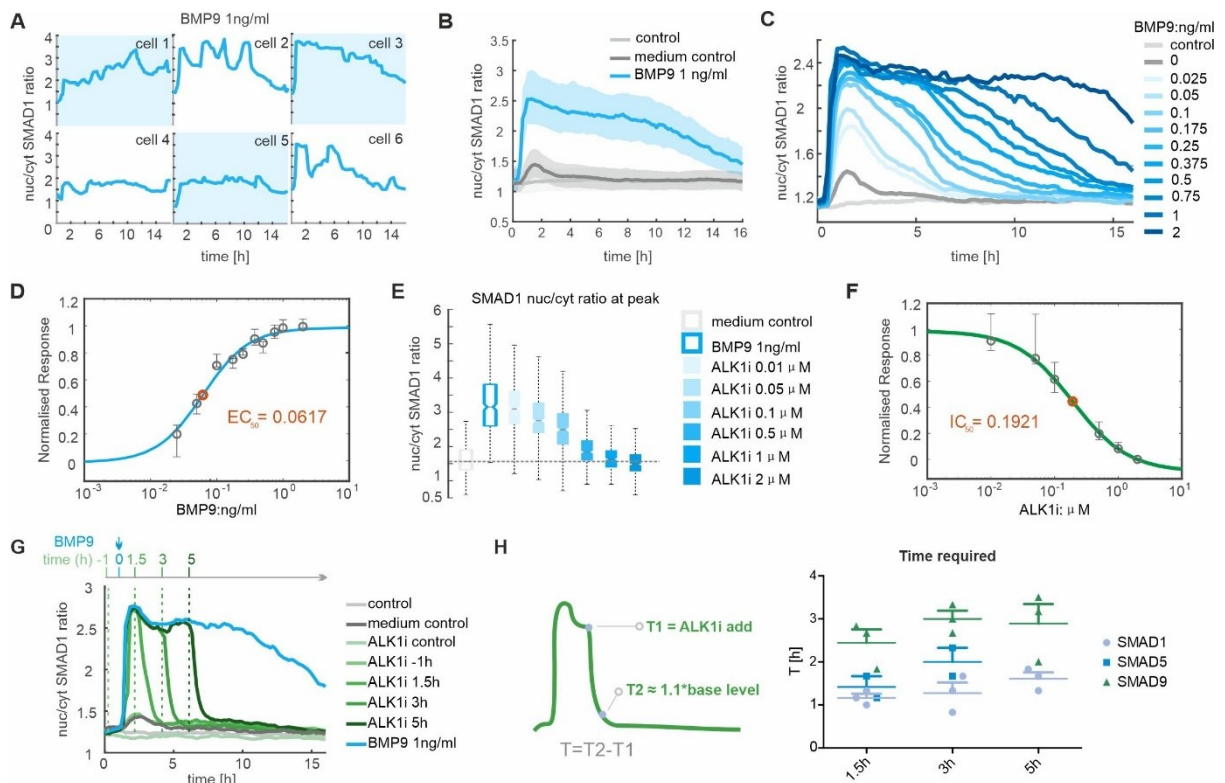


Figure 27 Dynamics of SMAD Signaling in Living Cells.

(A) Single-cell fluorescence intensity of nuclear-to-cytoplasmic YFP-SMAD1 ratio. Cells were cultured in 1.5% FBS medium for 20 hours prior to stimulation with 1 ng/ml BMP9 at 0.5 hours. Images were captured every 10 minutes for 16 hours. **(B)** Median nuclear-to-cytoplasmic SMAD1 ratio upon 1 ng/ml BMP9 stimulation (blue), unstimulated control (light gray), or medium control (dark gray). Solid lines represent median values; shaded areas indicate 25th to 75th percentiles. Cells were pre-cultured in 1.5% FBS medium for 20 hours. **(C)** Median nuclear-to-cytoplasmic SMAD1 ratio following stimulation with varying BMP9 concentrations over 16 hours. Cells were pre-cultured in 1.5% FBS medium for 20 hours. Imaging began 0.5 hours before BMP9 stimulation, with 10-minute intervals. **(D)** EC50 calculation (orange) based on peak median nuclear-to-cytoplasmic SMAD1 ratio for each BMP9 concentration. Data represent mean \pm SD from three independent experiments. **(E)** Peak median nuclear-to-cytoplasmic SMAD1 ratio in cells treated with various ALK1i (K02288) concentrations 1 hour before 1 ng/ml BMP9 stimulation. DMSO served as control. Cells were pre-cultured in 1.5% FBS medium for 20 hours and tracked for 16 hours. Dashed lines serve as guides to the eye. **(F)** EC50 calculation (orange) for ALK1 inhibitor based on peak median nuclear-to-cytoplasmic SMAD1 ratio. Data represent mean \pm SD from three independent experiments. **(G)** ALK1 inhibitor efficacy at different timepoints relative to BMP9 induction. Cells were treated with 1 μ M ALK1i at indicated timepoints (1 h before or 1.5 h, 3 h, 5 h post 1 ng/ml BMP9 stimulation). DMSO served as control. Cells were pre-cultured in 1.5% FBS medium for 20 hours and tracked for 16 hours. **(H)** Time required to reduce nuclear-to-cytoplasmic ratio from 90% to 10% for SMAD1 (lilac), SMAD5 (blue), and SMAD9 (green) upon 1 μ M ALK1i addition at 1.5 h, 3 h, or 5 h post BMP9 stimulation. Dots represent individual biological replicates (n=2 or 3).

To quantify SMAD dynamics, I used computer-aided image analysis to measure fluorescence intensities in both the nucleus and cytoplasm. This approach generated trajectories of the nuclear-to-cytoplasmic SMAD ratio, which served as a proxy for time-resolved pathway activation in individual cells. This analysis followed the same method used in Part 1 for assessing the SMAD2 nuclear-to-cytoplasmic ratio (see Methods 4.1.6). The analysis revealed significant heterogeneity in response to the saturating stimulus (Figure 27A). While cells generally displayed nuclear accumulation of SMAD1 shortly after initial stimulation, some cells adapted immediately to a low signaling plateau (e.g., cells 3 and 5), while others exhibited renewed nuclear translocation of SMAD1 (e.g., cells 2 and 6). The median nuclear-to-cytoplasmic SMAD1 ratio across the cell population further elucidated pathway activation dynamics (Figure 27B), showing an initial strong peak of SMAD1 translocation around 1.5 hours post-stimulation, followed by a gradual return to baseline levels. Shaded areas represent the 25th to 75th percentiles. Remarkably, even the control with medium alone showed a minor peak, underscoring SMAD1's heightened sensitivity to minimal BMP induction (Figure 27B). In addition, Supplemental Figures 39A and 39G depict the median responses of SMAD5 and SMAD9, respectively, to the same ligand stimulation, revealing that their responses closely mirrored that of SMAD1. Interestingly, SMAD5 did not exhibit a translocation peak in the stimulation control lacking ligands, indicating a lower sensitivity of this signaling mediator to BMP family ligands compared to SMAD1 and SMAD9.

To further explore SMADs sensitivity to BMP9, I systematically exposed reporter cells to varying concentrations of BMP9 (Figure 27C). Increasing BMP9 concentrations led to higher peak levels of SMAD1 translocation, saturating at approximately 0.375 ng/ml, with an EC50 of 0.0617 ng/ml (Figure 27C and D, see Method 4.2.8). Importantly, higher BMP9 doses also prolonged the duration of the

response, suggesting that ligand degradation determines the response duration in living cells, as previously demonstrated for TGF-beta signaling (Strasen et al., 2018). Similarly, both SMAD5 and SMAD9 exhibited dose-dependent responses (Figure 39B, H), although they required higher concentrations to reach saturation and peak levels compared to SMAD1. Notably, SMAD5 exhibited the highest EC50 among the SMAD proteins tested (Figure 39C, I).

To confirm the role of ALK1 in SMADs activation by BMP9, I treated reporter cells with varying concentrations of the ALK1 inhibitor K02288 (ALK1i) one hour before stimulation. Live-cell microscopy experiments demonstrated a dose-dependent decrease in SMAD1 translocation into the nucleus with increasing concentrations of the inhibitor (Figure 27E). The IC50 calculated from the peak nuclear to cytoplasmic (nuclear-to-cytoplasmic) SMAD1 ratio values was 192 nM (Figure 27F, see Method 4.2.8). Similar patterns of inhibition were observed for SMAD5 and SMAD9 in response to ALK1i treatment (Figure 39D, J), with lower half-maximal inhibitory concentrations (SMAD5 IC50: 66 nM, SMAD9 IC50: 145 nM; Figure 39E, K). Furthermore, sustained translocation of SMAD proteins was found to be reliant on receptor activity across all time points (Figure 27G, Figure 39F, L). Analysis of the time required for SMAD proteins to return to baseline cytoplasmic levels upon inhibitor treatment revealed that SMAD9 exhibited a slower return compared to SMAD1 and SMAD5 (Figure 27H).

In summary, my study using fluorescent reporters elucidates the dynamic patterns of SMAD1 activation mediated by ALK1-BMP9 signaling in endothelial cells. Additionally, comparative analysis of SMAD1, SMAD5, and SMAD9 translocation upon BMP9 stimulation reveals qualitatively similar dynamics. However, quantitative differences in their sensitivity to receptor activity and the kinetics of cytoplasmic relocation upon signal termination highlight distinct regulatory mechanisms within the SMAD signaling network.

2.2.2 FKBP12 Modulates the Activity of ALK2 in EA.hy926 Cells.

Following my investigation into BMP9-ALK1-mediated SMAD1/5/9 signaling in endothelial cells, I expanded my exploration to encompass the responses elicited by other ligands within the BMP and TGF-beta superfamily. This comprehensive study included ligands known to activate SMAD1/5/9 signaling, such as Activin A, BMP2, BMP6, BMP7, BMP9, and BMP10, alongside ligands that activate the SMAD2/3 pathway, such as TGF-beta and GDF11 (PIEK et al., 1999). Initially, I conducted Western blot analysis to assess the patterns of SMAD phosphorylation upon stimulation with these ligands. The analysis was supported by published RNA-seq data which confirmed the expression of both type I and type II receptors for these ligands in EA.hy926 cells, although at varying levels (Figure 28A,B) (Hiepen et al., 2019). Notably, BMP9 and BMP10 elicited significant phosphorylation of SMAD1/5/9, while BMP2 and BMP7 induced weaker signals (Figure 29A). The responses of SMAD2 and SMAD3 were more nuanced: BMP7, TGF-beta, GDF11, and Activin A clearly induced

phosphorylation of both SMAD2 and SMAD3. Interestingly, robust signals were also observed upon BMP9 and BMP10 stimulation. However, due to the detection of a band corresponding to exogenously expressed YFP-SMAD1, these signals were attributed to cross-reactivity of the phospho-specific antibodies used. Similar considerations affected the interpretation of SMAD2 and SMAD3 phosphorylation following BMP2 and BMP7 treatment.

A Gene Expression level [EA.hy926] derived from RNA-seq data (Hiepen, Christian et al. Dec. 2019)

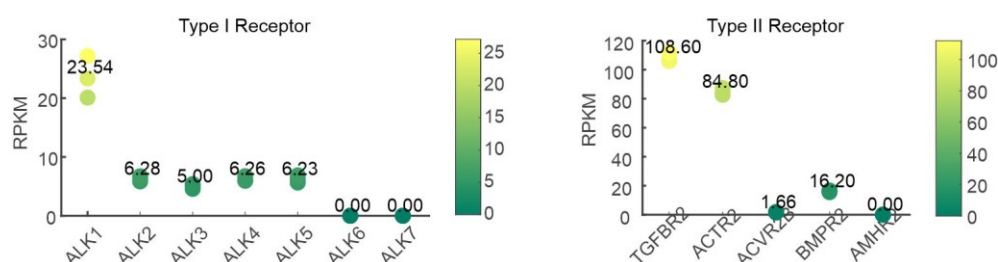


Figure 28 Analysis of Receptor Expression in SMAD Signaling Pathways.

RNA-seq data analysis (Hiepen et al., 2019) revealed receptor genes involved in SMAD signaling pathways. **(A)** Expression levels of type I receptor genes associated with SMAD signaling. **(B)** Expression levels of type II receptor genes associated with SMAD signaling.

To further validate these findings, I employed time-lapse microscopy of reporter cell lines to monitor SMAD translocation dynamics upon stimulation with these ligands. Remarkably, only BMP9 and BMP10 treatments resulted in robust translocation of SMAD1, SMAD5, and SMAD9 to the nucleus (Figure 29B and Figure 40A, B). The responses to BMP2 and BMP7 underscored differences in sensitivity among these proteins, with SMAD1 and SMAD9 showing slightly elevated nuclear accumulation upon stimulation, whereas SMAD5 exhibited no observable response.

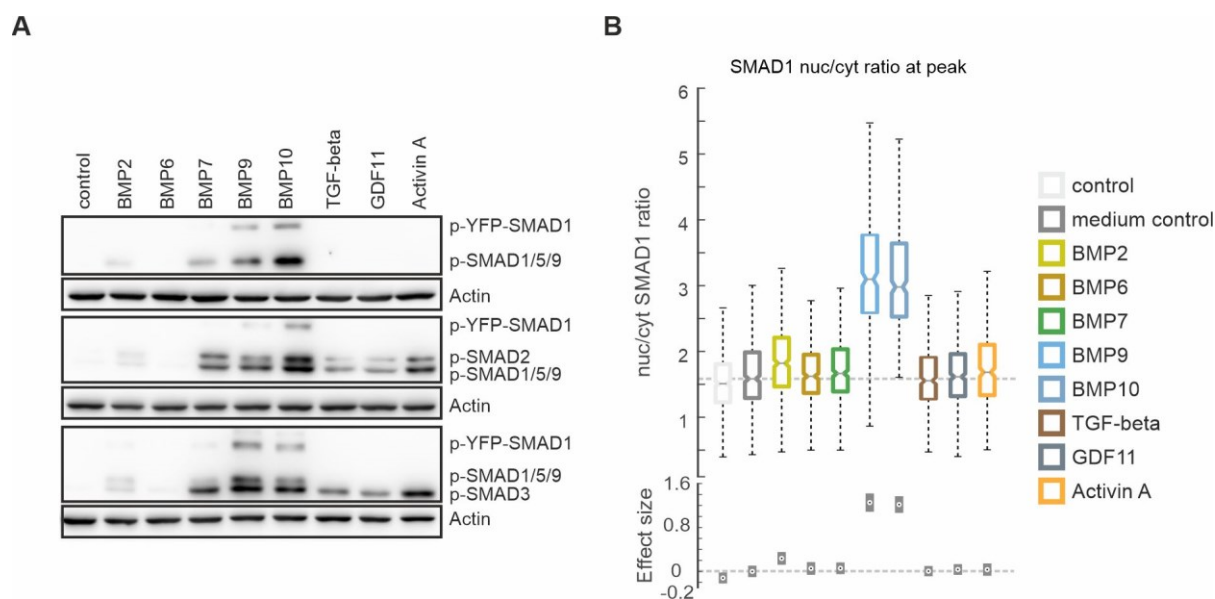


Figure 29 Different Ligands Induce Specific SMADs Responses.

(A) Western blot analysis of SMAD phosphorylation following stimulation with different ligands in SMAD1 reporter cells. Ligand concentrations used were: BMP2 (250 ng/ml), BMP6 (250 ng/ml), BMP7 (250 ng/ml), BMP9 (1 ng/ml), BMP10 (2 ng/ml), TGF-beta (50 ng/ml), GDF11 (250 ng/ml), and Activin A (250 ng/ml). Cells were cultured in 1.5% FBS medium for 20 hours prior to stimulation. Samples were harvested 1.5 hours after ligand stimulation. Upper panel: phosphorylation of SMAD1/5/9; middle panel: phosphorylation of SMAD2; bottom panel: phosphorylation of SMAD3. Actin served as the loading control. **(B)** Median nuclear-to-cytoplasmic SMAD1 ratio at peak following stimulation with varying ligands over 16 hours. Imaging began 0.5 hours before ligands stimulation, with 10-minute intervals. Cells were cultured in 1.5% FBS medium for 20 hours prior to stimulation. Ligand concentrations were identical to those used in panel A. Box plots represent data between the 25th and 75th percentiles of the cell population, with black lines indicating the median, and whiskers extending to maximum values within 1.5 times the interquartile range. Estimated changes compared to proliferating cells are depicted in the lower plot, with error bars representing 90% confidence intervals determined by permutation testing. Dashed lines are provided as guides to the eye.

These results underscore that despite the expression of multiple type I receptors, EA.hy926 cells predominantly respond to ALK1 activation. Given the robust SMAD translocation induced by BMP9 and BMP10, I excluded factors acting downstream of SMAD phosphorylation. Additionally, expression analysis revealed low or absent levels of extracellular inhibitory proteins known to block SMAD signaling (Figure 41B) (Canalis et al., 2003; Correns et al., 2021; Sidis et al., 2006; Y. Zhang et al., 2006). Moreover, the high concentration of exogenously supplied ligands was expected to saturate any remaining extracellular inhibitors. This led me to hypothesize that inhibitory factors may hinder the activity of other receptors. Therefore, my focus turned to factors potentially inhibiting the receptors themselves, leading me to observe high expression of FKBP12, a known inhibitor of ALK2 receptors (Huse et al., 1999), in EA.hy926 cells (Figure 41C). FKBP12 binds to receptors and impedes signaling by occupying the phosphorylation site in the glycine-serine-rich region, suggesting its role in pathway obstruction and thereby limiting SMAD activation by ligands using ALK2 as the type I receptor (Huse

et al., 1999). To test this hypothesis, I employed a FKBP12 PROTAC to induce FKBP12 protein degradation within the cells (Figure 30A). The FKBP12 PROTAC consists of a ligand that binds FKBP12 linked to a ligand that recruits the E3 ligase VHL, thereby facilitating FKBP12 degradation (Abdullah et al., 2023). Western blot analysis confirmed dose-dependent degradation of FKBP12 protein by the PROTAC, with complete degradation requiring an extended duration (Figure 30B). Subsequently, using the PROTAC to degrade FKBP12 before ligand stimulation, I observed rescue of the SMAD1 response to BMP7 and Activin A stimulation (Figure 30C, Figure 42A). Interestingly, BMP9 and BMP10, which can also utilize ALK2 or ALK3 to enhance the SMAD1 response (Ayuso-Íñigo et al., 2021; Herrera et al., 2009; Mazerbourg et al., 2005), did not show significant amplification (Figure 42A). Correspondingly, PROTAC treatment increased SMAD1/5/9 phosphorylation in response to BMP7 and Activin A, as evidenced by Western blot (Figure 30D). Following PROTAC treatment, I stimulated cells with varying doses of BMP7 and Activin A in the absence of FKBP12. Remarkably, BMP7 elicited a dose-dependent SMAD1 response in the presence of PROTAC (Figure 30E), consistent with findings from Activin A stimulation (Figure 30F). The dynamics of SMAD translocation were similar across all conditions eliciting a response. To assess the kinetics of FKBP12-mediated ALK2 inhibition, cells were pre-incubated with PROTAC for different durations before BMP7 stimulation (Figure 30G). Interestingly, several hours of PROTAC treatment were required to rescue SMAD1 dynamics at the peak time point. However, cells pre-incubated for shorter durations exhibited enhanced SMAD1 response at later time points, suggesting a direct relationship between FKBP12 degradation and heightened SMAD1 signaling. In summary, these findings strongly support the hypothesis that FKBP12 inhibits ALK2 in endothelial cells, thereby preventing SMAD1 activation by specific ligands.

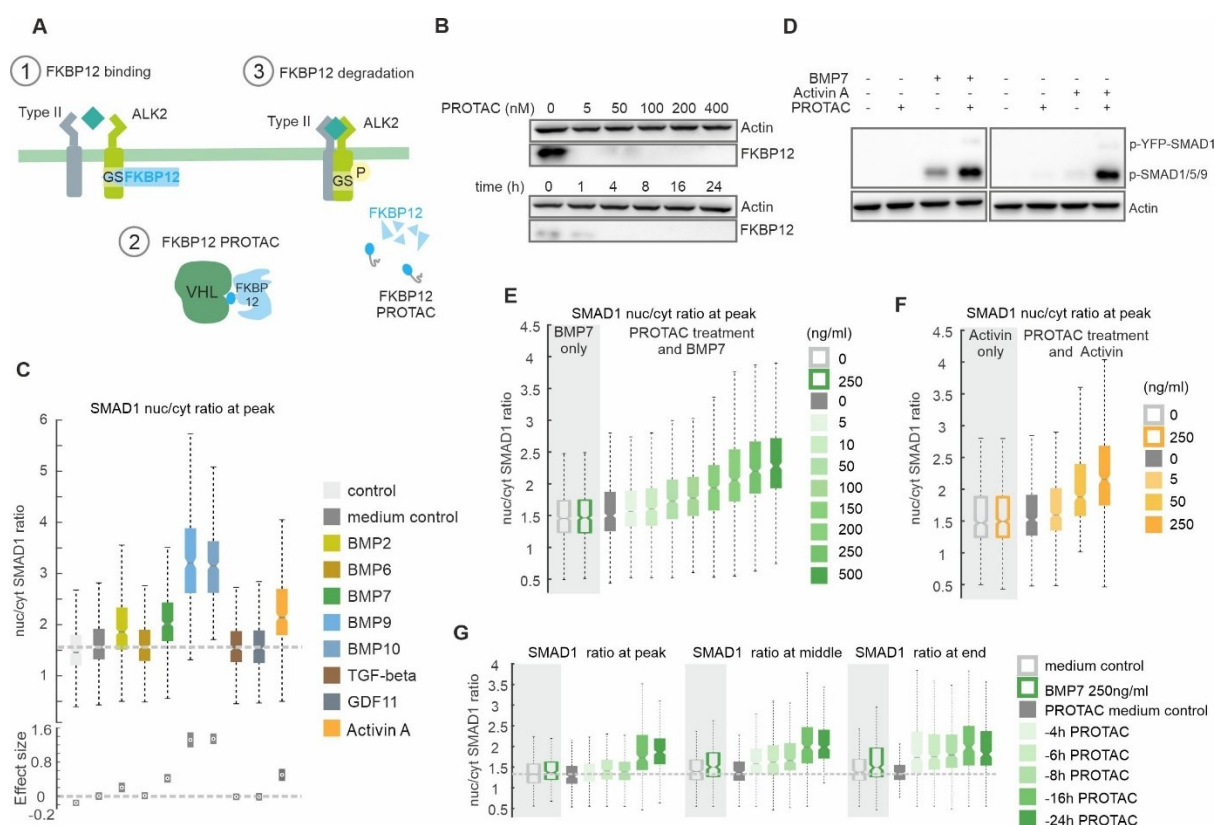


Figure 30 FKBP12 Absence Rescues SMAD Response to ALK2-Dependent Ligands.

(A) Schematic representation of FKBP12 inhibition of ALK2 activation and its degradation by FKBP12 PROTAC, enabling ALK2 activation by ligand stimulation. **(B)** Western blot analysis of FKBP12 degradation via PROTAC stimulation in SMAD1 reporter cells. Upper panel: Cells stimulated with varying PROTAC dosages; samples harvested after 24 hours. Lower panel: Cells stimulated with 200 nM PROTAC; samples harvested at indicated time points. Actin served as loading control. **(C)** Nuclear-to-cytoplasmic SMAD1 ratio in SMAD1 reporter cells at peak response following stimulation with different ligands. 200 nM PROTAC was added 24 hours before ligand stimulation in 1.5% FBS medium. Ligand concentrations as in Figure 29A. Box plots represent 25th to 75th percentiles, black lines indicate median, whiskers extend to maximum values within 1.5 times interquartile range. Lower plot shows estimated changes compared to medium control; error bars represent 90% confidence intervals. Dashed lines serve as guides to the eye. **(D)** Western blot analysis of SMAD1/5/9 phosphorylation following stimulation with BMP7 (250 ng/ml) and Activin A (250 ng/ml) in SMAD1 reporter cells, with or without 200 nM PROTAC was added 24 hours before ligand stimulation in 1.5% FBS medium. Samples harvested 1.5 hours after ligand stimulation. Actin served as loading control. **(E-F)** Analysis of peak nuclear-to-cytoplasmic SMAD1 ratio following stimulation with varying concentrations of **(E)** BMP7 or **(F)** Activin A over 16 hours, with or without PROTAC pre-treatment. 200 nM PROTAC added 24 hours before ligand stimulation in 1.5% FBS medium. Imaging began 0.5 hours before ligand stimulation. **(G)** Analysis of peak nuclear-to-cytoplasmic SMAD1 ratio following stimulation with 250 ng/ml BMP7 over 16 hours with different PROTAC addition times. Cells cultured in 1.5% FBS medium with or without PROTAC addition 24 hours before experiment start. Dashed lines serve as guides to the eye.

2.2.3 FKBP12 Regulates the Balance of SMAD1/5/9 and SMAD2/3 Activation by Ligands of the BMP Family.

Expanding on my prior findings that highlighted FKBP12's crucial role in suppressing SMAD responses to ALK2-based ligands like BMP7 and Activin A, I aimed to explore whether the activation of the SMAD1/5/9 pathway influences SMAD2/3 activation.

To begin, I conducted Western blot analysis to compare conditions with and without FKBP12 (Figure 43A). Unfortunately, these experiments did not yield conclusive results regarding SMAD2/3 activation in the absence of FKBP12. To delve deeper into understanding whether FKBP12 influences the balance between SMAD1/5/9 and SMAD2/3 pathways in live cells, I developed an mCherry-SMAD2 double reporter cell line based on our SMAD1 reporter cells (Figure 31A). This involved constructing an mCherry-SMAD2 plasmid under the UbCp with blasticidin selection, followed by lentiviral transduction and clonal selection for subsequent experiments (Figure 31B).

To validate the functionality of the double SMAD1-SMAD2-reporter cells in distinguishing SMAD2 responses while not detecting SMAD1 dynamics, I stimulated cells with varying doses of BMP9 and monitored SMAD1 and SMAD2 translocation in real-time. As anticipated, increasing doses of BMP9 did not induce SMAD2 translocation, clearly demonstrating that the SMAD1 pathway operates independently of SMAD2 activation upon BMP9 stimulation (Figure 31C). Subsequently, I stimulated the cells with various doses of TGF-beta to observe SMAD2 translocation using the double reporter system. Consistently, high doses of TGF-beta triggered robust SMAD2 translocation, peaking at 5 ng/ml, with a slight reduction observed at higher concentrations (Figure 31D), aligning well with previous studies indicating feedback inhibition at elevated TGF-beta levels (Yan et al., 2018). These results underscore the distinct and independent responses of the SMAD1/5/9 and SMAD2/3 branches to ligands that activate ALK1 and ALK5, respectively.

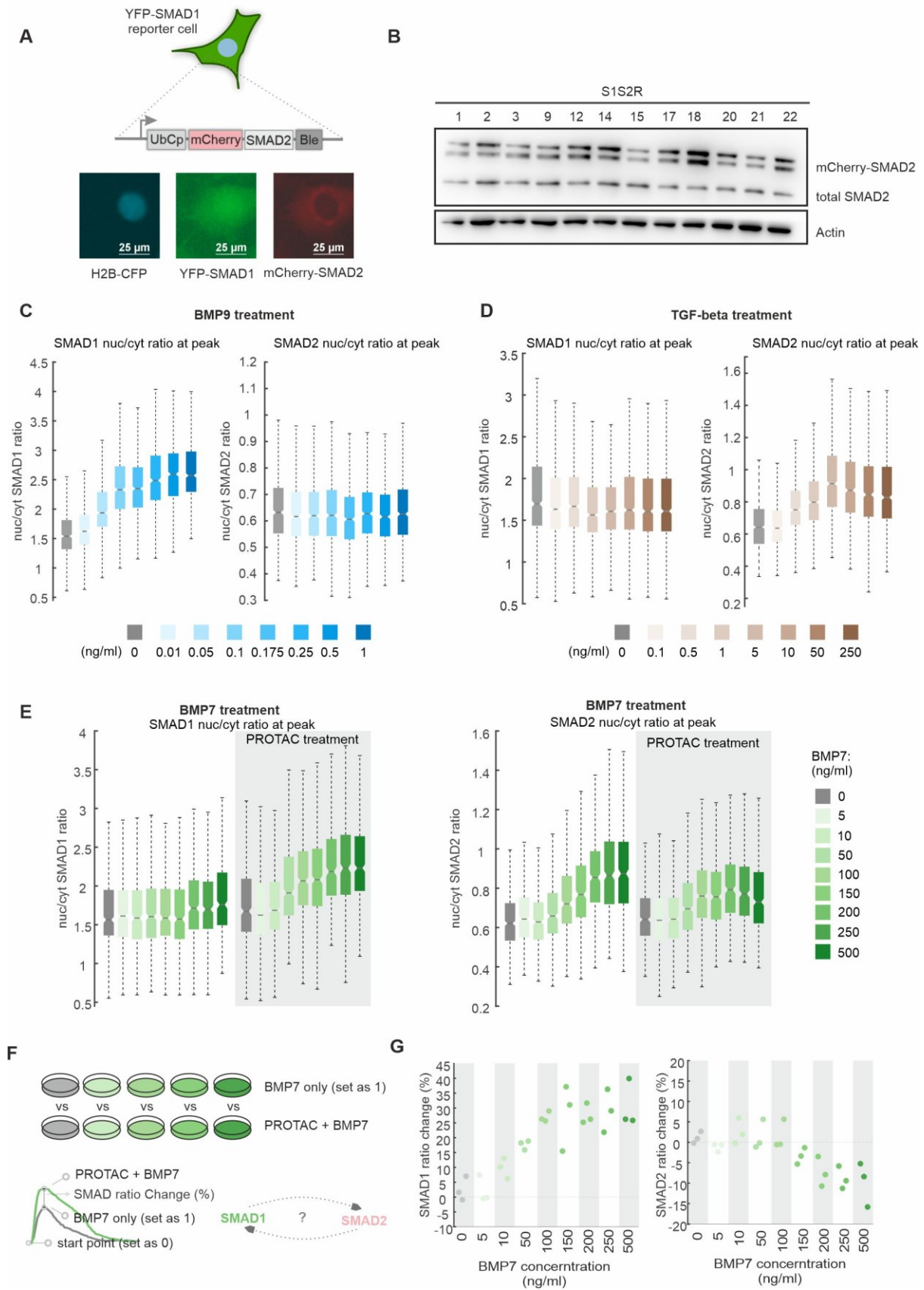


Figure 31 Dynamics of SMAD Signaling in Living Cells.

(A) Schematic of the fluorescent reporter system. SMAD2 was fused to mCherry (RFP) under the UbCp with blasticidin selection. **(B)** Western blot analysis of total SMAD2 in different SMAD1-SMAD2-reporter clones. Numbers correspond to specific clone identifiers. Actin served as loading control. **(C-D)** Analysis of peak nuclear-to-cytoplasmic SMAD1 and SMAD2 ratios upon stimulation with varying concentrations of (C) BMP9 or (D) TGF-beta over 16 hours. Cells were cultured in 1.5% FBS medium for 20 hours prior to stimulation. Ligands were added 0.5 hours after experiment start. **(E)** Analysis of peak nuclear-to-cytoplasmic SMAD1 and SMAD2 ratios upon stimulation with varying concentrations of BMP7 over 16 hours. PROTAC was added 24 hours before ligand stimulation, with cells cultured in 1.5% FBS medium simultaneously. BMP7 was added 0.5 hours after experiment start. **(F-G)** Normalization approach for (E). Median ratios of SMAD1 and SMAD2 responses with and without FKBP12 were calculated across all BMP7 concentrations, setting the starting point as 0. Peak ratio values in the presence of FKBP12 were normalized to 1 for each BMP7 concentration group. Percentage differences between FKBP12 absent and present conditions were calculated for both SMAD1 and SMAD2 responses. Each dot indicates one repeat experiment. Dashed lines serve as guides to the eye.

Using this double reporter cell system, I further investigated the dynamics between SMAD1 and SMAD2 to elucidate how FKBP12 influences the intricate cross-talk between these pathways. When treating cells with vary doses BMP7 alone, I observed the expected response: robust activation of SMAD2 while SMAD1 remained unresponsive (Figure 31E). However, upon depleting FKBP12, there was a noticeable shift in this response. The SMAD1 response to BMP7 significantly intensified and exhibited dose-dependence, whereas the SMAD2 response was attenuated, particularly at higher concentrations of BMP7 (Figure 31E).

To illustrate the significance of the shift between SMAD1 and SMAD2 responses at the population level, I employed a normalization approach (see Method 4.2.12). Initially, I calculated the median ratio of SMAD1 and SMAD2 responses with and without FKBP12 across all BMP7 concentrations, setting the starting point as 0 for the median ratio value. Subsequently, I normalized the peak ratio values in the presence of FKBP12 as 1 for each BMP7 concentration group (Figure 31F). Finally, I calculated the percentage difference between FKBP12 absent and present conditions for both SMAD1 and SMAD2 responses. This analysis revealed that the absence of FKBP12 significantly increased the SMAD1 response in a dose-dependent manner. Conversely, FKBP12 absence did not alter the SMAD2 response at lower BMP7 concentrations (0-100 ng/ml), but notably decreased it at higher concentrations (Figure 31G).

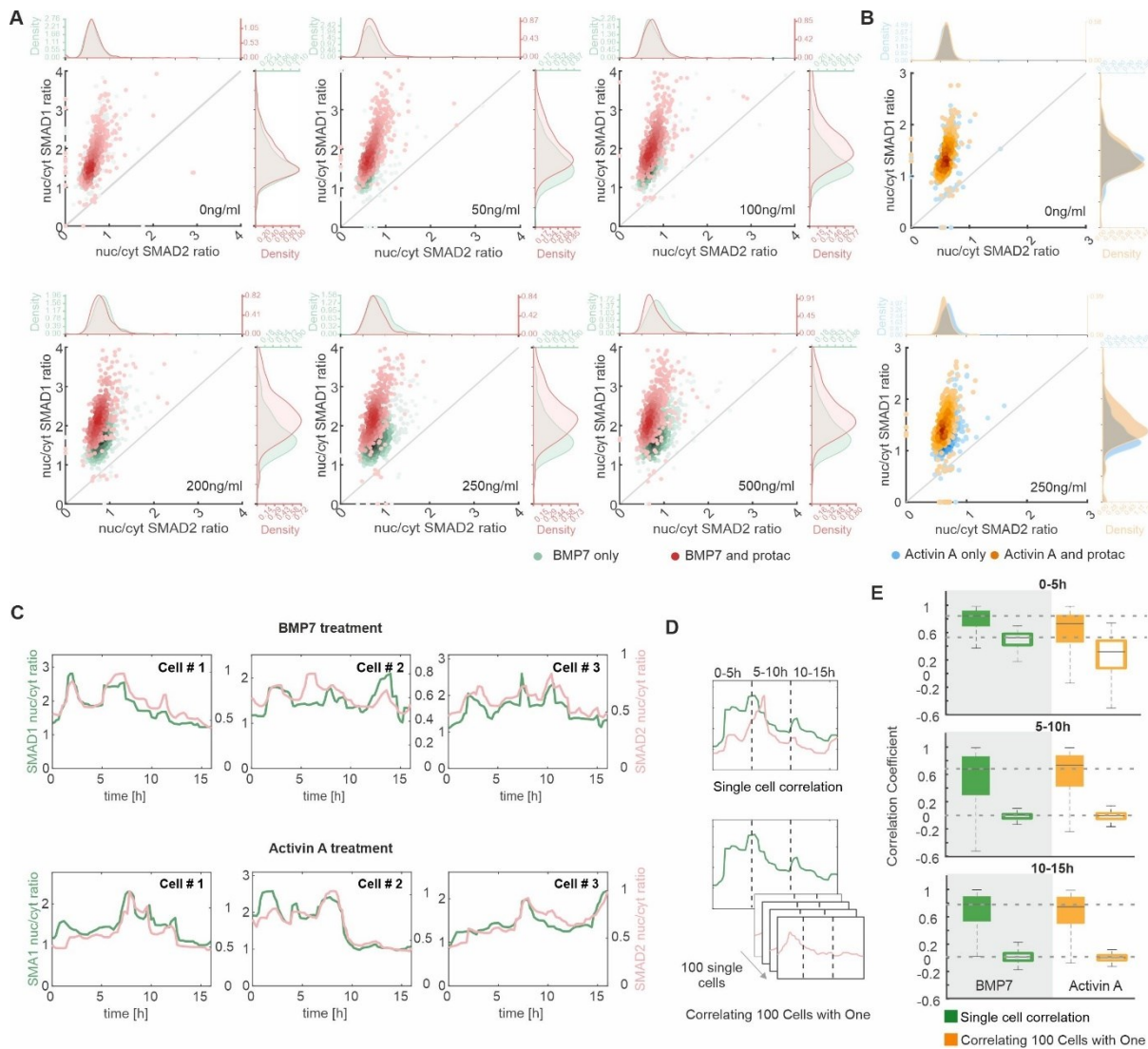


Figure 32 FKBP12 Modulation of SMAD1/2 Activation in Single Cells.

(A) Scatter plot showing single-cell quantification of peak nuclear-to-cytoplasmic ratios in the first 5h for SMAD2 (left) and SMAD1 (right) in cells treated with different doses of BMP7. Each dot represents one cell analyzed from Figure 31E microscopy experiments. (B) Similar analysis for 20 nM Activin A and untreated condition. (C) Single-cell fluorescence intensity of nuclear-to-cytoplasmic (nuclear-to-cytoplasmic) YFP-SMAD1 (green) and SMAD2 (pink) ratio. Cells were cultured in 1.5% FBS medium for 24 hours with FKBP12 PROTAC prior to stimulation with 250 ng/ml BMP7 (top) or Activin A (bottom) at 0.5 hours. Images were captured every 10 minutes for 16 hours. (D-E) Pearson correlation assays across different time frames, dividing the tracking period into three phases: initial response (0-5 hours), middle response (5-10 hours), and late response (10-15 hours). Correlation scores between SMAD1 and SMAD2 within individual cells were analyzed. To assess variability among individual cells, these scores were compared with a control where SMAD2 data from randomly selected 100 single cells were used to calculate correlations relative to SMAD1 data. Dashed lines serve as guides to the eye.

Following my investigation at the population level, I focused on examining the signaling changes at the single-cell level. To accomplish this, I analyzed the maximal initial response to varying doses of BMP7 in individual cells, comparing those treated with PROTAC to untreated cells. As expected, the analysis

confirmed that at higher BMP7 concentrations, the SMAD2 response decreased while the SMAD1 response increased when FKBP12 was absent (Figure 32A). This trend was particularly noticeable when BMP7 concentrations exceeded 200 ng/ml, reinforcing what I found at the population level. Similarly, when I studied cells treated with Activin A, I consistently observed reduced SMAD2 responses when FKBP12 was not present (Figure 32B).

Based on my observations, there is a noticeable shift in signaling from SMAD2 to SMAD1 at the single-cell level upon BMP7 and Activin A stimulation. This change in signal dynamics prompted me to investigate the correlation between SMAD1 and SMAD2 during dual pathway activation. First, I examined the single-cell SMAD1 and SMAD2 responses to BMP7 and Activin A. Interestingly, I found that these responses were highly correlated when FBBP12 was absent (Figure 32C). To explore this further, I conducted Pearson correlation assays across different time frames, dividing the tracking period into three phases: initial response (0-5 hours), middle response (5-10 hours), and late response (10-15 hours) (Figure 32D). Initially, I analyzed the correlation scores between SMAD1 and SMAD2 within individual cells to understand their relationship during the responses. To assess the variability among individual cells, I compared these scores with a control where SMAD2 data from randomly selected 100 single cells were used to calculate correlations relative to SMAD1 data (Figure 32D). Upon immediate stimulation, high correlation score was observed with both BMP7 and Activin A treatments (Figure 32E, see Method 4.2.11). However, at later time points (10-15 hours post-stimulation), the correlation between SMAD1 and SMAD2 markedly decreased, which suggests that although the initial response may show coordination, the pathways diverge over time due to distinct regulatory mechanisms.

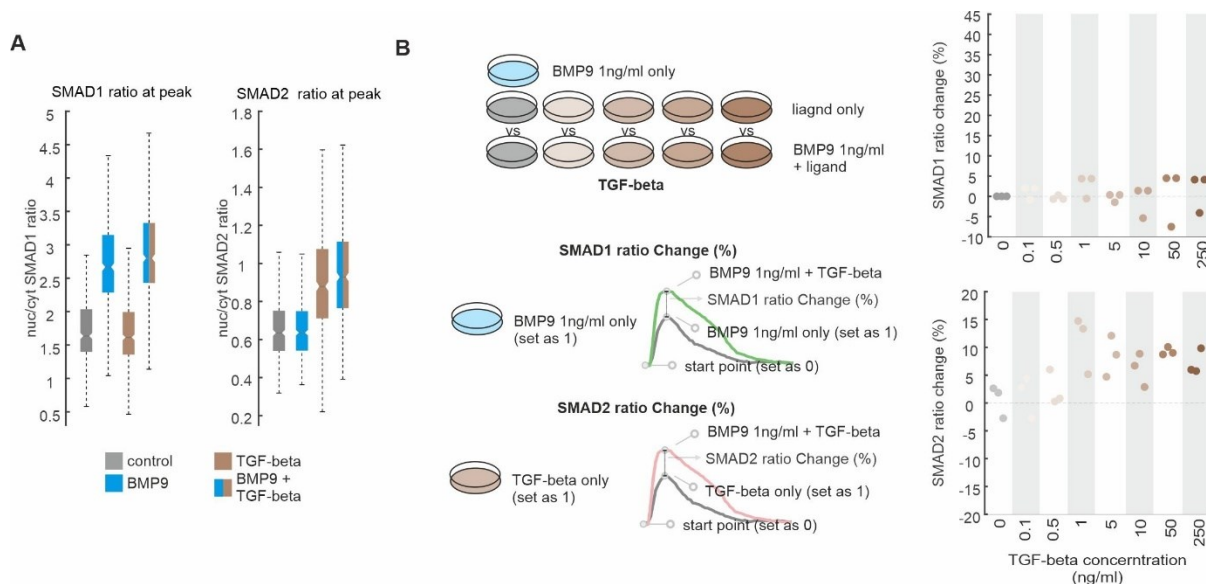


Figure 33 SMAD1 and SMAD2 Dynamics in Response to BMP9 and TGF-beta.

(A) Peak nuclear-to-cytoplasmic SMAD1 and SMAD2 ratios were measured upon stimulation with 1 ng/ml BMP9 (blue), 50 ng/ml TGF-beta, or a combination of both over 16 hours. Cells were cultured in 1.5% FBS medium for 20 hours, and ligands

were added 0.5 hours after the experiment started. **(B)** A dose titration experiment was conducted with varying TGF-beta concentrations, both alone and combined with 1 ng/ml BMP9. Normalization was done by calculating median SMAD1 and SMAD2 response ratios with and without FKBP12 across BMP7 concentrations, setting BMP9-only and TGF-beta-only treatments as references (set to 1). Each bar indicates one repeat experiment. Dashed lines serve as guides to the eye.

Observing correlated SMAD1-SMAD2 responses during dual pathway activation with both ligands, regardless of the dose, both at the population and single-cell levels, led me to question: How can such a rebalancing of SMAD1 and SMAD2 responses be explained mechanistically? Previous studies suggested that signal shifts during co-treatment with ligands could be attributed to receptor number limitations, feedback loop inhibition mechanisms, or competition between subpathways (Martinez-Hackert et al., 2021; Yan et al., 2018).

To test these hypotheses, I co-stimulated cells with BMP9 and TGF-beta, thereby activating both subpathways via distinct type I and type II receptors. If feedback loops or competition between the pathways existed, I would expect attenuated responses for SMAD1 and SMAD2 when comparing individual treatments with co-stimulation. However, co-stimulation induced unaltered SMAD responses (Figure 33A), which argues against competition between the subpathways or feedback inhibition. To further verify this phenomenon, I conducted a dose titration experiment. I treated cells with different doses of TGF-beta and, in parallel, treated another set of cells with the same TGF-beta concentrations along with 1 ng/ml BMP9 to activate the SMAD1/5/9 pathway. I employed a normalization approach similar to the BMP7 analysis (Figure 33B). For SMAD1 ratio changes, I used the BMP9-only treatment as a reference (set to 1). For SMAD2 Ratio changes, I used the cells treated with varying doses of TGF-beta only as a reference (set to 1). The SMAD1-SMAD2 dynamics in response to BMP9-TGF-beta co-stimulation across varying doses supported these conclusions (Figure 33B). Adding BMP9 did not change the SMAD1 ratio significantly. Interestingly, co-treatment with BMP9 slightly increased the SMAD2 response compared to TGF-beta alone. This indicates that the pathways operate independently without significant cross-inhibition or competition, reinforcing the idea that FKBP12's role is pivotal in modulating SMAD1/5/9 and SMAD2/3 activation without invoking pathway competition mechanisms.

2.2.4 Different Receptor Complexes Determine SMAD Response Branches for Various Ligands.

In my experiments, I did not find evidence supporting feedback inhibition or pathway competition between the two SMAD branches. Instead, I hypothesized that the observed interplay of SMAD2/3 and SMAD1/5/9 is based on the activation of differential receptor complexes. As the SMAD pathway initiates with ligand binding to a tetrameric receptor complex composed of two type I and two type II serine/threonine kinase receptors, which is essential for signal transduction, BMP7 and Activin A utilize

ALK2 and ALK4 as type I receptors, forming both homodimers and heterodimers with high affinity. Understanding the specific roles of different type I receptors is crucial, as they dictate the downstream SMAD pathways activated. Although there is a lack of research discussing the SMAD branch activated by homodimers and heterodimers within type I receptors, some studies have investigated how homodimers and heterodimers of type II receptors induce different SMAD branch responses. For instance, in human pulmonary artery endothelial cells, a related receptor, ALK1, activates SMAD1/5 through BMPRII and SMAD2/3 via ACVR2A (Upton et al., 2009). Importantly, the activation of these pathways shifts depending on the expression level of type II receptors. My observation regarding FKBP12 introduces a new perspective: FKBP12 influences the availability of receptor dimers that can be activated, potentially altering the activation of SMAD branches. To delve deeper into this idea, I employed several receptor inhibitors: K02288 (ALK1/2i), LDN-214117 (ALK2/1i), and SB525334 (ALK5/4i). These inhibitors allowed me to investigate how altering the number of available receptor dimers affects SMAD pathway activation and elucidate FKBP12's role in this regulatory mechanism.

Initially, to validate the efficacy of receptor blockade, I pre-incubated cells with inhibitors before stimulating them with BMP9 using the SMAD1-SMAD2 double reporter system in the presence or absence of FKBP12. As expected, the results clearly demonstrated that BMP9 specifically induces the SMAD1 response, primarily dependent on ALK1 activation, as observed with both ALK1/2i and ALK2/1i inhibitors (Figure 34A). Interestingly, even when SMAD1 was blocked, BMP9 did not trigger SMAD2 activation, indicating that BMP9 selectively activates the SMAD1 pathway in EA.hy926 cells, without cross-activating the SMAD2 pathway.

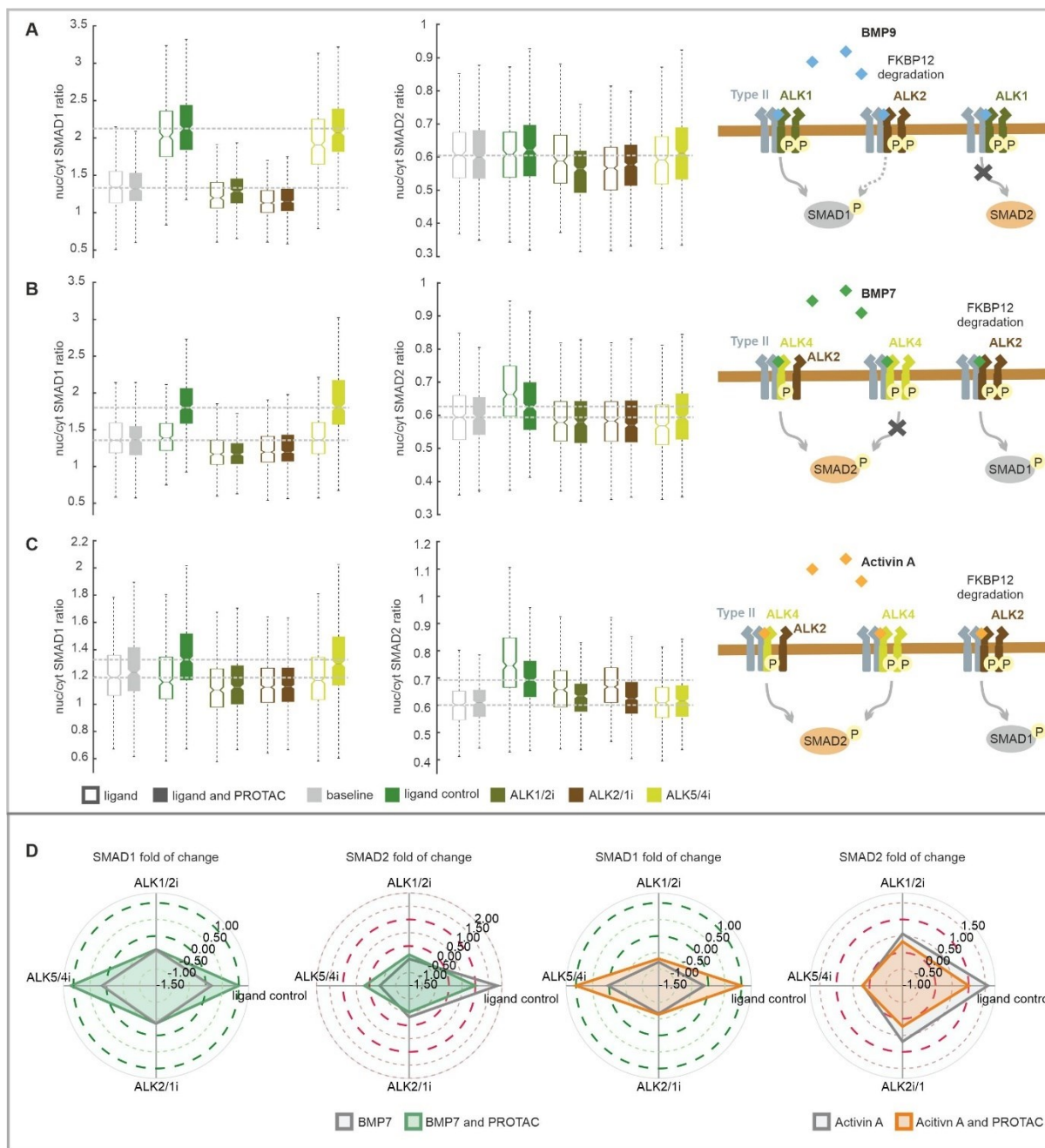


Figure 34 Differential SMAD Activation Due to Type I Receptor Homodimers or Heterodimers Depends on Specific Ligands.

(A-C) Analysis of peak nuclear-to-cytoplasmic (nuclear-to-cytoplasmic) ratios of SMAD1 and SMAD2 upon stimulation with **(A)** BMP9 (1 ng/ml), **(B)** BMP7 (250 ng/ml), or **(C)** Activin A (250 ng/ml) over a 16-hour period. PROTAC was added 24 hours before ligand stimulation in 1.5% FBS medium. Inhibitors ALK1/2i (K02288, 1 μ M), ALK5/4i (SB525334, 10 μ M), and ALK2/1i (LDN214117, 10 μ M) were added 0.5 hours after experiment start, with ligands added 1 hour later. Dashed lines indicate baseline and ligand-PROTAC values. Schematics illustrate SMAD activation by each ligand upon receptor binding. **(D)** Radar chart displaying fold change of SMAD signaling upon different inhibitor treatments. Baseline value (median from A-C) denoted as 0, ligand stimulation with PROTAC normalized to 1. This normalization enables comparison of fold changes across inhibitor treatments.

Next, I delved into understanding how the tetrameric receptor complex activates SMAD pathways and the specific role of FKBP12 in this process during BMP7 stimulation (Figure 34B). Interestingly, inhibiting ALK1/2 (using ALK1/2i and ALK2/1i inhibitors) significantly suppressed both SMAD1 and SMAD2 responses, regardless of FKBP12 status. This highlights the critical role of ALK2 in mediating dual SMAD activation following BMP7 treatment. Conversely, inhibition of ALK5/4 selectively blocked SMAD2 activation while leaving SMAD1 activation unaffected. This suggests that BMP7-induced SMAD2 activation relies on ALK4 and ALK2 heterodimers, whereas SMAD1 activation is solely dependent on the ALK2 homodimer complex (Figure 34B).

Activin A, like BMP7, utilizes ALK2 and ALK4 receptors to activate SMAD signaling in endothelial cells. During Activin A stimulation, inhibiting ALK5/4 resulted in identical SMAD1 and SMAD2 responses as observed with BMP7 stimulation (Figure 34C). This similarity suggests that both ligands activate SMAD1 through a comparable mechanism, regardless of FKBP12 status. However, when I inhibited ALK1/2 during Activin A stimulation, I observed a partial blockade of the SMAD2 response, regardless of whether FKBP12 was present or absent. In contrast, inhibiting ALK4/5 completely prevented SMAD2 activation, as confirmed by Western blot analysis (Figure 43A). These results suggest that Activin A-induced SMAD1 activation is solely dependent on the ALK2 homodimer complex, similar to the mechanism observed with BMP7, and is regulated by FKBP12. In contrast, SMAD2 activation exhibits more flexibility, relying not only on heterodimers formed by ALK4 and ALK2 but also on the ALK4 homodimer complex.

Overall, my results highlight how FKBP12 modulates the activity of specific receptor complexes, thereby influencing the balance between SMAD1/5/9 and SMAD2/3 activation in a ligand-specific manner (Figure 34D).

2.2.5 SMAD1/5/9 and SMAD2/3 Induce Distinct Cell Fates Independent of Activating Ligands.

As I revealed, cytokine-induced activation of the SMAD pathway leads to distinct cellular responses, such as EMT, in MCF10A cells. Building on this understanding, I aimed to answer a new question: how do single and dual pathway activations influence both immediate and prolonged cellular responses in endothelial cells, particularly focusing on how FKBP12 regulates ALK2-mediated cell fate?

To initiate this inquiry, I first wanted to understand the expression profiles of downstream genes regulated by these pathways over a brief temporal window. As expected, DLL4, a gene downregulated by the SMAD1/5/9 pathway, exhibited minimal alteration upon stimulation of the SMAD2/3 pathway (BMP7-treated and TGF-beta-treated) but demonstrated decreased expression upon activation of the SMAD1/5/9 axis (BMP9 treatment) (Figure 35A) (Rostama et al., 2015). Notably, FKBP12 degradation significantly downregulated DLL4 upon BMP7 stimulation, indicating that the FKBP12-ALK2-mediated SMAD1/5/9 pathway regulates the expression of specific downstream genes. Conversely,

genes such as ID2, which are regulated by both branches, showed different expression patterns following pathway activation. BMP7 alone increased ID2 expression, as ID2 is a downstream gene for SMAD2/3 (Figure 35A) (Veerasamy et al., 2013). The additional increase upon FKBP12 removal suggests that the FKBP12-ALK2-SMAD1/5/9 axis can regulate downstream gene expression synergistically with the SMAD2/3 pathway, further increasing ID2 expression.

To address prolonged cellular responses, I tracked individual cells over a 48-hour, quantifying the cumulative distance traversed under conditions of single pathway and dual pathway activation. My findings underscored that activation of the BMP9 treatment induced high cellular motility (Figure 35B). This high cell mobility could be entirely inhibited by inactivating ALK1 using an ALK1 inhibitor (ALK1i). Interestingly, BMP7 alone also increased cell motility (Figure 35B). Intriguingly, the removal of FKBP12 following activation of both pathways further augmented BMP7-induced single-cell movement. This enhancement was significantly mitigated by ALK4/5 inhibitors (ALK4/5i).

Next, I sought to determine whether FKBP12 influences cell fate decisions in vascular endothelial behavior. As discussed in the introduction, the SMAD pathway plays a crucial role in angiogenesis. To explore this, I employed a tube formation assay, a widely used in vitro method for evaluating the ability of endothelial cells to form capillary-like structures on an extracellular matrix. This assay effectively models the reorganization phase of angiogenesis, providing valuable insights into the angiogenic process (DeCicco-Skinner et al., 2014). To assess the role of FKBP12, I compared the tube formation capabilities of cells treated with BMP7 to those treated with BMP7 in the absence of FKBP12. Furthermore, I included a group treated with BMP9 to represent the activation of the SMAD1/5/9 pathway, thereby allowing for a broader understanding of FKBP12's role in relation to SMAD pathway signaling. The results indicated that removing FKBP12 alone does not significantly enhance the cells' tube formation ability, as measured by both tube total length and the number of nodes (Figure 35C). However, BMP9 treatment increased tube formation compared to the control group. BMP7 treatment alone markedly increased tube formation. As anticipated, cells treated with BMP7 in the absence of FKBP12 demonstrated a significant increase in endothelial behavior (Figure 35C, D). These findings corroborate the cell motility experiment, confirming that FKBP12 regulates pathway-induced cell fate decisions and influences cell behavior.

In summary, these investigations reveal the dynamic interplay within the SMAD pathway and its ramifications on cellular behavior. Understanding these intricacies holds promise for informing therapeutic interventions aimed at modulating SMAD signaling across diverse physiological and pathological contexts.

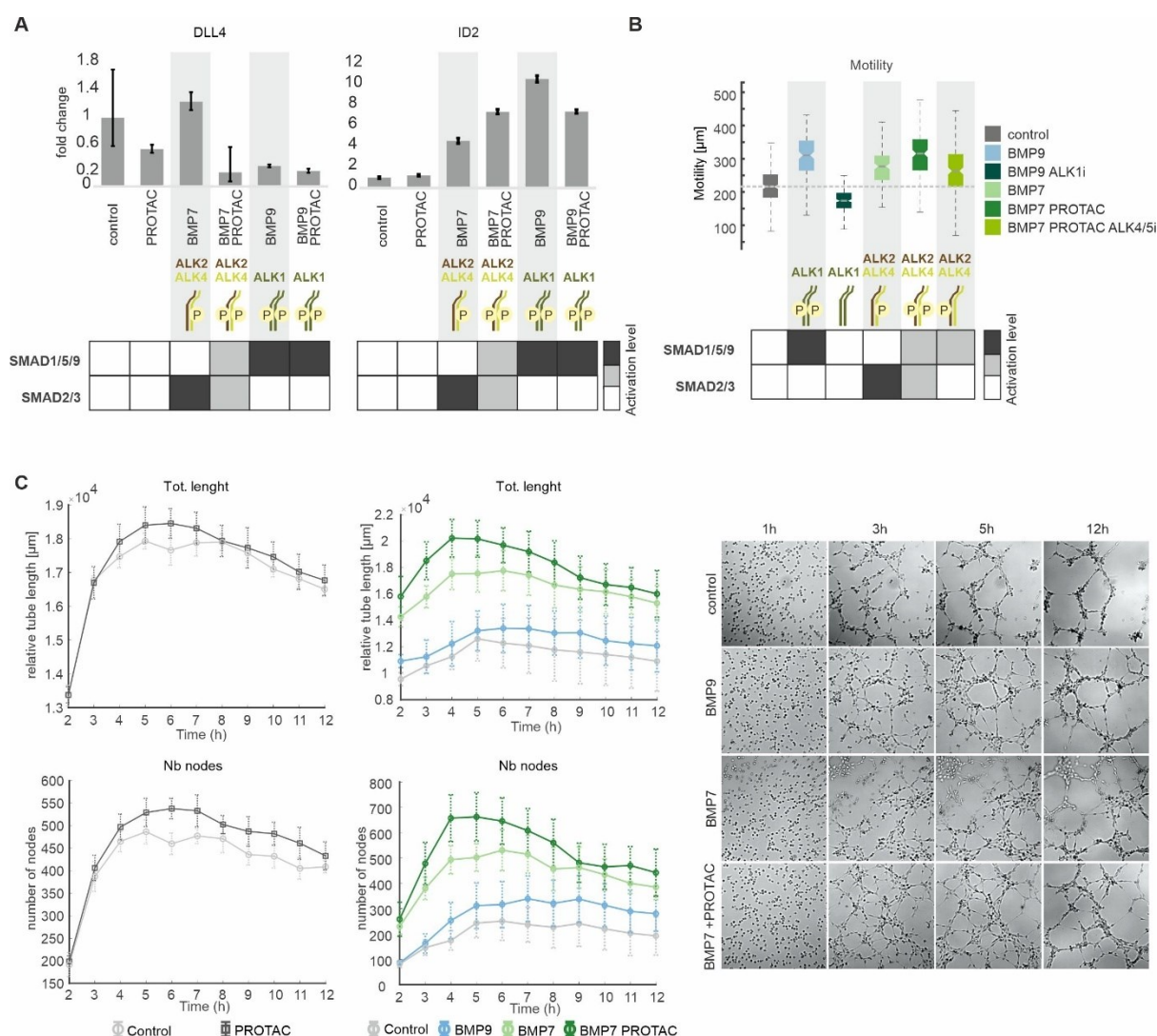


Figure 35 SMAD Activation and Downstream Effects on Gene Expression and Cellular Phenotype.

(A) The kinetics of SMAD target genes *DLL4* and *ID2* were measured by RT-qPCR in SMAD1 reporter cell lines after stimulation with BMP9 (1 ng/ml), BMP7 (250 ng/ml), and PROTAC (200 nM), with PROTAC added 24 hours prior to ligand stimulation in cells cultured in 1.5% FBS medium. Samples were harvested 1.5 hours post-stimulation, with beta-Actin serving as an internal control; error bars depict the standard deviation of technical triplicates. **(B)** Median cell motility was quantified across the population following treatment with BMP9 (1 ng/ml), BMP7 (250 ng/ml), PROTAC (200 nM), K02288 (1 µM), and SB525334 (10 µM) for 48 hours in 1.5% FBS medium. PROTAC was added concurrently, and inhibitors were administered 1 hour before ligand stimulation, with medium refreshed 24 hours post-imaging start; error bars indicate standard deviations across the cell population. Dashed lines serve as guides to the eye. **(C)** Tube formation assays were conducted by treating cells with BMP9 (5 ng/ml) and BMP7 (250 ng/ml) in 1.5% FBS medium, with or without PROTAC, for 48 hours. Cells were subsequently seeded on Matrigel and monitored via microscopy over 12 hours; tube length and nodes were quantified using ImageJ. **(D)** Representative images from the tube formation assay captured at specified time points illustrate cells treated as described in (C).

3 Discussion

3.1 Discussion of Part 1:

In this study, I aimed to understand how SMAD proteins respond to different signals and cellular conditions. Firstly, I found that the dependence of SMAD2 on cellular phenotype is closely linked to its nuclear accumulation, which is influenced both by the cell's state and by the specific ligand. Additionally, I discovered that EGF modifies the SMAD2 response network, revealing new insights into the complex interactions between signaling pathways. Through the investigation of cells with mutations in the SMAD2 linker region, I found that while this region is crucial for SMAD2's nuclear translocation, it does not alter the protein's overall responsiveness to different signals or states. Most notably, my research with SMAD3 knockout and reconstitution demonstrated that SMAD3 is essential for modulating SMAD2 responses, especially in the context of GDF11 signaling. To further elucidate the mechanisms behind state- and ligand-specific SMAD signaling, I utilized RNA-seq to identify additional proteins that influence the SMAD3-mediated GDF11-induced SMAD2 response. In this discussion, I will explore the implications of SMAD2 nuclear accumulation on cellular phenotype, delve into EGF's role in reshaping the SMAD2 response network, analyze the impact of the SMAD2 linker region on nuclear translocation and signaling, and examine SMAD3's pivotal role in modulating SMAD2 responses, particularly in relation to GDF11 signaling.

3.1.1 Conservation of SMAD Signaling Mechanisms in TGF-beta Family.

In the first part of this study, I investigated whether TGF-beta family ligands beyond TGF-beta and GDF11 could induce SMAD responses linked to cell phenotypes in both quiescent and proliferating states.

My findings highlighted a consistent correlation between SMAD nuclear accumulation and cellular phenotypes across TGF-beta, GDF11, and Activin A. This correlation was observed in both quiescent and proliferating states. Specifically, the intensity of SMAD nuclear accumulation strongly predicted cellular responses, such as changes in cell motility (Figure 6B, C) and apoptosis (Figure 6G, H). This consistency across different ligands and cellular states supports the hypothesis that SMAD nuclear accumulation acts as a universal indicator of signal strength and cellular response in TGF-beta signaling and acts as a common language through which cells interpret and respond to these diverse ligands (Bohn et al., 2023). My findings align with previous research, which emphasized the significance of SMAD nuclear translocation in signal transduction (Heldin & Moustakas, 2012; Moustakas & Heldin, 2002, 2009; Schmierer & Hill, 2007; Ten Dijke & Hill, 2004).

Besides, the roles of SMAD signaling in cancer progression are illustrated by its ability to induce epithelial-mesenchymal transition (EMT) in MCF10A cells, observed during wound healing experiments (Figure 6D, E). High SMAD activation correlates with increased EMT, making cells more cancer-like (Costanza et al., 2017; Sánchez-Tilló et al., 2012; J. Zhang et al., 2016). My observations in MCF10A cells show a pronounced induction of EMT in response to TGF-beta stimulation, resembling the behavior of advanced-stage cancer cells (Figure 6E). Specifically, this increased SMAD activation results in enhanced motility and invasiveness, as evidenced by faster wound healing, reflecting a higher migratory capacity characteristic of metastatic cancer cells (N. Dumont et al., 2003; Hao et al., 2019). Moreover, these cells exhibited morphological changes characteristic of EMT, such as the loss of cell-cell adhesion and the acquisition of an elongated, fibroblast-like shape, similar to those observed in cells treated with TGF-beta during the experiment (Figure 6E) (T. Chen et al., 2017; Marconi et al., 2021). These changes are consistent with the loss of epithelial markers (e.g., E-cadherin) and gain of mesenchymal markers (e.g., vimentin, N-cadherin) often seen in cancer cells undergoing EMT (Lamouille et al., 2014; Mittal, 2018; Rubtsova et al., 2022; Usman et al., 2021).

In summary, my study demonstrates a conserved mechanism of SMAD signaling across multiple TGF-beta family ligands and highlights the critical role of SMAD nuclear accumulation in determining cellular responses. The inclusion of Activin A provided a broader perspective, revealing that despite different response patterns, the fundamental signaling mechanism remains consistent.

3.1.2 EGF-Induced Rewiring of SMAD Signaling.

Next, I investigated how EGF influences the SMAD response in quiescent MCF10A cells, shedding light on the interplay between growth factor signaling and the TGF-beta pathway.

Previous research showed that EGF stimulation induces a shift from quiescence to active proliferation in MCF10A cells (Chou et al., 1999; LeVeal et al., 2004; Worster et al., 2012), which likely alters TGF-beta signaling by impacting receptor expression or modifying intracellular components, thereby affecting SMAD target gene accessibility. The critical role of temporal order in pathway cross-talk in determining cell fate has been highlighted by recent studies. For example, a validated multiscale systems model demonstrates that sequential BMP-2 followed by IGF-1 optimally activates key pathways—Runx2 via TAK1-p38 MAPK and SMAD1/5, and osterix and β -catenin via ERK and AKT—essential for osteoblastic differentiation and bone regeneration (Tan et al., 2017). Similarly, my results indicate that EGF enhances SMAD2 responses to TGF-beta in a time-dependent manner (Figure 7A), suggesting mechanisms such as EGF-induced upregulation of TGF-beta receptors or co-factors, alterations in signaling intermediates.

Notably, EGF's effect extends to GDF11-induced SMAD2 responses, indicating that EGF impacts TGF-beta family signaling broadly, not just TGF-beta-specific pathways (Figure 7B). This observation aligns with the concept of signaling pathway crosstalk, as elucidated by David and Massagué (David & Massagué, 2018). In their comprehensive review, they emphasized the intricate integration of TGF-beta signaling with other cellular pathways across diverse biological contexts. Additionally, my research revealed that EGF can rescue cells from apoptosis at any time, demonstrating a strong pro-survival effect (Figure 7C). This finding is consistent with studies showing that EGF protects cells by activating the PI3K/AKT pathway (Jost et al., 2001), which overrides TGF-beta-induced apoptosis by upregulating anti-apoptotic proteins like Bcl-2 and Bcl-XL. Additionally, the PI3K/AKT pathway, enhanced by EGF, is crucial for cell survival and proliferation, further supporting EGF's role in counteracting apoptotic signals (Henson & Gibson, 2006; Y. Zhang et al., 2017). The interplay between EGF and TGF-beta is vital for tissue homeostasis and regeneration, with disruptions potentially leading to pathological conditions like cancer.

3.1.3 Role of SMAD2 Linker Region Phosphorylation in Signal Integration and Cellular Response.

The impact of EGF on SMAD2 dynamics highlights a significant interaction between these pathways. Previous research by Kretzschmar demonstrated that Ras-ERK signaling can phosphorylate the SMAD2/3 linker region, affecting their activity and nuclear accumulation (Kretzschmar et al., 1999). The linker region of SMAD2 serves as a crucial integration point for various signaling inputs, enabling cells to adjust SMAD2 activity based on the cellular context (Kamoto et al., 2020; Luo, 2017; Lutz & Knaus, 2002; L. Xu, 2006). Additionally, modifications to the linker region, such as phosphorylation or ubiquitination, further regulate SMAD function (Wrighton et al., 2009; P. Xu et al., 2016). In contrast, C-terminal phosphorylation generally reflects canonical TGF-beta signaling and maintains a baseline activation state (Figure 8A) (Wrighton et al., 2009). EGF-induced phosphorylation of the linker region can impact SMAD2's interactions with transcriptional cofactors, as well as its stability and nuclear translocation (De Caestecker et al., 1998).

To investigate the function of the SMAD2 linker region, I silenced the endogenous gene and reconstituted cells with various SMAD2 mutants, enabling precise assessment of how individual phosphorylation sites affect SMAD2's nuclear translocation at the single-cell level using live-cell reporters. Specifically, not all phosphorylation sites in the SMAD2 linker region have the same regulatory effect. The loss of T220 and S255 promoted SMAD2's nuclear accumulation across TGF-beta stimulations in proliferating MCF10A cells (Figure 10C, D), whereas S245 and S250 did not (Figure 10A, B). In addition, to investigate how multiple phosphorylation sites, affect SMAD2 function, I created the SRv2 3x-mutation (S245, S250, S255) and SRv2 4x-mutation (T220, S245, S250, S255)

cell lines. The results showed increased SMAD2 nuclear accumulation with both mutations, but no additional enhancement with those two compared to the single site mutation (Figure 10E, F).

Studies indicated that phosphorylation of the SMAD linker region can prevent the SMAD complex from translocating to the nucleus, thereby inhibiting TGF-beta signaling and its downstream pathways (Kamoto & Little, 2020). For instance, in Mv1Lu cells, Mek1-mediated inhibition of Smad3 nuclear accumulation was shown to be dependent on phosphorylation within the linker domain (Kretzschmar et al., 1999). Additionally, research demonstrated that specifically inhibiting CDK4/6 in human embryonic stem cells (hESCs) using the small molecule PD0332991 led to an increased localization of SMAD2/3 in the chromatin fraction (Pauklin & Vallier, 2013). However, the specific mechanisms by which phosphorylation at various sites influences SMAD localization and transcriptional activity remain unclear. My research provides insights into how both single-site and multi-site phosphorylations affect SMAD2 nuclear shuttling, highlighting the critical role of the linker region in non-canonical SMAD pathways.

Interesting, despite the introduction of multiple mutations in the linker region, the SMAD response pattern to TGF-beta stimulation remained comparable to that of the wild-type SMAD2. Specifically, both the SRv2 3x-mutation and SRv2 4x-mutation clones exhibited similar dose-dependence in their SMAD2 responses (Figure 10G) and showed that their translocation was still dependent on ALK5 (Figure 10H). This observation supports that, despite the modification of the linker region, the C-terminal phosphorylation of SMAD2 plays a crucial role in its regulation (Macias et al., 2015; Wrighton et al., 2009). In conclusion, these findings underscore the robustness and adaptability of SMAD2 regulation, which is crucial for effectively integrating and responding to multiple signaling pathways.

In examining the role of EGF-mediated SMAD2 linker region phosphorylation, it's essential to consider how this modification influences SMAD2 dynamics across different cell states. To address this, I extended the analysis to quiescent cells.

The rationale behind using the SRv2 4x-mutation was based on the hypothesis that if EGF-mediated phosphorylation significantly impacts the linker region, then this mutation would alter SMAD2 responses pattern between proliferating and quiescent states. Contrary to expectations, SRv2 4x-mutation cells exhibited a significantly reduced response to TGF-beta stimulation compared to proliferating cells, similar to the response in quiescent SRv2 WT cells, suggesting that the linker mutations alone do not restore the SMAD response to proliferating cell levels (Figure 11A, B). Interestingly, despite the quiescent state, the SRv2 4x-mutation cells exhibited enhanced SMAD2 nuclear translocation upon TGF-beta stimulation relative to SRv2 WT cells (Figure 11B). This enhanced response was also observed with GDF11 treatment, confirming that the effect is not limited to TGF-beta (Figure 11C, D). This aligns with other findings, which highlighted the linker region's role

in modulating SMAD2's activity and subcellular localization (Burch et al., 2011; Kamato et al., 2013). My results further emphasize that the linker region modulates SMAD2's activity and localization regardless of the cell's state. This consistent response pattern supports the idea that the linker region primarily modulates the strength of the signaling response rather than its specificity (Feng & Derynck, 2005).

3.1.4 Impact of Receptor Expression and SMAD Proteins on TGF-beta Signaling.

The SMAD2 C-terminal region is crucial for regulating its shuttling and activation, especially in the context of EGF's indirect effects (Derynck & Budi, 2019; Javelaud & Mauviel, 2005). Variations in receptor expression between quiescent and proliferating cells can alter SMAD2 dynamics (Bhaskaran et al., 2007). This flexible regulation of receptor expression allows cells to adjust their response to TGF-beta based on their physiological state or developmental stage.

Our previous RNA-seq data showing changes in TGFBR2 expression support the idea that receptor levels may influence SMAD2 dynamics across different cell states (Figure 11A). The observation of decreased TGFBR2 expression in growth-factor deprived cells highlights how cellular state impacts signaling sensitivity. Notably, EGF treatment can restore TGFBR2 levels. Further investigation into whether TGFBR2 overexpression can partially restore SMAD2 activation in quiescent cells could shed light on the role of receptor expression in pathway activation.

While receptor expression levels are crucial, the role of SMAD proteins, particularly SMAD3, is also important in regulating cellular responses to TGF-beta. Unlike SMAD2, SMAD3 exhibits varying expression levels across different cell states (Figure 11B).

Functionally, SMAD2 and SMAD3 respond differently to TGF-beta signaling. SMAD2 remains in the cytoplasm until phosphorylated by TGF-beta receptors, after which it forms a complex with SMAD4 and translocates to the nucleus to regulate target gene expression (Moustakas & Heldin, 2009; Nakao, Imamura, et al., 1997; Tzavlaki & Moustakas, 2020). Research using single-molecule Förster resonance energy transfer data demonstrate that, in TGF-beta1-treated cells, Smad2/Smad4 heterocomplexes concentrate in the nucleus due to a nuclear import rate that is almost four times higher than their export rate, whereas in the absence of TGF-beta1, Smad2 and Smad4 fail to accumulate in the nucleus because their nuclear export efficiency is approximately twofold greater than their import rate (Li et al., 2018). In contrast, research shown that in HEK 293 cells, SMAD2, is phosphorylated by activated type I receptors and then forms a robust complex with SMAD4, which efficiently translocates into the nucleus to regulate target genes. SMAD3 predominantly resides in the nucleus even in the absence of stimulation, resulting in its reduced ability to be recruited by activated receptors for phosphorylation and thus limiting its role as a signaling transducer. Additionally, SMAD3 shows weaker interaction

with SMAD4, even when its SSXS motif is phosphorylated, highlighting a differential binding affinity compared to SMAD2 (L. Liu et al., 2016). This constitutive presence in the nucleus suggests that SMAD3 may play a critical role in maintaining basal transcriptional activity and ensuring the readiness of the TGF-beta pathway.

This could be particularly important for processes that require constant regulation, such as cell cycle control, differentiation, and maintaining cellular homeostasis. For example, in certain cellular contexts, SMAD3 might be involved in regulating genes that are essential for maintaining the epithelial phenotype or preventing uncontrolled cell proliferation (Flanders, 2004; Hata & Chen, 2016; Mithani et al., 2004). Additionally, SMAD3 expression is regulated by the MEK1/ERK pathway (Kretzschmar et al., 1999; Ross et al., 2007), linking MAPK and TGF-beta pathways and influencing cellular behaviors such as migration, proliferation, and apoptosis (Ma et al., 2024; Papageorgis & Stylianopoulos, 2015). For instance, in breast cancer cells, ERK-mediated phosphorylation of SMAD3 has been shown to inhibit its anti-proliferative effects, thereby promoting tumor growth (Matsuura et al., 2005). Given these complexities, I investigated how the absence of SMAD3 affects SMAD2 responses by removing SMAD3 from reporter cells.

3.1.5 SMAD3 Knockout Reveals Ligand-Specific Regulation of SMAD2 Dynamics.

In SMAD3 knockout cells, the effects of SMAD3 enhance SMAD2 responses to GDF11 stimulation (Figure 14D). Interestingly, the absence of SMAD3 did not alter the SMAD2 response to TGF-beta stimulation, which remained consistent across different cell states (Figure 14E). This specificity highlights the unique role of SMAD3 in GDF11-mediated pathways, as opposed to broader TGF-beta signaling. By applying different ligands from the TGF-beta family, my results confirmed that the ligand-specific role of SMAD3 in regulating SMAD2 responses is evident for GDF8 and GDF11, but not for other ligands (Figure 15A).

GDF8, also known as myostatin, and GDF11 are both members of the TGF-beta superfamily and share about 90% amino acid sequence identity in their mature forms (Suh & Lee, 2020; Walker et al., 2017). They signal through similar receptors, primarily activin type II receptors (ActRIIA and ActRIIB) and ALK4/5/7 type I receptors. For those reason, it is not surprising that GDF8 and GDF11 had similar effects on SMAD2 dynamics.

In the EGF pre-incubation experiment, I found that EGF rescues SMAD2 translocation and reshapes SMAD2 shuttling in response to both TGF-beta and GDF11, with this effect requiring approximately three hours of pre-incubation (Figure 7C). Initially, I assumed the underlying mechanism was similar for both ligands; however, SMAD3 knockout investigation revealed significant differences in their regulatory networks. The SMAD2 response to TGF-beta is independent of SMAD3, whereas the

response to GDF11 is entirely dependent on SMAD3. This distinction highlights the non-redundant roles of SMAD2 and SMAD3, even though both ligands activate the SMAD2/3 pathway. Additionally, Activin A, which uses receptors similar to those of GDF11, elicits a SMAD2 response independent of SMAD3 in both cell states, further emphasizing the unique regulatory mechanisms of each ligand.

3.1.6 Dissecting the Roles of SMAD2 and SMAD3 in Cellular Apoptosis and Motility.

Following, I investigated the impact of SMAD3 removal on cellular outcomes. My results show that while removing SMAD3 significantly reduces apoptosis in MCF10A cells, it does not eliminate it entirely (Figure 16B). This finding contrasts with microarray analysis showing that, out of 2,039 TGF-beta-regulated target genes, 190 are differentially controlled by SMAD2-SMAD4 versus SMAD3-SMAD4 signaling, with SMAD3-SMAD4 signaling being more crucial for TGF-beta-induced apoptosis in Hep3B cells through the up-regulation of cell death (Yu et al., 2008). In MCF10A cells, both SMAD2 and SMAD3 play roles in apoptotic signaling, potentially through overlapping or distinct sets of pro-apoptotic genes. This partial redundancy may serve as a safeguard to ensure that apoptotic pathways remain functional even when one SMAD protein is missing.

Moreover, my results indicate that SMAD3, rather than SMAD2, primarily regulates cell mobility genes in MCF10A cells (Figure 16D, E). This aligns with the established role of SMAD3 in facilitating TGF-beta-induced EMT and cell migration (H. Yu et al., 2008). Specifically, SMAD3 is essential for the expression of genes involved in cytoskeletal reorganization, cell adhesion, and extracellular matrix remodeling (Arany et al., 2006). For example, SMAD3 regulates the alternative splicing of CD44, a gene critical for cell migration and adhesion, through phosphorylation events that enhance its activity in cancer cells (Tripathi et al., 2016). Additionally, the activation of HER2/EGFR signaling pathways can alter TGF-beta's role from inhibition to promotion of cancer progression by phosphorylating SMAD3, further emphasizing SMAD3's pivotal role in cell motility and EMT (F. Huang et al., 2018).

Interestingly, the correlation between SMAD2 nuclear accumulation and cell motility—reflecting SMAD3 function—highlights their interaction, likely due to heteromeric complexes between SMAD2 and SMAD3 that translocate to the nucleus together (Hill, 2009). Thus, SMAD2's nuclear presence may indicate SMAD3 activity.

In addition, removing SMAD3 from the SRv2 4x-mutation clones did not significantly impact SMAD2's functionality, contrary to initial expectations. Specifically, while deleting the SMAD2 linker region increased its nuclear accumulation, it did not alter SMAD2's response to ligands, cell state, or the presence of SMAD3 (Figure 17B, C). These results suggest that although the linker region contributes to regulating SMAD2, its loss does not disrupt SMAD2's nuclear accumulation or its

response to external signals. Thus, in MCF10A cells, the linker region's role in SMAD2's nuclear translocation appears to be less critical than previously thought.

3.1.7 Exploring SMAD3's Role in SMAD2 Modulation.

To explore whether reintroducing SMAD3 into SRv2 WT SMAD3KO cells would affect the SMAD2 response to GDF11 in proliferating cells, I utilized a double reporter system. This system provided a more detailed comparison of SMAD2 and SMAD3 dynamics compared to traditional methods like Western blotting or immunofluorescence.

My double reporter system revealed that SMAD2 and SMAD3 respond similarly to high doses of TGF-beta in MCF10A cells, both relying on ALK5 for activation (Figure 19B). As ALK5 phosphorylates both SMAD2 and SMAD3 at the C-terminal SXS motif, crucial for their activation and nuclear translocation (Ten Dijke & Hill, 2004). Notably, the nuclear-to-cytoplasm translocation times for SMAD2 and SMAD3 were nearly identical, even with ALK5 inhibition, suggesting similar activation and translocation dynamics under these conditions. This contrasts with the results from part two, where SMAD1, SMAD5, and SMAD9 showed distinct nuclear-to-cytoplasm translocation times (Figure 27H). My dose titration experiments with TGF-beta further support the similar behaviors of SMAD2 and SMAD3 (Figure 19C). Both proteins showed dose-dependent activation in quiescent and proliferating cells, consistent with Zi, who observed that TGF-beta levels regulate SMAD protein activation precisely (Zi et al., 2012).

Using my double reporter clone, I confirmed that SMAD3 modulates SMAD2 activity during GDF11 stimulation (Figure 20A). This effect was consistent in both proliferating and quiescent cells, indicating that SMAD3's regulation of SMAD2 is effective across different cell states. However, the unexpectedly weak SMAD2 response in quiescent cells suggests that cells, even in a non-dividing state, maintain some responsiveness to GDF11 mediated by SMAD3. This supports the idea that SMAD3 actively modulates SMAD2 rather than being a passive participant.

Further experiments with various SMAD3 clones, each exhibiting different levels of overexpression, revealed that SMAD3 has a dose-dependent effect on the GDF11-mediated SMAD2 response in both quiescent and proliferating cells (Figure 21A). This highlights the essential role of SMAD3 in gene regulation and points to the often-overlooked balance between SMAD2 and SMAD3 expression. SMAD2 and SMAD3 can form different complexes with SMAD4—namely, S2S4, S3S4, and S2S3S4—each influencing gene regulation in unique ways. Massagué demonstrated that these complexes regulate distinct target genes (Massagué et al., 2005). For instance, the Mix2 promoter may be targeted by a heterotrimeric S2S4 complex bound to FoxH1, while a S3S4 heterodimer, along with an unknown cofactor, may target the JunB promoter (G. J. Inman & Hill, 2002).

The balance between SMAD2 and SMAD3 levels is crucial in determining the formation of these complexes (Brown et al., 2007). Higher levels of SMAD2 favor the formation of S2S4 complexes, whereas higher levels of SMAD3 promote the formation of S3S4 and S2S3S4 complexes. This balance is vital not only for cellular responses but also for maintaining homeostasis. Early research indicates that proteins like TLP exist to regulate this balance. TLP modulates TGF-beta signaling by influencing the SMAD2 and SMAD3 pathways, enhancing SMAD2/4-mediated transcription while repressing SMAD3/4 signaling, potentially by regulating the intracellular localization of SMAD4 (Felici et al., 2003). This comprehensive understanding of how SMAD3 modulates SMAD2 activity across different cellular states, along with the impact of their complex formation and the role of regulatory proteins like TLP, highlights the intricate balance essential for precise TGF-beta signaling and its diverse biological outcomes.

Interestingly, SMAD3's regulatory effect on SMAD2 was specific to GDF11, as it did not alter SMAD2's response to TGF-beta. This specificity, observed also in SMAD3 knockout cells, reinforces that SMAD3's regulation of SMAD2 varies depending on the ligand. I therefore explore the specificity of SMAD3 in modulating SMAD2 responses to various ligands, including GDF8, Activin A, and GDF3. My findings reveal that reconstituting SMAD3 specifically attenuates the SMAD2 response to GDF8 and GDF11, but not to Activin A and GDF3 (Figure 22A), which aligned with the SMAD3 KO result.

In summary, my findings emphasize the crucial role of SMAD3 in modulating SMAD2 activity, especially in response to GDF11, and highlight the importance of balancing SMAD2 and SMAD3 expression due to their dose-dependent effects and specific regulatory impacts.

3.1.8 Upstream Regulation of SMAD3 and Its Impact on SMAD2 Dynamics.

In this section, I investigate the upstream regulation of SMAD3 and its role in modulating SMAD2 responses to GDF11, focusing on the expression and activation of phosphorylated SMAD3 in different cellular contexts and the impact of EGF and ALK5 on this process.

My western blot results reveal significant differences in p-SMAD3 activation between quiescent and proliferating cells, with elevated levels in proliferating cells (Figure 23A). Besides, the interaction between EGF signaling and TGF-beta pathways adds another layer to SMAD3 regulation. My findings indicate that EGF affects p-SMAD3 levels, highlighting significant cross-talk between these pathways. This is supported, who reported that EGF receptor signaling can modulate TGF-beta pathways (Q. Shi & Chen, 2017). Furthermore, the dependency of p-SMAD3 activation on ALK5 is particularly noteworthy. This finding is consistent with Goumans, who demonstrated ALK5's essential role in SMAD3 activation in endothelial cells (Goumans et al., 2002).

Following, the wash-off experiment revealed that ALK5 inhibition enhances SMAD2 responses to GDF11, but not to TGF-beta (Figure 23C). This context-specific modulation aligns with previous studies demonstrating that SMAD2 and SMAD3 interact differently depending on the ligand and cellular environment. Goumans demonstrated that ALK5 is crucial for TGF-beta signaling and that its inhibition can shift downstream signaling dynamics (Goumans et al., 2002). My study extends this understanding by showing that this shift specifically affects SMAD2 dynamics in response to GDF11, rather than TGF-beta.

In addition, my double reporter system revealed that inhibiting ALK5 enhances the GDF11-induced SMAD3 response, suggesting that SMAD3 can regulate its own signaling, not just influence SMAD2 (Figure 23D). This self-regulation connects with another mechanism in the SMAD pathway known as "self-enabling" (Ten Dijke & Hill, 2004). In "self-enabling" TGF-beta transcriptional responses, SMAD target genes, once activated, reinforce and sustain the TGF-beta signaling. For instance, during NODAL/Activin signaling, SMAD2 not only opens chromatin on a genome-wide scale but also initiates a self-enabling transcriptional cascade where activated SMADs, along with transcription factors like ZIC3, promote the expression of genes such as WNT3. This, in turn, cooperates with SMAD pathways to sustain and amplify delayed gene expression (Coda et al., 2022). While both mechanisms enhance the TGF-beta pathway, SMAD3 self-regulation focuses on fine-tuning the pathway's immediate response, whereas self-enabling loops ensure that the pathway's effects are sustained over time. Together, these concepts illustrate the complexity of TGF-beta signaling, where different layers of regulation ensure that cellular responses are both precise and enduring, crucial for processes such as development, differentiation, and disease progression.

In conclusion, my study sheds light on the complex and context-specific modulation of SMAD2 dynamics by SMAD3, with a particular focus on ALK5-dependent mechanisms.

3.1.9 Exploring SMAD2-Regulation through Gene Expression Profiling.

By comparing gene expression profiles across experimental conditions and SvR2 WT cells, my RNA-seq analysis provided candidates which might alter the SMAD2 response network (Figure 24 D, E).

Moustakas and Heldin emphasized the importance of cellular context and ligand type in determining TGF-beta signaling outcomes, suggesting that extracellular factors modulate ligand-receptor interactions and subsequent signaling responses (Moustakas & Heldin, 2009). Membrane proteins are vital for cellular signaling due to their direct interactions with receptors and co-receptors (Nickel et al., 2018; Pawlak & Blobel, 2022). For instance, the Smad anchor for receptor activation (SARA) protein was identified as a key regulator that facilitates the localization of SMADs to TGF-beta receptors during the activation of TGF-beta signaling (Rozés-Salvador et al., 2018). This supports the notion that

membrane proteins regulate SMAD2 responses in a context-dependent manner. Secreted proteins also play a critical role in regulating SMAD signaling. These proteins can act as antagonists or inhibitors, binding to ligands and preventing their interaction with receptors, which in turn alters downstream signaling. Massagué discussed how extracellular antagonists shape cellular responses, which changes in secreted protein expression can influence SMAD2 activation based on the cellular context (Massagué, 2012).

However, studies of LTBP2, MMP9, and PMEPA1 in SMAD3KO cells revealed that restoring their expression did not significantly alter SMAD2 responses to GDF11 or TGF-beta (Figure 25D). One possible explanation for the lack of effect is that the overexpression levels of these proteins may have been too low to significantly influence SMAD2 signaling. For example, in rescue experiments, LTBP2 expression was lower than in control cells, indicating that higher expression levels might be required for a functional impact. This highlights the importance of having sufficient levels of signaling components, as their abundance is crucial for pathway output and achieving significant effects (Lee & Yaffe, 2016). Another possibility is that effective regulation of SMAD2 signaling relies on the coordinated action of multiple proteins, rather than the overexpression of just one. Similar to how extracellular matrix components and secreted factors collectively regulate TGF-beta signaling, a balanced interaction among various proteins may be necessary for proper SMAD2 activity (Verrecchia & Mauviel, 2002).

Future research should focus on exploring the combined effects of multiple proteins on SMAD2 signaling. Techniques such as combinatorial overexpression, gene editing to restore multiple components, and high-throughput screening could provide deeper insights into these regulatory mechanisms.

3.1.10 Future research.

The research still leaves open questions regarding the key proteins that regulate and influence SMAD2 responses based on ligand type and cellular state. Future work should focus on identifying these critical proteins and their impact on SMAD2 signaling. Our RNA-seq results indicate that Decorin (DCN) is upregulated in quiescent cells. DCN is known to sequester TGF-beta, which could potentially impact EGFR signaling as well (Hildebrand et al., 1994; Kolb et al., 2001; Zafiropoulos & Tzanakakis, 2008). Future studies should explore whether elevated levels of DCN in quiescent cells inhibit TGF-beta binding and affect SMAD2 activation.

Additionally, other proteins from my list, such as ligand traps and membrane proteins, may modulate SMAD signaling. While my focus has been on the downregulated genes, it is also crucial to examine the upregulated genes. For example, the upregulation of p-SMAD3 in proliferating cells and its rescue

by EGF in quiescent cells indicate that SMAD3 activation in proliferating cells increases some inhibitors, which ultimately inhibit the GDF11-induced high SMAD2 response. Overall, focusing on these areas could advance our understanding of how specific proteins influence SMAD2 responses and contribute to the regulation of TGF-beta signaling.

Results from the second part of the study suggest crosstalk between the SMAD2/3 and SMAD1/5/9 pathways. It is possible that the SMAD1/5/9 pathway could influence the SMAD2 response during changes in cellular states. Future research should investigate how the activation of the SMAD1/5/9 pathway impacts the SMAD2/3 pathway upon two cell states. Specifically, it is crucial to determine whether SMAD1/5/9 activation synergizes with or antagonizes SMAD2/3 signaling. To explore this further, creating a dual-reporter cell line that uses different fluorescent markers SMAD1 and SMAD2 could help track both pathways in real time, showing how they interact within the single cell.

3.2 Discussion of Part 2:

This study aimed to elucidate the dynamics and regulatory mechanisms underlying SMAD activation in the BMP signaling pathway. Through the development of fluorescent reporter cell lines for SMAD1, SMAD5, and SMAD9 in human vascular endothelial cells, I have uncovered several key findings. First, I observed qualitatively similar but quantitatively distinct dynamics in SMAD1, SMAD5, and SMAD9 translocation in response to BMP9 stimulation. Second, and perhaps most importantly, I identified FKBP12 as a critical inhibitor of ALK2-mediated SMAD activation, effectively modulating the balance between SMAD1/5/9 and SMAD2/3 activation in a ligand-specific manner. Third, using a dual reporter system, I revealed dynamic shifts in the activation of SMAD1 and SMAD2 during concurrent ligand stimulation following FKBP12 removal. In this discussion, I will first examine the differential dynamics of SMAD1, SMAD5, and SMAD9 activation, followed by an analysis of the pivotal role of FKBP12 in modulating SMAD activation. I will then explore the implications of FKBP12 removal on the balance between SMAD1/5/9 and SMAD2/3 signaling, and conclude with a consideration of the potential impact of our findings on understanding and treating vascular disorders.

3.2.1 Live-Cell Imaging of SMAD Dynamics in Response to BMP9 Stimulation.

In the first part of my study, I established SMAD reporter system and used time-resolved imaging to observe SMAD behavior in the endothelial cell line EA.hy926. By investigating SMAD1 dynamics in response to BMP9, I was able to provide comprehensive insights into the differential activation of SMAD1, SMAD5, and SMAD9.

My results demonstrate that SMAD1, SMAD5, and SMAD9 exhibit dose-dependent responses to stimulation (Figure 27C, 39B, H), which aligns with our previous findings showing similar patterns for SMAD2 and SMAD3 in MCF10A cells (Figure 19C, 20B). This consistent behavior across different SMAD proteins suggests that the SMAD pathway functions as a unified signaling mechanism, with all SMAD proteins responding proportionally to varying input levels.

The dose-dependent nature of SMAD activation is particularly relevant in the context of embryonic development, where TGF-beta family ligands often act as morphogens. These morphogens create concentration gradients that induce distinct cell fates along their distribution (Green & Smith, 1990; Gurdon et al., 1994). My findings support the notion that differential TGF-beta receptor occupancy, resulting from varying ligand concentrations, leads to graded levels of SMAD activation (Dyson & Gurdon, 1998). This graded activation can, in turn, induce different sets of target genes, thus facilitating the diverse cellular responses observed in developmental processes (Schmierer & Hill, 2007; Ten Dijke & Hill, 2004; Wilson et al., 1997).

One of the most intriguing findings from our imaging studies was the preferential activation of SMAD1 over SMAD5 and SMAD9 at lower BMP9 concentrations (Figure 27D, Figure 39C, I). As BMP9 concentrations increase, the involvement of SMAD5 becomes more pronounced, indicating its role in modulating more robust vascular responses, such as inhibiting angiogenesis and balancing vascular maintenance with new vessel formation (Benn et al., 2020; Yang et al., 1999). Interestingly, RNA-seq data from EA.hy926 cells revealed that SMAD5 expression levels are higher than those of SMAD1 and SMAD9 (Figure 41A). The significance of SMAD5 in vascular biology is further underscored by studies showing that endothelial-specific deletion of *Smad5* leads to embryonic lethality due to cardiovascular defects (Chang et al., 1999). This highlights that while SMAD1 and SMAD9 may respond to lower BMP9 levels, SMAD5 plays a critical role in mediating robust BMP9 signaling essential for vascular development and function.

BMP9 is constitutively produced by the liver and secreted into the bloodstream (Bidart et al., 2012). Physiological concentrations in human circulation range from 2-12 ng/ml (L. David et al., 2007). Although circulating BMP9 levels are relatively high, the effective concentration at the cellular level can vary significantly due to factors such as extracellular matrix composition, co-receptors, and local BMP9 antagonists (L. David et al., 2007, 2008). This may explain why EA.hy926 cells maintain sensitivity to lower BMP9 concentrations as observed in my experiments. The local microenvironment allows for BMP signaling control in different tissues and physiological conditions, enabling cells to respond appropriately to both subtle changes and substantial fluctuations in BMP levels (Migliorini et al., 2020).

Following my investigation into SMADs responses to BMP9, I examined the dynamics of SMAD C-terminal activation via ALK1. My findings confirm that the nuclear shuttling of SMAD1, SMAD5, and SMAD9 is mediated by the ALK1 receptor (Figure 27E, Figure 39C, I). Besides, I observed that SMAD proteins show varying sensitivities to different concentrations of the ALK1 inhibitor, with SMAD1 being more sensitive to low doses (Figure 27F, Figure 39E, K). This supports my earlier conclusions about the differential sensitivity of SMADs to BMP9 signaling.

This observation of extended nuclear retention for SMAD9 suggests it may have distinct functional characteristics or regulatory mechanisms (Figure 27H). David's kinetic model of Smad signaling showed that R-SMAD nuclear accumulation is highly influenced by the rates of phosphorylation, dephosphorylation, and R-SMAD/Co-SMAD complex dissociation (Clarke & Liu, 2008). These findings suggest that the distinct nuclear retention of SMAD9, compared to SMAD1 and SMAD5, could be due to differences in these key processes. The duration of SMAD proteins' nuclear retention plays a critical role in TGF-beta signaling, with sustained SMAD activity in epithelial cells leading to growth arrest, while transient responses in pancreatic tumor cells enable them to avoid growth arrest but still respond to TGF-beta (Nicolás & Hill, 2003; Ten Dijke & Hill, 2004). SMAD9's longer nuclear

retention may be crucial for contexts requiring sustained gene expression, such as in vascular development (Z. Huang et al., 2009). In contrast, the shorter nuclear retention of SMAD1 and SMAD5 could facilitate rapid responses to stress, enabling quicker adaptation to changing conditions. Further research is needed to fully elucidate the functional implications of these differences in nuclear retention.

The prolonged nuclear retention of SMAD9 suggests it could play a key role in sustaining BMP9 signaling activity even after the initial stimulus has diminished. In pathological contexts like pulmonary arterial hypertension (PAH), where BMP2 mutations reduce pathway activity, SMAD9's extended nuclear presence could serve as a compensatory mechanism, partially offsetting the decreased signaling. This could explain why SMAD9 mutations are associated with PAH development; if SMAD9 acts as a backup system for BMP signaling in the presence of BMP2 mutations, mutations in SMAD9 would eliminate this compensation, exacerbating signaling deficiencies and contributing to PAH pathogenesis (Figure 5C) (Shintani et al., 2009).

Compared to SMAD1 and SMAD5, SMAD9 has received less research focus. However, my results represent the first comprehensive comparison and quantification of SMAD behavior in live cells, highlighting differences between these three SMADs. This suggests that SMAD9 might serve a specialized role in BMP signaling, potentially offering a unique mechanism to modulate the duration and specificity of gene expression.

Future research should explore gene expression profiles associated with prolonged SMAD9 nuclear localization versus SMAD1 and SMAD5. Investigating how SMAD9's extended nuclear presence correlates with sustained gene expression of critical markers like FOXE3 (Yoshimoto et al., 2005), compared to the more transient regulation by SMAD1 and SMAD5, will provide deeper insights into their functional specificity. Moreover, combining this with downstream gene reporter assays and advanced computational modeling could offer a comprehensive picture of SMAD signaling pathways at a single-cell level. Additionally, the observed differences in sensitivity between SMAD1, SMAD5, and SMAD9 may be due to structural variations. SMAD activation begins when the receptor interacts closely with the SMAD proteins, leading to their activation and subsequent shuttling into the nucleus. In future studies, based on the results from my experiments, we can continue to investigate if the affinity between the receptor and different SMADs is different. To this end, we can collaborate with researchers specializing in protein structure and combine our reporter system, mutating different parts of the SMADs—particularly the parts crucial for receptor-mediated activation—to figure out why they work differently.

In summary, my research contributes significantly to our understanding of SMAD dynamics by employing live-cell imaging to observe SMAD behavior at the single-cell level. This work reveals the

differential sensitivity and nuclear retention times of SMAD1, SMAD5, and SMAD9, highlighting the specialized roles these proteins play in BMP signaling.

3.2.2 Investigating the Role of FKBP12 and Non-Signaling Complexes (NSCs) in BMP Signaling.

Next, I performed a ligand screening experiment to analyze SMAD dynamics in response to various ligands. BMP ligands are produced in partially overlapping patterns, and genetic studies indicate that closely related BMP family members can activate the BMP signaling pathway via SMAD1/5/9. This activation leads to downstream gene expression and results in functional redundancy among these ligands, as demonstrated by Dudley and Robertson, Lyons, and Solloway and Robertson (Dudley & Robertson, 1997; Lyons et al., 1995; Solloway & Robertson, 1999). Research has shown that BMP4 can effectively substitute for BMP7 in kidney development, underscoring the interchangeable nature of BMP family members in crucial signaling pathways for organogenesis (Oxburgh et al., 2005). Additionally, a certain threshold level of BMP signaling is essential for chondrogenesis. Although BMP2 and BMP4-deficient limbs may fail to form some chondrogenic condensations, differentiation can proceed normally without BMP2 and BMP7 or BMP2 and BMP4. However, the absence of both BMP2 and BMP4 severely disrupts osteogenesis, leading to limb deformities (Bandyopadhyay et al., 2006). Those substantial evidence highlights the functional redundancy of BMP signals (Arnold et al., 2006). The ongoing presence of functional redundancy among BMP ligands through evolution prompts an inquiry into their roles in regulating cellular functions. To explore this, I plan to use various ligands as inputs and study the SMAD protein responses in vascular system.

My results revealed a surprising specificity: only BMP9 and BMP10 induced strong SMAD1/5/9 responses, as confirmed by both western blot analysis (Figure 28A) and live-cell imaging (Figure 28B). Research has shown that BMP9 can activate the BMP response element (BRE) at concentrations as low as 0.01 ng/mL (L. David et al., 2007), a sensitivity confirmed by my live-cell imaging (Figure 27C). The potency of BMP9 and BMP10 in activating SMAD1/5/9 signaling can be primarily attributed to the predominant expression of their type I receptor, ALK1, in vascular endothelial cells (Figure 28A) (Desroches-Castan et al., 2022). Besides, the high sensitivity of BMP9 and BMP10 can also be attributed to their exceptionally high affinity for the ALK1 receptor (Desroches-Castan et al., 2022).

In contrast, other BMPs, which signal through alternative receptors such as ALK2, ALK3, or ALK6, exhibited limited activity in my experimental system (Figure 28A, B), which raises questions about BMP signaling specificity in vascular biology. First reason is that the differential expression levels of BMP receptors significantly influence signaling dynamics. For example, ALK3 (BMPRI1A) and ALK6 (BMPRI1B) receptors for BMP2 and BMP4 are expressed at lower levels compared to ALK1 (Figure 28A). This disparity in receptor expression could affect signaling dynamics, as high ALK1 expression

may preferentially drive the formation of ALK1-type II receptor heterodimers, which are highly responsive to BMP9 and BMP10 but not to BMP2 or BMP4 (Mitchell et al., 2010). Consequently, the limited availability of type II receptor may prevent effective signaling through their respective pathways, even in the presence of BMP2.

Another contributing factor may be the presence of different inhibitors within the SMAD signaling pathway. Although high concentrations of ligands were used to overcome potential extracellular inhibition, intracellular inhibitors such as SMAD6 and SMAD7 could still mask weak SMAD responses (Miyazawa & Miyazono, 2017). For instance, Smad6 inhibits BMP/Smad1 signaling in *Xenopus* embryos and mammalian cells by competing with Smad4 for binding to phosphorylated Smad1, forming an inactive Smad1-Smad6 complex and acting as a Smad4 decoy (Hata et al., 1998). In addition, the composition of the extracellular matrix and the presence of specific co-receptors also significantly influence ligand availability and signaling efficiency. Heparan sulfate proteoglycans (HSPGs) modulate the activity of BMP ligands, potentially contributing to the observed specificity (O'Connell et al., 2007; Rider & Mulloy, 2017; Xie & Li, 2019). Studies have shown that heparinase, present in my EA.hy926 culture medium, diminishes BMP2 signaling in C2C12 cells (Jiao et al., 2007). This could explain why BMP2 did not induce a strong SMAD response in my reporter system.

The final factor contributing factor to the observed phenomenon may be the presence of non-signaling complexes (NSCs) in the BMP signaling pathway. One type of NSC involves Activin A binding to ALK2-type II receptor complexes, which prevents both the ligand and receptors from participating in signaling with other ligands, such as BMPs (Aykul et al., 2020; Olsen et al., 2015). Another type includes FKBP12, which binds to type I and II BMP receptors, forming inactive tetrameric complexes before ligand binding (Quist-Løkken et al., 2023). These FKBP12-containing complexes help maintain signaling homeostasis and prevent inappropriate activation of the pathway in the absence of ligands (Sánchez-Duffhues et al., 2015). Following the discovery that FKBP12 is the NSC factor within our experimental system, my investigation using FKBP12 PROTAC highlighted the pivotal role of FKBP12 in modulating the SMAD response to BMP7 and Activin A (Figure 29 C, D).

Interestingly, my observations reveal that ligands capable of utilizing ALK2 as a type I receptor, such as BMP9 and BMP10 (Quist-Løkken et al., 2023), did not show a significant increase in signaling upon FKBP12 degradation (Figure 42A). This finding suggests that BMP9 and BMP10 might have a higher affinity for other receptors, like ALK1, which could be primarily responsible for their strong SMAD1/5/9 responses (Townson et al., 2012). In contrast, BMP2 induces only a minimal SMAD1/5/9 response when FKBP12 is present, and this response remains unchanged even after FKBP12 is removed (Figure 42A). Previous studies suggested that BMP2, BMP4, and BMP10, which normally signal through ALK3, can instead signal through ALK2, provided that FKBP12 is removed and BMP2 is present (Quist-Løkken et al., 2023). However, my results do not support this result. This discrepancy

suggests that BMP2 signaling may involve the formation of heterodimeric complexes with other BMP ligands for effective receptor activation, or other factors might be influencing BMP2 signaling in my experimental system. Moreover, BMP6 raises additional questions. Although BMP6 and BMP7 share structural similarities and use the same receptor for pathway activation, they exhibit distinct functional properties (Gipson et al., 2020). For instance, BMP6 is resistant to the antagonist Noggin, while BMP7 remains sensitive to its inhibitory effects (Song et al., 2010). This differential sensitivity underscores that structural homology does not always equate to functional equivalence in biological systems. The subtle structural differences between BMP6 and BMP7 thus result in significant variations in their signaling properties and regulatory mechanisms.

3.2.3 Novel Insights into the Balance of SMAD1 and SMAD2 Signaling.

To quantify the balance of SMAD1 and SMAD2 signaling over time, I had used a double reporter system to analyze ligands activating the dual-signaling pathway for the first time. A key observation was the role of FKBP12 in modulating this balance. Removal of FKBP12 led to a shift towards SMAD1/5/9 signaling (Figure 30E).

Maintaining the balance between SMAD1/5/9 and SMAD2/3 signaling is essential for vascular homeostasis, influencing key processes such as angiogenesis, vascular integrity, and endothelial-to-mesenchymal transition (Hiepen et al., 2020). Research by Goumans demonstrated the critical nature of this balance. They showed that ALK1-mediated SMAD1/5/9 signaling promotes endothelial cell proliferation and migration, crucial for angiogenesis, while ALK5-mediated SMAD2/3 signaling acts as an inhibitor, stabilizing newly formed blood vessels (Goumans et al., 2003). Building on these insights, my results suggest that FKBP12 inhibits SMAD1/5/9 signaling.

Following my population-level investigation, single-cell analysis confirmed that higher BMP7 concentrations decrease the SMAD2 response while increasing the SMAD1 response in the absence of FKBP12 (Figure 31A). This trend, especially pronounced at BMP7 concentrations above 200 ng/ml.

Besides, my single-cell analysis revealed a more complex picture. At first, SMAD1 and SMAD2 responses were highly correlated at the single-cell level (Figure 31E), mirroring the population-level findings. Yet, over time (10-15 hours post-stimulation), this correlation decreased, indicating that while the initial response was coordinated, pathways began to diverge due to distinct regulatory mechanisms within individual cells. This behavior parallels observations in other signaling pathways, like NF- κ B, where initial uniformity gives way to variability due to feedback and regulatory processes (Nelson et al., 2004). The initial uniform response ensures a robust activation of SMAD pathways, crucial for immediate cellular reactions. However, the later divergence underscores the complexity of intracellular signaling, where individual cells adjust their responses based on specific regulatory mechanisms. For

instance, in cancer, both population-level and single-cell-level insights can shed light on tumor heterogeneity and treatment resistance (Altschuler & Wu, 2010).

In summary, my research enhances our understanding of BMP signaling by revealing how SMAD1/5/9 and SMAD2/3 pathways balance and how FKBP12 regulates this balance.

3.2.4 Investigating Mechanisms Underlying the shift from SMAD2 to SMAD1 Signaling and Pathway Integration.

Following the discovery of the SMAD1-SMAD2 signaling shift after FKBP12 removal, I investigated the mechanisms underlying this phenomenon. My experiments, which involved co-treating cells with TGF-beta and BMP9, did not reveal evidence of feedback inhibition or pathway competition between the SMAD2/3 and SMAD1/5/9 branches at the population level (Figure 32A). Interestingly, my findings complement yet contrast with previous studies, which demonstrated BMP and TGF-beta antagonism through competition in multi-ligand environments (Guo & Wang, 2009; Ning et al., 2019).

Building on studies that developed a mathematical model predicting responses to TGF-beta and BMP combinations (Zi et al., 2011), I result further described the intensities between SMAD2 and SMAD1 signaling in live cell. Additional TGF-beta did not significantly change the SMAD1 ratio, but co-treatment with BMP9 slightly increased the SMAD2 response compared to TGF-beta alone. The lack of observed competition implies that cells use sophisticated mechanisms to maintain pathway specificity, even when exposed to multiple ligands. Cellular responses in complex signaling environments involve orchestrated integration of multiple inputs rather than simple additive effects. Mechanisms such as spatial receptor segregation, differential receptor trafficking, and pathway-specific modulators could contribute to maintaining signal fidelity (Hoch & Soriano, 2014). Further research, incorporating mathematical models, FKBP12 impact, reporter systems, and deep learning techniques, could enhance understanding of signal integration and pathway specificity

3.2.5 Unveiling the Complexity of TGF-beta Family Signaling: Receptor Dynamics and FKBP12 Modulation.

Receptors play a pivotal role in mediating ligand binding and pathway activation, serving as crucial determinants of cellular responses (Vander Ark et al., 2018; Weiss & Attisano, 2013; Y. E. Zhang, 2018). Variations in receptor expression levels, dimer diversity, and ligand affinity can significantly impact pathway activation and downstream signaling outcomes (Klemm et al., 1998; Krall et al., 2011; Rojas et al., 2009). Building on this, my research reveals that FKBP12 modulates ALK2 activation, acting as an on-off switch.

My result highlight that both BMP7 and Activin A, despite being distinct ligands, activate the SMAD1/5/9 pathway through ALK2 and utilize the same receptor dimerization complex (Figure 33 B, C). The common receptor dimerization complex for BMP7 and Activin A implies that the specificity of SMAD1/5/9 activation might depend more on the presence of FKBP12. In contrast, my research has uncovered significant differences in receptor dimerization complexes for SMAD2/3 activation (Figure 33 B, C). This suggests that BMP7-induced SMAD2 activation relies on ALK4/ALK2 heterodimers, while Activin A-induced SMAD2 activation is more flexible, depending on both ALK4/ALK2 heterodimers and ALK4 homodimers.

Previous reviews have highlighted how different type I receptors phosphorylate specific R-SMADs (Chaikuad & Bullock, 2016; Hata & Chen, 2016; Miyazono, 1999). My findings add an important layer of complexity at the receptor complex level, suggesting that signaling specificity is influenced not only by the type I receptor but also by the configuration of the FKBP12-receptor complex. This distinction could significantly impact the cell's ability to generate ligand-specific responses within the SMAD pathway, with different ligands potentially activating the same SMAD proteins through distinct receptor complex configurations. This diversity aligns with the work on the structural basis for TGF-beta family signaling specificity (Hinck et al., 2016), suggesting that these variations reflect evolutionary adaptations of the signaling system.

3.2.6 Investigating Single and Dual Pathway Inputs: Insights into Endothelial Cell Responses regulated by FKBP12.

In the final segment of my study, I investigated how single versus dual pathway inputs affect both short-term and long-term cellular responses, with a particular focus on FKBP12's role. Contrary to previous research that suggested a competitive balance between SMAD1/5/9 and SMAD2/3 pathways in shaping endothelial cell (EC) phenotypes (Hiepen et al., 2020), my findings show no evidence of such competition. This conclusion was supported by short-term gene expression analyses through qPCR and long-term functional assays, including mobility and tube formation studies.

My qPCR results revealed that SMAD2/3 and SMAD1/5/9 signaling pathways have an additive effect on gene regulation (Figure 34A). While BMP7 alone did not affect DLL4 expression, DLL4 was downregulated upon FKBP12 degradation, highlighting the FKBP12-ALK2-SMAD1/5/9 pathway's role in gene regulation. Conversely, ID2 expression was increased by BMP7 and further enhanced by FKBP12 removal, demonstrating a synergistic effect of the SMAD1/5/9 and SMAD2/3 pathways on ID2 regulation. This additive effect reinforces the concept of threshold effects, where combined signaling inputs enable cells to integrate multiple pathways and exceed specific activation thresholds (Raj et al., 2010). For instance, TGF-beta 1 induces epithelial-to-mesenchymal transition in NMuMG cells by surpassing a signaling threshold via ALK5 and Smad proteins, whereas activin A and BMP-7

do not trigger this transformation due to insufficient activation (Piek et al., 1999). Similarly, dual bioluminescence imaging studies have shown that surpassing a threshold of SMAD4, but not SMAD2, increases the likelihood of sustained CTGF transcription (Tidin et al., 2019). These findings indicate that overlapping expression of downstream genes like ID2 under certain stimuli can lead to threshold effects, driving specific cellular outcomes such as angiogenesis or differentiation states that single pathways alone cannot achieve.

Long-term functional assays, including cell mobility and tube formation, further illustrate no competitive interaction between the pathways (Figure 34B, C). BMP7 alone increased cell motility, and FKBP12 removal further enhanced this effect. This enhancement was significantly reduced by ALK4/5 inhibitors.

Besides, the roles of SMAD1/5/9 and SMAD2/3 in angiogenesis are critical, and the tube formation assay provides valuable insights into how activation of these pathways influences the ability of vascular endothelial cells (ECs) to form tubes (Gaengel et al., 2009). Additionally, research has shown that BMP2/6/7 promotes the formation of tip cells, which gain capabilities such as EMT, proliferation, and characteristics of tip cells through the SMAD1/5/9 pathway. In contrast, the SMAD2/3 pathway is associated with the development of stalk-like cells (Benn et al., 2017). In my tube formation experiments, the SMAD2/3 pathway, active upon BMP7 stimulation, can induce tube formation. Furthermore, when FKBP12 was removed to activate the SMAD1/5/9 pathway, there was a notable enhancement in the cells' ability to form tubes, supporting the idea that SMAD1/5/9 activation contributes significantly to angiogenesis. Both pathways contribute additively to the observed cellular behaviors (Figure 34B, C), suggesting a cooperative or parallel operation rather than competitive interaction. This challenges the traditional view of SMAD pathway competition. Contrary to previous studies that emphasized competitive interactions between ALK1 and ALK5 signaling in endothelial cells (Goumans et al., 2002), my findings reveal a cooperative effect between the SMAD2/3 and SMAD1/5/9 pathways in endothelial cells. This cooperative signaling may enhance endothelial cell plasticity in various vascular contexts and during angiogenesis. For example, it could enable endothelial cells to dynamically adapt to changing microenvironments as they transition from quiescence to activation, potentially explaining how they maintain their identity while adapting to the demands of different vessel types (Hiepen et al., 2020).

However, while my research focused primarily on SMAD pathways, it is crucial to recognize that different ligands also activate non-SMAD pathways, which can significantly influence gene expression and cell fate decisions (Schmierer & Hill, 2007; Y. E. Zhang, 2009). For instance, while SMAD signaling regulates key genes involved in cellular differentiation and morphogenesis, non-SMAD pathways such as ERK or PI3K/AKT can modulate cell survival, proliferation, and migration—all essential processes in tissue formation and remodeling (Aashaq et al., 2022; Guo & Wang, 2009). In

my tube formation assays, BMP7 effectively induces tube formation despite not strongly activating SMAD2/3. This suggests that BMP7 likely activates critical non-SMAD pathways for tube formation. Notably, BMP7 continues to strongly induce tube formation even in the presence of FKBP12. Removal of FKBP12 further enhances endothelial cell (EC) tube formation, indicating that the SMAD1/5/9 and SMAD2/3 pathways cooperate rather than compete in the tube formation process.

Overall, my study highlights the cooperative nature of SMAD signaling in endothelial cells. Both SMAD pathways work together to affect gene expression and functional responses, without directly competing.

3.2.7 Implications for Disease and Therapeutic Strategies.

My research underscores the pivotal role of FKBP12 in modulating the balance between SMAD1/5/9 and SMAD2/3 signaling pathways in endothelial cells. The shift towards SMAD1/5/9 signaling upon FKBP12 removal highlights its potential as a therapeutic target for various vascular disorders. For instance, FKBP12-targeted PROTAC represent a promising intervention, potentially offering more tailored treatments for BMP-related disorders by selectively enhancing or inhibiting specific SMAD pathways.

Recent developments have positioned FK506 (tacrolimus) as a potential treatment for HHT (Albiñana et al., 2011). FK506 functions by displacing FKBP12 from the TGF-beta receptor complex, thereby enhancing ALK1-SMAD1/5/9 signaling (Robert et al., 2020). Clinical studies have demonstrated that low-dose tacrolimus effectively mitigates bleeding complications associated with HHT, improving symptoms such as epistaxis, hemoglobin levels, and overall quality of life (Al-Samkari, 2022; Hessels et al., 2022). This therapeutic benefit is attributed to the increased expression of endoglin and ALK1 in endothelial cells, which may correct the vascular anomalies seen in HHT1 and HHT2 (Albiñana et al., 2011). Besides, in the context of PAH, FKBP12 plays a significant role by inhibiting BMPR2 signaling. Given that loss-of-function mutations in BMPR2 are a major genetic risk factor for PAH, targeting FKBP12 could provide a therapeutic advantage (Orriols et al., 2017; Shah et al., 2023). This approach is particularly promising as it bypasses the need for functional BMPR2 by amplifying signaling through remaining receptors.

Emerging insights into FKBP12's role in BMP signaling and other pathways highlight the potential of FKBP12-specific PROTACs as a novel therapeutic strategy (Geiger et al., 2024; Hähle et al., 2019). While FK506 is a clinically utilized drug, it is an immunosuppressor through mediating the interaction of FKBP12 with calcineurin and has therefore strong side effects (F. J. Dumont, 2012; Inomata et al., 1996). FKBP12-specific PROTACs, in contrast, offer increased selectivity by exclusively targeting FKBP12 for degradation (Geiger et al., 2024; Williams et al., 2021). This specificity could minimize

unintended effect of the immune system as well as interactions with other FKBP family members, potentially reducing off-target effects and enhancing therapeutic efficacy.

FKBP12 is a promising target for a range of disorders, including depression, chronic pain, obesity, cancer, and neurodegenerative diseases (Caminati & Procacci, 2020; Chattopadhyaya et al., 2011; Christner et al., 2005; Häusl et al., 2019; Kolos et al., 2018; Moschetta et al., 2014; Schmidt et al., 2012). For example, FKBP12's interaction with mTOR influences cellular processes linked to cancer progression and neuronal survival (Lipton & Sahin, 2014; Takei & Nawa, 2014). In cancer, FKBP12's role in modulating MDM2 can enhance chemotherapy by promoting MDM2 degradation, which sensitizes cancer cells to apoptosis (T. Liu et al., 2017). In the context of neurodegenerative diseases, FKBP12's involvement in mTOR signaling pathways suggests potential benefits for conditions like Alzheimer's disease by influencing neuronal health and survival (C. Wang et al., 2014). Additionally, FKBP12 has been implicated in chronic pain management, where its modulation could affect pain signaling pathways (Lisi et al., 2015). These examples underscore the potential of FKBP12-targeted PROTACs to address a variety of complex therapeutic challenges.

My study significantly enhances the understanding of SMAD signaling dynamics in endothelial cells by uncovering the complex regulatory mechanisms that govern pathway activation in response to diverse ligands in live cell. I have elucidated how different SMAD pathways interact and how receptor complexes, along with FKBP12 modulation, contribute to this intricate signaling network. These findings offer a new perspective on how cells interpret and respond to various signaling cues, laying the groundwork for developing novel therapeutic strategies targeting SMAD pathways.

4 Material and Methods

4.1 Material and Methods of Part 1:

4.1.1 Cell Lines.

MCF10A cells were cultured in Dulbecco's Modified Eagle Medium (DMEM/F12, Thermo Fisher Scientific) supplemented with:

5% horse serum (Thermo Fisher Scientific)
20 ng/ml EGF (PeproTech)
0.5 µg/ml hydrocortisone (Sigma Aldrich)
100 ng/ml cholera toxin (Sigma Aldrich)
10 µg/ml insulin (Sigma Aldrich)
2 mM GlutaMAX (Thermo Fisher Scientific)
100 U/ml penicillin (Thermo Fisher Scientific)
100 µg/ml streptomycin (Thermo Fisher Scientific)

This medium is referred to as the "growth medium." For starvation experiments, the cells were cultured in a modified version of the growth medium, referred to as the "deprivation medium," which contains:

DMEM/F12 with 0.3% tissue culture grade BSA (Sigma Aldrich)
0.5 µg/ml hydrocortisone
100 ng/ml cholera toxin
2 mM GlutaMAX
100 U/ml penicillin
100 µg/ml streptomycin

Cells were incubated in the deprivation medium for 48 hours to induce a quiescent state.

Reporter Clones and Antibiotic Selection: MCF10A cell lines and various reporter clones were maintained in DMEM/F12 growth medium supplemented with specific antibiotics to ensure transgene expression:

400 µg/ml geneticin disulfate
50 µg/ml hygromycin B
5 µg/ml blasticidin S hydrochloride
150 µg/ml Zeocin

HEK293 cells were cultured in DMEM - High Glucose medium supplemented with:

10% fetal bovine serum (FBS)
100 U/ml penicillin
100 µg/ml streptomycin
2 mM GlutaMAX

All cell lines were maintained at 37°C in a humidified atmosphere containing 5% CO₂. For passaging, the culture medium was aspirated, and the cells were washed with 10 ml of 1x PBS. After removing the PBS, 1 ml of 1x trypsin/EDTA solution in 1x PBS was added (for MCF10A cells), and the cells were incubated at 37°C with 5% CO₂ for 20 minutes (for MCF10A cells) or 3 minutes (for HEK293) to facilitate detachment from the plate. Once the cells had detached, the trypsinization was stopped by adding 3 ml of medium to dilute the trypsin. The cells were then transferred to a 15 ml conical tube and centrifuged at 300 g for 5 minutes. After centrifugation, the supernatant was aspirated, and the cell pellet was resuspended in medium at the desired dilution, typically around 1:6. Finally, 1 ml of the diluted cell suspension was added to 9 ml of medium in new 10 cm petri dishes. On average, MCF10A cells were passaged every 3 to 4 days and HEK293 passaged every 2 days.

4.1.2 Generating SMAD2 Knockout Cell Line.

I utilized the CRISPR/Cas9 system to create a SMAD2 knockout cell line in MCF10A H2B-CFP cells, targeting both alleles of the SMAD2 gene to ensure complete loss of the corresponding protein. To achieve this, I cloned donor DNA and an sgRNA, which were co-transfected with Cas9 endonuclease into the cells (Huang & Loewer., 2022).

Donor DNA cloning:

The donor DNA comprised a knock-in sequence (SV40-Blasticidin_R) flanked by left and right homology arms, homologous to the genomic DNA regions upstream and downstream of SMAD2 exon 2. I generated the homology arms by PCR amplification from MCF10A genomic DNA using specific primers (list below), yielding fragments of 707bp (left arm) and 609bp (right arm). The knock-in sequence, containing the SV40 promoter and blasticidin resistance gene, was amplified from the pVE10 vector. All PCR products were purified from agarose gels and assembled with the pDONR221 (pDO18) vector using NEBuilder. The resulting construct, pDONR221-SMAD2-Blast, was amplified in *E. coli* and validated by control digestion and sequencing.

Component	Amount
NEBuilder HiFi DNA Assembly Master Mix (2X)	10 μ g
Vector DNA (pDONR221 \times EcoRV+AflII)	2 μ l
Insert DNA	
HAL	25 ng
HAR	35 ng
SV40-Blasticidin R	28.5 ng
ddH ₂ O	Up to 20 μ l

To design the sgRNA, I used the online tool CHOPCHOP v3 to select a 20bp guide sequence specific to SMAD2 exon 2. I then annealed corresponding oligos and cloned them into the sgRNA_AL vector, which had been digested with AgeI. A Gibson Assembly reaction was then performed using the purified vector and annealed oligos. The assembly product was transformed into electrocompetent cells and plated on LB-Kan agar. Colonies were screened by restriction digestion with NdeI and XbaI, and positive clones were verified by Sanger sequencing using the CS1_U6_Fwd primer.

For the transfection, I co-transfected 495 ng of sgRNA, 10 ng of NotI-linearized donor DNA, and 495 ng of Cas9 endonuclease into MCF10A H2B-CFP cells.

To analyze the resulting clones and determine whether they were heterozygous, homozygous, or negative for the insertion, I isolated genomic DNA using the QIAamp DNA Mini Kit. I performed PCR with two different primer pairs to assess the presence and zygosity of the knock-in.

The program for oligo annealing was set up as follows:

Temperature	Time	Cycles
95 °C	10 min	1
95-85 °C, -2 °C /s		
85 °C	1 min	1
85-75 °C, 0.3 °C/s		
75 °C	1 min	1
75-65 °C, -0.3 °C /s		
65 °C	1 min	1
65-55 °C, -0.3 °C /s		

55 °C	1 min	1
55-45 °C, -0.3 °C /s		
45 °C	1 min	1
45-35 °C, -0.3 °C /s		
35 °C	1 min	1
35-25 °C, -0.3 °C /s		
25 °C	1 min	1

Vector digestion:

Component	Amount
DNA (sgRNA AL vector)	5 µg
CutSmart buffer	5 µl
AgeI enzyme	5 µl
H ₂ O	Up to 50 µl total volume

Gibson assembly:

Component	Amount
Digested vector (sgRNA AL)	50 ng (0.02047 pmol)
Annealed oligos	1.02 µl (0.10235 pmol)
Gibson Assembly Master Mix (2x)	5 µl
H ₂ O	Up to 10 µl total volume
Incubation	60 minutes at 50°C

sgRNA cloning:

Component	Amount
NEBuilder HiFi DNA Assembly Master Mix (2X)	10 µg
sgRNA AL×AgeI	50 ng
Annealed oligos	2.8 ng
ddH ₂ O	Up to 20 µl

To perform the NEBuilder HiFi DNA Assembly, combine all components in a PCR tube on ice and gently mix by pipetting. Incubate the reaction mixture in a thermocycler at 50°C for 1 hour, then cool on ice. Use 1-5 µl of the cooled assembly mixture for transformation into NEB 5-alpha Competent E. coli following standard transformation protocols. This method ensures efficient assembly of DNA fragments, with the flexibility to adjust incubation times based on the number of fragments being assembled (15-30 minutes for 2-3 fragments, 60 minutes for 4-6 fragments).

Primer list:

Primer name	Sequence (5'→3')
SMAD2_e2_gen_forward	ACACGTGGCACATTGCCAGATTAC
SMAD2_e2_gen_reverse	TGCTATATGCTAGCCCACGGTATG
SMAD2_e2_HAL_forward	TTGTAAAACGACGGCCAGTCGCGGCCGCGAGCAGGTGA AACCGGACTAC
SMAD2_e2_HAL_reverse	AAATCGGCAGACTTCTTCCATCCCAGCAGTCTC
SMAD2_e2_HAR_forward	TGCACCTCTAGGAGAGCAGAATGGGCAGGAAG

SMAD2_e2_HAR_reverse	TACGACTCACTATAGGGGATGCGGCCGCGGAAGCAATG CTGCAACGCAAAG
Bsd_SMAD2_e2_forward	TGGAAGAAGTCTGCCGATTTTCGGCCTATTGG
Bsd_SMAD2_e2_reverse	TCTGCTCTCCTAGAGGTCGACGGTATACAG
SMAD2_sgRNA_29_forward	CACCGATGGAAGAAGTCAGCTGGTGTTTTAGAGCTAGA AATAGCA
SMAD2_sgRNA_29_reverse	AAACACCAGCTGACTTCTTCCATCGGTGTTTCGTCCTTT CC
SMAD2_sgRNA_33_forward	CACCGCAGGCGGAGGAGAGCAGAAGTTTTAGAGCTAG AAATAGCA
SMAD2_sgRNA_33_reverse	AAACTTCTGCTCTCCTCCGCCTGCGGTGTTTCGTCCTTTC C

4.1.3 Generating SMAD3 Knockout Cell Line.

To generate SMAD3 knockout (KO) cell lines based on SRv2 WT and SRv2 4x-mutation cells, I employed a CRISPR-Cas9 approach similar to the previously described SMAD2 KO method (Z. Huang & Loewer, 2022).

The donor DNA was designed to enable antibiotic selection with puromycin and comprised a knock-in sequence (SV40-puro_R) flanked by homology arms corresponding to genomic regions upstream and downstream of SMAD3 exon 6. These homology arms were generated by PCR amplification from MCF10A genomic DNA using specific primers, resulting in fragments of 775 bp (left arm) and 940 bp (right arm), with a total length of 1982bp. The knock-in sequence, containing the SV40 promoter and puromycin resistance gene, was amplified from the pDE009 vector. All PCR products were purified from agarose gels and assembled with the pDONR221 (pDO18) vector using NEBuilder as described SMAD2 KO method.

The sgRNA targeting SMAD3 exon 6 was designed (Primers sequence list below) and the plasmid construct was generated using methods identical to those employed for the SMAD2 knockout, as previously described. The resulting construct, pDONR221-SMAD3-puro, was amplified in *E. coli* and subsequently validated through control digestion and sequencing to ensure its accuracy and integrity.

Primer list:

Primer name	Sequence (5' -> 3')
SMAD3_e6_gen_for	GGCATAGCGTTAAACCATCC
SMAD3_e6_gen_rev	TTACCTGCTCCACTAGTCTG
SMAD3_e6_HAL_for	TTGTA AAAACGACGGCCAGTCGCGGCCGCCTGCAAGGGT AGAGGTTATC
SMAD3_e6_HAL_rev	ATTCCACAGGGGGAGACTGGACAAAAATAG
SMAD3_e6_HAR_for	CGGTGCCTGAGCAAGATCCCACCAGGTAAAC
SMAD3_e6_HAR_rev	TACGACTCACTATAGGGGATGCGGCCGCGGAAGAGG CCTTAGATGG
puro SMAD3_e6_for	CCAGTCTCCCCCTGTGGAATGTGTGTCAGTTAGGG
puro SMAD3_e6_rev	GGGATCTTGCTCAGGCACCGGGCTTGCGGGTC

SMAD3_exon6_sgRNA2_for	CACCGCTGGTTACAGTTGGGAGACGTTTTAGAGCTAGA AATAGCA
SMAD3_exon6_sgRNA2_rev	AAAC GTCTCCCAACTGTAACCAGCGGTGTTTCGTCCTTTCC
SMAD3_exon6_sgRNA3_for	CACCGGATCTTGCAGACGGTGGCCGTTTTAGAGCTAGA AATAGCA
SMAD3_exon6_sgRNA3_rev	AAACGGCCACCGTCTGCAAGATCCGGTGTTCGTCCTTT CC

4.1.4 Generating SMAD2-Replacement Cell Lines.

For this part, all the plasmids with the SMAD2 label fused to the YFP protein (including SMAD2-WT, SMAD2-T220, SMAD2-S245, SMAD2-S250, SMAD2-S255, SMAD2-3x-mutation, and SMAD2-4x-mutation) were generated by Anne-Sophie Lindemann for her Master's thesis (Anne-Sophie Lindemann, 2018). Using the CRISPR/Cas9 system, I inserted the YFP-SMAD2 wildtype or mutant constructs into the AAVS1 locus base on the H2B-CFP SMAD2KO MCF10A cell line. The resulting construct, pDONR221-SMAD3-puro, was amplified in *E. coli* and validated through control digestion and sequencing to ensure accuracy and integrity.

4.1.5 Generating SMAD3 Knockin Cell Line.

To generate the mCherry-SMAD3 fluorescent construct, I first needed to create a lentiviral vector with Zeocin resistance and a separate SMAD3 lentiviral construct.

To generate the mCherry-SMAD3 fluorescent construct, I first needed to clone a lentiviral vector with Zeocin resistance. The initial step involved amplifying the sh_Zeocin ORF using pTEMP53 as a template. The PCR reaction was set up as follows:

Component	Amount
pTEMP53	5 ng
5x Q5 Reaction Buffer	10 μ l
dNTP's (10 mM)	1 μ l
ble_PmlI_fwd (10 μ M)	1.5 μ l
ble_NheI_rev (10 μ M)	1.5 μ l
Q5 Polymerase	0.5 μ l
H ₂ O	up to 50 μ l

The PCR cycling conditions were as follows:

Stage	Temperature	Time	Cycles
Initial denaturation	98°C	3 min	1
Denaturation	98°C	15 seconds	10
Annealing	70-60°C (touchdown)	20 seconds	
Elongation	72°C	15 seconds	
Denaturation	98°C	15 seconds	25
Annealing	60°C	20 seconds	

Elongation	72°C	15 seconds	
Final elongation	72°C	7 min	1

Following PCR amplification, the product underwent several processing steps to ensure purity and quality. First, 1 µl of DpnI enzyme was added to the PCR product and incubated at 37°C for 1 hour to digest any remaining template DNA. The product was then purified using a PCR purification kit to remove enzymes, primers, and other contaminants. To verify the success of the amplification and purification, 5 µl of the purified product was analyzed on a 1% agarose gel.

To clone the ble fragment into pMiniT2.0, I first mixed the linearized pMiniT vector, the PCR product, and water to a total volume of 5 µl. Cloning Mix 1 and 2 were then added sequentially to prevent the reaction from starting prematurely. The mixture was incubated at room temperature for 15 minutes before transforming 2 µl into electro-competent TOP10 E. coli cells, which were subsequently plated on LB-amp agar. For verification, minipreps were prepared from the resulting colonies and subjected to test digestion with PmlI and NheI-HF, expecting band sizes of 2600 bp and 386 bp.

The reaction was set up as follows:

Component	Amount
Linearized pMiniT 2.0	25 ng
PCR product (sh Zeocin fragment)	60 ng
H ₂ O	up to 5 µl
Cloning Mix 1	4 µl
Cloning Mix 2	1 µl

Following created the pMiniT2- Zeocin vector, I need to make the Linearized pMiniT2- Zeocin and Linearized pDE8 by usingt he digested with PmlI and NheI-HF before Ligation of those frame to generated the final lentiviral vector with Zeocin resistance.

Component	Amount
pMiniT2- Zeocin / pDE8	5 µg
CutSmart Buffer	5 µl
PmlI-HF	1 µl
NheI-HF	4 µl
H ₂ O	up to 50 µl

The digestion reactions for both pDE8 and pMiniT2- Zeocin were incubated for 2 hours at 37°C. For pDE8, an additional step was performed by adding 1 µl of Antarctic Phosphatase, followed by a 30-minute incubation at 37°C and a brief 5-minute incubation at 70°C. Both digestion products were then purified by gel electrophoresis, with pDE8 using a 0.7% agarose gel for better separation of larger fragments. The desired bands were subsequently extracted: the 8245 bp band from the pDE8 digestion and the 386 bp band from the pMiniT2- Zeocin digestion. These purified fragments were then ready for the subsequent ligation step in the cloning process.

The digested vector backbone and ble insert were ligated using Quick ligase. A control reaction without insert was also prepared. The ligation mixture contained:

Component	Amount
pRRLB x PmlI x NheI	100 ng
Zeocin x PmlI x NheI	25 ng
Quick ligase buffer	10 μ l
Quick ligase	1 μ l
H ₂ O	up to 20 μ l

The reaction was incubated at 25°C for 30 minutes. Then 2 μ l of the ligation mixture was transformed into ccdB survival E. coli cells and plated on LB-amp/chloramphenicol at 30°C for 24 hours. Minipreps were prepared using amp + chloramphenicol at 30°C for 24 hours. Clones were verified by test digestion with AatII (expected bands: 7.8 + 0.75 + 50 bp) and EagI (expected bands: 5.1 + 2.6 + 884 bp).

pVE078 which is a vector which SMADd3 cDNA ORF Clone in Cloning Vector, Human, buy from sino biological.

touch down PCR was using to amplifying the SMAD3 ORF using pVE078 as a template. and the touch down PCR is following the touch down protocol as before (xxx), times and temperatures need to be adjusted according to the characteristics of the primers and the insert. and afterward, the BP reaction was preformed to insert the SMAD3 OFR into the pDONR-P2R-P3 (pDO003).

BP reaction was set up as follows:

Component	Amount
SMAD3 ORF PCR product	25 fmol
pDO003	75 ng
BP Clonase MIX II	1 μ l
TE Buffer	add to 5 μ l

The reaction tube was placed in a PCR machine and incubated at 25°C for 1 hour. Following this, 0.5 μ l of Proteinase K was added to inactivate the enzyme, and the mixture was incubated at 37°C for 10 minutes. Next, 1 μ l of the ligation mixture was transformed into TOP10 E. coli cells, which were then plated on LB-kanamycin agar and incubated at 37°C for 16 hours. Minipreps were prepared from the resulting colonies, with kanamycin selection at 37°C for 16 hours. The clones were verified by test digestion with EcoRV and NdeI, expecting band sizes of 2.4 kbp and 1.5 kbp.

The final step in this process involved using the LR reaction, as previously described (xxx), to generate the complete construct. For this reaction, I combined the following plasmids: pDONR221-mCherry (pDO47), pDONR-UbCp (pDO52), pDONR-P2R-P3-SMAD3 (pDO150), and pDONR221-Zeocin (pDE014). This multiplasmid LR reaction facilitated the assembly of all necessary components into a

single vector, resulting in the final mCherry-SMAD3 fluorescent construct with Zeocin resistance under the control of the UbC promoter.

Primer List:

Primer name	Sequence (5'→3')
Zeocin PmlI forward	GACCACGTGCCATGGATGCCAAGTTGACCAGTG
Zeocin NheI reverse	GACGCTAGCTCAGTCCTGCTCCTCGG
SMAD3 OFR forward	GGGGACAGCTTTCTTGTAACAAGTGGGAATGTCCTCCATC CTGCCTTTC
SMAD3 OFR reverse	GGGGACAACCTTTGTATAATAAAGTTGCCTAAGACACACTG GAACAGC

4.1.6 Generating LTBP2, MMP9, PMEPA1 Overexpression Cell Line.

The first step in overexpressing the target gene in the cells involved creating a new lentiSAMv2-Zeocin construct, as other antibiotics were already being used to select for previous insertions in the SRv2 SMAD2 WT SMAD3KO cells. To achieve this, it was necessary to develop three key components: the EF1a promoter, the U6 promoter, and the dCas9-SAM construct. By assembling these elements, we aimed to establish a lentiSAMv2 system with Zeocin resistance, enabling selective overexpression of our target gene.

To begin, I designed specific primers to amplify the EF1a promoter from the pEX003 plasmid. The amplification was performed using a touchdown PCR protocol. Following successful amplification, I employed a BP reaction to insert the EF1a fragment into the pDONR221 vector (pDO018). The resulting constructs were selected using kanamycin resistance. To ensure the integrity of the inserted sequence, the final plasmid was sent for sequencing.

To generate the U6 entry vector, I followed a process similar to that used for the EF1a promoter. I began by using the pEX003 plasmid as the PCR template to amplify the U6 promoter, employing the same touchdown PCR protocol as before. After successful amplification, I performed a BP reaction to insert the U6 fragment into the pDORNP4P1R vector (pDO001).

Last, I proceeded to create the dCas9-SAM entry vector using a method similar to the previous steps. The dCas9-SAM fragment was amplified from the pEX003 plasmid using PCR. Following successful amplification, we performed a BP reaction to insert this fragment into the pDONRP2RP3 vector (pDO003).

The final step involved assembling all the components using an LR reaction to build the complete construct, which utilized EF1a as the promoter for dCas9 and included Zeocin as the selection antibiotic. The LR reaction protocol was identical to the one used previously and combined the following plasmids: pDONRP221-EF1a (pDO152) as the entry vector with the EF1a promoter, pDORNP4P1R-U6

(pDO151) as the entry vector with the U6 promoter, pDONRP2RP3-dCas9 (pDO153) as the entry vector containing dCas9, and pRRLZeo (pDE014) as the destination vector with Zeocin resistance.

The next step is using this construct, to generate the sgRNA which can recognize the target genes. For this reason, I followed the methodology described by Konermann et al., 2015, employing a dead Cas9-VP64 complex. Optimized sgRNAs for any coding gene can be found using SAM Cas9 activator design tool designed by ZhangLab, MIT at the following website: (sam.genome-engineering.org/database/) to avoid off-target effects and ensure that the target sequence is located close to the TSS. Insert the SgRNA oligo into lentiSAMv2-Zeocin plasmid. It involved denaturing and annealing the corresponding oligos using a PCR machine. After the oligos were annealed and had 4 bp overhangs, they were joined together with the lentiviral vector lentiSAMv2-Zeocin.

Oligo annealing was set up as follows:

Component	Amount
Each oligo	100 μ M (1 μ l each)
10x T4 ligase buffer (New England BioLabs)	1 μ l
T4 PNK (New England BioLabs)	1 μ l
TE Buffer	0.5 μ l
ddH ₂ O	6.5 μ l

The PCR cycling conditions were as follows:

Temperature	Time	Cycles
37 °C	30 min	1
95 °C	5 min	1
95-25 °C, -5° C/min		1

After the reaction, dilute the sample by adding 90 μ l of ddH₂O. Then, mix the following components for the Golden Gate reaction:

Component	Amount
2×T7 Ligase Reaction Buffer (New England BioLabs)	1 μ l
T7 ligase (New England BioLabs)	0.125 μ l
BSA (20 mg/ml)	0.125 μ l
Restriction enzyme BsmBI (New England BioLabs)	1 μ l
Diluted oligo anneals	1 μ l
Backbone vector lentiSAMv2-Zeocin	1 μ l
ddH ₂ O	

The PCR cycling conditions were as follows:

Temperature	Time	Cycles
37 °C	5 min	15
20 °C	5 min	15

Transform 2 μ l of the Golden Gate reaction mixture into Stb13 competent cells and plate them on agar plates containing Ampicillin. Incubate the plates at 30°C for 24 hours. Verify the positive clones by performing PCR or digestion, followed by sequencing to confirm their accuracy. Next, infect the cells with the corresponding lentiviral particles to create stable cell lines that overexpress the target gene.

Primer name	Sequence (5'→3')
EF1a forward	GGGGACAAGTTTGTACAAAAAAGCAGGCTTCGAAAGGAGTGG GAATTGG
EF1a reverse	GGGGACCACTTTGTACAAGAAAGCTGGGTCCTGTGTTCTGGCG GCAAACC
U6 forward	GGGGACAACCTTTGTATAGAAAAGTTGGAGAGGGCCTATTTC ATGATTC
U6 reverse	GGGGACTGCTTTTTTTGTACAACTTGCGAGCCAATTCCCCTCC TTTC
dCas9-SAM forward	GGGGACAGCTTTCTTGTACAAAGTGGGAGTTTGCCGCCAGAAC ACAG
dCas9-SAM reverse	GGGGACAACCTTTGTATAATAAAGTTGCTTCCTCTGCCCTCTCCA CTG
MMP9 sg1 forward	CACCGTGTAAGCCCTTTCATGC
MMP9 sg1 reverse	AAACGCATGAGAAAGGGCTTACAC
MMP9 sg3 forward	CACCGTGGGAACTGTATGAAAGGG
MMP9 sg3 reverse	AAACCCCTTTCATACAGTCCCAC
LTBP2 sg1 forward	CACCGGATTAACCCGTGCGGAGCA
LTBP2 sg1 reverse	AAACTGCTCCGCACGGGTTAATCC
LTBP2 sg2 forward	CACCGATTAACCCGTGCGGAGCAGG
LTBP2 sg2 reverse	AAACCCTGCTCCGCACGGGTTAATC
PMEPA1 sg4 forward	CACCGTATTTGCAGTGGCACCCCAA
PMEPA1 sg4 reverse	AAACTTGGGGTGCCACTGCAAATAC
PMEPA1 sg6 forward	CACCGCTGACCGTCTTCTGTTGGG
PMEPA1 sg6 reverse	AAACCCCAAACAGAAGACGGTCAGC

4.1.7 Transfection and Generation of Monoclonal Cell Lines.

For plasmid DNA insertion into MCF10A cell lines, I seeded 2.5×10^5 cells per well in a 12-well plate and cultured them in growth medium for 18 to 24 hours. The plasmid DNA was then diluted in 50 μ l of preheated Opti-MEM I reduced-serum medium (Thermo Fisher Scientific) and mixed with 2 μ l of P3000 reagent from the Lipofectamine 3000 Kit (Thermo Fisher Scientific). This mixture was incubated for 5 minutes. Meanwhile, 3 μ l of Lipofectamine 3000 reagent was added to another 50 μ l of preheated Opti-MEM I medium. The two mixtures were combined and incubated for 15 minutes at room temperature. The resulting transfection mixture was added dropwise to different areas of the wells, and the plate was gently rocked to ensure homogeneous distribution. After 3 days of incubation, the cells were trypsinized with 1 \times Trypsin-EDTA (Thermo Fisher Scientific) and transferred to 15 cm plates containing antibiotic-selective medium. The medium was changed twice per week. After 14 to 21 days, individual colonies were picked by trypsinizing and aspirating them with a 1 ml pipette, then transferring each colony to a 24-well plate with antibiotic-containing medium. Upon reaching

confluency, the cells were washed with PBS, trypsinized, and transferred to a 6-well plate. This process was repeated until the cells were successfully transferred to 10 cm plates, ensuring proper expansion and selection of transfected cell lines.

4.1.8 PCR Amplification of DNA Fragments.

PCR amplification of DNA fragments was performed using Q5 High-Fidelity DNA Polymerase (New England BioLabs) with specific primers. To improve PCR efficiency, a touchdown PCR approach was typically used. The initial annealing temperature for the touchdown cycles was set 3°C above the lower melting temperature of the two primers. The elongation time was calculated at 30 seconds per 1 kb of target fragment length. To further enhance PCR effectiveness, GC enhancer or DMSO was added to the reaction mixture.

PCR reaction was set up as follows:

Component	Amount
5X Q5 Reaction Buffer	10 µl
10 mM dNTPs (200 µM final)	1 µl
Forward Primer (0.5 µM final)	2.5 µg
Reverse Primer (0.5 µM final)	2.5 µl
Template DNA (< 1000 ng)	Variable
Q5 High-Fidelity DNA Polymerase	0.5 µl
Nuclease-free water	Up to 50 µl

4.1.9 Analysis and Purification of DNA by Agarose Gel Electrophoresis.

For DNA fragment separation, 0.75-1.5% agarose gels containing the fluorescent dye peqGREEN (Peqlab) were prepared. To prepare a 1% (w/v) agarose gel, 1 g of agarose was dissolved in 100 ml of 1× TAE buffer by heating until fully dissolved. After the mixture cooled to a safe handling temperature, 5 µl of peqGREEN dye was added to the solution and mixed thoroughly. DNA samples were prepared by adding 6× loading dye (New England BioLabs) to the samples to facilitate tracking during electrophoresis. For molecular weight estimation, the 1 kb plus DNA Ladder (New England BioLabs) was used as a size reference. The gels were run at approximately 130 V for 30 minutes, but the running time and voltage were adjusted as needed based on the size of the DNA fragments being separated. When DNA fragments were needed for further experiments, specific bands were excised from the gel and purified using the QIAquick Gel Extraction Kit (Qiagen), following the manufacturer's instructions. The purified DNA was eluted with 30 µl of EB buffer and quantified using a NanoDrop 2000c spectrophotometer (Thermo Fisher Scientific) to ensure accurate concentration measurements for downstream applications.

4.1.10 Electroporation and Cultivation of Escherichia coli.

Electrocompetent *E. coli* cells (TOP10 or Stable3 strains) were prepared for electroporation by thawing them on ice. For the transformation, 1 μ l of diluted NEBuilder assembly products (1:3 dilution) or 2 μ l of Golden Gate reaction products were added to the cells. The mixture was then transferred into an electroporation cuvette (Bulldog Bio, Inc.) and subjected to a 1.8 kV electric pulse using an Eppendorf AG electroporator, which facilitates the uptake of DNA into the bacterial cells. Immediately following electroporation, 1 ml of SOC medium or Stable3 medium (New England BioLabs) was added to the cuvette to provide essential nutrients and promote cell recovery. The cells were incubated for 1 hour at 37°C, allowing time for the expression of antibiotic resistance genes and recovery from the electroporation process. This step is crucial for ensuring that the cells are viable and capable of growing on selective media. After the recovery period, 50 μ l of the transformed cell suspension was spread onto LB agar plates containing the appropriate antibiotics—100 μ g/ml Ampicillin or 50 μ g/ml Kanamycin (Sigma). The plates were incubated overnight at 37°C for TOP10 strains or for 24 hours for Stable3 strains at 30°C. The following day, individual colonies were selected and transferred to 4 ml of LB medium (Carl Roth) with the corresponding antibiotics. These cultures were then grown overnight at 37°C with shaking to amplify the transformed colonies for further experiments.

4.1.11 Genomic and Plasmid DNA Isolation.

Plasmid DNA was isolated and purified from overnight bacterial cultures using the QIAprep Spin Miniprep Kit (Qiagen). The procedure followed the manufacturer's instructions, and the purified plasmid DNA was eluted with 30 μ l of EB buffer. Genomic DNA was extracted from cultured MCF10A cells using the QIAamp Mini DNA Kit (Qiagen). The isolation process was conducted according to the manufacturer's protocol, and the genomic DNA was eluted with 200 μ l of EB buffer.

4.1.12 Restriction Digest.

To verify the presence of desired DNA fragments in plasmids or to prepare DNA for subsequent procedures, we performed restriction digest analysis. This technique involves using specific restriction enzymes to cleave DNA molecules at predetermined sites. The restriction digest reaction was prepared in a total volume of 20 μ l, containing the following components:

Component	Amount
DNA (200-1,000 ng)	10 μ g
10 \times CutSmart Buffer (New England BioLabs)	2 μ l
Enzyme I (10 U/ μ l)	0.5 μ l
Enzyme II (10 U/ μ l) (if need)	0.5 μ l
ddH ₂ O	Up to 20 μ l

The DNA concentration used ranged from 200 to 1,000 ng, depending on the specific requirements of each experiment. CutSmart Buffer was used to provide optimal conditions for enzyme activity. Two

different restriction enzymes (Enzyme I and Enzyme II) were added to the reaction mixture, each at a concentration of 10 U/ μ l. The final volume was adjusted to 20 μ l using ddH₂O.

4.1.13 Sequencing.

Sequencing reactions were performed by Eurofins Genomics in Ebersberg, utilizing Sanger DNA sequencing to identify the nucleotide sequence. For this purpose, I prepared the sequencing reaction by diluting 1.2 μ g of DNA with 3 μ l of an appropriate primer (10 μ M) in nuclease-free water, bringing the total volume to 12 μ l. This preparation ensured that the DNA and primer concentrations were suitable for the sequencing process.

4.1.14 Live-Cell Time-Lapse Imaging.

For live-cell imaging experiments, $0.2-0.4 \times 10^4$ cells were seeded in 24-well ibidi imaging plates and incubated in growth medium for 36 hours for proliferating cells. The medium was then replaced with deprivation medium (DMEM/F12 with 0.3% BSA, 0.5 μ g/ml hydrocortisone, 100 ng/ml cholera toxin, and antibiotics) for 48 hours to induce quiescence for the quiescent cell experiment. Prior to imaging, cells were switched to deprivation-microscopy medium (FluoroBrite with similar supplements plus 2 mM GlutaMAX and 10 mM HEPES). Imaging was performed using a Nikon Eclipse Ti-E inverted microscope with a 20 \times CFI Plan Fluor objective, Nikon DS-Qi2 camera, and X-Cite 120 LED illumination system. Specific filter sets were utilized for Venus (500/20 nm excitation, 515 nm dichroic beam splitter, 535/30 nm emission), CFP (436/20 nm excitation, 455 nm beam splitter, 480/40 nm emission), and mCherry (562/40 nm excitation, 593 nm beam splitter, 641/75 nm emission). Images were captured every 20 minutes for 72 hours in long-term experiments or every 10 minutes for 24 hours in short-term experiments, controlled by Nikon NIS Elements AR software. This setup allowed for detailed analysis of cellular behavior and signaling dynamics under various conditions.

4.1.15 Ligand and Inhibitor Treatment.

Inhibitor and ligand treatments were performed using the appropriate culture medium. Recombinant proteins, including TGF-beta, GDF8, and GDF11, were stored at -80°C in 4 mM HCl with 1 mg/ml bovine serum albumin, while activin A and GDF3 were stored at -80°C in 1 mg/ml bovine serum albumin. Inhibitors were typically diluted in DMSO and stored at -20°C unless otherwise specified. Prior to treatment, cells were imaged for 0.5 hour to establish baseline conditions. Ligands and inhibitors were prepared in 125 μ l of medium and added to the cells to achieve the desired concentration in a final volume of 625 μ l for 24-hour microscopy experiment, and 1 ml for 72-hour experiment. The old medium was replaced with new medium containing the specified concentration of ligand or inhibitor every 48 hour, and control cells received either medium only or medium containing DMSO. The

prepared solutions were added directly to the culture medium, ensuring accurate concentrations and consistent experimental conditions throughout the treatments.

For the wash-off experiment, cells are first treated with 0.5 μM ALK5 inhibitor for 8 hours. Following this, the medium is replaced with 1 mL of fresh medium, and the cells are washed three times. Finally, ligands are reintroduced, adjusting the final volume to 625 μL .

Inhibitors and ligands used:

Gefitinib (EGFR inhibitor) (Selleckchem)	10 μM
SB525334 (ALK5 inhibitor) (Selleckchem)	10 μM
Activin A (PeproTech)	20 nM
GDF3 (PeproTech)	20 nM
GDF8 (PeproTech)	20 nM
GDF11 (PeproTech)	Various concentrations
TGF-beta (PeproTech)	Various concentrations

4.1.16 Wound Healing Assay.

For wound healing assay experiments, 8×10^4 cells per plate were seeded in 35 mm imaging dishes (μ -Dish, ibidi GmbH) and cultured in growth medium for 40 to 46 hours to allow for sufficient cell attachment and growth, forming a confluent monolayer. Where indicated, cells were treated with 250 pM TGF-beta, 10 nM GDF11, or only growth medium as a control for 72 hours to investigate the effect of these ligands on cell migration. To ensure sustained ligand stimulation, the medium was exchanged at 48 hours with fresh medium containing the respective ligands or control. Prior to imaging, a scratch was made in the cell monolayer using a 10 μL pipette tip to create a straight line across the dish, reliably removing a section of cells and creating a defined gap or "wound" in the cell layer. The cells were then gently washed with PBS to remove debris and unattached cells resulting from the scratching process, followed by replenishment with phenol-red-free medium (Fluorobrite, Thermo Fisher) containing the appropriate ligands or control medium. Live cell imaging was utilized to capture the dynamics of cell migration and wound closure, with dishes placed in an incubator equipped with a live-cell imaging system to maintain optimal growth conditions (37°C, 5% CO₂) throughout the imaging period. Images of the scratch area were captured every 20 minutes over a 20-hour period to provide detailed temporal resolution of cell movements. The resulting data from the H2B-CFP nuclear marker was quantified using qCMA software (Zeisel et al., 2013) and displayed as average migration distance, which corresponds to the difference of the initial gap width and the width of the gap at a given time point.

4.1.17 RNA Sequencing.

For RNA sequencing, proliferating SRv2 WT cells were treated with 1nM ALK5i for 1 hour, while SRv2 WT SMAD3KO reporter cells and SRv2 WT cells treated with DMSO served as additional

conditions. All experiments were performed in biological duplicates, with biological triplicates generated for each. RNA was isolated from cell pellets as previously described. The IMB Genomics Core Facility (Mainz) performed RNA sequencing and initial data processing using the TruSeq stranded mRNA LT Sample Prep Kit (Illumina) according to manufacturer's instructions. Libraries were prepared with 500 ng RNA, amplified in 11 PCR cycles, and profiled using a DNA 1000 kit and a 2100 Bioanalyzer (Agilent). Library quantification was done using a Qubit 2.0 Fluorometer with the dsDNA HS Assay Kit (Thermo Fisher). Pooled libraries in equimolar ratios were sequenced on the NextSeq 500 system (Illumina) using a high-output flow cell in single-read mode, with 84 cycles plus 7 cycles index read. The RNA sequencing was conducted in a non-strand specific mode with 50 bp reads. The RNA sequencing and subsequent data processing were carried out by the Genomics Core Facility at IMB (Mainz).

4.1.18 Bioinformatic Analysis of RNA Sequencing Data.

The bioinformatic analysis of RNA sequencing data involved several key steps. First, samples were demultiplexed using `bcl2fastq` (v.2.19.1.403, Illumina) to generate FastQ files. The raw sequence reads were then assessed for quality using `FastQC` (v.0.11.5, Babraham Bioinformatics). Following this, the reads were aligned to the human reference genome GRCh38.p7, utilizing the GTF annotation file from Gencode human release 25, with the STAR aligner (v.2.5.2b). Mapped data were summarized at the gene level using `featureCounts` software (v.1.6.2, Subread). Finally, further data evaluation, normalization, and pairwise differential expression analyses were conducted in R (v.3.5.0) with the Bioconductor package `DESeq2` (v.1.20.0), adhering to the recommended analysis workflow. RPKMs for each gene were calculated with the Bioconductor packages `GenomicRanges` (v.1.32.1) and `rtracklayer` (v.1.40.6), utilizing a GTF annotation file and FPM data computed by `DESeq2`. Fold changes were determined using a maximum likelihood model based on a negative binomial distribution of reads, fitting these to the read counts across all sample conditions. P-values for each fold change, indicating differential expression relative to a reference condition, were also calculated. The RNA sequencing and subsequent data processing were carried out by the Genomics Core Facility at IMB (Mainz).

4.1.19 Filter the Data.

To filter the RNA-seq data, I developed a custom MATLAB script to identify genes with a p-value significance threshold of $p < 0.05$ and a \log_2 fold change greater than 1 from the final analysis table. This initial filtering step ensured the selection of statistically significant and biologically relevant genes. Subsequently, I wrote another MATLAB script to compare two groups of filtered genes, identifying those that were consistently up- or down-regulated across both lists. The genes identified through this

comprehensive filtering and comparative analysis process are listed in Figure 37, providing a robust set of candidates for further investigation.

Following the identification of genes, I used The Human Protein Atlas (<https://www.proteinatlas.org/>) to verify the subcellular localization of the corresponding proteins. Since not all proteins from the list had available information on this website, I also utilized the Compartments database (<https://compartments.jensenlab.org/>) as an additional tool to check protein locations. By combining data from these two resources, I was able to summarize and predict the subcellular localization of the proteins more comprehensively.

4.1.20 Data Analysis of Live-Cell Microscopy Experiments.

Cells were tracked throughout the experiment using custom MATLAB scripts based on code developed by the Alon lab and the CellProfiler project. Initially, raw images underwent flat-field correction and background subtraction. Individual nuclei were then segmented from nuclear marker images using adaptive thresholding and seeded watershed algorithms. A greedy match algorithm was applied to assign segmented cells to their corresponding positions in subsequent images, ensuring that only cells tracked from the first to the last time point were included. In cases of cell division, the daughter cell closest to the last position of the mother cell was followed, and tracks from mothers and offspring were merged. For quantification, nuclear fluorescence intensity was measured alongside cytoplasmic fluorescence, which was assessed using a 4-pixel wide annulus around the nucleus. Automated image analysis results were processed and normalized to remove artifacts, such as spikes caused by fluorescent lamp flickering. To account for cell division, nuclear area and integrated fluorescence intensity were normalized and smoothed. The median fluorescence for both nuclear and cytoplasmic measurements was calculated to provide robustness against fluctuations. Finally, the nucleus-to-cytoplasm ratio for each cell over time was estimated, allowing for a comprehensive analysis of single-cell trajectories. This approach enabled accurate tracking and quantification of cellular responses, accounting for changes in nuclear shape and cell division, ultimately ensuring a precise analysis of SMAD signaling dynamics in live cells.

To assess effect sizes and their significance between conditions, we performed permutation testing with 1000 permutations. This involved calculating changes in population means from subsamples of 20% of the imaged cells within each condition and establishing corresponding 90% confidence intervals.

4.1.21 Quantification of Cell Death.

Cell death was assessed in tracked cells based on decreases in nuclear size and cellular detachment. A cell was considered dying if its nucleus fragmented during apoptosis and its diameter fell below a defined threshold, calculated as the average nuclear area of cells at the initial time point minus 1.5

standard deviations. The fraction of dead cells per field of view was determined by counting the number of cells with a nuclear area above the threshold at each time point, dividing this number by the initial cell count, and subtracting the result from 1. This method allowed for the quantification of cell death over time by accounting for both nuclear shrinkage and cell detachment, characteristic features of apoptosis.

4.1.22 Quantification of Cell Motility.

Cell motility was quantified by calculating the Euclidean distances between consecutive positions of individual cells using their x and y coordinates, measured in pixels. To minimize the impact of tracking errors, any trajectories where the distance covered between two time points exceeded three times the average distance covered by all cells were excluded from further analysis. The motility score for each cell was determined by calculating the mean distance covered between consecutive time points. These pixel-based distances were then converted to actual distances using the resolution of the objective and camera (0.24 $\mu\text{m}/\text{pixel}$). This approach allowed for a robust quantification of cell movement by focusing on average displacement while filtering out any anomalous jumps in cell position that could arise from tracking errors.

4.1.23 Statistical Assessment of Differences in Cell Motility.

To assess statistically significant differences between the mean motilities of the TGF-beta, GDF11, and control groups within the same SMAD AUC bin, a resampling technique was employed due to the non-normality of the data. A two-step approach was utilized: first, a Gaussian kernel-density estimator (`scipy.stats.gaussian_kde`) was used to resample the motility and model the distribution of the respective mean in the control for each AUC group. Subsequently, the estimated distribution was integrated (`gaussian_kde.integrate_box_1d`) to calculate the p-values for the mean values observed in the TGF-beta and GDF11 conditions from the same AUC group. This method allowed for robust statistical comparison despite the non-normal distribution of the data, providing a reliable assessment of the differences in cell motility across treatment conditions and SMAD AUC bins.

4.1.24 Protein Quantification and Western Blot Assay.

Cells were seeded at a density of 6×10^5 cells per 6 cm tissue culture plate and cultured in growth medium for 2 days. After 48 hours of growth factor and serum deprivation, cells were stimulated for specified time points and harvested in 2 ml PBS by scraping. The harvested cells were centrifuged and flash-frozen in liquid nitrogen. Protein extraction was performed by lysing cells on ice for 30 min with 50 μl of RIPA buffer containing protease and phosphatase inhibitors. The lysis buffer composition was as follows:

1% protease inhibitor
 1% phosphatase inhibitor
 50 mM Tris
 100 mM NaCl
 1% Triton X-100
 0.5% Na-deoxycholate
 0.1% SDS

After centrifugation at 4°C for 30 min, protein concentration was determined using the Bradford protein assay. Extracted proteins were denatured with NuPAGE 4× Sample buffer and 50 mM reducing agent at 70°C for 10 minutes. Protein samples (20 µg) were loaded onto a 10% SDS-PAGE gel and separated for 1.5-3 hour at 120 V using the Mini Trans-Blot® Cell System. Precision Plus Protein™ Dual Color Standards were used for molecular weight estimation. Following electrophoresis, proteins were transferred to a PVDF membrane for 1.5 hours at 200 mA. The membrane was then blocked with 5% nonfat-dried milk or BSA in TBS-T for 1 hour at room temperature to prevent non-specific binding. Primary antibodies were diluted in the respective blocking solution and incubated with the membrane overnight at 4°C. The next day, the membrane was washed with TBS-T and incubated with an HRP-conjugated secondary antibody for 1 hour at room temperature. After washing, proteins on the membrane were detected using the Amersham ECL Prime Western Blotting Detection Kit. Chemiluminescent images were captured with a Fusion Fx documentation system.

Primary antibodies:

Total SMAD2 (D43B4, #5339, Cell Signaling Technology)
 Total SMAD3 (C67H9, #4088, Cell Signaling Technology)
 Phospho-Smad2 (Ser465/467) (Cell Signaling, #3108)
 Phospho-Smad3 (Ser423, Ser425) (Bioss, #BS-3425R)
 beta-actin (Sigma-Aldrich, #A5316)

Secondary antibodies:

HRP conjugated anti-mouse IgG (Thermo Fisher Scientific, #31430)

HRP conjugated anti-rabbit IgG (Thermo Fisher Scientific, #31460)

4.1.25 RNA Isolation and Quantification.

For RNA isolation, cells were processed following the protocol described in section 4.1.23. Total RNA extraction was carried out using the High Pure RNA Isolation Kit from Roche, according to the manufacturer's instructions. The eluted RNA was quantified using a NanoDrop 2000c spectrophotometer.

1 µg of RNA from each sample was reverse transcribed into cDNA using oligo dT primers and reverse transcriptase from the NEB First Strand cDNA Synthesis Kit. The reaction mixture was heated at 70°C for 5 minutes to initiate the process. The components used in the initial reaction mixture are listed below:

Component	Amount
RNA	1 µg
dNTP mix (10 mM)	1 µl
Oligo dT	2 µl
DEPC-treated H ₂ O	Up to 12 µl

After the initial heating step, the following components were added to the reaction mixture, which was then incubated for 1 hour at 42°C:

Component	Amount
5× Reaction Buffer	4 µl
DTT (1 M)	2 µl
RNase inhibitor	1 µl
DEPC-treated H ₂ O	1 µl

The enzymes were inactivated by heating the mixture at 80°C for 5 minutes. Finally, 180 µl of DEPC-treated H₂O was added to the mixture for dilution.

RT-qPCR was performed using the StepOnePlus™ Real-Time PCR System (Thermo Fisher Scientific) with a 96-well plate (Applied Biosystems) sealed with adhesive foil (Biozym). All samples were analyzed in triplicate.

The reaction mixture for each sample contained:

Component	Amount
cDNA	3 µl
SYBR Green Master Mix (Roche)	12.5 µl
Forward primer (640 nM)	4.75 µl
Reverse primer (640 nM)	4.75 µl

The PCR cycling conditions were as follows:

Stage	Temperature	Time	Cycles
Holding stage	95°C	10 minutes	1
Cycling stage	95°C	15 seconds	40
	60°C	1 minute	40
Melt curve analysis	95°C	15 seconds	1
	60°C	1 minute	1
	60-95°C	15 seconds	10

Gene expression levels were assessed using the comparative CT ($\Delta\Delta\text{CT}$) method. This involved calculating ΔCT , which is the difference between the CT value of the housekeeping gene (Actin) and the gene of interest, and then calculating $\Delta\Delta\text{CT}$, which is the difference in ΔCT values between experimental and control samples.

The primers as follows:

Primer name	Sequence (5'-3')
Actin Froward	GGCACCCAGCACAAATGAAGATCAA
Actin Reverse	TAGAAGCATTTGCGGTGGACGATG
LTBP2 Froward	TTACAAGCAGAGACTCACT
LTBP2 Reverse	ACAACAGAAGAGACCAGAT
MMP9 Froward	AGCGGGCGGCGCCTCTGGAGGTTCTGA
MMP9 Reverse	CCTGGCAGAAATAGGCTTTCTCTCGGT
PMEPA1 Froward	CTGAGCCACTACAAGCTGTCTG
PMEPA1 Reverse	CTTCTGAGGACAGGGCATCTTC
SMAD3 Froward	GGGCTCCCTCATGTCATCTA
SMAD3 Reverse	GGCTCGCAGTAGGTAAGTGG

4.1.26 Software and Website.

For the microscopy data analysis, we utilized MATLAB R2021a (MathWorks). The microscopy experiments themselves were conducted using NIS-Elements AR 4.50.00 (Nikon). For designing primers for PCR, Clone Manager (Sci Ed Software) was used, while Primer BLAST (<https://www.ncbi.nlm.nih.gov/tools/primer-blast/>) from PubMed was used for designing primers for QPCR. StepOne™ Software v2.3 (Thermo Fisher Scientific) facilitated the setup and analysis of QPCR data. CorelDRAW was used for preparing all charts and figures, including color adjustments, adding labels, and assembling images. The Human Protein Atlas (<https://www.proteinatlas.org/>) was referenced to verify the subcellular localization of proteins. For proteins not covered by this resource, the Compartments database (<https://compartments.jensenlab.org/>) was consulted. Additionally, Perplexity (<https://www.perplexity.ai/>) was used to refine the text and enhance the quality of the writing. Mendeley was used to insert and manage references.

4.2 Material and Methods of Part 2:

4.2.1 Cell Maintenance of EA.hy926 Cell Lines.

EA.hy926 wildtype cells and reporter cell lines were cultured in M199 medium supplemented with growth factors and antibiotics. Reporter cell lines additionally received selective antibiotics to maintain transgene expression. Cells were passaged every 2-3 days upon reaching over 90% confluency using a standard protocol: washing with 10 ml PBS, trypsinization for 2-3 minutes at 37°C with 2 ml trypsin, collection in 8 ml PBS, centrifugation for 3 minutes at 200 g, aspiration of supernatant, resuspension in fresh culture medium, and seeding at the desired dilution. All cultures were maintained at 37°C with 5% CO₂ to ensure optimal growth conditions and stability of transgene expression in EA.hy926 cell lines.

M199 medium components for cell culture:

M199 Medium (Sigma Aldrich)
20% Fetal Bovine Serum (FBS) (Life Technologies)
25 µg/ml Heparin (Sigma Aldrich)
50 µg/ml Endothelial Cell Growth Supplement (ECGS) (Corning)
1% Penicillin/Streptomycin (Thermo Fisher Scientific)
1% Glutamine (Thermo Fisher Scientific)

Formulating starvation medium for experimental applications:

M199 Medium
1.5% Fetal Bovine Serum (FBS)
25 µg/ml Heparin
50 µg/ml Endothelial Cell Growth Supplement (ECGS)
1% Penicillin/Streptomycin
1% Glutamine

Selective antibiotics for reporter cell lines:

200 µg/ml (selection), 100 µg/ml (culture) G418 (Merck)

100 µg/ml (selection), 50 µg/ml (culture) Hygromycin (Invitrogen)

10 ng/ml (selection), 5 ng/ml (culture) Blasticidin (Thermo Fisher Scientific)

4.2.2 Generated the Reporter Cell Line.

Lentiviral reporter constructs for SMAD1, SMAD5, and SMAD9 were generated using the MultiSite-Gateway recombination system (Invitrogen). The SMAD1 plasmid was originally produced by Jette Strasen for her PhD thesis (Strasen Henriette Sophie, 2018), while SMAD5 and SMAD9 plasmids were created by Sonja Gabriele Lenhardt for her Bachelor's thesis (Sonja Lenhardt, 2019). These constructs fused the protein-coding sequence of each SMAD protein to the yellow fluorescent protein Venus (YFP), under the control of the constitutive human Ubiquitin C promoter (UbCp). EA.hy926 cells were transduced with these lentiviral particles, along with viruses expressing histone 2B fused to cyan fluorescent protein (H2B-CFP) under the UbCp as a nuclear marker. Additionally, a SMAD1-SMAD2 double reporter cell line was established by introducing SMAD2 fused to the red fluorescent protein mCherry (also under the UbC promoter) into the existing SMAD1 reporter cell line. The SMAD2 plasmid was also created by Jette Strasen. Following transduction, stable clonal cell lines were established and validated for their ability to monitor SMAD protein activity effectively.

4.2.3 Live-Cell Time-Lapse Microscopy.

For live-cell time-lapse microscopy, 0.48×10^5 cells were seeded in 35-mm poly-D-lysine-coated glass-bottom dishes (ibidi) two days prior to experimentation. Twenty-four hours before imaging, the medium was changed to phenol red- and riboflavin-free medium supplemented with growth factors, 1.5% FBS, and penicillin/streptomycin. Imaging was conducted using a 20× CFI Plan Fluor objective and an Andor iXon Ultra 888 camera on a Nikon Eclipse Ti-E inverted microscope equipped with a perfect focus system. Specific filter sets were utilized for Venus (500/20 nm excitation, 515 nm dichroic beam splitter, 535/30 nm emission), CFP (436/20 nm excitation, 455 nm beam splitter, 480/40 nm emission), and mCherry (562/40 nm excitation, 593 nm beam splitter, 641/75 nm emission). Prior to treatment, cells were imaged for 30 minutes to establish baseline conditions. Images were captured at 10-20-minute intervals over a duration of 12-48 hours using Nikon Elements software within a custom enclosure maintaining conditions of 37°C, 5% CO₂, and controlled humidity.

4.2.4 Ligand and Inhibitor Treatments.

Ligands and inhibitors were prepared and stored according to specific protocols to maintain their efficacy. TGF-beta and GDF11 were stored at -80°C in 4 mM HCl with 1 mg/ml BSA, while other ligands were kept at -20°C in 1 mg/ml BSA. All inhibitors and FKBP12 PROTAC were diluted in DMSO and stored at -20°C. Twenty hours before the microscopy experiment, the cell medium was

changed to one containing 1.5% FBS instead of 20%. For FKBP12 removal, FKBP12 PROTAC was added during this medium change. Prior to the experiment, ligands and inhibitors were prepared in 125/250 μ l of medium and added to cells to achieve desired concentrations in a final volume of 1 ml. Control cells received either medium alone or medium with DMSO.

Inhibitors and ligands used:

TGF-beta (Peprotech)	Various concentrations
GDF11 (Peprotech)	250 ng/ml
Activin A (Peprotech)	Various concentrations
BMP2 (Peprotech)	250 ng/ml
BMP6 (Peprotech)	250 ng/ml
BMP7 (Peprotech)	Various concentrations
BMP9 (Peprotech)	Various concentrations
BMP10 (Peprotech)	2 ng/ml
K02288 (ALK1i) (Selleckchem)	1 μ M
LDN-214117 (ALK2/1i) (Selleckchem)	10 μ M
SB525334 (ALK5/4i) (Selleckchem)	10 μ M
FKBP12 PROTAC (synthesized by Hausch lab)	200 nM

4.2.5 Western Blot Assay.

Cells were initially seeded in 6-cm dishes at a density of $5-6 \times 10^5$ cells per plate and allowed to grow for 48 hours before the experiment. To induce a SMAD response to ligands, the regular growth medium was replaced with 1.5% FBS medium 20 hours prior to treatment initiation. For FKBP12 removal, FKBP12 PROTAC was added during this medium change. On the day of the experiment, cells were treated with specific ligands as required and harvested at designated time points for further analysis. The detail western blot experiment was the same as it described in the 4.1.23. In brief, proteins were isolated in the presence of protease and phosphatase inhibitors, and concentrations were measured by BCA assay (Thermo Fisher Scientific). Equal amounts of protein were separated by electrophoresis on 10-12.5% SDS-polyacrylamide gels and transferred to PVDF membranes (GE Healthcare) by electroblotting (Bio-Rad). Membranes were blocked with 5% non-fat dried milk or 5% bovine serum albumin, incubated overnight with primary antibodies, washed, incubated with secondary antibodies, washed again, and detected using chemiluminescence (ECL Prime, GE Healthcare).

Primary antibodies:

Total SMAD1 (Invitrogen, MA5-41184)

Total SMAD2 (D43B4, #5339, Cell Signaling Technology)

Phospho-Smad1(Ser463/465)/5(Ser463/465)/9(Ser463/465) (Cell Signaling Technology, #13820)

Phospho-Smad2 (Ser465/467) (Cell Signaling, #3108)

Phospho-Smad3 (Ser423, Ser425) (Bioss, #BS-3425R)

FKBP12 (Biozol, HBO-ET1703-55)

beta-actin (Sigma-Aldrich, #A5316)

Secondary antibodies:

HRP conjugated anti-mouse IgG (Thermo Fisher Scientific, #31430)

HRP conjugated anti-rabbit IgG (Thermo Fisher Scientific, #31460)

4.2.6 Real-Time Quantitative PCR (RT-qPCR).

Cells were plated and harvested at specified time points following stimulation using the same as the western did in 4.2.4. The following same as it described in 4.1.24. in brief, total RNA extraction was performed using the High Pure RNA Isolation kit (Roche), with RNA concentration determined using a NanoDrop 2000 spectrophotometer (Thermo Fisher Scientific). Complementary DNA (cDNA) was synthesized from 1 µg of RNA using either M-MuLV or ProtoScript II reverse transcriptase (both from NEB) with oligo-dT primers. Quantitative PCR (qPCR) was conducted in triplicates using SYBR Green reagent (Roche) on a StepOnePlus PCR machine (Applied Biosystems). Data were collected and analyzed using StepOne Software v2.3.5.7.

The following primer sequences were utilized:

Primer name	Sequence (5'-3')
beta-actin forward	GGCACCCAGCACAATGAAGATCAA
beta-actin reverse	TAGAAGCATTGCGGTGGACGATG
ID2 forward	TCCCAGGGTGTCTCTTACTTGGACT
ID2 reverse	GGATCCTTCTGGTATTTCACGCTCCA
EDN1 forward	ACTTCTGCCACCTGGACATC
EDN1 reverse	GGCAAAAATTCCAGCACTTC
DLL4 forward	TGCAACTGCCCTTATGGCTTTGTG
DLL4 reverse	ACAAGTTGTTTCATGGCTTCCCTGC

4.2.7 Image Analysis and Cell Tracking.

Cells were tracked throughout experiments using custom MATLAB scripts based on code from the Alon laboratory and the CellProfiler project, as described in section 4.1.19. In brief, the process involved extracting images, performing flat-field correction and fluorescence normalization, and segmenting cells using the nuclear marker H2B-CFP. Cells were tracked over time, excluding those

that left the field of view or died. For each cell, nuclear and cytoplasmic (4-pixel annulus) fluorescence intensities were quantified, and the nuclear-to-cytoplasmic ratio was calculated over time, with values interpolated during mitosis. This method allowed for comprehensive analysis of cellular dynamics and fluorescence distribution throughout the experiment. In order to quantified cell motility, I am using the same method as it describes in 4.1.21.

4.2.8 EC50 and IC50 analysis.

The EC50 and IC50 analysis script by Sonja Lenhardt involves a detailed and systematic approach to analyzing dose-response relationships (Sonja Lenhardt, 2022). Firstly, calculated the median values for each condition to obtain a representative dataset. From these median values, the script identified the peak (maximum) value and its corresponding time point for each condition, and these peak values were then extracted and stored separately. Concentrations corresponding to each condition were manually defined to reflect the experimental setup accurately. To assess variability, the first (Q1) and third (Q3) quartiles of the peak data for each condition were calculated, and the error margins were computed based on these quartiles. The concentration and peak data, along with the computed error margins, were then prepared for the EC50 calculation. Using a dose-response function, these prepared data points were incorporated to calculate the EC50 value. Finally, the results were visualized using appropriate plotting functions to clearly present the findings.

4.2.9 Timing of Nuclear Translocation.

To analyze turning points and changes in the normalized data values, I first normalized the dataset by dividing each value by the initial value for the relevant condition. The median of these normalized values was calculated to provide a summary of the data. I then identified the most significant drop by detecting the largest change between consecutive time points and recorded the time at which this drop occurred. Following this, I located the time point closest to a specified target value by finding the smallest deviation from this target. I visualized the normalized data with a plot that highlighted both the most significant drop and the point nearest to the target value using distinct markers.

To assess the recovery time of the signal after inhibitor treatment, I identified the time point where the signal returned to approximately 1.1 times the baseline value. I then calculated the time difference between the most significant drop and this recovery point.

4.2.10 Investigating Single-Cell SMAD1 and SMAD2 First Response Dynamics.

To analyze the first response dynamics of single-cell SMAD1 and SMAD2, a MATLAB script was developed utilizing the 'findpeaks' function. The script focused on the first 5 hours post-ligand addition to identify peak responses. If multiple peaks were detected within this timeframe, the maximum value

was selected. In instances where no distinguishable peak was found, the value was set to $1e-10$. The results were visualized using a dot chart, with SMAD2 values on the x-axis and SMAD1 values on the y-axis. To represent the density of single-cell responses, the 'ksdensity' function was employed, overlaying a density plot on the dot chart. Additionally, corresponding histograms and the 'density2C' function were used to color the dots in the scatter chart according to their density. This approach enabled a comprehensive visualization of the distribution and relationship between SMAD1 and SMAD2 responses at the single-cell level following ligand stimulation.

4.2.11 Single Cell Dual Single Correlation Assay.

To analyze the correlation between two channels at the single-cell level, a MATLAB script was developed. Initially, the data were normalized using the `bsxfun` function. The normalized SMAD1 and SMAD2 data for the condition of interest were extracted. A correlation matrix was then computed to determine the Pearson correlation coefficients between SMAD1 and SMAD2 for each cell. Any NaN values in the matrix were replaced with a small value ($1e-10$) to ensure computational stability. A bootstrap analysis was conducted with 100 iterations to validate the correlation results. For each cell, a temporary matrix was created by randomly permuting the order of the SMAD2 data. The correlation coefficients were calculated between the SMAD1 data and the permuted SMAD2 data for each iteration.

4.2.12 Peak Value for Dual Single Assay.

To assess the impact of FKBP12 on SMAD1 and SMAD2 responses across various BMP7 concentrations, data were organized into a matrix of maximum values at different time points for each BMP7 concentration. The median of these values was calculated for each condition and time point, with normalization performed by dividing by the initial median value from the baseline (no FKBP12 treatment), setting this baseline to zero. Peak ratio values in the presence of FKBP12 were standardized to a reference value of 1 for each BMP7 concentration by dividing the normalized peak values with FKBP12 by baseline values and expressing changes as percentages. Percentage differences between FKBP12-treated and untreated conditions were then computed, these effects were visualized using scatter plots of percentage changes against conditions. In the TGF-beta and BMP9 co-treatment experiment, SMAD1 and SMAD2 responses were analyzed using different reference points. For SMAD1, BMP9-only treatment was used as the reference (value of 1). For SMAD2, TGF-beta-only treatments at various doses served as the reference (value of 1).

4.2.13 Radar Chart.

To create the radar chart, conditions of interest were selected, and data corresponding to these conditions were extracted. The peak values of the SMAD2 nuc/cyt ratio over specified time intervals were

identified for each condition. These values were organized into a matrix where missing values were set to NaN. The median values for each condition were calculated, and the median of the base condition without the FKBP12 PROTAC was subtracted to normalize the data, setting it to zero. The ligand simulation with PROTAC condition was then set as the reference with a median value of one. The resulting normalized data were divided into two groups and combined into a single matrix for plotting. The radar chart was generated using the 'radarChart' function. The radial limits and tick intervals were adjusted, and the chart was drawn with customized line widths and colors for the theta and radial ticks.

4.2.14 Tube Formation Assay.

The tube formation assay was used to assess the angiogenic potential of endothelial cells. To begin, Matrigel (Corning, USA) was thawed overnight on ice at 4°C. A μ -Slide 15 Well 3D plate (ibidi Cat.No:81506) was also pre-chilled overnight at 4°C. Once chilled, 10 μ L of Matrigel was added to each well of the plate, which was then incubated at 37°C for 30 minutes to allow the Matrigel to solidify. To verify the volume, place the slide 1-2 cm above a scale paper and observe the scale through the filled wells. If the grid on the scale paper appears reduced, increase the pipetting volume. If the grid appears magnified, decrease the volume.

For the assay, SMAD1 reporter cells were seeded in a 6-well plate and 24 hours later, the medium was replaced with 1.5% FBS instead of 20%. If required, FKBP12 PROTAC was added at this time. After another 24 hours, cells were treated with BMP9 (3 ng/mL) and BMP7 (250 ng/mL) for 48 hours. The cells were then harvested, resuspended in endothelial cell growth medium (Lonza, USA) to a final concentration of 2×10^5 cells/mL, and 50 μ L of this cell suspension was added to each well containing solidified Matrigel. The plate was incubated at 37°C with 5% CO₂ for 1 hour to allow for tube formation. During the incubation, the plate was monitored using a microscope. Images were captured every hour for 12 hours, focusing on different layers with the help of the software's perfect focus feature. After the incubation period, images of the tube networks were analyzed using ImageJ software (NIH, USA) with the custom Angiogenesis Analyzer plugin. Key metrics such as the number of branches, total tube length, and number of closed loops were quantified. All experiments were conducted in triplicate to ensure accuracy and reproducibility.

4.2.15 Softwares Used for the Assay.

For the microscopy data analysis, I utilized MATLAB R2021a (MathWorks). The microscopy experiments were conducted using NIS-Elements AR 4.50.00 (Nikon). ImageJ (Public Domain) was employed to analyze the tube formation assay. For designing primers for PCR, Clone Manager (Sci Ed Software) was used, while Primer BLAST (<https://www.ncbi.nlm.nih.gov/tools/primer-blast/>) from PubMed was used for designing primers for QPCR. StepOne™ Software v2.3 (Thermo Fisher Scientific)

facilitated the setup and analysis of QPCR data. CorelDRAW was used for preparing all charts and figures, including color adjustments, adding labels, and assembling images. Additionally, Perplexity (<https://www.perplexity.ai/>) was used to refine the text and enhance the quality of the writing. Mendeley was used to insert and manage references.

5 Reference

- Aashaq, S., Batool, A., Mir, S. A., Beigh, M. A., Andrabi, K. I., & Shah, Z. A. (2022). TGF- β signaling: A recap of SMAD-independent and SMAD-dependent pathways. In *Journal of Cellular Physiology* (Vol. 237, Issue 1). <https://doi.org/10.1002/jcp.30529>
- Abdullah, A., Herdenberg, C., & Hedman, H. (2023). Ligand-specific regulation of transforming growth factor beta superfamily factors by leucine-rich repeats and immunoglobulin-like domains proteins. *PLoS ONE*, *18*(8 August). <https://doi.org/10.1371/journal.pone.0289726>
- Albiñana, V., Sanz-Rodríguez, F., Recio-Poveda, L., Bernabéu, C., & Botella, L. M. (2011). Immunosuppressor FK506 increases endoglin and activin receptor-like kinase 1 expression and modulates transforming growth factor- β 1 signaling in endothelial cells. *Molecular Pharmacology*, *79*(5). <https://doi.org/10.1124/mol.110.067447>
- Al-Samkari, H. (2022). Systemic Antiangiogenic Therapies for Bleeding in Hereditary Hemorrhagic Telangiectasia: A Practical, Evidence-Based Guide for Clinicians. In *Seminars in Thrombosis and Hemostasis* (Vol. 48, Issue 5). <https://doi.org/10.1055/s-0042-1743467>
- Altschuler, S. J., & Wu, L. F. (2010). Cellular Heterogeneity: Do Differences Make a Difference? In *Cell* (Vol. 141, Issue 4). <https://doi.org/10.1016/j.cell.2010.04.033>
- Ankers, J. M., Spiller, D. G., White, M. R., & Harper, C. V. (2008). Spatio-temporal protein dynamics in single living cells. In *Current Opinion in Biotechnology* (Vol. 19, Issue 4). <https://doi.org/10.1016/j.copbio.2008.07.001>
- Anne-Sophie Lindemann. (2018). *Title German: Untersuchung der Rolle von Smad2-Phosphorylierung in nukleärem shuttling von Smad2 in einzelnen Zellen Title English: Investigating the role of Smad2 phosphorylation on nuclear shuttling of Smad2 in single cells.*
- Aragón, E., Wang, Q., Zou, Y., Morgani, S. M., Ruiz, L., Kaczmarek, Z., Su, J., Torner, C., Tian, L., Hu, J., Shu, W., Agrawal, S., Gomes, T., Márquez, J. A., Hadjantonakis, A. K., Macias, M. J., & Massagué, J. (2019). Structural basis for distinct roles of SMAD2 and SMAD3 in FOXH1 pioneer-directed TGF- β signaling. *Genes & Development*, *33*(21–22). <https://doi.org/10.1101/gad.330837.119>
- Arany, P. R., Flanders, K. C., Kobayashi, T., Kuo, C. K., Stuelten, C., Desai, K. V., Tuan, R., Rennard, S. I., & Roberts, A. B. (2006). Smad3 deficiency alters key structural elements of the extracellular matrix and mechanotransduction of wound closure. *Proceedings of the National Academy of Sciences of the United States of America*, *103*(24). <https://doi.org/10.1073/pnas.0602473103>
- Arnold, S. J., Maretto, S., Islam, A., Bikoff, E. K., & Robertson, E. J. (2006). Dose-dependent Smad1, Smad5 and Smad8 signaling in the early mouse embryo. *Developmental Biology*, *296*(1). <https://doi.org/10.1016/j.ydbio.2006.04.442>
- Attisano, L., & Wrana, J. L. (2002). Signal transduction by the TGF- β superfamily. In *Science* (Vol. 296, Issue 5573). <https://doi.org/10.1126/science.1071809>
- Aykul, S., Corpina, R. A., Goebel, E. J., Cunanan, C. J., Dimitriou, A., Kim, H. J., Zhang, Q., Rafique, A., Leidich, R., Wang, X., McClain, J., Jimenez, J., Nannuru, K. C., Rothman, N. J., Lees-Shepard, J. B., Martinez-Hackert, E., Murphy, A. J., Thompson, T. B., Economides, A. N., & Idone, V. (2020). Activin forms a non-signaling complex with acvr1 and type ii activin/bmp receptors via its finger 2 tip loop. *ELife*, *9*. <https://doi.org/10.7554/eLife.54582>

- Ayuso-Íñigo, B., Méndez-García, L., Pericacho, M., & Muñoz-Félix, J. M. (2021). The dual effect of the BMP9–ALK1 pathway in blood vessels: An opportunity for cancer therapy improvement? In *Cancers* (Vol. 13, Issue 21). <https://doi.org/10.3390/cancers13215412>
- Bandyopadhyay, A., Tsuji, K., Cox, K., Harfe, B. D., Rosen, V., & Tabin, C. J. (2006). Genetic analysis of the roles of BMP2, BMP4, and BMP7 in limb patterning and skeletogenesis. *PLoS Genetics*, 2(12). <https://doi.org/10.1371/journal.pgen.0020216>
- Batchelor, E., Loewer, A., Mock, C., & Lahav, G. (2011). Stimulus-dependent dynamics of p53 in single cells. *Molecular Systems Biology*, 7. <https://doi.org/10.1038/msb.2011.20>
- Benn, A., Alonso, F., Mangelschots, J., Génot, E., Lox, M., & Zwijsen, A. (2020). BMP-SMAD1/5 signaling regulates retinal vascular development. *Biomolecules*, 10(3). <https://doi.org/10.3390/biom10030488>
- Benn, A., Hiepen, C., Osterland, M., Schütte, C., Zwijsen, A., & Knaus, P. (2017). Role of bone morphogenetic proteins in sprouting angiogenesis: Differential BMP receptor-dependent signaling pathways balance stalk vs. tip cell competence. *FASEB Journal*, 31(11). <https://doi.org/10.1096/fj.201700193RR>
- Bhaskaran, M., Kolliputi, N., Wang, Y., Gou, D., Chintagari, N. R., & Liu, L. (2007). Trans-differentiation of alveolar epithelial type II cells to type I cells involves autocrine signaling by transforming growth factor β 1 through the Smad pathway. *Journal of Biological Chemistry*, 282(6). <https://doi.org/10.1074/jbc.M609060200>
- Bidart, M., Ricard, N., Levet, S., Samson, M., Mallet, C., David, L., Subileau, M., Tillet, E., Feige, J. J., & Bailly, S. (2012). BMP9 is produced by hepatocytes and circulates mainly in an active mature form complexed to its prodomain. *Cellular and Molecular Life Sciences*, 69(2). <https://doi.org/10.1007/s00018-011-0751-1>
- Blanpain, C., & Simons, B. D. (2013). Unravelling stem cell dynamics by lineage tracing. In *Nature Reviews Molecular Cell Biology* (Vol. 14, Issue 8). <https://doi.org/10.1038/nrm3625>
- Bohn, S., Hexemer, L., Huang, Z., Strohmaier, L., Lenhardt, S., Legewie, S., & Loewer, A. (2023). State- And stimulus-specific dynamics of SMAD signaling determine fate decisions in individual cells. *Proceedings of the National Academy of Sciences of the United States of America*, 120(10). <https://doi.org/10.1073/pnas.2210891120>
- Brown, K. A., Pietenpol, J. A., & Moses, H. L. (2007). A tale of two proteins: Differential roles and regulation of Smad2 and Smad3 in TGF- β signaling. In *Journal of Cellular Biochemistry* (Vol. 101, Issue 1). <https://doi.org/10.1002/jcb.21255>
- Burch, M. L., Zheng, W., & Little, P. J. (2011). Smad linker region phosphorylation in the regulation of extracellular matrix synthesis. In *Cellular and Molecular Life Sciences* (Vol. 68, Issue 1). <https://doi.org/10.1007/s00018-010-0514-4>
- Cai, J., Pardali, E., Sánchez-Duffhues, G., & Ten Dijke, P. (2012). BMP signaling in vascular diseases. In *FEBS Letters* (Vol. 586, Issue 14). <https://doi.org/10.1016/j.febslet.2012.04.030>
- Caminati, G., & Procacci, P. (2020). Mounting evidence of FKBP12 implication in neurodegeneration. In *Neural Regeneration Research* (Vol. 15, Issue 12). <https://doi.org/10.4103/1673-5374.284980>
- Canalis, E., Economides, A. N., & Gazzerro, E. (2003). Bone morphogenetic proteins, their antagonists, and the skeleton. In *Endocrine Reviews* (Vol. 24, Issue 2). <https://doi.org/10.1210/er.2002-0023>

- Carmeliet, P., & Jain, R. K. (2011). Molecular mechanisms and clinical applications of angiogenesis. In *Nature* (Vol. 473, Issue 7347). <https://doi.org/10.1038/nature10144>
- Chaikuad, A., & Bullock, A. N. (2016). Structural basis of intracellular TGF- β signaling: Receptors and smads. *Cold Spring Harbor Perspectives in Biology*, 8(11). <https://doi.org/10.1101/cshperspect.a022111>
- Chang, H., Huylebroeck, D., Verschueren, K., Guo, Q., Matzuk, M. M., & Zwijsen, A. (1999). Smad5 knockout mice die at mid-gestation due to multiple embryonic and extraembryonic defects. *Development*, 126(8). <https://doi.org/10.1242/dev.126.8.1631>
- Chattopadhyaya, S., Harikishore, A., & S. Yoon, H. (2011). Role of FK506 Binding Proteins in Neurodegenerative Disorders. *Current Medicinal Chemistry*, 18(35). <https://doi.org/10.2174/092986711798194441>
- Chen, C., Uludağ, H., Wang, Z., & Jiang, H. (2012). Noggin suppression decreases BMP-2-induced osteogenesis of human bone marrow-derived mesenchymal stem cells in Vitro. *Journal of Cellular Biochemistry*, 113(12). <https://doi.org/10.1002/jcb.24240>
- Chen, D., Zhao, M., & Mundy, G. R. (2004). Bone morphogenetic proteins. *Growth Factors*, 22(4). <https://doi.org/10.1080/08977190412331279890>
- Chen, T., You, Y., Jiang, H., & Wang, Z. Z. (2017). Epithelial–mesenchymal transition (EMT): A biological process in the development, stem cell differentiation, and tumorigenesis. In *Journal of Cellular Physiology* (Vol. 232, Issue 12). <https://doi.org/10.1002/jcp.25797>
- Chou, J. L., Fan, Z., DeBlasio, T., Koff, A., Rosen, N., & Mendelsohn, J. (1999). Constitutive overexpression of cyclin D1 in human breast epithelial cells does not prevent G1 arrest induced by deprivation of epidermal growth factor. *Breast Cancer Research and Treatment*, 55(3). <https://doi.org/10.1023/A:1006217413089>
- Christner, C., Herdegen, T., & Fischer, G. (2005). FKBP Ligands as Novel Therapeutics for Neurological Disorders. *Mini-Reviews in Medicinal Chemistry*, 1(4). <https://doi.org/10.2174/1389557013406675>
- Clarke, D. C., & Liu, X. (2008). Decoding the quantitative nature of TGF- β /Smad signaling. In *Trends in Cell Biology* (Vol. 18, Issue 9). <https://doi.org/10.1016/j.tcb.2008.06.006>
- Coda, D. M., Patel, H., Gori, I., Gaarenstroom, T. E., Song, O. R., Howell, M., & Hill, C. S. (2022). A network of transcription factors governs the dynamics of NODAL/Activin transcriptional responses. *Journal of Cell Science*, 135(8). <https://doi.org/10.1242/jcs.259972>
- Connolly, E. C., Freimuth, J., & Akhurst, R. J. (2012). Complexities of TGF- β targeted cancer therapy. In *International Journal of Biological Sciences* (Vol. 8, Issue 7). <https://doi.org/10.7150/ijbs.4564>
- Conway, E. M., Collen, D., & Carmeliet, P. (2001). Molecular mechanisms of blood vessel growth. In *Cardiovascular Research* (Vol. 49, Issue 3). [https://doi.org/10.1016/S0008-6363\(00\)00281-9](https://doi.org/10.1016/S0008-6363(00)00281-9)
- Correns, A., Zimmermann, L. M. A., Baldock, C., & Sengle, G. (2021). BMP antagonists in tissue development and disease. In *Matrix Biology Plus* (Vol. 11). <https://doi.org/10.1016/j.mbplus.2021.100071>
- Costanza, B., Umelo, I. A., Bellier, J., Castronovo, V., & Turtoi, A. (2017). Stromal modulators of TGF- β in cancer. In *Journal of Clinical Medicine* (Vol. 6, Issue 1). <https://doi.org/10.3390/jcm6010007>

- David, C. J., & Massagué, J. (2018). Publisher Correction: Contextual determinants of TGF β action in development, immunity and cancer (Nature Reviews Molecular Cell Biology (2018) DOI: 10.1038/s41580-018-0007-0). In *Nature Reviews Molecular Cell Biology* (Vol. 19, Issue 7). <https://doi.org/10.1038/s41580-018-0018-x>
- David, L., Mallet, C., Keramidas, M., Lamandé, N., Gasc, J. M., Dupuis-Girod, S., Plauchu, H., Feige, J. J., & Bailly, S. (2008). Bone morphogenetic protein-9 is a circulating vascular quiescence factor. *Circulation Research*, 102(8), 914–922. <https://doi.org/10.1161/CIRCRESAHA.107.165530>
- David, L., Mallet, C., Mazerbourg, S., Feige, J. J., & Bailly, S. (2007). Identification of BMP9 and BMP10 as functional activators of the orphan activin receptor-like kinase 1 (ALK1) in endothelial cells. *Blood*, 109(5). <https://doi.org/10.1182/blood-2006-07-034124>
- De Caestecker, M. P., Parks, W. T., Frank, C. J., Castagnino, P., Bottaro, D. P., Roberts, A. B., & Lechleider, R. J. (1998). Smad2 transduces common signals from receptor serine/threonine and tyrosine kinases. *Genes and Development*, 12(11). <https://doi.org/10.1101/gad.12.11.1587>
- DeCicco-Skinner, K. L., Henry, G. H., Cataisson, C., Tabib, T., Curtis Gwilliam, J., Watson, N. J., Bullwinkle, E. M., Falkenburg, L., O'Neill, R. C., Morin, A., & Wiest, J. S. (2014). Endothelial cell tube formation assay for the in vitro study of angiogenesis. *Journal of Visualized Experiments*, 91. <https://doi.org/10.3791/51312>
- Deheuninck, J., & Luo, K. (2009). Ski and SnoN, potent negative regulators of TGF- β signaling. In *Cell Research* (Vol. 19, Issue 1). <https://doi.org/10.1038/cr.2008.324>
- Derynck, R., Akhurst, R. J., & Balmain, A. (2001). TGF- β signaling in tumor suppression and cancer progression. In *Nature Genetics* (Vol. 29, Issue 2). <https://doi.org/10.1038/ng1001-117>
- Derynck, R., & Budi, E. H. (2019). Specificity, versatility, and control of TGF- β family signaling. In *Science Signaling* (Vol. 12, Issue 570). <https://doi.org/10.1126/scisignal.aav5183>
- Derynck, R., & Zhang, Y. E. (2003). Smad-dependent and Smad-independent pathways in TGF- β family signalling. In *Nature* (Vol. 425, Issue 6958). <https://doi.org/10.1038/nature02006>
- Desroches-Castan, A., Tillet, E., Bouvard, C., & Bailly, S. (2022). BMP9 and BMP10: Two close vascular quiescence partners that stand out. In *Developmental Dynamics* (Vol. 251, Issue 1, pp. 178–197). John Wiley and Sons Inc. <https://doi.org/10.1002/dvdy.395>
- Dijke, P. Ten, Goumans, M. J., Itoh, F., & Itoh, S. (2002). Regulation of cell proliferation by Smad proteins. In *Journal of Cellular Physiology* (Vol. 191, Issue 1). <https://doi.org/10.1002/jcp.10066>
- Dongre, A., & Weinberg, R. A. (2019). New insights into the mechanisms of epithelial–mesenchymal transition and implications for cancer. In *Nature Reviews Molecular Cell Biology* (Vol. 20, Issue 2). <https://doi.org/10.1038/s41580-018-0080-4>
- Dudley, A. T., & Robertson, E. J. (1997). Overlapping expression domains of bone morphogenetic protein family members potentially account for limited tissue defects in BMP7 deficient embryos. *Developmental Dynamics*, 208(3). [https://doi.org/10.1002/\(SICI\)1097-0177\(199703\)208:3<349::AID-AJA6>3.0.CO;2-I](https://doi.org/10.1002/(SICI)1097-0177(199703)208:3<349::AID-AJA6>3.0.CO;2-I)
- Dumont, F. J. (2012). FK506, An Immunosuppressant Targeting Calcineurin Function. *Current Medicinal Chemistry*, 7(7). <https://doi.org/10.2174/0929867003374723>

- Dumont, N., Bakin, A. V., & Arteaga, C. L. (2003). Autocrine transforming growth factor- β signaling mediates Smad-independent motility in human cancer cells. *Journal of Biological Chemistry*, 278(5). <https://doi.org/10.1074/jbc.M204623200>
- Dyson, S., & Gurdon, J. B. (1998). The interpretation of position in a morphogen gradient as revealed by occupancy of activin receptors. *Cell*, 93(4). [https://doi.org/10.1016/S0092-8674\(00\)81185-X](https://doi.org/10.1016/S0092-8674(00)81185-X)
- Ebisawa, T., Fukuchi, M., Murakami, G., Chiba, T., Tanaka, K., Imamura, T., & Miyazono, K. (2001). Smurf1 Interacts with Transforming Growth Factor- β Type I Receptor through Smad7 and Induces Receptor Degradation. *Journal of Biological Chemistry*, 276(16). <https://doi.org/10.1074/jbc.C100008200>
- Edgell, C. J. S., McDonald, C. C., & Graham, J. B. (1983). Permanent cell line expressing human factor VIII-related antigen established by hybridization. *Proceedings of the National Academy of Sciences of the United States of America*, 80(12 I). <https://doi.org/10.1073/pnas.80.12.3734>
- Falanga, V., Schrayner, D., Cha, J., Butmarc, J., Carson, P., Roberts, A. B., & Kim, S. J. (2004). Full-thickness wounding of the mouse tail as a model for delayed wound healing: Accelerated wound closure in Smad3 knock-out mice. *Wound Repair and Regeneration*, 12(3). <https://doi.org/10.1111/j.1067-1927.2004.012316.x>
- Felici, A., Wurthner, J. U., Parks, W. T., Giam, L. R. Y., Reiss, M., Karpova, T. S., McNally, J. G., & Roberts, A. B. (2003). TLP, a novel modulator of TGF- β signaling, has opposite effects on Smad2- and Smad3-dependent signaling. *EMBO Journal*, 22(17). <https://doi.org/10.1093/emboj/cdg428>
- Feng, X. H., & Derynck, R. (2005). Specificity and versatility in TGF- β signaling through smads. In *Annual Review of Cell and Developmental Biology* (Vol. 21). <https://doi.org/10.1146/annurev.cellbio.21.022404.142018>
- Finnson, K. W., McLean, S., Di Guglielmo, G. M., & Philip, A. (2013). Dynamics of Transforming Growth Factor Beta Signaling in Wound Healing and Scarring. *Advances in Wound Care*, 2(5). <https://doi.org/10.1089/wound.2013.0429>
- Finzel, A., Grybowski, A., Strasen, J., Cristiano, E., & Loewer, A. (2016). Hyperactivation of ATM upon DNA-PKcs inhibition modulates p53 dynamics and cell fate in response to DNA damage. *Molecular Biology of the Cell*, 27(15). <https://doi.org/10.1091/mbc.E16-01-0032>
- Flanders, K. C. (2004). Smad3 as a mediator of the fibrotic response. In *International Journal of Experimental Pathology* (Vol. 85, Issue 2). <https://doi.org/10.1111/j.0959-9673.2004.00377.x>
- Gaengel, K., Genové, G., Armulik, A., & Betsholtz, C. (2009). Endothelial-mural cell signaling in vascular development and angiogenesis. In *Arteriosclerosis, Thrombosis, and Vascular Biology* (Vol. 29, Issue 5). <https://doi.org/10.1161/ATVBAHA.107.161521>
- Gajos-Michniewicz, A., Piastowska, A. W., Russell, J. A., & Ochedalski, T. (2010). Follistatin as a potent regulator of bone metabolism. In *Biomarkers* (Vol. 15, Issue 7). <https://doi.org/10.3109/1354750X.2010.495786>
- Gallione, C. J., Repetto, G. M., Legius, E., Rustgi, A. K., Schelley, S. L., Tejpar, S., Mitchell, G., Drouin, É., Westermann, C. J. J., & Marchuk, D. A. (2004). A combined syndrome of juvenile polyposis and hereditary haemorrhagic telangiectasia associated with mutations in MADH4 (SMAD4). *Lancet*, 363(9412). [https://doi.org/10.1016/S0140-6736\(04\)15732-2](https://doi.org/10.1016/S0140-6736(04)15732-2)

- Garcia-Rivas, G., Jerjes-Sánchez, C., Rodriguez, D., Garcia-Pelaez, J., & Trevino, V. (2017). A systematic review of genetic mutations in pulmonary arterial hypertension. *BMC Medical Genetics*, *18*(1). <https://doi.org/10.1186/s12881-017-0440-5>
- Geiger, T. M., Walz, M., Meyners, C., Kuehn, A., Dreizler, J. K., Sugiarto, W. O., Maciel, E. V. S., Zheng, M., Lermyte, F., & Hausch, F. (2024). Discovery of a Potent Proteolysis Targeting Chimera Enables Targeting the Scaffolding Functions of FK506-Binding Protein 51 (FKBP51). *Angewandte Chemie - International Edition*, *63*(3). <https://doi.org/10.1002/anie.202309706>
- Gipson, G. R., Goebel, E. J., Hart, K. N., Kappes, E. C., Kattamuri, C., McCoy, J. C., & Thompson, T. B. (2020). Structural perspective of BMP ligands and signaling. In *Bone* (Vol. 140). <https://doi.org/10.1016/j.bone.2020.115549>
- Gordon, G. M., Ledee, D. R., Feuer, W. J., & Fini, M. E. (2009). Cytokines and signaling pathways regulating matrix metalloproteinase-9 (MMP-9) expression in corneal epithelial cells. *Journal of Cellular Physiology*, *221*(2). <https://doi.org/10.1002/jcp.21869>
- Goumans, M. J., Liu, Z., & Ten Dijke, P. (2009). TGF- β signaling in vascular biology and dysfunction. In *Cell Research* (Vol. 19, Issue 1, pp. 116–127). <https://doi.org/10.1038/cr.2008.326>
- Goumans, M. J., Valdimarsdottir, G., Itoh, S., Lebrin, F., Larsson, J., Mummery, C., Karlsson, S., & Ten Dijke, P. (2003). Activin receptor-like kinase (ALK)1 is an antagonistic mediator of lateral TGF β /ALK5 signaling. *Molecular Cell*, *12*(4). [https://doi.org/10.1016/S1097-2765\(03\)00386-1](https://doi.org/10.1016/S1097-2765(03)00386-1)
- Goumans, M. J., Valdimarsdottir, G., Itoh, S., Rosendahl, A., Sideras, P., & Ten Dijke, P. (2002). Balancing the activation state of the endothelium via two distinct TGF- β type I receptors. *EMBO Journal*, *21*(7). <https://doi.org/10.1093/emboj/21.7.1743>
- Goumans, M. J., Zwijsen, A., ten Dijke, P., & Bailly, S. (2018). Bone morphogenetic proteins in vascular homeostasis and disease. *Cold Spring Harbor Perspectives in Biology*, *10*(2). <https://doi.org/10.1101/cshperspect.a031989>
- Green, J. B. A., & Smith, J. C. (1990). Graded changes in dose of a *Xenopus* activin A homologue elicit stepwise transitions in embryonic cell fate. *Nature*, *347*(6291). <https://doi.org/10.1038/347391a0>
- Guo, X., & Wang, X. F. (2009). Signaling cross-talk between TGF- β /BMP and other pathways. In *Cell Research* (Vol. 19, Issue 1). <https://doi.org/10.1038/cr.2008.302>
- Gurdon, J. B., Harger, P., Mitchell, A., & Lemaire, P. (1994). Activin signalling and response to a morphogen gradient. *Nature*, *371*(6497). <https://doi.org/10.1038/371487a0>
- Hähle, A., Merz, S., Meyners, C., & Hausch, F. (2019). The many faces of FKBP51. In *Biomolecules* (Vol. 9, Issue 1). <https://doi.org/10.3390/biom9010035>
- Hao, Y., Baker, D., & Dijke, P. Ten. (2019). TGF- β -mediated epithelial-mesenchymal transition and cancer metastasis. In *International Journal of Molecular Sciences* (Vol. 20, Issue 11). MDPI AG. <https://doi.org/10.3390/ijms20112767>
- Hata, A., & Chen, Y. G. (2016). TGF- β signaling from receptors to smads. *Cold Spring Harbor Perspectives in Biology*, *8*(9). <https://doi.org/10.1101/cshperspect.a022061>
- Hata, A., Lagna, G., Massagué, J., & Hemmati-Brivanlou, A. (1998). Smad6 inhibits BMP/Smad1 signaling by specifically competing with the Smad4 tumor suppressor. *Genes and Development*, *12*(2). <https://doi.org/10.1101/gad.12.2.186>

- Häusl, A. S., Balsevich, G., Gassen, N. C., & Schmidt, M. V. (2019). Focus on FKBP51: A molecular link between stress and metabolic disorders. In *Molecular Metabolism* (Vol. 29). <https://doi.org/10.1016/j.molmet.2019.09.003>
- Heinke, J., Wehofsits, L., Zhou, Q., Zoeller, C., Baar, K. M., Helbing, T., Laib, A., Augustin, H., Bode, C., Patterson, C., & Moser, M. (2008). BMPER is an endothelial cell regulator and controls bone morphogenetic protein-4-dependent angiogenesis. *Circulation Research*, *103*(8). <https://doi.org/10.1161/CIRCRESAHA.108.178434>
- Heldin, C. H., Landström, M., & Moustakas, A. (2009). Mechanism of TGF- β signaling to growth arrest, apoptosis, and epithelial-mesenchymal transition. In *Current Opinion in Cell Biology* (Vol. 21, Issue 2). <https://doi.org/10.1016/j.ceb.2009.01.021>
- Heldin, C. H., Miyazono, K., & Ten Dijke, P. (1997). TGF- β signalling from cell membrane to nucleus through SMAD proteins. In *Nature* (Vol. 390, Issue 6659). <https://doi.org/10.1038/37284>
- Heldin, C. H., & Moustakas, A. (2012). Role of Smads in TGF β signaling. In *Cell and Tissue Research* (Vol. 347, Issue 1). <https://doi.org/10.1007/s00441-011-1190-x>
- Heldin, C. H., & Moustakas, A. (2016). Signaling receptors for TGF- β family members. *Cold Spring Harbor Perspectives in Biology*, *8*(8). <https://doi.org/10.1101/cshperspect.a022053>
- Henson, E. S., & Gibson, S. B. (2006). Surviving cell death through epidermal growth factor (EGF) signal transduction pathways: Implications for cancer therapy. In *Cellular Signalling* (Vol. 18, Issue 12). <https://doi.org/10.1016/j.cellsig.2006.05.015>
- Herrera, B., Van Dinther, M., Ten Dijke, P., & Inman, G. J. (2009). Autocrine bone morphogenetic protein-9 signals through activin receptor-like kinase-2/Smad1/Smad4 to promote ovarian cancer cell proliferation. *Cancer Research*, *69*(24). <https://doi.org/10.1158/0008-5472.CAN-09-2912>
- Hessels, J., Kroon, S., Boerman, S., Nelissen, R. C., Grutters, J. C., Snijder, R. J., Lebrin, F., Post, M. C., Mummery, C. L., & Mager, J. J. (2022). Efficacy and Safety of Tacrolimus as Treatment for Bleeding Caused by Hereditary Hemorrhagic Telangiectasia: An Open-Label, Pilot Study. *Journal of Clinical Medicine*, *11*(18). <https://doi.org/10.3390/jcm11185280>
- Heyer, J., Escalante-Alcalde, D., Lia, M., Boettinger, E., Edelmann, W., Stewart, C. L., & Kucherlapati, R. (1999). Postgastrulation Smad2-deficient embryos show defects in embryo turning and anterior morphogenesis. *Proceedings of the National Academy of Sciences of the United States of America*, *96*(22). <https://doi.org/10.1073/pnas.96.22.12595>
- Hiepen, C., Jatzlau, J., Hildebrandt, S., Kampfrath, B., Goktas, M., Murgai, A., Cuellar Camacho, J. L., Haag, R., Ruppert, C., Sengle, G., Cavalcanti-Adam, E. A., Blank, K. G., & Knaus, P. (2019). BMPR2 acts as a gatekeeper to protect endothelial cells from increased TGF β responses and altered cell mechanics. *PLoS Biology*, *17*(12). <https://doi.org/10.1371/journal.pbio.3000557>
- Hiepen, C., Mendez, P. L., & Knaus, P. (2020). It Takes Two to Tango: Endothelial TGF β /BMP Signaling Crosstalk with Mechanobiology. In *Cells* (Vol. 9, Issue 9). NLM (Medline). <https://doi.org/10.3390/cells9091965>
- Hildebrand, A., Romaris, M., Rasmussen, L. M., Heinegard, D., Twardzik, D. R., Border, W. A., & Ruoslahti, E. (1994). Interaction of the small interstitial proteoglycans biglycan, decorin and fibromodulin with transforming growth factor β . *Biochemical Journal*, *302*(2). <https://doi.org/10.1042/bj3020527>

- Hill, C. S. (2009). Nucleocytoplasmic shuttling of Smad proteins. In *Cell Research* (Vol. 19, Issue 1). <https://doi.org/10.1038/cr.2008.325>
- Hill, C. S. (2016). Transcriptional control by the SMADs. In *Cold Spring Harbor Perspectives in Biology* (Vol. 8, Issue 10). <https://doi.org/10.1101/cshperspect.a022079>
- Hinck, A. P., Mueller, T. D., & Springer, T. A. (2016). Structural biology and evolution of the TGF- β family. *Cold Spring Harbor Perspectives in Biology*, 8(12). <https://doi.org/10.1101/cshperspect.a022103>
- Hoch, R. V., & Soriano, P. (2014). Generating Diversity and Specificity through Developmental Cell Signaling. In *Principles of Developmental Genetics: Second Edition*. <https://doi.org/10.1016/B978-0-12-405945-0.00001-6>
- Huang, F., Shi, Q., Li, Y., Xu, L., Xu, C., Chen, F., Wang, H., Liao, H., Chang, Z., Liu, F., Zhang, X. H. F., Feng, X. H., Han, J. D. J., Luo, S., & Chen, Y. G. (2018). HER2/EGFR–AKT signaling switches TGF β from inhibiting cell proliferation to promoting cell migration in breast cancer. *Cancer Research*, 78(21), 6073–6085. <https://doi.org/10.1158/0008-5472.CAN-18-0136>
- Huang, Z., & Loewer, A. (2022). Generating Somatic Knockout Cell Lines with CRISPR-Cas9 Technology to Investigate SMAD Signaling. In *Methods in Molecular Biology* (Vol. 2488). https://doi.org/10.1007/978-1-0716-2277-3_7
- Huang, Z., Wang, D., Ihida-Stansbury, K., Jones, P. L., & Martin, J. F. (2009). Defective pulmonary vascular remodeling in Smad8 mutant mice. *Human Molecular Genetics*, 18(15). <https://doi.org/10.1093/hmg/ddp214>
- Humbert, M., Morrell, N. W., Archer, S. L., Stenmark, K. R., MacLean, M. R., Lang, I. M., Christman, B. W., Weir, E. K., Eickelberg, O., Voelkel, N. F., & Rabinovitch, M. (2004). Cellular and molecular pathobiology of pulmonary arterial hypertension. *Journal of the American College of Cardiology*, 43(12 SUPPL.). <https://doi.org/10.1016/j.jacc.2004.02.029>
- Huse, M., Chen, Y. G., Massagué, J., & Kuriyan, J. (1999). Crystal structure of the cytoplasmic domain of the type I TGF β receptor in complex with FKBP12. *Cell*, 96(3). [https://doi.org/10.1016/S0092-8674\(00\)80555-3](https://doi.org/10.1016/S0092-8674(00)80555-3)
- Ikushima, H., & Miyazono, K. (2010). TGF β 2 signalling: A complex web in cancer progression. In *Nature Reviews Cancer* (Vol. 10, Issue 6). <https://doi.org/10.1038/nrc2853>
- Imamura, T., Takase, M., Nishihara, A., Oeda, E., Hanai, J. I., Kawabata, M., & Miyazono, K. (1997). Smad6 inhibits signalling by the TGF- β superfamily. *Nature*, 389(6651). <https://doi.org/10.1038/39355>
- Inman, G. J., & Hill, C. S. (2002). Stoichiometry of active Smad-transcription factor complexes on DNA. *Journal of Biological Chemistry*, 277(52). <https://doi.org/10.1074/jbc.M208532200>
- Inman, J. L., Robertson, C., Mott, J. D., & Bissell, M. J. (2015). Mammary gland development: Cell fate specification, stem cells and the microenvironment. In *Development (Cambridge)* (Vol. 142, Issue 6, pp. 1028–1042). Company of Biologists Ltd. <https://doi.org/10.1242/dev.087643>
- Inomata, Y., Tanaka, K., Egawa, H., Uemoto, S., Ozaki, N., Okajima, H., Satomura, K., Kiuchi, T., Yamaoka, Y., & Hashida, T. (1996). The evolution of immunosuppression with FK506 in pediatric living-related liver transplantation. *Transplantation*, 61(2). <https://doi.org/10.1097/00007890-199601270-00015>

- Ito, C., Akimoto, T., Ioka, T., Kobayashi, T., & Kusano, E. (2009). TGF- β inhibits vascular sprouting through TGF- β type I receptor in the mouse embryonic aorta. *Tohoku Journal of Experimental Medicine*, 218(1). <https://doi.org/10.1620/tjem.218.63>
- Javelaud, D., & Mauviel, A. (2005). Crosstalk mechanisms between the mitogen-activated protein kinase pathways and Smad signaling downstream of TGF- β : Implications for carcinogenesis. In *Oncogene* (Vol. 24, Issue 37). <https://doi.org/10.1038/sj.onc.1208928>
- Jiao, X., Billings, P. C., O'Connell, M. P., Kaplan, F. S., Shore, E. M., & Glaser, D. L. (2007). Heparan Sulfate Proteoglycans (HSPGs) modulate BMP2 osteogenic bioactivity in C2C12 cells. *Journal of Biological Chemistry*, 282(2). <https://doi.org/10.1074/jbc.M513414200>
- Jost, M., Huggett, T. M., Kari, C., & Rodeck, U. (2001). Matrix-independent survival of human keratinocytes through an EGF receptor/MAPK-kinase-dependent pathway. *Molecular Biology of the Cell*, 12(5). <https://doi.org/10.1091/mbc.12.5.1519>
- Kamato, D., Burch, M. L., Piva, T. J., Rezaei, H. B., Rostam, M. A., Xu, S., Zheng, W., Little, P. J., & Osman, N. (2013). Transforming growth factor- β signalling: Role and consequences of Smad linker region phosphorylation. In *Cellular Signalling* (Vol. 25, Issue 10, pp. 2017–2024). <https://doi.org/10.1016/j.cellsig.2013.06.001>
- Kamato, D., Do, B. H., Osman, N., Ross, B. P., Mohamed, R., Xu, S., & Little, P. J. (2020). Smad linker region phosphorylation is a signalling pathway in its own right and not only a modulator of canonical TGF- β signalling. In *Cellular and Molecular Life Sciences* (Vol. 77, Issue 2). <https://doi.org/10.1007/s00018-019-03266-3>
- Kamato, D., & Little, P. J. (2020). Smad2 linker region phosphorylation is an autonomous cell signalling pathway: Implications for multiple disease pathologies. In *Biomedicine and Pharmacotherapy* (Vol. 124). <https://doi.org/10.1016/j.biopha.2020.109854>
- Katsuno, Y., Lamouille, S., & Derynck, R. (2013). TGF- β signaling and epithelial-mesenchymal transition in cancer progression. In *Current Opinion in Oncology* (Vol. 25, Issue 1, pp. 76–84). <https://doi.org/10.1097/CCO.0b013e32835b6371>
- Kavsak, P., Rasmussen, R. K., Causing, C. G., Bonni, S., Zhu, H., Thomsen, G. H., & Wrana, J. L. (2000). Smad7 binds to Smurf2 to form an E3 ubiquitin ligase that targets the TGF β receptor for degradation. *Molecular Cell*, 6(6). [https://doi.org/10.1016/S1097-2765\(00\)00134-9](https://doi.org/10.1016/S1097-2765(00)00134-9)
- Klemm, J. D., Schreiber, S. L., & Crabtree, G. R. (1998). Dimerization as a regulatory mechanism in signal transduction. In *Annual Review of Immunology* (Vol. 16). <https://doi.org/10.1146/annurev.immunol.16.1.569>
- Kolb, M., Margetts, P. J., Sime, P. J., & Gauldie, J. (2001). Proteoglycans decorin and biglycan differentially modulate TGF- β -mediated fibrotic responses in the lung. *American Journal of Physiology - Lung Cellular and Molecular Physiology*, 280(6 24-6). <https://doi.org/10.1152/ajplung.2001.280.6.11327>
- Kolos, J. M., Voll, A. M., Bauder, M., & Hausch, F. (2018). FKBP Ligands—Where We Are and Where to Go? In *Frontiers in Pharmacology* (Vol. 9). <https://doi.org/10.3389/fphar.2018.01425>
- Konermann, S., Brigham, M. D., Trevino, A. E., Joung, J., Abudayyeh, O. O., Barcena, C., Hsu, P. D., Habib, N., Gootenberg, J. S., Nishimasu, H., Nureki, O., & Zhang, F. (2015). Genome-scale transcriptional activation by an engineered CRISPR-Cas9 complex. *Nature*, 517(7536). <https://doi.org/10.1038/nature14136>

- Krall, J. A., Beyer, E. M., & MacBeath, G. (2011). High- and low-affinity epidermal growth factor receptor-ligand interactions activate distinct signaling pathways. *PLoS ONE*, 6(1). <https://doi.org/10.1371/journal.pone.0015945>
- Kramer, Ij. M. (2016). TGF β and Signaling through Receptor Serine/Threonine Protein Kinases. In *Signal Transduction*. <https://doi.org/10.1016/b978-0-12-394803-8.00017-6>
- Kretzschmar, M., Doody, J., Timokhina, I., & Massagué, J. (1999). A mechanism of repression of TGF β /Smad signaling by oncogenic Ras. *Genes and Development*, 13(7). <https://doi.org/10.1101/gad.13.7.804>
- Kubiczkova, L., Sedlarikova, L., Hajek, R., & Sevcikova, S. (2012). TGF- β - an excellent servant but a bad master. In *Journal of Translational Medicine* (Vol. 10, Issue 1). <https://doi.org/10.1186/1479-5876-10-183>
- Labelle, M., Begum, S., & Hynes, R. O. (2011). Direct Signaling between Platelets and Cancer Cells Induces an Epithelial-Mesenchymal-Like Transition and Promotes Metastasis. *Cancer Cell*, 20(5). <https://doi.org/10.1016/j.ccr.2011.09.009>
- Lahav, G., Rosenfeld, N., Sigal, A., Geva-Zatorsky, N., Levine, A. J., Elowitz, M. B., & Alon, U. (2004). Dynamics of the p53-Mdm2 feedback loop in individual cells. *Nature Genetics*, 36(2). <https://doi.org/10.1038/ng1293>
- Lamouille, S., Xu, J., & Derynck, R. (2014). Molecular mechanisms of epithelial-mesenchymal transition. In *Nature Reviews Molecular Cell Biology* (Vol. 15, Issue 3). <https://doi.org/10.1038/nrm3758>
- La Rosa, I., Camargo, L. S. A., Pereira, M. M., Fernandez-Martin, R., Paz, D. A., & Salamone, D. F. (2011). Effects of bone morphogenic protein 4 (BMP4) and its inhibitor, Noggin, on in vitro maturation and culture of bovine preimplantation embryos. *Reproductive Biology and Endocrinology*, 9. <https://doi.org/10.1186/1477-7827-9-18>
- Lastres, P., Letamendía, A., Zhang, H., Rius, C., Almendro, N., Raab, U., López, L. A., Langa, C., Fabra, A., Letarte, M., & Bernabéu, C. (1996). Endoglin modulates cellular responses to TGF- β 1. *Journal of Cell Biology*, 133(5). <https://doi.org/10.1083/jcb.133.5.1109>
- Lebrin, F., Goumans, M. J., Jonker, L., Carvalho, R. L. C., Valdimarsdottir, G., Thorikay, M., Mummery, C., Arthur, H. M., & Ten Dijke, P. (2004). Endoglin promotes endothelial cell proliferation and TGF- β /ALK1 signal transduction. *EMBO Journal*, 23(20). <https://doi.org/10.1038/sj.emboj.7600386>
- Lee, M. J., & Yaffe, M. B. (2016). Protein regulation in signal transduction. *Cold Spring Harbor Perspectives in Biology*, 8(6). <https://doi.org/10.1101/cshperspect.a005918>
- Lesca, G., Burnichon, N., Raux, G., Tosi, M., Pinson, S., Marion, M. J., Babin, E., Gilbert-Dussardier, B., Rivière, S., Goizet, C., Faivre, L., Plauchu, H., Frébourg, T., Calender, A., & Giraud, S. (2006). Distribution of ENG and ACVRL1 (ALK1) mutations in French HHT patients. *Human Mutation*, 27(6). <https://doi.org/10.1002/humu.9421>
- LeVea, C. M., Reeder, J. E., & Mooney, R. A. (2004). EGF-dependent cell cycle progression is controlled by density-dependent regulation of Akt activation. *Experimental Cell Research*, 297(1). <https://doi.org/10.1016/j.yexcr.2004.03.026>

- Lewis, K. A., Gray, P. C., Blount, A. L., MacConell, L. A., Wiater, E., Bitezikjian, L. M., & Vate, W. (2000). Betaglycan binds inhibin and can mediate functional antagonism of activin signalling. *Nature*, *404*(6776). <https://doi.org/10.1038/35006129>
- Lin, S. Y., Morrison, J. R., Phillips, D. J., & de Kretser, D. M. (2003). Regulation of ovarian function by the TGF- β superfamily and follistatin. In *Reproduction* (Vol. 126, Issue 2). <https://doi.org/10.1530/rep.0.1260133>
- Lipton, J. O., & Sahin, M. (2014). The Neurology of mTOR. In *Neuron* (Vol. 84, Issue 2). <https://doi.org/10.1016/j.neuron.2014.09.034>
- Lisi, L., Aceto, P., Navarra, P., & Dello Russo, C. (2015). MTOR kinase: A possible pharmacological target in the management of chronic pain. *BioMed Research International*, *2015*. <https://doi.org/10.1155/2015/394257>
- Liu, L., Liu, X., Ren, X., Tian, Y., Chen, Z., Xu, X., Du, Y., Jiang, C., Fang, Y., Liu, Z., Fan, B., Zhang, Q., Jin, G., Yang, X., & Zhang, X. (2016). Smad2 and Smad3 have differential sensitivity in relaying TGF β signaling and inversely regulate early lineage specification. *Scientific Reports*, *6*. <https://doi.org/10.1038/srep21602>
- Liu, T., Xiong, J., Yi, S., Zhang, H., Zhou, S., Gu, L., & Zhou, M. (2017). FKBP12 enhances sensitivity to chemotherapy-induced cancer cell apoptosis by inhibiting MDM2. *Oncogene*, *36*(12). <https://doi.org/10.1038/onc.2016.331>
- Li, Y., Luo, W., & Yang, W. (2018). Nuclear Transport and Accumulation of Smad Proteins Studied by Single-Molecule Microscopy. *Biophysical Journal*, *114*(9). <https://doi.org/10.1016/j.bpj.2018.03.018>
- Loewer, A., Batchelor, E., Gaglia, G., & Lahav, G. (2010). Basal Dynamics of p53 Reveal Transcriptionally Attenuated Pulses in Cycling Cells. *Cell*, *142*(1). <https://doi.org/10.1016/j.cell.2010.05.031>
- Loewer, A., & Lahav, G. (2011). We are all individuals: Causes and consequences of non-genetic heterogeneity in mammalian cells. In *Current Opinion in Genetics and Development* (Vol. 21, Issue 6). <https://doi.org/10.1016/j.gde.2011.09.010>
- López-Casillas, F., Cheifetz, S., Doody, J., Andres, J. L., Lane, W. S., & Massague, J. (1991). Structure and expression of the membrane proteoglycan betaglycan, a component of the TGF- β receptor system. *Cell*, *67*(4). [https://doi.org/10.1016/0092-8674\(91\)90073-8](https://doi.org/10.1016/0092-8674(91)90073-8)
- Lowery, J. W., & de Caestecker, M. P. (2010). BMP signaling in vascular development and disease. In *Cytokine and Growth Factor Reviews* (Vol. 21, Issue 4). <https://doi.org/10.1016/j.cytogfr.2010.06.001>
- Luo, K. (2017). Signaling cross talk between TGF- β /Smad and other signaling pathways. In *Cold Spring Harbor Perspectives in Biology* (Vol. 9, Issue 1). <https://doi.org/10.1101/cshperspect.a022137>
- Lutz, M., & Knaus, P. (2002). Integration of the TGF- β pathway into the cellular signalling network. In *Cellular Signalling* (Vol. 14, Issue 12). [https://doi.org/10.1016/S0898-6568\(02\)00058-X](https://doi.org/10.1016/S0898-6568(02)00058-X)
- Lyons, K. M., Hogan, B. L. M., & Robertson, E. J. (1995). Colocalization of BMP 7 and BMP 2 RNAs suggests that these factors cooperatively mediate tissue interactions during murine development. *Mechanisms of Development*, *50*(1). [https://doi.org/10.1016/0925-4773\(94\)00326-I](https://doi.org/10.1016/0925-4773(94)00326-I)

- Machado, R. D., Southgate, L., Eichstaedt, C. A., Aldred, M. A., Austin, E. D., Best, D. H., Chung, W. K., Benjamin, N., Elliott, C. G., Eyries, M., Fischer, C., Gräf, S., Hinderhofer, K., Humbert, M., Keiles, S. B., Loyd, J. E., Morrell, N. W., Newman, J. H., Soubrier, F., ... Grünig, E. (2015). Pulmonary Arterial Hypertension: A Current Perspective on Established and Emerging Molecular Genetic Defects. In *Human Mutation* (Vol. 36, Issue 12). <https://doi.org/10.1002/humu.22904>
- Macias, M. J., Martin-Malpartida, P., & Massagué, J. (2015). Structural determinants of Smad function in TGF- β signaling. In *Trends in Biochemical Sciences* (Vol. 40, Issue 6). <https://doi.org/10.1016/j.tibs.2015.03.012>
- Malhotra, N., & Kang, J. (2013). SMAD regulatory networks construct a balanced immune system. *Immunology*, 139(1). <https://doi.org/10.1111/imm.12076>
- Mallet, C., Vittet, D., Feige, J., & Bailly, S. (2006). TGF β 1 Induces Vasculogenesis and Inhibits Angiogenic Sprouting in an Embryonic Stem Cell Differentiation Model: Respective Contribution of ALK1 and ALK5. *STEM CELLS*, 24(11). <https://doi.org/10.1634/stemcells.2005-0494>
- Ma, Q., Ye, S., Liu, H., Zhao, Y., Mao, Y., & Zhang, W. (2024). HMGA2 promotes cancer metastasis by regulating epithelial–mesenchymal transition. In *Frontiers in Oncology* (Vol. 14). <https://doi.org/10.3389/fonc.2024.1320887>
- Marc-Andre Fiedler. (2022). *Bachelor_Abschlussarbeit_Marc-Andre_Fiedler_Mtrn_2625399*.
- Marconi, G. D., Fonticoli, L., Rajan, T. S., Pierdomenico, S. D., Trubiani, O., Pizzicannella, J., & Diomede, F. (2021). Epithelial-mesenchymal transition (Emt): The type-2 emt in wound healing, tissue regeneration and organ fibrosis. In *Cells* (Vol. 10, Issue 7). <https://doi.org/10.3390/cells10071587>
- Martinez-Hackert, E., Sundan, A., & Holien, T. (2021). Receptor binding competition: A paradigm for regulating TGF- β family action. In *Cytokine and Growth Factor Reviews* (Vol. 57). <https://doi.org/10.1016/j.cytogfr.2020.09.003>
- Massagué, J. (2000). How cells read TGF- β signals. In *Nature Reviews Molecular Cell Biology* (Vol. 1, Issue 3). <https://doi.org/10.1038/35043051>
- Massagué, J. (2012). TGF β signalling in context. In *Nature Reviews Molecular Cell Biology* (Vol. 13, Issue 10). <https://doi.org/10.1038/nrm3434>
- Massagué, J., & Gomis, R. R. (2006). The logic of TGF β signaling. In *FEBS Letters* (Vol. 580, Issue 12). <https://doi.org/10.1016/j.febslet.2006.04.033>
- Massagué, J., Seoane, J., & Wotton, D. (2005). Smad transcription factors. In *Genes and Development* (Vol. 19, Issue 23). <https://doi.org/10.1101/gad.1350705>
- Matsuura, I., Wang, G., He, D., & Liu, F. (2005). Identification and characterization of ERK MAP kinase phosphorylation sites in Smad3. *Biochemistry*, 44(37). <https://doi.org/10.1021/bi050560g>
- Mazerbourg, S., Sangkuhl, K., Luo, C. W., Sudo, S., Klein, C., & Hsueh, A. J. W. (2005). Identification of receptors and signaling pathways for orphan bone morphogenetic protein/growth differentiation factor ligands based on genomic analyses. *Journal of Biological Chemistry*, 280(37). <https://doi.org/10.1074/jbc.M504629200>
- McReynolds, L. J., Gupta, S., Figueroa, M. E., Mullins, M. C., & Evans, T. (2007). Smad1 and Smad5 differentially regulate embryonic hematopoiesis. *Blood*, 110(12). <https://doi.org/10.1182/blood-2007-04-085753>

- Meng, X. M., Nikolic-Paterson, D. J., & Lan, H. Y. (2016). TGF- β : The master regulator of fibrosis. In *Nature Reviews Nephrology* (Vol. 12, Issue 6). <https://doi.org/10.1038/nrneph.2016.48>
- Migliorini, E., Guevara-Garcia, A., Albiges-Rizo, C., & Picart, C. (2020). Learning from BMPs and their biophysical extracellular matrix microenvironment for biomaterial design. In *Bone* (Vol. 141). <https://doi.org/10.1016/j.bone.2020.115540>
- Mitchell, D., Pobre, E. G., Mulivor, A. W., Grinberg, A. V., Castonguay, R., Monnell, T. E., Solban, N., Ucran, J. A., Pearsall, R. S., Underwood, K. W., Seehra, J., & Kumar, R. (2010). ALK1-Fc inhibits multiple mediators of angiogenesis and suppresses tumor growth. *Molecular Cancer Therapeutics*, 9(2). <https://doi.org/10.1158/1535-7163.MCT-09-0650>
- Mithani, S. K., Balch, G. C., Shiou, S. R., Whitehead, R. H., Datta, P. K., & Beauchamp, R. D. (2004). Smad3 has a critical role in TGF- β -mediated growth inhibition and apoptosis in colonic epithelial cells. *Journal of Surgical Research*, 117(2). [https://doi.org/10.1016/S0022-4804\(03\)00335-4](https://doi.org/10.1016/S0022-4804(03)00335-4)
- Mittal, V. (2018). Epithelial Mesenchymal Transition in Tumor Metastasis. *Annual Review of Pathology: Mechanisms of Disease*, 13. <https://doi.org/10.1146/annurev-pathol-020117-043854>
- Miyazawa, K., & Miyazono, K. (2017). Regulation of TGF- β family signaling by inhibitory smads. *Cold Spring Harbor Perspectives in Biology*, 9(3). <https://doi.org/10.1101/cshperspect.a022095>
- Miyazawa, K., Shinozaki, M., Hara, T., Furuya, T., & Miyazono, K. (2002). Two major Smad pathways in TGF- β superfamily signalling. In *Genes to Cells* (Vol. 7, Issue 12). <https://doi.org/10.1046/j.1365-2443.2002.00599.x>
- Miyazono, K. (1999). Signal transduction by bone morphogenetic protein receptors: Functional roles of Smad proteins. *Bone*, 25(1). [https://doi.org/10.1016/S8756-3282\(99\)00113-1](https://doi.org/10.1016/S8756-3282(99)00113-1)
- Miyazono, K., Kamiya, Y., & Morikawa, M. (2010). Bone morphogenetic protein receptors and signal transduction. In *Journal of Biochemistry* (Vol. 147, Issue 1, pp. 35–51). <https://doi.org/10.1093/jb/mvp148>
- Morrell, N. W., Aldred, M. A., Chung, W. K., Elliott, C. G., Nichols, W. C., Soubrier, F., Trembath, R. C., & Loyd, J. E. (2019). Genetics and genomics of pulmonary arterial hypertension. *European Respiratory Journal*, 53(1). <https://doi.org/10.1183/13993003.01899-2018>
- Moschetta, M., Reale, A., Marasco, C., Vacca, A., & Carratù, M. R. (2014). Therapeutic targeting of the mTOR-signalling pathway in cancer: Benefits and limitations. In *British Journal of Pharmacology* (Vol. 171, Issue 16). <https://doi.org/10.1111/bph.12749>
- Moustakas, A., & Heldin, C. H. (2002). From mono- to oligo-Smads: The heart of the matter in TGF- β signal transduction. In *Genes and Development* (Vol. 16, Issue 15). <https://doi.org/10.1101/gad.1016802>
- Moustakas, A., & Heldin, C. H. (2005). Non-Smad TGF- β signals. In *Journal of Cell Science* (Vol. 118, Issue 16). <https://doi.org/10.1242/jcs.02554>
- Moustakas, A., & Heldin, C. H. (2009). The regulation of TGF β signal transduction. In *Development* (Vol. 136, Issue 22). <https://doi.org/10.1242/dev.030338>
- Nakao, A., Afrakhte, M., Morén, A., Nakayama, T., Christian, J. L., Heuchef, R., Itoh, S., Kawabata, M., Heldin, N. E., Heldin, C. H., & Ten Dijke, P. (1997). Identification of Smad7, a TGF β -inducible antagonist of TGF- β signalling. *Nature*, 389(6651). <https://doi.org/10.1038/39369>

- Nakao, A., Imamura, T., Souchelnytskyi, S., Kawabata, M., Ishisaki, A., Oeda, E., Tamaki, K., Hanai, J. I., Heldin, C. H., Miyazono, K., & Ten Dijke, P. (1997). TGF- β receptor-mediated signalling through Smad2, Smad3 and Smad4. *EMBO Journal*, *16*(17). <https://doi.org/10.1093/emboj/16.17.5353>
- Nelson, D. E., Ihekweba, A. E. C., Elliott, M., Johnson, J. R., Gibney, C. A., Foreman, B. E., Nelson, C., See, V., Horton, C. A., Spiller, D. G., Edwards, S. W., McDowell, H. P., Unitt, J. F., Sullivan, E., Grimley, R., Benson, N., Broomhead, D., Kell, D. B., & White, M. R. H. (2004). Oscillations in NF- κ B signaling control the dynamics of gene expression. *Science*, *306*(5696). <https://doi.org/10.1126/science.1099962>
- Nickel, J., Ten Dijke, P., & Mueller, T. D. (2018). TGF- β family co-receptor function and signaling. In *Acta Biochimica et Biophysica Sinica* (Vol. 50, Issue 1, pp. 12–36). Oxford University Press. <https://doi.org/10.1093/abbs/gmx126>
- Nicolás, F. J., & Hill, C. S. (2003). Attenuation of the TGF- β -Smad signaling pathway in pancreatic tumor cells confers resistance to TGF- β -induced growth arrest. *Oncogene*, *22*(24). <https://doi.org/10.1038/sj.onc.1206420>
- Ning, J., Zhao, Y., Ye, Y., & Yu, J. (2019). Opposing roles and potential antagonistic mechanism between TGF- β and BMP pathways: Implications for cancer progression. In *EBioMedicine* (Vol. 41). <https://doi.org/10.1016/j.ebiom.2019.02.033>
- Ninkovic, J., Pinto, L., Petricca, S., Lepier, A., Sun, J., Rieger, M. A., Schroeder, T., Cvekl, A., Favor, J., & Götz, M. (2010). The transcription factor Pax6 regulates survival of dopaminergic olfactory bulb neurons via crystallin α A. *Neuron*, *68*(4). <https://doi.org/10.1016/j.neuron.2010.09.030>
- O'Connell, M. P., Billings, P. C., Fiori, J. L., Deirmengian, G., Roach, H. I., Shore, E. M., & Kaplan, F. S. (2007). HSPG modulation of BMP signaling in fibrodysplasia ossificans progressiva cells. *Journal of Cellular Biochemistry*, *102*(6). <https://doi.org/10.1002/jcb.21370>
- Olsen, O. E., Wader, K. F., Hella, H., Mylin, A. K., Turesson, I., Nesthus, I., Waage, A., Sundan, A., & Holien, T. (2015). Activin A inhibits BMP-signaling by binding ACVR2A and ACVR2B. *Cell Communication and Signaling*, *13*(1). <https://doi.org/10.1186/s12964-015-0104-z>
- Ooshima, A., Park, J., & Kim, S. J. (2019). Phosphorylation status at Smad3 linker region modulates transforming growth factor- β -induced epithelial-mesenchymal transition and cancer progression. In *Cancer Science* (Vol. 110, Issue 2). <https://doi.org/10.1111/cas.13922>
- Orriols, M., Gomez-Puerto, M. C., & ten Dijke, P. (2017). BMP type II receptor as a therapeutic target in pulmonary arterial hypertension. In *Cellular and Molecular Life Sciences* (Vol. 74, Issue 16). <https://doi.org/10.1007/s00018-017-2510-4>
- Oxburgh, L., Dudley, A. T., Godin, R. E., Koonce, C. H., Islam, A., Anderson, D. C., Bikoff, E. K., & Robertson, E. J. (2005). BMP4 substitutes for loss of BMP7 during kidney development. *Developmental Biology*, *286*(2). <https://doi.org/10.1016/j.ydbio.2005.08.024>
- Papageorgis, P., & Stylianopoulos, T. (2015). Role of TGF β in regulation of the tumor microenvironment and drug delivery (review). *International Journal of Oncology*, *46*(3). <https://doi.org/10.3892/ijo.2015.2816>
- Pardali, E., Goumans, M. J., & ten Dijke, P. (2010). Signaling by members of the TGF- β family in vascular morphogenesis and disease. In *Trends in Cell Biology* (Vol. 20, Issue 9, pp. 556–567). <https://doi.org/10.1016/j.tcb.2010.06.006>

- Pauklin, S., & Vallier, L. (2013). XThe cell-cycle state of stem cells determines cell fate propensity. *Cell*, *155*(1). <https://doi.org/10.1016/j.cell.2013.08.031>
- Pawlak, J. B., & Blobe, G. C. (2022). TGF- β superfamily co-receptors in cancer. In *Developmental Dynamics* (Vol. 251, Issue 1). <https://doi.org/10.1002/dvdy.338>
- Perrimon, N., Pitsouli, C., & Shilo, B. Z. (2012). Signaling mechanisms controlling cell fate and embryonic patterning. *Cold Spring Harbor Perspectives in Biology*, *4*(8). <https://doi.org/10.1101/cshperspect.a005975>
- PIEK, E., HELDIN, C., & DIJKE, P. TEN. (1999). Specificity, diversity, and regulation in TGF- β superfamily signaling. *The FASEB Journal*, *13*(15). <https://doi.org/10.1096/fasebj.13.15.2105>
- Piek, E., Moustakas, A., Kurisaki, A., Heldin, C. H., & Ten Dijke, P. (1999). TGF- β type I receptor/ALK-5 and Smad proteins mediate epithelial to mesenchymal transdifferentiation in NMuMG breast epithelial cells. *Journal of Cell Science*, *112*(24). <https://doi.org/10.1242/jcs.112.24.4557>
- Pregizer, S. K., & Mortlock, D. P. (2015). Dynamics and cellular localization of Bmp2, Bmp4, and noggin transcription in the postnatal mouse skeleton. *Journal of Bone and Mineral Research*, *30*(1). <https://doi.org/10.1002/jbmr.2313>
- Purvis, J. E., Karhohs, K. W., Mock, C., Batchelor, E., Loewer, A., & Lahav, G. (2012). p53 dynamics control cell fate. *Science*, *336*(6087). <https://doi.org/10.1126/science.1218351>
- Quist-Løkken, I., Andersson-Rusch, C., Kastnes, M. H., Kolos, J. M., Jatzlau, J., Hella, H., Olsen, O. E., Sundan, A., Knaus, P., Hausch, F., & Holien, T. (2023). FKBP12 is a major regulator of ALK2 activity in multiple myeloma cells. *Cell Communication and Signaling*, *21*(1). <https://doi.org/10.1186/s12964-022-01033-9>
- Rajagopal, S., & Yu, Y. R. A. (2022). The Pathobiology of Pulmonary Arterial Hypertension. In *Cardiology Clinics* (Vol. 40, Issue 1). <https://doi.org/10.1016/j.ccl.2021.08.001>
- Raj, A., Rifkin, S. A., Andersen, E., & Van Oudenaarden, A. (2010). Variability in gene expression underlies incomplete penetrance. *Nature*, *463*(7283). <https://doi.org/10.1038/nature08781>
- Retting, K. N., Song, B., Yoon, B. S., & Lyons, K. M. (2009). BMP canonical Smad signaling through Smad1 and Smad5 is required for endochondral bone formation. *Development*, *136*(7). <https://doi.org/10.1242/dev.029926>
- Richardson, L., Wilcockson, S. G., Guglielmi, L., & Hill, C. S. (2023). Context-dependent TGF β family signalling in cell fate regulation. In *Nature Reviews Molecular Cell Biology* (Vol. 24, Issue 12). <https://doi.org/10.1038/s41580-023-00638-3>
- Rider, C. C., & Mulloy, B. (2017). Heparin, heparan sulphate and the TGF- Cytokine superfamily. In *Molecules* (Vol. 22, Issue 5). <https://doi.org/10.3390/molecules22050713>
- Robert, F., Desroches-Castan, A., Bailly, S., Dupuis-Girod, S., & Feige, J. J. (2020). Future treatments for hereditary hemorrhagic telangiectasia. In *Orphanet Journal of Rare Diseases* (Vol. 15, Issue 1). <https://doi.org/10.1186/s13023-019-1281-4>
- Robertson, I. B., Horiguchi, M., Zilberberg, L., Dabovic, B., Hadjiolova, K., & Rifkin, D. B. (2015). Latent TGF- β -binding proteins. In *Matrix Biology* (Vol. 47). <https://doi.org/10.1016/j.matbio.2015.05.005>

- Rojas, A., Padidam, M., Cress, D., & Grady, W. M. (2009). TGF- β receptor levels regulate the specificity of signaling pathway activation and biological effects of TGF- β . *Biochimica et Biophysica Acta - Molecular Cell Research*, 1793(7). <https://doi.org/10.1016/j.bbamcr.2009.02.001>
- Ross, K. R., Corey, D. A., Dunn, J. M., & Kelley, T. J. (2007). SMAD3 expression is regulated by mitogen-activated protein kinase kinase-1 in epithelial and smooth muscle cells. *Cellular Signalling*, 19(5). <https://doi.org/10.1016/j.cellsig.2006.11.008>
- Rostama, B., Turner, J. E., Seavey, G. T., Norton, C. R., Gridley, T., Vary, C. P. H., & Liaw, L. (2015). DLL4/Notch1 and BMP9 Interdependent Signaling Induces Human Endothelial Cell Quiescence via P27KIP1 and Thrombospondin-1. *Arteriosclerosis, Thrombosis, and Vascular Biology*, 35(12). <https://doi.org/10.1161/ATVBAHA.115.306541>
- Rozés-Salvador, V., Siri, S. O., Musri, M. M., & Conde, C. (2018). New Player in Endosomal Trafficking: Differential Roles of Smad Anchor for Receptor Activation (SARA) Protein. *Molecular and Cellular Biology*, 38(24). <https://doi.org/10.1128/mcb.00446-18>
- Rubtsova, S. N., Zhitnyak, I. Y., & Gloushankova, N. A. (2022). Dual role of E-cadherin in cancer cells. In *Tissue Barriers* (Vol. 10, Issue 4). <https://doi.org/10.1080/21688370.2021.2005420>
- Salazar, V. S., Gamer, L. W., & Rosen, V. (2016). BMP signalling in skeletal development, disease and repair. In *Nature Reviews Endocrinology* (Vol. 12, Issue 4). <https://doi.org/10.1038/nrendo.2016.12>
- Sánchez-Duffhues, G., Hiepen, C., Knaus, P., & ten Dijke, P. (2015). Bone morphogenetic protein signaling in bone homeostasis. In *Bone* (Vol. 80). <https://doi.org/10.1016/j.bone.2015.05.025>
- Sánchez-Tilló, E., Liu, Y., De Barrios, O., Siles, L., Fanlo, L., Cuatrecasas, M., Darling, D. S., Dean, D. C., Castells, A., & Postigo, A. (2012). EMT-activating transcription factors in cancer: Beyond EMT and tumor invasiveness. In *Cellular and Molecular Life Sciences* (Vol. 69, Issue 20). <https://doi.org/10.1007/s00018-012-1122-2>
- Schmidt, M. V., Paez-Pereda, M., Holsboer, F., & Hausch, F. (2012). The Prospect of FKBP51 as a Drug Target. *ChemMedChem*, 7(8). <https://doi.org/10.1002/cmdc.201200137>
- Schmierer, B., & Hill, C. S. (2007). TGF β -SMAD signal transduction: Molecular specificity and functional flexibility. In *Nature Reviews Molecular Cell Biology* (Vol. 8, Issue 12). <https://doi.org/10.1038/nrm2297>
- Schwarte-Waldhoff, I., & Schmiegel, W. (2002). Smad4 transcriptional pathways and angiogenesis. In *International Journal of Gastrointestinal Cancer* (Vol. 31, Issues 1–3). <https://doi.org/10.1385/ijgc:31:1-3:47>
- Shah, A. J., Beckmann, T., Vorla, M., & Kalra, D. K. (2023). New Drugs and Therapies in Pulmonary Arterial Hypertension. In *International Journal of Molecular Sciences* (Vol. 24, Issue 6). <https://doi.org/10.3390/ijms24065850>
- Shintani, M., Yagi, H., Nakayama, T., Saji, T., & Matsuoka, R. (2009). A new nonsense mutation of SMAD8 associated with pulmonary arterial hypertension. *Journal of Medical Genetics*, 46(5). <https://doi.org/10.1136/jmg.2008.062703>
- Shi, Q., & Chen, Y. G. (2017). Interplay between TGF- β signaling and receptor tyrosine kinases in tumor development. In *Science China Life Sciences* (Vol. 60, Issue 10). <https://doi.org/10.1007/s11427-017-9173-5>

- Shi, Y., Wang, Y. F., Jayaraman, L., Yang, H., Massagué, J., & Pavletich, N. P. (1998). Crystal structure of a Smad MH1 domain bound to DNA: Insights on DNA binding in TGF- β signaling. *Cell*, *94*(5). [https://doi.org/10.1016/S0092-8674\(00\)81600-1](https://doi.org/10.1016/S0092-8674(00)81600-1)
- Sidis, Y., Mukherjee, A., Keutmann, H., Delbaere, A., Sadatsuki, M., & Schneyer, A. (2006). Biological activity of follistatin isoforms and follistatin-like-3 is dependent on differential cell surface binding and specificity for activin, myostatin, and bone morphogenetic proteins. *Endocrinology*, *147*(7). <https://doi.org/10.1210/en.2006-0089>
- Singha, P. K., Pandeswara, S., Geng, H., Lan, R., Venkatachalam, M. A., & Saikumar, P. (2014). TGF- β induced TMEPAI/PMEPA1 inhibits canonical smad signaling through R-smad sequestration and promotes noncanonical PI3K/Akt signaling by reducing PTEN in triple negative breast cancer. *Genes and Cancer*, *5*(9–10). <https://doi.org/10.18632/genesandcancer.30>
- Smith, A. L., Robin, T. P., & Ford, H. L. (2012). Molecular pathways: Targeting the TGF- β pathway for cancer therapy. *Clinical Cancer Research*, *18*(17). <https://doi.org/10.1158/1078-0432.CCR-11-3224>
- Solloway, M. J., & Robertson, E. J. (1999). Early embryonic lethality in Bmp5;Bmp7 double mutant mice suggests functional redundancy within the 60A subgroup. *Development*, *126*(8). <https://doi.org/10.1242/dev.126.8.1753>
- Song, K., Krause, C., Shi, S., Patterson, M., Suto, R., Grgurevic, L., Vukicevic, S., Van Dinther, M., Falb, D., Ten Dijke, P., & Alaoui-Ismaili, M. H. (2010). Identification of a key residue mediating bone morphogenetic protein (BMP)-6 resistance to noggin inhibition allows for engineered BMPs with superior agonist activity. *Journal of Biological Chemistry*, *285*(16). <https://doi.org/10.1074/jbc.M109.087197>
- Sonja Lenhardt. (2019). *Investigating SMAD mediated signaling in endothelial cells Untersuchung der SMAD vermittelten Signalverarbeitung in Endothelzellen.*
- Sonja Lenhardt. (2022). *Investigating BMP-induced nuclear shuttling of SMAD5 in endothelial cells.*
- Strasen Henriette Sophie. (2018). *Dynamics and variability of SMAD signaling in single cells.*
- Strasen, J., Sarma, U., Jentsch, M., Bohn, S., Sheng, C., Horbelt, D., Knaus, P., Legewie, S., & Loewer, A. (2018). Cell-specific responses to the cytokine TGF β are determined by variability in protein levels. *Molecular Systems Biology*, *14*(1). <https://doi.org/10.15252/msb.20177733>
- Suh, J., & Lee, Y. S. (2020). Similar sequences but dissimilar biological functions of GDF11 and myostatin. In *Experimental and Molecular Medicine* (Vol. 52, Issue 10). <https://doi.org/10.1038/s12276-020-00516-4>
- Sun, X., Essalmani, R., Susan-Resiga, D., Prat, A., & Seidah, N. G. (2011). Latent transforming growth factor β -binding proteins-2 and -3 inhibit the proprotein convertase 5/6A. *Journal of Biological Chemistry*, *286*(33). <https://doi.org/10.1074/jbc.M111.242479>
- Takei, N., & Nawa, H. (2014). mTOR signaling and its roles in normal and abnormal brain development. In *Frontiers in Molecular Neuroscience* (Vol. 7, Issue 1 APR). <https://doi.org/10.3389/fnmol.2014.00028>
- Tan, H., Chen, R., Li, W., Zhao, W., Zhang, Y., Yang, Y., Su, J., & Zhou, X. (2017). A systems biology approach to studying the molecular mechanisms of osteoblastic differentiation under cytokine combination treatment. *Npj Regenerative Medicine*, *2*(1). <https://doi.org/10.1038/s41536-017-0009-0>

- Tay, S., Hughey, J. J., Lee, T. K., Lipniacki, T., Quake, S. R., & Covert, M. W. (2010). Single-cell NF- κ B dynamics reveal digital activation and analogue information processing. *Nature*, *466*(7303). <https://doi.org/10.1038/nature09145>
- Ten Dijke, P., & Arthur, H. M. (2007). Extracellular control of TGF β signalling in vascular development and disease. In *Nature Reviews Molecular Cell Biology* (Vol. 8, Issue 11). <https://doi.org/10.1038/nrm2262>
- Ten Dijke, P., & Hill, C. S. (2004). New insights into TGF- β -Smad signalling. In *Trends in Biochemical Sciences* (Vol. 29, Issue 5). <https://doi.org/10.1016/j.tibs.2004.03.008>
- Thenappan, T., Ormiston, M. L., Ryan, J. J., & Archer, S. L. (2018). Pulmonary arterial hypertension: Pathogenesis and clinical management. In *BMJ (Online)* (Vol. 360). <https://doi.org/10.1136/bmj.j5492>
- Tidin, O., Friman, E. T., Naef, F., & Suter, D. M. (2019). Quantitative relationships between SMAD dynamics and target gene activation kinetics in single live cells. *Scientific Reports*, *9*(1). <https://doi.org/10.1038/s41598-019-41870-2>
- Tomic, D., Brodie, S. G., Deng, C., Hickey, R. J., Babus, J. K., Malkas, L. H., & Flaws, J. A. (2002). Smad 3 may regulate follicular growth in the mouse ovary. *Biology of Reproduction*, *66*(4). <https://doi.org/10.1095/biolreprod66.4.917>
- Townson, S. A., Martinez-Hackert, E., Greppi, C., Lowden, P., Sako, D., Liu, J., Ucran, J. A., Liharska, K., Underwood, K. W., Seehra, J., Kumar, R., & Grinberg, A. V. (2012). Specificity and structure of a high affinity activin receptor-like kinase 1 (ALK1) signaling complex. *Journal of Biological Chemistry*, *287*(33). <https://doi.org/10.1074/jbc.M112.377960>
- Tremblay, K. D., Dunn, N. R., & Robertson, E. J. (2001). Mouse embryos lacking Smad1 signals display defects in extra-embryonic tissues and germ cell formation. *Development*, *128*(18). <https://doi.org/10.1242/dev.128.18.3609>
- Tripathi, V., Sixt, K. M., Gao, S., Xu, X., Huang, J., Weigert, R., Zhou, M., & Zhang, Y. E. (2016). Direct Regulation of Alternative Splicing by SMAD3 through PCBP1 Is Essential to the Tumor-Promoting Role of TGF- β . *Molecular Cell*, *64*(3). <https://doi.org/10.1016/j.molcel.2016.09.013>
- Tzavlaki, K., & Moustakas, A. (2020). TGF-B signaling. In *Biomolecules* (Vol. 10, Issue 3). MDPI AG. <https://doi.org/10.3390/biom10030487>
- Upton, P. D., Davies, R. J., Trembath, R. C., & Morrell, N. W. (2009). Bone morphogenetic protein (BMP) and activin type II receptors balance BMP9 signals mediated by activin receptor-like kinase-1 in human pulmonary artery endothelial cells. *Journal of Biological Chemistry*, *284*(23), 15794–15804. <https://doi.org/10.1074/jbc.M109.002881>
- Usman, S., Waseem, N. H., Nguyen, T. K. N., Mohsin, S., Jamal, A., Teh, M. T., & Waseem, A. (2021). Vimentin is at the heart of epithelial mesenchymal transition (Emt) mediated metastasis. In *Cancers* (Vol. 13, Issue 19). <https://doi.org/10.3390/cancers13194985>
- Vander Ark, A., Cao, J., & Li, X. (2018). TGF- β receptors: In and beyond TGF- β signaling. In *Cellular Signalling* (Vol. 52). <https://doi.org/10.1016/j.cellsig.2018.09.002>
- Veerasingam, M., Phanish, M., & Dockrell, M. E. C. (2013). Smad Mediated Regulation of Inhibitor of DNA Binding 2 and Its Role in Phenotypic Maintenance of Human Renal Proximal Tubule Epithelial Cells. *PLoS ONE*, *8*(1). <https://doi.org/10.1371/journal.pone.0051842>

- Verrecchia, F., & Mauviel, A. (2002). Transforming growth factor- β signaling through the Smad pathway: Role in extracellular matrix gene expression and regulation. In *Journal of Investigative Dermatology* (Vol. 118, Issue 2). <https://doi.org/10.1046/j.1523-1747.2002.01641.x>
- Villalba, M., Evans, S. R., Vidal-Vanaclocha, F., & Calvo, A. (2017). Role of TGF- β in metastatic colon cancer: it is finally time for targeted therapy. In *Cell and Tissue Research* (Vol. 370, Issue 1). <https://doi.org/10.1007/s00441-017-2633-9>
- Waldrip, W. R., Bikoff, E. K., Hoodless, P. A., Wrana, J. L., & Robertson, E. J. (1998). Smad2 signaling in extraembryonic tissues determines anterior-posterior polarity of the early mouse embryo. *Cell*, 92(6). [https://doi.org/10.1016/S0092-8674\(00\)81407-5](https://doi.org/10.1016/S0092-8674(00)81407-5)
- Walker, R. G., Czepnik, M., Goebel, E. J., McCoy, J. C., Vujic, A., Cho, M., Oh, J., Aykul, S., Walton, K. L., Schang, G., Bernard, D. J., Hinck, A. P., Harrison, C. A., Martinez-Hackert, E., Wagers, A. J., Lee, R. T., & Thompson, T. B. (2017). Structural basis for potency differences between GDF8 and GDF11. *BMC Biology*, 15(1). <https://doi.org/10.1186/s12915-017-0350-1>
- Wang, C., Yu, J. T., Miao, D., Wu, Z. C., Tan, M. S., & Tan, L. (2014). Targeting the mTOR signaling network for alzheimer's disease therapy. In *Molecular Neurobiology* (Vol. 49, Issue 1). <https://doi.org/10.1007/s12035-013-8505-8>
- Wang, Y., Shi, J., Chai, K., Ying, X., & Zhou, B. (2014). The Role of Snail in EMT and Tumorigenesis. *Current Cancer Drug Targets*, 13(9). <https://doi.org/10.2174/15680096113136660102>
- Weinstein, M., Yang, X., Li, C., Xu, X., Gotay, J., & Deng, C. X. (1998). Failure of egg cylinder elongation and mesoderm induction in mouse embryos lacking the tumor suppressor smad2. *Proceedings of the National Academy of Sciences of the United States of America*, 95(16). <https://doi.org/10.1073/pnas.95.16.9378>
- Weiss, A., & Attisano, L. (2013). The TGFbeta superfamily signaling pathway. In *Wiley Interdisciplinary Reviews: Developmental Biology* (Vol. 2, Issue 1). <https://doi.org/10.1002/wdev.86>
- Williams, E., Riesebos, E., Kerr, G., & Bullock, A. N. (2021). Alk2 receptor kinase association with fkbp12.6 is structurally conserved with the alk2-fkbp12 complex. *Biomedicines*, 9(2). <https://doi.org/10.3390/biomedicines9020129>
- Wilson, P. A., Lagna, G., Suzuki, A., & Hemmati-Brivanlou, A. (1997). Concentration-dependent patterning of the *Xenopus* ectoderm by BMP4 and its signal transducer Smad1. *Development*, 124(16). <https://doi.org/10.1242/dev.124.16.3177>
- Worster, D. T., Schmelzle, T., Solimini, N. L., Lightcap, E. S., Millard, B., Mills, G. B., Brugge, J. S., & Albeck, J. G. (2012). Akt and ERK control the proliferative response of mammary epithelial cells to the growth factors IGF-1 and EGF through the cell cycle inhibitor p57 Kip2. *Science Signaling*, 5(214). <https://doi.org/10.1126/scisignal.2001986>
- Wrighton, K. H., & Feng, X. H. (2008). To (TGF) β or not to (TGF) β : Fine-tuning of Smad signaling via post-translational modifications. In *Cellular Signalling* (Vol. 20, Issue 9). <https://doi.org/10.1016/j.cellsig.2008.02.003>
- Wrighton, K. H., Lin, X., & Feng, X. H. (2009). Phospho-control of TGF- β superfamily signaling. In *Cell Research* (Vol. 19, Issue 1). <https://doi.org/10.1038/cr.2008.327>

- Wu, M., Chen, G., & Li, Y. P. (2016). TGF- β and BMP signaling in osteoblast, skeletal development, and bone formation, homeostasis and disease. *Bone Research*, 4. <https://doi.org/10.1038/boneres.2016.9>
- Wu, M. Y., & Hill, C. S. (2009). TGF- β Superfamily Signaling in Embryonic Development and Homeostasis. In *Developmental Cell* (Vol. 16, Issue 3). <https://doi.org/10.1016/j.devcel.2009.02.012>
- Xie, M., & Li, J. ping. (2019). Heparan sulfate proteoglycan – A common receptor for diverse cytokines. *Cellular Signalling*, 54. <https://doi.org/10.1016/j.cellsig.2018.11.022>
- Xu, L. (2006). Regulation of Smad activities. In *Biochimica et Biophysica Acta - Gene Structure and Expression* (Vol. 1759, Issues 11–12). <https://doi.org/10.1016/j.bbaexp.2006.11.001>
- Xu, P., Lin, X., & Feng, X. H. (2016). Posttranslational regulation of smads. *Cold Spring Harbor Perspectives in Biology*, 8(12). <https://doi.org/10.1101/cshperspect.a022087>
- Xu, Y., Yuan, J., & Lipinski, M. M. (2013). Live imaging and single-cell analysis reveal differential dynamics of autophagy and apoptosis. *Autophagy*, 9(9). <https://doi.org/10.4161/auto.25080>
- Yagi, K., Furuhashi, M., Aoki, H., Goto, D., Kuwano, H., Sugamura, K., Miyazono, K., & Kato, M. (2002). c-myc is a downstream target of the Smad pathway. *Journal of Biological Chemistry*, 277(1). <https://doi.org/10.1074/jbc.M104170200>
- Yang, X. (1999). Targeted disruption of SMAD3 results in impaired mucosal immunity and diminished T cell responsiveness to TGF-beta. *The EMBO Journal*, 18(5). <https://doi.org/10.1093/emboj/18.5.1280>
- Yang, X., Castilla, L. H., Xu, X., Li, C., Gotay, J., Weinstein, M., Liu, P. P., & Deng, C. X. (1999). Angiogenesis defects and mesenchymal apoptosis in mice lacking SMAD5. *Development*, 126(8). <https://doi.org/10.1242/dev.126.8.1571>
- Yan, X., Xiong, X., & Chen, Y. G. (2018). Feedback regulation of TGF- β signaling. In *Acta Biochimica et Biophysica Sinica* (Vol. 50, Issue 1). <https://doi.org/10.1093/abbs/gmx129>
- Yoshimoto, A., Saigou, Y., Higashi, Y., & Kondoh, H. (2005). Regulation of ocular lens development by Smad-interacting protein 1 involving Foxe3 activation. *Development*, 132(20). <https://doi.org/10.1242/dev.02022>
- Yu, H., Königshoff, M., Jayachandran, A., Handley, D., Seeger, W., Kaminski, N., & Eickelberg, O. (2008). Transgelin is a direct target of TGF- β /Smad3-dependent epithelial cell migration in lung fibrosis. *The FASEB Journal*, 22(6). <https://doi.org/10.1096/fj.07-083857>
- Yu, J., Zhang, L., Chen, A., Xiang, G., Wang, Y., Wu, J., Mitchelson, K., Cheng, J., & Zhou, Y. (2008). Identification of the gene transcription and apoptosis mediated by TGF- β -Smad2/3-Smad4 signaling. *Journal of Cellular Physiology*, 215(2). <https://doi.org/10.1002/jcp.21325>
- Zafiroopoulos, A., & Tzanakakis, G. N. (2008). Decorin-mediated effects in cancer cell biology. *Connective Tissue Research*, 49(3–4). <https://doi.org/10.1080/03008200802147746>
- Zeisel, A., Yitzhaky, A., Koerner, C., Lauriola, M., Cohen-Dvashi, H., Köstler, W. J., Yarden, Y., Wiemann, S., & Domany, E. (2013). QCMA: A desktop application for quantitative collective cell migration analysis. *Journal of Biomolecular Screening*, 18(3). <https://doi.org/10.1177/1087057112461940>

- Zhang, J., Thorikay, M., van der Zon, G., van Dinther, M., & Dijke, P. Ten. (2020). Studying $\text{tgf-}\beta$ signaling and $\text{tgf-}\beta$ -induced epithelial-to-mesenchymal transition in breast cancer and normal cells. *Journal of Visualized Experiments*, 2020(164). <https://doi.org/10.3791/61830>
- Zhang, J., Tian, X. J., & Xing, J. (2016). Signal transduction pathways of EMT induced by TGF- β , SHH, and WNT and their crosstalks. In *Journal of Clinical Medicine* (Vol. 5, Issue 4). <https://doi.org/10.3390/jcm5040041>
- Zhang, Y., Alexander, P. B., & Wang, X. F. (2017). TGF- β family signaling in the control of cell proliferation and survival. *Cold Spring Harbor Perspectives in Biology*, 9(4). <https://doi.org/10.1101/cshperspect.a022145>
- Zhang, Y. E. (2009). Non-Smad pathways in TGF- β signaling. In *Cell Research* (Vol. 19, Issue 1). <https://doi.org/10.1038/cr.2008.328>
- Zhang, Y. E. (2018). Mechanistic insight into contextual TGF- β signaling. In *Current Opinion in Cell Biology* (Vol. 51). <https://doi.org/10.1016/j.ceb.2017.10.001>
- Zhang, Y., Ge, G., & Greenspan, D. S. (2006). Inhibition of bone morphogenetic protein 1 by native and altered forms of α 2-macroglobulin. *Journal of Biological Chemistry*, 281(51). <https://doi.org/10.1074/jbc.M601362200>
- Zhu, H., Kavsak, P., Abdollah, S., Wrana, J. L., & Thomsen, G. H. (1999). A SMAD ubiquitin ligase targets the BMP pathway and affects embryonic pattern formation. *Nature*, 400(6745). <https://doi.org/10.1038/23293>
- Zi, Z., Chapnick, D. A., & Liu, X. (2012). Dynamics of TGF- β /Smad signaling. In *FEBS Letters* (Vol. 586, Issue 14). <https://doi.org/10.1016/j.febslet.2012.03.063>
- Zi, Z., Feng, Z., Chapnick, D. A., Dahl, M., Deng, D., Klipp, E., Moustakas, A., & Liu, X. (2011). Quantitative analysis of transient and sustained transforming growth factor- β signaling dynamics. *Molecular Systems Biology*, 7. <https://doi.org/10.1038/msb.2011.22>

6 Appendix

6.1 List of Abbreviation

µg	micrograms
µl	microliter
µM	micromolar
ACVR2A	activin A receptor 2A
ACVR2B	activin A receptor 2B
ALK1/ ACVRL1	Activin A Receptor Like Type 1
ALK1i	Activin A Receptor Like Type 1 inhibitor
ALK2/ ACVR1	Activin Receptor Type I
ALK2i	Activin Receptor Type I inhibitor
ALK3/ BMPR1A	Bone Morphogenetic Protein Receptor Type 1A
ALK4	Activin A Receptor Type 1B
ALK4i/ ACVR1B	Activin A Receptor Type 1B inhibitor
ALK5/ TGF- BR1	Transforming Growth Factor Beta Receptor 1
ALK5i	Transforming Growth Factor Beta Receptor 1 inhibitor
ALK6/ BMPR1B	Bone Morphogenetic Protein Receptor Type 1B
ALK7/ ACVR1C	Activin A Receptor Type 1C
Amp	amplitude
au	arbitrary unit
AUC	area under the curve
Blast R	blasticidin resistance
BMP	bone morphogenetic protein
BMP2	bone morphogenetic protein 2
BMP4	bone morphogenetic protein 4
BMP6	bone morphogenetic protein 6
BMP7	bone morphogenetic protein 7
BMP9	bone morphogenetic protein 9
BMP10	bone morphogenetic protein 10
BMPR2	Bone Morphogenetic Protein Receptor Type 2
bp	base pairs
BSA	bovine serum albumine
Cas9	CRISPR-associated 9
CDK	cyclin-dependent kinases
cDNA	complementary DNA
CFP	cyan fluorescent protein
cm	centimeter
CMV	cauliflower mosaic virus
Co-SMAD	common-mediator SMAD; isoform 4
CRISPR	clustered regularly interspaced short palindromic repeats
crRNA	CRISPR RNA
CT	cycle threshold
dCas9	dead Cas9
DCN	Decorin
ddH ₂ O	double-distilled water

DEPC-treated H ₂ O	diethyl pyrocarbonate treated water
DLL4	Delta Like Canonical Notch Ligand 4
DMEM	Dulbecco's Modified Eagle Medium
DMEM/F12	Dulbecco's Modified Eagle Medium/Nutrient Mixture F-12
DMSO	dimethyl sulfoxide
DNA	deoxyribonucleic acid
dNTP	deoxyribose nucleotide triphosphate
DSB	double-strand breaks
dsDNA	double-stranded DNA
DTT	dithiothreitol
EA.hy 926	Immortalized Human Vascular Endothelial Cells (somatic hybrid from HUVEC and A549)
E. col	Escherichia col
ECGS	Endothelial Cell Growth Supplement
EDN1	Endothelin 1
EDTA	ethylenediaminetetraacetic acid
EGF	epidermal growth factor
EGFR	EGF receptor
EGFRi	EGFR inhibitor
EMT	epithelial to mesenchymal transition
ENG	Endoglin
ERK	extracellular signal-regulated kinase
FBS	fetal bovine serum
FC	fold change
FOXH1	forkhead box protein H1
FOXO	forkhead box protein O
FRA1/FOSL1	fos-related antigen 1
FRET	fluorescence resonance energy transfer
FST	follistatin
G1-phase	first gap phase (cell cycle)
G418	Geneticin
GDF2	growth differentiation factor 2
GDF3	growth differentiation fact 3
GDF8	growth differentiation factor 8; also called myostati
GDF11	growth differentiation factor 11
h	hours
H2B	histone 2b
HA	homology arm
HAL	homology arm left
HAR	homology arm right
HCl	hydrogen chloride
HDR	homology-directed repair
HEK293T	human embryonic kidney cells expressing SV40 large T antigen
HUVEC	human umbilical vein endothelial cells
ID2	inhibitor of DNA binding 2
IGF	insulin-like growth factor
I-SMAD	inhibitory SMADs; isoforms 6 and 7
JNK	c-Jun N-terminal kinase
kDa	kilodalton
KO	knockout
kV	kilovolt
LTBP2	latent-transforming growth factor beta-binding protein 2

m	slope of linear model
mA	milliampere
MAPK	mitogen-activated protein kinase
MCF10A	immortalized human breast epithelial cell line (Michigan Cancer Foundation-10A)
MEK	MAPK kinase
mg	milligrams
MH1	mad homology 1
MH2	mad homology 2
min	minutes
ml	milliliter
mM	millimolar
MMP9	Matrix Metalloproteinase 9
mRNA	messenger RNA
mTOR	mechanistic target of rapamycin kinase
MYC	myelocytomatosis oncogene
NF- κ B	nuclear factor 'kappa-light-chain-enhancer' of activated B-cells
ng	nanograms
NLS	nuclear localization sequence
nM	nanomolar
nuc/cyt	nuclear-to-cytoplasmic
OE	overexpression
PBS	phosphate buffered saline
PCR	polymerase chain reaction
PI3K	phosphatidylinositol 3-kinase
pM	picomolar
PMEPA1	Prostate Transmembrane Protein, Androgen Induced 1
poly(A)	polyadenylation
puro	Puromycin
pSMAD1/5/9	phosphorylated SMAD1/5/9
pSMAD2	phosphorylated SMAD2
pSMAD3	phosphorylated SMAD3
PVDF	polyvinylidene difluoride
RFP	red fluorescent protein
RNA	ribonucleic acid
RNase	ribonuclease
RPKM	reads per kilobase of transcript per million mapped reads
R-SMADs	receptor-regulated SMADs; isoforms 1, 2, 3, 5, 8
RT-qPCR	real-time quantitative PCR
s	seconds
STBL-3	Stable competent E. Coli
S2R	MCF10A SMAD2-reporter cell line
S2vR	MCF10A SMAD2-reporter version 2 cell line
S2vR S245	MCF10A SMAD2-reporter version 2 linker region S245 site mutation
S2vR S250	MCF10A SMAD2-reporter version 2 linker region S250 site mutation
S2vR S255	MCF10A SMAD2-reporter version 2 linker region S255 site mutation
S2vR T220	MCF10A SMAD2-reporter version 2 linker region T220 site mutation
S2Vr 3x-mutation	MCF10A SMAD2-reporter version 2 linker region S245, S250, S255 site mutation
S2vR 4x-mutation	MCF10A SMAD2-reporter version 2 linker region S245, S250, S255, T220 site mutation
SDS	sodium dodecyl sulfate
sgRNA	single guide RNA

SMAD	SMA ('small') and MAD ('mothers against decapentaplegic')
SOC	super optimal broth with catabolite repression
Sv40	simian virus 40
TAE	tris-acetate-EDTA
TBS-T	tris-buffered saline with Tween20
TEMED	tetramethylethylenediamine
TGF-beta	transforming growth factor beta
TGFBR2	transforming growth factor beta receptor 2
TGFBR3	transforming growth factor beta receptor 3
tracrRNA	trans-activating crRNA
Top10	Top10 electro competent E. Coli
TSS	transcriptional start site
U/ml	units per milliliter
UbCp	ubiquitin C promoter
V	volt
w/v	weight per volume
WT	wild-type
YFP	yellow fluorescent protein
Zeo	Zeocin

6.2 List of Figures

Figure 1 Schematic Representation of the SMAD Pathway Elements.	1
Figure 2 Schematic Representation of Live-Cell Time-Lapse Microscopy and Single-Cell Analysis... 7	7
Figure 3 Context-Dependent Effects of TGF-beta Signaling on Cellular Outcomes..... 8	8
Figure 4 SMAD Signaling in Angiogenesis and Vascular Homeostasis. 10	10
Figure 5 Genetic Basis and Vascular Manifestations of Hereditary Hemorrhagic Telangiectasia (HHT) and Pulmonary Arterial Hypertension (PAH)..... 12	12
Figure 6 Phenotypic Responses Correlate with SMAD Translocation in a State-Specific Manner Independent of Ligand Type. 16	16
Figure 7 EGF treatment Rewrite SMAD Response to Ligands in Quiescent Cells and Rescues Cells from Apoptosis..... 18	18
Figure 8 Generation of SMAD2 Linker Region Mutation Clones..... 20	20
Figure 9 Validation of SRv2 WT Clone. 22	22
Figure 10 Analysis of SMAD2 Dynamics in Different Clones with TGF-beta Induction. 23	23
Figure 11 SMAD2 Linker Region Inhibits SMAD2 Nuclear Translocation Upon Stimulation Independent of Cellular State..... 24	24
Figure 12 SMAD2 Linker Region Does Not Alter Cell Mobility Upon TGF-beta Stimulation..... 26	26
Figure 13 Gene Expression Analysis Identifies Receptors and SMADs in TGF-beta Pathway..... 27	27
Figure 14 Loss of SMAD3 Enhances GDF11-Regulated SMAD2 response in Proliferating Cells. 29	29
Figure 15 SMAD2 Nuclear Translocation in SMAD3KO Cells in Response to TGF-beta Superfamily Ligands..... 30	30
Figure 16 Loss of SMAD3 Alters Cell Phenotype Response Upon Ligand Stimulation. 32	32
Figure 17 Loss of SMAD3 Does Not Alter SMAD2 response in Cells Lacking the SMAD2 Linker Region Upon Ligand Stimulation. 33	33
Figure 18 Generation and Validation of mCherry-SMAD3 Double Reporter Clones..... 34	34
Figure 19 SMAD2 and SMAD3 Dynamics in Double Reporter Clones in Response to TGF-beta. 35	35
Figure 20 SMAD2 and SMAD3 Dynamics in Double Reporter Clones in Response to GDF11. 36	36
Figure 21 SMAD3 Regulates GDF11-Mediated SMAD2 Dynamics in a Dose-Dependent Manner... 37	37
Figure 22 SMAD2 and SMAD3 Responses to TGF-beta Superfamily Ligands. 38	38
Figure 23 SMAD3 Regulates GDF11-Mediated SMAD2 response via ALK5. 40	40

Figure 24 Global Gene Expression Analysis Identifies Potential Key Regulators of SMAD Signaling.	42
Figure 25 LTBP2, MMP9, and PMEPA1 Do Not Regulate GDF11-Mediated SMAD2 response in Proliferating Cells.	45
Figure 26 Selection and Validation of SMAD1 Reporter Clone.	48
Figure 27 Dynamics of SMAD Signaling in Living Cells.	49
Figure 28 Analysis of Receptor Expression in SMAD Signaling Pathways.	52
Figure 29 Different Ligands Induce Specific SMADs Responses.	53
Figure 30 FKBP12 Absence Rescues SMAD Response to ALK2-Dependent Ligands.	55
Figure 31 Dynamics of SMAD Signaling in Living Cells.	57
Figure 32 FKBP12 Modulation of SMAD1/2 Activation in Single Cells.	59
Figure 33 SMAD1 and SMAD2 Dynamics in Response to BMP9 and TGF-beta.	60
Figure 34 Differential SMAD Activation Due to Type I Receptor Homodimers or Heterodimers Depends on Specific Ligands.	63
Figure 35 SMAD Activation and Downstream Effects on Gene Expression and Cellular Phenotype.	66
Figure 36 Western Blot Assay Verifies p-SMAD3 Bands Following Inhibitor Treatment.	146
Figure 37 Global Gene Expression Analysis Identifies Potential Key Regulators of SMAD Signaling.	147
Figure 38 Verification of the SMADs Reporter.	148
Figure 39 Dynamics of SMAD5 and SMAD9 Signaling in Living Cells.	149
Figure 40 Different Ligands Induce Specific SMADs Responses.	150
Figure 41 Gene Expression Analysis Identified Protein in SMAD Signaling.	151
Figure 42 Different Ligands Induce Specific SMADs Responses after Removed FKBP12.	151
Figure 43 Differential SMAD Activation Due to Type I Receptor Homodimers or Heterodimers Depends on Specific Ligands.	152

6.3 Supplementary Figures

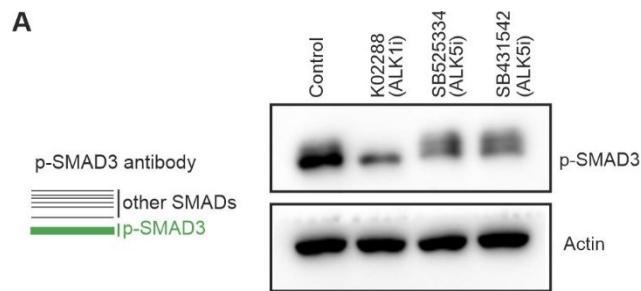


Figure 36 Western Blot Assay Verifies p-SMAD3 Bands Following Inhibitor Treatment.

(A) Western blot analysis of SMAD3 phosphorylation in MCF10A wildtype cells. Proliferating cells were treated with ALK1 inhibitor (K02288) (1 μ M), ALK5 inhibitor (SB525334) (10 μ M), or ALK5 inhibitor (SB431542) (10 μ M) as indicated. The figure shows the phosphorylation status of SMAD3, with Actin serving as the loading control. Specifically, the lower band corresponds to phosphorylated SMAD3, and the upper band corresponds to phosphorylated SMAD1/5/9.

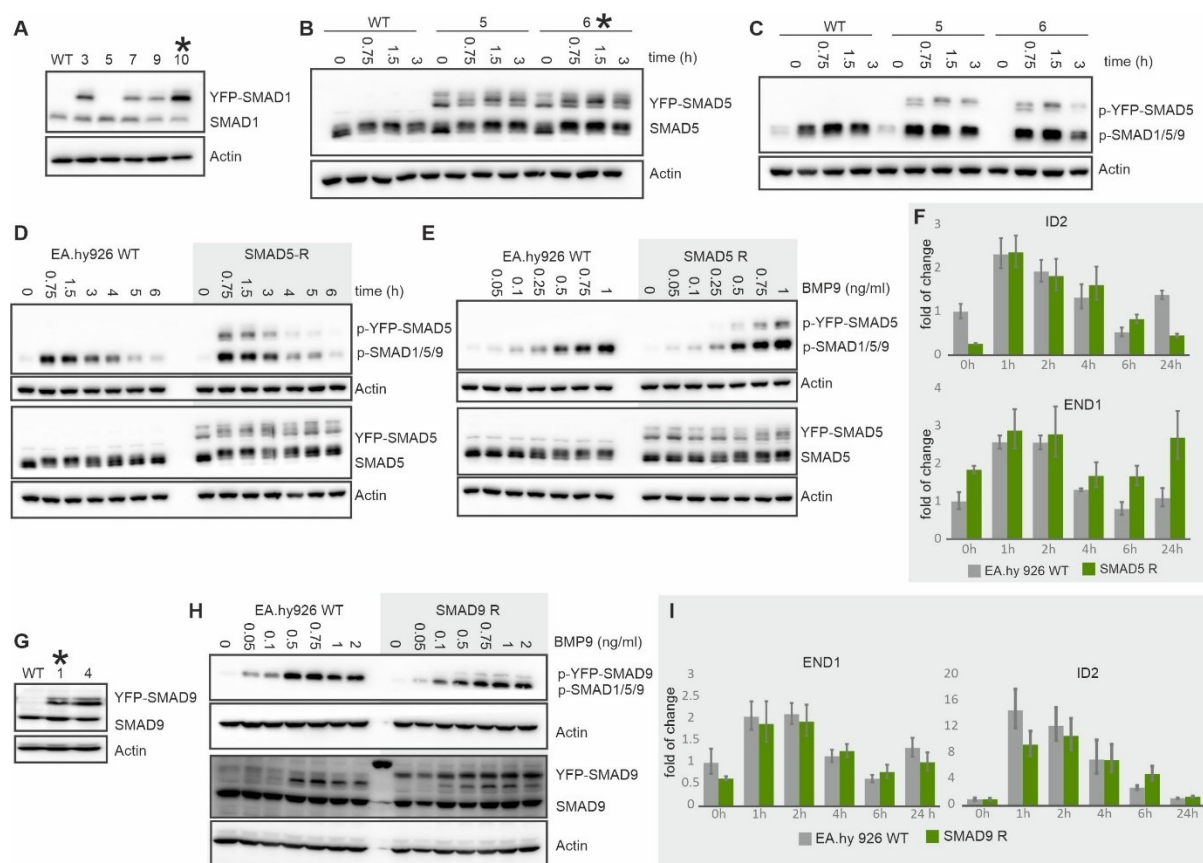


Figure 38 Verification of the SMADs Reporter.

Cells were grown in 1.5% FBS medium for 20 hours before stimulation with 1 ng/ml BMP9 and were harvested at the indicated time points. All experiments involving the SMAD5 reporter verification were conducted by Sonja Lenhardt for her Master's thesis, and all experiments for SMAD9 reporter verification were conducted by Marc-André Fiedler for his Bachelor's thesis. **(A)** Western blot comparison of EA.hy926 SMAD1 reporter cell lines (#3, #5, #7, #9, #10) with EA.hy926 WT cells using a Total SMAD1 antibody. In the end, cell line #10 was selected for further experiments, with Actin serving as the loading control. **(B)** Western blot comparison of EA.hy926 SMAD5 reporter cell lines (#5, #6) with EA.hy926 WT cells using a Total SMAD5 antibody. **(C)** Western blot comparison of EA.hy926 SMAD5 reporter cell lines (#5, #6) with EA.hy926 WT cells using a p-SMAD1/5/9 antibody. In the end, cell line #6 was selected for further experiments. **(D)** SMAD5 reporter cells were stimulated with 1 ng/ml BMP9 and harvested at the indicated time points and compare with EA.hy926 WT cells. p-SMAD1/5/9 is shown on the top, and total SMAD5 is shown on the bottom. **(E)** SMAD5 reporter cells were stimulated with the indicated BMP9 concentrations and harvested after 1.5 hours and compare with EA.hy926 WT cells. p-SMAD1/5/9 antibody results are shown on the top, and total SMAD5 results are shown on the bottom. **(F)** RT-qPCR analysis comparing SMAD target gene expression kinetics in EA.hy926 WT and EA.hy926 SMAD5 reporter cells following 1 ng/ml BMP9 stimulation. β -Actin served as the control. Data represent mean \pm SD of technical triplicates. **(G)** Western blot comparison of EA.hy926 SMAD9 reporter cell lines (#1, #4) with EA.hy926 WT cells using a Total SMAD9 antibody. In the end, cell line #1 was selected as the SMAD9 reporter. **(H)** SMAD9 reporter cells were stimulated with the indicated BMP9 concentrations and harvested after 1.5 hours and compare with EA.hy926 WT cells. p-SMAD1/5/9 antibody results are shown on the top, and total SMAD9 results are shown on the bottom. **(I)** RT-qPCR analysis comparing SMAD target gene expression kinetics in EA.hy926 WT and EA.hy926 SMAD9 reporter cells following 1 ng/ml BMP9 stimulation. β -Actin served as the control. Data represent mean \pm SD of technical triplicates.

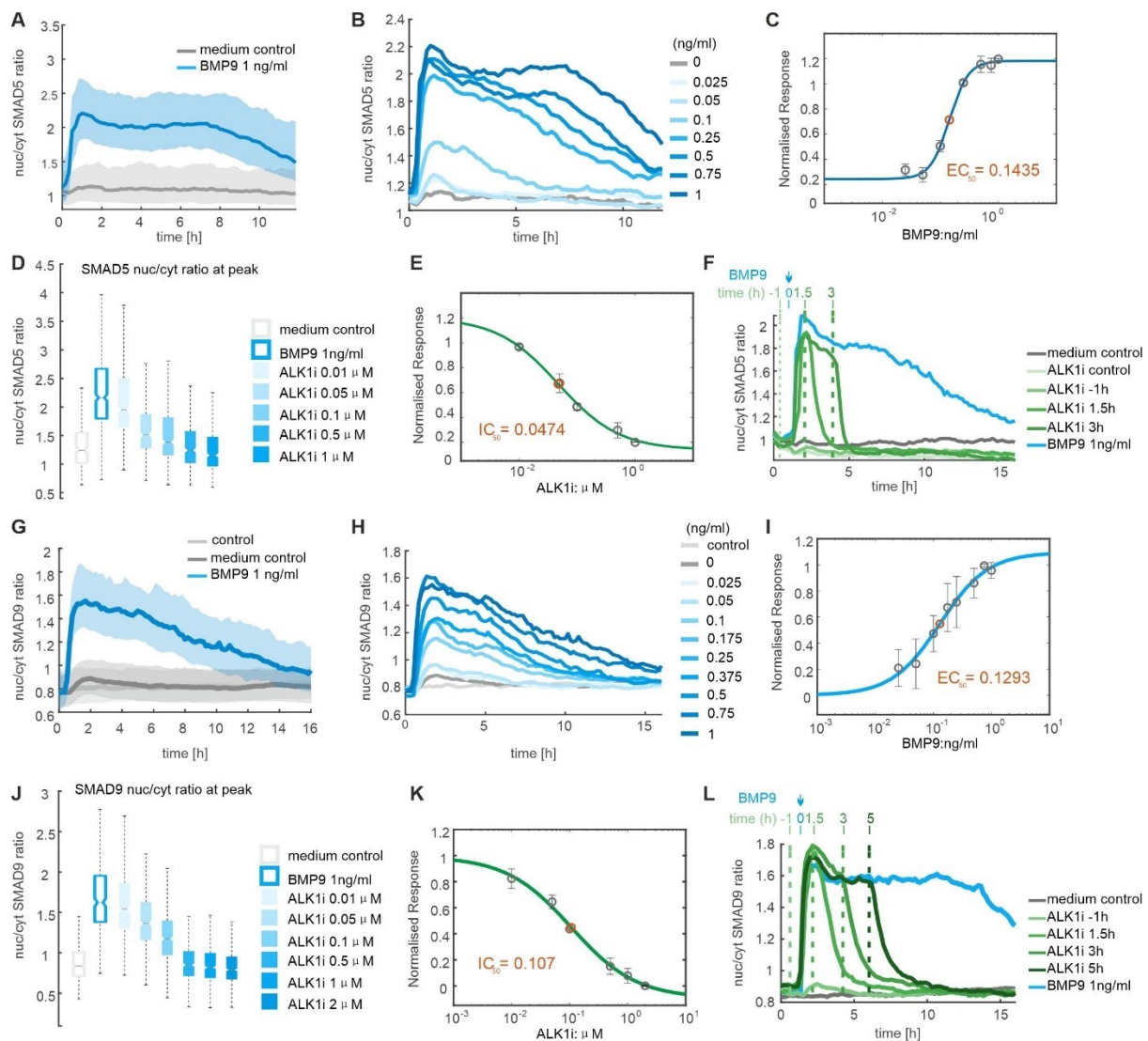


Figure 39 Dynamics of SMAD5 and SMAD9 Signaling in Living Cells.

(A) Median nuclear-to-cytoplasmic (nuc/cyt) SMAD5 ratio upon stimulation with 1 ng/ml BMP9 (blue), unstimulated control (light gray), or medium control (dark gray). Solid lines represent median values, and shaded areas indicate the 25th to 75th percentiles. Cells were pre-cultured in 1.5% FBS medium for 20 hours. Experiment performed by Sonja Gabriele Lenhardt for her Master's thesis. **(B)** Median nuc/cyt SMAD5 ratio following stimulation with varying BMP9 concentrations over 16 hours. Cells were pre-cultured in 1.5% FBS medium for 20 hours. Imaging began 0.5 hours before BMP9 stimulation, with 10-minute intervals. Experiment performed by Sonja Gabriele Lenhardt for her Master's thesis. **(C)** EC₅₀ calculation (orange) based on peak median nuc/cyt SMAD5 ratio for each BMP9 concentration. Data represent mean ± SD from two independent experiments. **(D)** Peak median nuc/cyt SMAD5 ratio in cells treated with various concentrations of ALK1 inhibitor (K02288) 1 hour before 1 ng/ml BMP9 stimulation. DMSO served as the control. Cells were pre-cultured in 1.5% FBS medium for 20 hours and tracked for 16 hours. Experiment performed by Sonja Gabriele Lenhardt for her Master's thesis. **(E)** IC₅₀ calculation (orange) for the ALK1 inhibitor based on peak median nuc/cyt SMAD5 ratio. Data represent mean ± SD from two independent experiments. **(F)** ALK1 inhibitor efficacy at different time points relative to BMP9 induction. Cells were treated with 1 μM ALK1 inhibitor at indicated time points (1 hour before or 1.5, 3, and 5 hours post 1 ng/ml BMP9 stimulation). DMSO served

as the control. Cells were pre-cultured in 1.5% FBS medium for 20 hours and tracked for 16 hours. Experiment performed by Sonja Gabriele Lenhardt for her Master's thesis. **(G)** Median nuc/cyt SMAD9 ratio upon stimulation with 1 ng/ml BMP9 (blue), unstimulated control (light gray), or medium control (dark gray). Solid lines represent median values, and shaded areas indicate the 25th to 75th percentiles. Cells were pre-cultured in 1.5% FBS medium for 20 hours. Experiment performed by Marc-André Fiedler for his Bachelor's thesis. **(H)** Median nuc/cyt SMAD9 ratio following stimulation with varying BMP9 concentrations over 16 hours. Cells were pre-cultured in 1.5% FBS medium for 20 hours. Imaging began 0.5 hours before BMP9 stimulation, with 10-minute intervals. Experiment performed by Marc-André Fiedler for his Bachelor's thesis. **(I)** EC50 calculation (orange) based on peak median nuc/cyt SMAD9 ratio for each BMP9 concentration. Data represent mean \pm SD from two independent experiments. **(J)** Peak median nuc/cyt SMAD9 ratio in cells treated with various concentrations of ALK1 inhibitor (K02288) 1 hour before 1 ng/ml BMP9 stimulation. DMSO served as the control. Cells were pre-cultured in 1.5% FBS medium for 20 hours and tracked for 16 hours. Experiment performed by Marc-André Fiedler for his Bachelor's thesis. **(K)** IC50 calculation (orange) for the ALK1 inhibitor based on peak median nuc/cyt SMAD9 ratio. Data represent mean \pm SD from two independent experiments. **(L)** ALK1 inhibitor efficacy at different time points relative to BMP9 induction. Cells were treated with 1 μ M ALK1 inhibitor at indicated time points (1 hour before or 1.5, 3, and 5 hours post 1 ng/ml BMP9 stimulation). DMSO served as the control. Cells were pre-cultured in 1.5% FBS medium for 20 hours and tracked for 16 hours. Experiment performed by Marc-André Fiedler for his Bachelor's thesis.

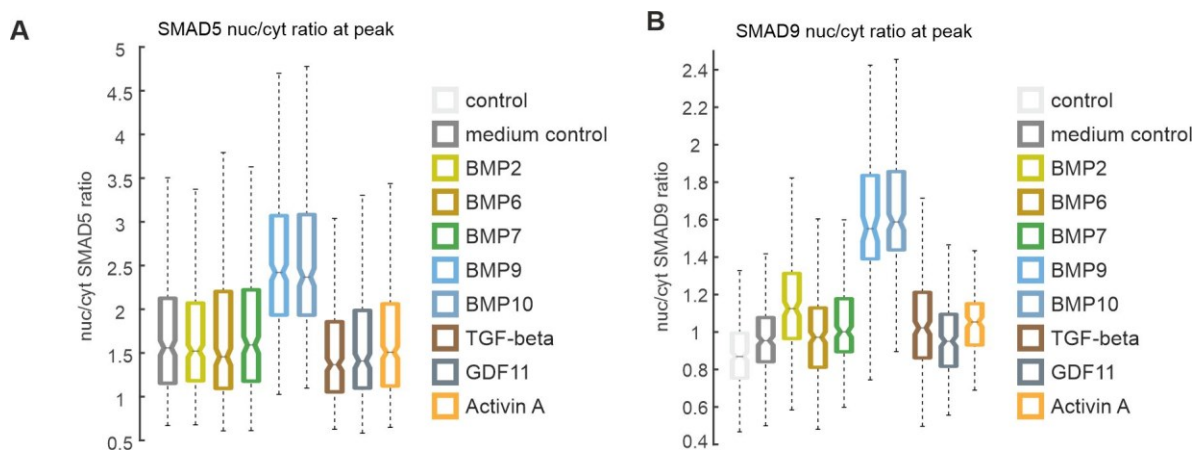


Figure 40 Different Ligands Induce Specific SMADs Responses.

Median nuc/cyt SMAD5 **(A)** and SMAD9 **(B)** ratio at peak following stimulation with varying ligands over 16 hours. SMAD5 experiment performed by Sonja Gabriele Lenhardt for her Master's thesis. SMAD9 experiment performed by Marc-André Fiedler for his Bachelor's thesis. Imaging began 0.5 hours before ligands stimulation, with 10-minute intervals. Cells were cultured in 1.5% FBS medium for 20 hours prior to stimulation. Ligand concentrations were identical to those used in panel A. Box plots represent data between the 25th and 75th percentiles of the cell population, with black lines indicating the median, and whiskers extending to maximum values within 1.5 times the interquartile range.

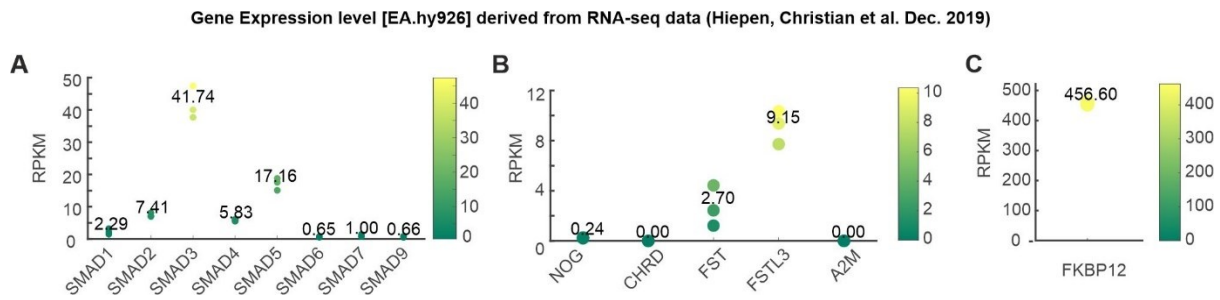


Figure 41 Gene Expression Analysis Identified Protein in SMAD Signaling.

The data was from the RNA-seq data (Hiepen et al., 2019). **(A)** List of SMAD expression levels in EA.hy926 cells. **(B)** List of inhibited protein expression levels in the BMP pathway. **(C)** FKBP12 expression level.

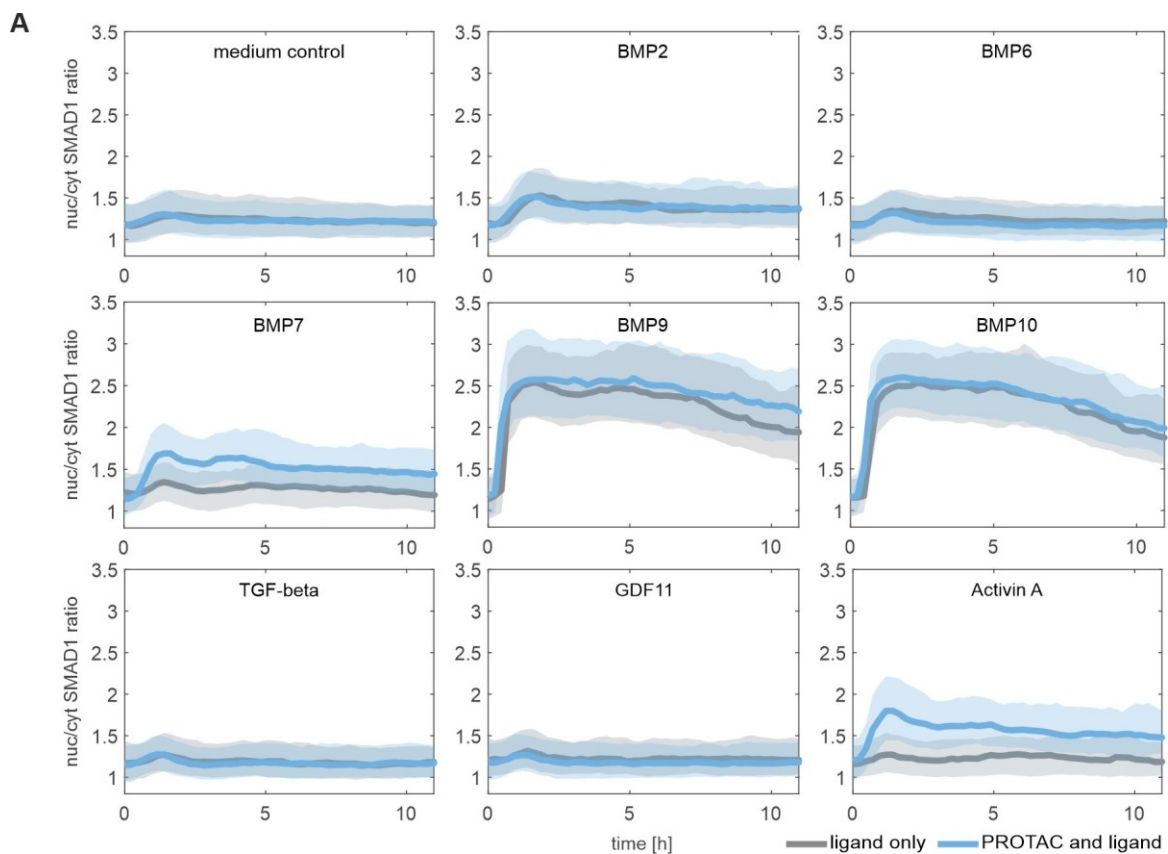


Figure 42 Different Ligands Induce Specific SMADs Responses after Removed FKBP12.

(A) Median nuclear-to-cytoplasmic SMAD1 ratio stimulation with different ligands in SMAD1 reporter cells. Ligand concentrations used were: BMP2 (250 ng/ml), BMP6 (250 ng/ml), BMP7 (250 ng/ml), BMP9 (1 ng/ml), BMP10 (1 ng/ml), TGF-beta (50 ng/ml), GDF11 (250 ng/ml), and Activin A (250 ng/ml). Cells were cultured in 1.5% FBS medium for 20 hours prior to stimulation. Cells were treated with ligand only (grey) and compare with the cell pre-incubated with FKBP12 PROTAC (blue). Solid lines represent the median values, and shaded areas indicate the 25th to 75th percentiles of the population.

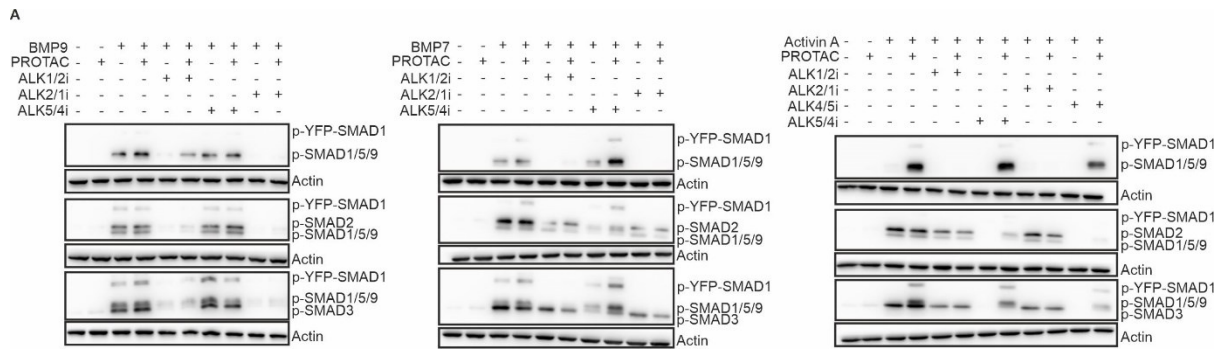


Figure 43 Differential SMAD Activation Due to Type I Receptor Homodimers or Heterodimers Depends on Specific Ligands.

(A) Western blot analysis was conducted to assess the phosphorylation of SMAD1/5/9 (top), SMAD2 (middle), and SMAD3 (bottom) in SMAD1 reporter cells following treatment with BMP9 (1 ng/ml, left), BMP7 (250 ng/ml, middle), or Activin A (250 ng/ml, right). The figure illustrates the phosphorylation status of these SMADs, with Actin serving as the loading control. Specifically, the lower band corresponds to phosphorylated SMAD3 (p-SMAD3 antibody), while the upper band corresponds to phosphorylated SMAD2 (SMAD2 antibody). PROTAC was added 24 hours before ligand stimulation in 1.5% FBS medium. Inhibitors ALK1/2i (K02288, 1 μ M), ALK2/1i (LDN214117, 10 μ M), ALK4/5i (TEW7179, 10 μ M), and ALK5/4i (SB525334, 10 μ M) were added 1 hour before ligand addition. Samples were harvested 1.5 hours after ligand addition.

6.4 Number of Tracked Cells in Time-Lapse Microscopy Experiments

6.4.1 Number of Tracked Cells in Time-Lapse Microscopy Experiments (Part 1):

Condition	Number of tracked cells
Figure 6 A, B, C	
Proliferating control	170
Proliferating TGF-beta	91
Proliferating GDF11	124
Proliferating Activin A	77
Figure 6 F, G, H	
Quiescent control	3019
Quiescent TGF-beta	2200
Quiescent GDF11	596
Quiescent Activin A	878
Figure 7 A	
Control	2186
Control + EGF	2403
TGF-beta	2587
TGF-beta + EGF 0 h	2339
TGF-beta + EGF 0.5 h	2257
TGF-beta + EGF 1 h	2665
TGF-beta + EGF 2 h	2528
TGF-beta + EGF 3 h	2363
TGF-beta + EGF 4 h	2496
TGF-beta + EGF 6 h	2843
TGF-beta + EGF 8 h	2648
Figure 7 B	
Control	2486
Control + EGF	2291
GDF11	2339
GDF11+ EGF 0 h	2287
GDF11+ EGF 0.5 h	2578
GDF11+ EGF 1 h	2510
GDF11+ EGF 2 h	2547
GDF11+ EGF 3 h	2635
GDF11+ EGF 4 h	2380
GDF11+ EGF 6 h	2698
GDF11+ EGF 8 h	2800
Figure 7 C	
Control	845
TGF-beta	1256
GDF11	227
Control – EGF -8h	333

TGF-beta – EGF -8h	271
GDF11 – EGF -8h	329
Control – EGF -1h	424
TGF-beta – EGF -1h	248
GDF11 – EGF -1h	351
Control – EGF 16h	702
TGF-beta – EGF 16h	334
GDF11 – EGF 16h	386
Figure 9 D	
SMAD2-R	624
SRv2 WT	365
Figure 9 E	
SMAD2-R TGF-beta 0 pM	323
SMAD2-R TGF-beta 1 pM	349
SMAD2-R TGF-beta 2.5 pM	339
SMAD2-R TGF-beta 5 pM	389
SMAD2-R TGF-beta 25 pM	404
SMAD2-R TGF-beta 100 pM	370
SRv2 WT TGF-beta 0 pM	280
SRv2 WT TGF-beta 1 pM	311
SRv2 WT TGF-beta 2.5 pM	260
SRv2 WT TGF-beta 5 pM	257
SRv2 WT TGF-beta 25 pM	312
SRv2 WT TGF-beta 100 pM	389
Figure 9 F	
SMAD2-R GDF11 0 nM	418
SMAD2-R GDF11 0.1 nM	372
SMAD2-R GDF11 0.5 nM	252
SMAD2-R GDF11 1 nM	408
SMAD2-R GDF11 2.5 nM	385
SMAD2-R GDF11 10 nM	405
SRv2 WT GDF11 0 nM	441
SRv2 WT GDF11 0.1 nM	302
SRv2 WT GDF11 0.5 nM	371
SRv2 WT GDF11 1 nM	399
SRv2 WT GDF11 2.5 nM	306
SRv2 WT GDF11 10 nM	345
Figure 10 A	
SRv2 WT	510
SRv2 S245	386
Figure 10 B, C, D	
SRv2 WT	297
SRv2 S250	158
SRv2 S255	365

SRv2 T220	201		
Figure 10 E, F			
SRv2 WT	451		
SRv2 3x-mutation	471		
SRv2 4x-mutation	538		
Figure 10 G, 12 A			
SRv2 WT TGF-beta 0 pM	326		
SRv2 WT TGF-beta 20 pM	171		
SRv2 WT TGF-beta 50 pM	234		
SRv2 WT TGF-beta 100 pM	236		
SRv2 3x-mutation TGF-beta 0 pM	365		
SRv2 3x-mutation TGF-beta 20 pM	294		
SRv2 3x-mutation TGF-beta 50 pM	275		
SRv2 3x-mutation TGF-beta 100 pM	190		
SRv2 4x-mutation TGF-beta 0 pM	285		
SRv2 4x-mutation TGF-beta 20 pM	181		
SRv2 4x-mutation TGF-beta 50 pM	137		
SRv2 4x-mutation TGF-beta 100 pM	161		
Figure 10 H			
SRv2 WT TGF-beta	486		
SRv2 WT TGF-beta ALK5i -1h	421		
SRv2 3x-mutation TGF-beta	648		
SRv2 3x-mutation TGF-beta ALK5i -1h	631		
SRv2 4x-mutation TGF-beta	707		
SRv2 4x-mutation TGF-beta ALK5i -1h	565		
Figure 10 I			
SRv2 WT TGF-beta	392		
SRv2 WT TGF-beta ALK5i 3h	256		
SRv2 3x-mutation TGF-beta	506		
SRv2 3x-mutation TGF-beta ALK5i 3h	270		
SRv2 4x-mutation TGF-beta	566		
SRv2 4x-mutation TGF-beta ALK5i 3h	425		
Figure 11 A, B, C, D, Fiugr 14 D, E, F, Figure 16 B, C	Repeat 1	Repeat 2	Repeat 3
SRv2 WT quiescent	898	674	1461
SRv2 WT quiescent TGF-beta	1002	948	1223
SRv2 WT proliferating	740	383	448
SRv2 WT proliferating TGF-beta	556	222	431
SRv2 4x-mutation quiescent	986	1099	1591
SRv2 4x-mutation quiescent TGF-beta	997	755	1148
SRv2 4x-mutation proliferating	703	437	500
SRv2 4x-mutation proliferating TGF-beta	627	279	492
SRv2 WT quiescent GDF11	1014	857	1438
SRv2 WT proliferating GDF11	736	266	528
SRv2 4x-mutation quiescent GDF11	1094	1236	1416

SRv2 4x-mutation proliferating GDF11	679	384	584
SRv2 WT SMAK3KO quiescent	840	985	1714
SRv2 WT SMAK3KO quiescent TGF-beta	924	844	1556
SRv2 WT SMAK3KO proliferating	636	302	396
SRv2 WT SMAK3KO proliferating TGF-beta	733	216	384
SRv2 4x-mutation SMAK3KO quiescent	949	954	992
SRv2 4x-mutation SMAK3KO quiescent TGF-beta	982	828	1135
SRv2 4x-mutation SMAK3KO proliferating	536	462	370
SRv2 4x-mutation SMAK3KO proliferating TGF-beta	522	303	410
SRv2 WT SMAK3KO quiescent GDF11	971	945	1283
SRv2 WT SMAK3KO proliferating GDF11	642	235	403
SRv2 4x-mutation SMAK3KO quiescent GDF11	934	825	1086
SRv2 4x-mutation SMAK3KO proliferating GDF11	638	358	319
Figure 15 A, Figure 22 A			
SRv2 WT SMAK3KO quiescent	1050		
SRv2 WT SMAK3KO quiescent TGF-beta	1148		
SRv2 WT SMAK3KO quiescent Activin A	1020		
SRv2 WT SMAK3KO quiescent GDF3	1040		
SRv2 WT SMAK3KO quiescent GDF8	1039		
SRv2 WT SMAK3KO quiescent GDF11	1115		
SRv2 WT SMAK3KO proliferating	298		
SRv2 WT SMAK3KO proliferating TGF-beta	181		
SRv2 WT SMAK3KO proliferating Activin A	446		
SRv2 WT SMAK3KO proliferating GDF3	322		
SRv2 WT SMAK3KO proliferating GDF8	457		
SRv2 WT SMAK3KO proliferating GDF11	247		
SRv2 WT SMAK3 R quiescent	1026		
SRv2 WT SMAK3 R quiescent TGF-beta	876		
SRv2 WT SMAK3 R quiescent Activin A	1133		
SRv2 WT SMAK3 R quiescent GDF3	1219		
SRv2 WT SMAK3 R quiescent GDF8	855		
SRv2 WT SMAK3 R quiescent GDF11	958		
SRv2 WT SMAK3 R proliferating	514		
SRv2 WT SMAK3 R proliferating TGF-beta	522		
SRv2 WT SMAK3 R proliferating Activin A	393		
SRv2 WT SMAK3 R proliferating GDF3	409		
SRv2 WT SMAK3 R proliferating GDF8	554		
SRv2 WT SMAK3 R proliferating GDF11	389		
Figure 16 A, B			
SRv2 WT quiescent	1795		
SRv2 WT quiescent TGF-beta	1326		
SRv2 WT quiescent GDF11	815		
SRv2 WT SMAK3KO quiescent	2289		

SRv2 WT SMAK3KO quiescent TGF-beta	1808		
SRv2 WT SMAK3KO quiescent GDF11	1440		
Figure 16 C, D, E			
SRv2 WT proliferating	172		
SRv2 WT proliferating TGF-beta	325		
SRv2 WT proliferating GDF11	196		
SRv2 WT SMAK3KO proliferating	201		
SRv2 WT SMAK3KO proliferating TGF-beta	159		
SRv2 WT SMAK3KO proliferating GDF11	276		
Figure 19 A			
SRv2 WT SMAD3 R control	319		
SRv2 WT SMAD3 R TGF-beta	216		
Figure 19 B			
SRv2 WT SMAD3 R control	136		
SRv2 WT SMAD3 R TGF-beta	263		
SRv2 WT SMAD3 R TGF-beta ALK5i -1h	120		
SRv2 WT SMAD3 R TGF-beta ALK5i 3h	143		
SRv2 WT SMAD3 R TGF-beta ALK5i 6h	153		
SRv2 WT SMAD3 R TGF-beta ALK5i 21h	155		
Figure 19 C			
SRv2 WT SMAD3 R quiescent control	1250		
SRv2 WT SMAD3 quiescent TGF-beta 5 pM	1073		
SRv2 WT SMAD3 quiescent TGF-beta 25 pM	1134		
SRv2 WT SMAD3 quiescent TGF-beta 100 pM	852		
Figure 19 C			
SRv2 WT SMAD3 R proliferating control	266		
SRv2 WT SMAD3 proliferating TGF-beta 5 pM	286		
SRv2 WT SMAD3 proliferating TGF-beta 25 pM	325		
SRv2 WT SMAD3 proliferating TGF-beta 100 pM	277		
Figure 20 A	Repeat 1	Repeat 2	Repeat 3
SRv2 WT SMAD3 quiescent TGF-beta	281	735	870
SRv2 WT SMAD3 quiescent GDF11	317	825	796
SRv2 WT SMAD3 proliferating TGF-beta	132	325	248
SRv2 WT SMAD3 proliferating GDF11	151	259	312
Figure 20 B			
SRv2 WT SMAD3 R quiescent control	701		
SRv2 WT SMAD3 quiescent GDF11 0.1 nM	716		
SRv2 WT SMAD3 quiescent GDF11 1 nM	675		
SRv2 WT SMAD3 quiescent GDF11 10 nM	696		
SRv2 WT SMAD3 R proliferating control	332		
SRv2 WT SMAD3 proliferating GDF11 0.1 nM	382		
SRv2 WT SMAD3 proliferating GDF11 1 nM	312		
SRv2 WT SMAD3 proliferating GDF11 10 nM	353		
Figure 21 A			

SRv2 WT quiescent TGF-beta	911	
SRv2 WT SMAD3KO quiescent TGF-beta	1146	
SRv2 WT SMAD3 R1 quiescent TGF-beta	1144	
SRv2 WT SMAD3 R quiescent TGF-beta	1406	
SRv2 WT SMAD3 R2 quiescent TGF-beta	920	
SRv2 WT quiescent GDF11	844	
SRv2 WT SMAD3KO quiescent GDF11	1322	
SRv2 WT SMAD3 R1 quiescent GDF11	1196	
SRv2 WT SMAD3 R quiescent GDF11	1146	
SRv2 WT SMAD3 R2 quiescent GDF11	1199	
SRv2 WT proliferating TGF-beta	213	
SRv2 WT SMAD3KO proliferating TGF-beta	216	
SRv2 WT SMAD3 R1 proliferating TGF-beta	294	
SRv2 WT SMAD3 R proliferating TGF-beta	290	
SRv2 WT SMAD3 R2 proliferating TGF-beta	246	
SRv2 WT proliferating GDF11	201	
SRv2 WT SMAD3KO proliferating GDF11	310	
SRv2 WT SMAD3 R1 proliferating GDF11	254	
SRv2 WT SMAD3 R proliferating GDF11	314	
SRv2 WT SMAD3 R2 proliferating GDF11	294	
Figure 23 C, D	Repeat 1 (Figure 23 C)	Repeat 2
Control	249	274
Control ALK5i wash off	312	172
TGF-beta	255	284
TGF-beta ALK5i wash off	193	187
GDF11	256	286
GDF11 ALK5i wash off	330	248
Figure 23 E, F	Repeat 1	Repeat 2
Control	301	463
Control ALK5i wash off	525	539
TGF-beta	344	364
TGF-beta ALK5i wash off	512	579
GDF11	464	429
GDF11 ALK5i wash off	514	632
Figure 23 G, H	Repeat 1	Repeat 2
Control	353	344
Control ALK5i wash off	380	483
TGF-beta	297	306
TGF-beta ALK5i wash off	419	391
GDF11	335	331
GDF11 ALK5i wash off	327	415
Figure 25 D		
LTBP2 sg1-11 TGF-beta	1045	
LTBP2 sg1-11 GDF11	896	

LTBP2 sg1-14 TGF-beta	835
LTBP2 sg1-14 GDF11	1131
LTBP2 sg2-2 TGF-beta	527
LTBP2 sg2-2 GDF11	571
LTBP2 sg2-3 TGF-beta	870
LTBP2 sg2-3 GDF11	755
MMP9 sg1-1 TGF-beta	376
MMP9 sg1-1 GDF11	396
MMP9 sg3-2 TGF-beta	337
MMP9 sg3-2 GDF11	283
MMP9 sg3-3 TGF-beta	316
MMP9 sg3-3 GDF11	226
MMP9 sg3-4 TGF-beta	243
MMP9 sg3-4 GDF11	240
PMEPA1 sg4-2 TGF-beta	411
PMEPA1 sg4-2 GDF11	472
PMEPA1 sg4-22 TGF-beta	552
PMEPA1 sg4-22 GDF11	635
PMEPA1 sg6-1 TGF-beta	375
PMEPA1 sg6-1 GDF11	326
PMEPA1 sg6-10 TGF-beta	677
PMEPA1 sg6-10 GDF11	671

6.4.2 Number of Tracked Cells in Time-Lapse Microscopy Experiments (Part 2):

Condition	Number of tracked cells		
	Repeat 1 (Figure 27 B, C)	Repeat 2	Repeat 3
Figure 27 B, C, D	Repeat 1 (Figure 27 B, C)	Repeat 2	Repeat 3
Control	567	558	407
BMP9 0 ng/ml	502	602	359
BMP9 0.025 ng/ml	385	537	431
BMP9 0.05 ng/ml	332	508	376
BMP9 0.1 ng/ml	354	559	369
BMP9 0.175 ng/ml	441	439	423
BMP9 0.25 ng/ml	425	316	458
BMP9 0.375 ng/ml	358	260	406
BMP9 0.5 ng/ml	390	251	351
BMP9 0.75 ng/ml	359	348	394
BMP9 1 ng/ml	353	220	377
BMP9 2 ng/ml	288	397	409
Figure 27 E, F	Repeat 1	Repeat 2	Repeat 3 (Figure 27 E)
Medium control	685	100	547
BMP9 1 ng/ml	469	251	442
ALK1i 0.01 μ M	554	114	367
ALK1i 0.05 μ M	539	110	432
ALK1i 0.1 μ M	522	85	469
ALK1i 0.5 μ M	585	224	603
ALK1i 1 μ M	622	253	576
ALK1i 2 μ M	558	282	655
Figure 27 G, H	Repeat 1	Repeat 2 (Figure 27 E)	Repeat 3
Control	440	590	571
Medium control	465	522	493
ALK1i control	398	454	602
ALK1i -1h	428	545	556
ALK1i 1.5h	422	443	657
ALK1i 3h	469	499	527
ALK1i 5h	443	546	471
BMP9 1 ng/ml	363	486	439
Figure 29 B			
Control	620		
Medium control	513		
BMP2	452		
BMP6	428		
BMP7	414		
BMP9	346		
BMP10	364		

TGF-beta	421
GDF11	429
Activin A	333
Figure 30 C	
Control	627
Medium control	545
BMP2	400
BMP6	504
BMP7	438
BMP9	338
BMP10	464
TGF-beta	494
GDF11	519
Activin A	334
Figure 30 E	
Control	496
BMP7 250 ng/ml	432
PROTAC control	582
PROTAC BMP7 5 ng/ml	517
PROTAC BMP7 10 ng/ml	487
PROTAC BMP7 50 ng/ml	463
PROTAC BMP7 100 ng/ml	451
PROTAC BMP7 150 ng/ml	422
PROTAC BMP7 200 ng/ml	465
PROTAC BMP7 250 ng/ml	434
PROTAC BMP7 500 ng/ml	368
Figure 30 F	
Control	496
Activin A 250 ng/ml	564
PROTAC control	582
PROTAC Actvin A 5 ng/ml	566
PROTAC Actvin A 50 ng/ml	456
PROTAC Actvin A 250 ng/ml	367
Figure 30 G	
Mediun control	311
BMP7 250 ng/ml	258
PROTAC medium control	325
PROTAC -4h	254
PROTAC -6h	272
PROTAC -8h	297
PROTAC -16h	228
PROTAC -24h	322
Figure 31 C	
BMP9 0 ng/ml	727

BMP9 0.01 ng/ml	703		
BMP9 0.05 ng/ml	687		
BMP9 0.1 ng/ml	759		
BMP9 0.175 ng/ml	717		
BMP9 0.25 ng/ml	729		
BMP9 0.5 ng/ml	726		
BMP 1 ng/ml	783		
Figure 31 D			
TGF-beta 0 ng/ml	833		
TGF-beta 0.1 ng/ml	919		
TGF-beta 0.5 ng/ml	861		
TGF-beta 1 ng/ml	943		
TGF-beta 5 ng/ml	999		
TGF-beta 10 ng/ml	884		
TGF-beta 50 ng/ml	915		
TGF-beta 250 ng/ml	911		
Figure 31 E, Figure 32 A	Repeat 1 (Figure 31 E, Figure 32 A)	Repeat 2	Repeat 3
BMP7 0 ng/ml	539	691	467
BMP7 5 ng/ml	558	705	493
BMP7 10 ng/ml	485	679	345
BMP7 50 ng/ml	487	581	297
BMP7 100 ng/ml	405	595	453
BMP7 150 ng/ml	410	608	341
BMP7 200 ng/ml	430	548	434
BMP7 250 ng/ml	454	648	445
BMP7 500 ng/ml	434	664	384
PROTAC BMP7 0 ng/ml	503	625	404
PROTAC BMP7 5 ng/ml	563	676	448
PROTAC BMP7 10 ng/ml	523	700	480
PROTAC BMP7 50 ng/ml	528	640	482
PROTAC BMP7 100 ng/ml	510	652	482
Prtoac BMP7 150 ng/ml	453	691	511
PROTAC BMP7 200 ng/ml	354	649	455
PROTAC BMP7 250 ng/ml	440	641	528
PROTAC BMP7 500 ng/ml	543	708	506
Figure 32 E			
BMP7 250 ng/ml correated	506		
Activin A 250 ng/ml correated	521		
Figure 33 A			
Medium control	464		
BMP9 TGF-beta contreated	521		
TGF-beta	541		
BMP9 TGF-beta	524		
Figure 33 B	Repeat 1 (Figure 33 B)	Repeat 2	Repeat 3

BMP9 0 ng/ml	727	355	374
BMP9 0.01 ng/ml	703	278	411
BMP9 0.05 ng/ml	687	311	404
BMP9 0.1 ng/ml	759	266	389
BMP9 0.175 ng/ml	717	295	359
BMP9 0.25 ng/ml	729	279	345
BMP9 0.5 ng/ml	726	246	326
BMP9 1 ng/ml	783	323	394
TGF-beta BMP9 0 ng/ml	703	294	308
TGF-beta BMP9 0.01 ng/ml	792	279	368
TGF-beta BMP9 0.05 ng/ml	814	340	385
TGF-beta BMP9 0.1 ng/ml	832	321	422
TGF-beta BMP9 0.175 ng/ml	783	336	362
TGF-beta BMP9 0.25 ng/ml	794	346	381
TGF-beta BMP9 0.5 ng/ml	780	293	414
TGF-beta BMP9 1 ng/ml	706	204	299
Figure 34 A, D			
Medium control	379		
BMP9	368		
BMP9 ALK1/2/i	352		
BMP9 ALK2/1i	746		
BMP9 ALK4/5i	365		
PROTAC medium control	516		
PROTAC BMP9	417		
PROTAC BMP9 ALK1/2/i	406		
PROTAC BMP9 ALK2/1i	806		
PROTAC BMP9 ALK4/5i	446		
Figure 34 B, D			
Medium control	396		
BMP7	346		
BMP7 ALK1/2i	497		
BMP7 ALK2/1i	739		
BMP7 ALK4/5i	488		
PROTAC medium control	311		
PROTAC BMP7	370		
PROTAC BMP7 ALK1/2/i	349		
PROTAC BMP7 ALK2/1i	703		
PROTAC BMP7 ALK4/5i	381		
Figure 34 C, D			
Medium control	455		
Activin A	431		
Activin ALK1/2/i	443		
Activin A ALK2/1i	792		
Activin A ALK4/5i	486		

PROTAC mediun control	403
PROTAC Activin A	442
PROTAC Activin A ALK1/2/i	427
PROTAC Activin A ALK2/1i	842
PROTAC Activin A ALK4/5i	565
Figure 35 B	
Control	262
BMP9	164
BMP9 AKL1i	277
BMP7	175
BMP7 prtoac	182
BMP7 PROTAC ALK4/5i	202

Acknowledgments

First and foremost, I would like to express my deepest gratitude to Alex, my supervisor, for his invaluable guidance, encouragement, and unwavering support throughout this research journey. From the outset of this project to the most challenging moments I encountered, both academically and personally, Alex has been a constant source of strength and reassurance, always believing in my potential. His insightful suggestions and advice—ranging from laboratory techniques to programming, and even the nuances of thesis writing—have not only shaped this research but also contributed significantly to my development as a scientist and as an individual. His encouragement during times of doubt and stress provided me with the courage and determination to persevere, ultimately enabling me to complete this thesis.

I am also immensely grateful to Stefan and the Petra group members for their constructive feedback and invaluable suggestions, which significantly enhanced the quality of my work. Stefan was always ready to offer his support, providing the best advice whenever I needed it. I would also like to extend my heartfelt thanks to Petra and her team for their invaluable assistance when I embarked on the SMAD1/5/9 project. Their feedback and encouragement were instrumental in advancing the project.

This work would not have been possible without the financial support of the China Scholarship Council (CSC), whose generous funding enabled me to pursue this research.

I extend my heartfelt thanks to my wonderful colleagues in the lab. From the day I arrived, Petra has been a constant source of support, helping me navigate both the complexities of lab work and the nuances of life here. To Laura, Anna, and Stefan, I am deeply grateful for their kindness and support, especially during those overwhelming early days. Flavia, her thoughtful feedback and the warmth she showed by inviting me to celebrate Christmas with her family are moments I will treasure forever. Theresa, she brought light to my darkest days in the lab, and I will always cherish our fun conversations. Sonja, even as my first student, I felt that we grew together under Alex's mentorship. We faced many challenges side by side, and I learned just as much from her as she did from me. The trips we took and the laughter we shared will always hold a special place in my heart. Annkathrin, her encouraging words and positivity always lifted my spirits when I needed them most. Ahmed and Yunwei, I am grateful for their patience and understanding, and for standing by me during stressful times. Caibin, even though we have yet to meet in person, his invaluable help has made a difference in my journey. Lastly, I extend my sincere thanks to Bettina, Jenni, and Sabine for their vital assistance in the lab and with all the necessary documentation. On a personal note, I would like to express my heartfelt thanks to my family and friends for their unwavering support and understanding throughout this journey.

To my grandparents, your love and strict guidance have shaped me into who I am today (感谢我的爷爷奶奶，外公外婆，你们充满爱的照顾和培养塑造了今天的我。). To my parents, your support has been my anchor; I would not have persevered without you. You are my safe harbor, always (感谢我的花哥，罗姐，黄老大和伯伯，你们的支持是我的支柱；没有你们，我不可能坚持下去。你们永远是我的避风港。). To my dearest friend, Yuting, words cannot express how grateful I am for you. Thank you for being my daily source of comfort, for patiently listening to my worries and negative thoughts, and for always radiating positivity. You kept me connected to the world and grounded, even from afar. I truly cannot imagine these past six years without you by my side. Houma and Wan, we've known each other for nearly 15 years, and through it all, your unwavering care and protection have been constants in my life. You both are more than friends; you are a gift that life has given me. Zhiwei, my friend of over a decade, thank you for standing by me and encouraging me, especially during those times when scientific challenges felt insurmountable. Despite the physical distance between us, your support has meant more to me than I could ever put into words.

Ehrenwörtliche Erklärung

Ich erkläre hiermit, dass ich die vorliegende Arbeit ohne unzulässige Hilfe Dritter angefertigt habe. Sämtliche aus fremden Quellen direkt oder indirekt übernommenen Gedanken sowie sämtliche von Anderen direkt oder indirekt übernommenen Daten, Techniken und Materialien sind als solche kenntlich gemacht.

Ferner erkläre ich, dass ich bei der Verfassung der Dissertation die "Grundsätze zur Sicherung guter wissenschaftlicher Praxis an der Technischen Universität Darmstadt" und die "Leitlinien zum Umgang mit digitalen Forschungsdaten an der TU Darmstadt" in den jeweils aktuellen Versionen beachtet habe. Die Arbeit wurde bisher bei keiner anderen Hochschule zu Prüfungszwecken eingereicht.

.....

Ort, Datum

Curriculum Vitae

Zixin Huang
M.S. Genetics

Born on 4th June 1992 in Guangdong, China

Academic Career

Ph.D. Student in Systems Biology

Technical University Darmstadt, Darmstadt, Germany
10/2018 – 10/2024

M.S. in Genetics

Sun Yat-sen University, Guangzhou, P.R. China
09/2014 – 06/2018

B.S. in Biotechnology

Guangzhou Medical University, Guangzhou, P.R. China
09/2010 – 06/2014

Awards

CSC (China Scholarship Council) Scholarship 2018-2022

Sun Yat-sen University Scholarship (first-class prize) 2016-2017

Sun Yat-sen University Scholarship (first-class prize) 2015-2016

Sun Yat-sen University Scholarship (third-class prize) 2014-2015

Publications

Bohn, S., Hexemer, L., **Huang, Z.**, Strohmaier, L., Lenhardt, S., Legewie, S., & Loewer, A. (2023). State- And stimulus-specific dynamics of SMAD signaling determine fate decisions in individual cells. *Proceedings of the National Academy of Sciences of the United States of America*, 120(10). <https://doi.org/10.1073/pnas.2210891120>

Huang, Z., & Loewer, A. (2022). Generating Somatic Knockout Cell Lines with CRISPR-Cas9 Technology to Investigate SMAD Signaling. In *Methods in Molecular Biology* (Vol. 2488). https://doi.org/10.1007/978-1-0716-2277-3_7